1995-08-01

A New Photopolymer Recording Material for Holographic Applications: Photochemical and Holographic Studies Towards an Optimized System

Suzanne Martin
Technological University Dublin, suzanne.martin@tudublin.ie

Recommended Citation

Martin, S. (1995). *A new photopolymer recording material for holographic applications: photochemical and holographic studies towards an optimized system*. Doctoral thesis. Technological University Dublin. doi:10.21427/D7DP4B

A NEW PHOTOPOLYMER RECORDING MATERIAL FOR HOLOGRAPHIC APPLICATIONS: PHOTOCHEMICAL AND HOLOGRAPHIC STUDIES TOWARDS AN OPTIMIZED SYSTEM

A thesis submitted for the degree of Doctor of Philosophy to

the Department of Pure and Applied Physics

University of Dublin

August 1995

by

Suzanne Martin B. Sc(Appl. Sc.)

Department of Physics

Dublin Institute of Technology

CONTENTS

Acknowledgments

During the years it took to complete this thesis I received advice, support and encouragement from many people. I would particularly like to thank my supervisor at the Dublin Institute of Technology, Dr. Vincent Toal for his constant encouragement, support and practical help.

I would also like to thank Prof. Werner Blau and Dr. Andy Davy of the Physics department, Trinity College for their interest in the work and for many helpful and interesting discussions.

I am indebted to Prof. Yves Lion, Dr. Yvon Renotte, Dr Philippe Leclere and the postgrads and employees of HoloLab in the University of Liege, Belgium for inviting me to work with them and for their help and kindness during my stay in their laboratories last year.

I would like to acknowledge the help of research students Clodagh Feeley and Brian Bowe for their work in methylene blue sensitized systems and reflection holography, and Howard McQuaid of Forbairt for his assistance with surface profilometry. Thanks also to the staff of the Physics department in Kevin street, particularly Dr. Matt Hussey, Mr. Art O' Hare, and the physics technicians, and also to the staff of chemistry department for valuable assistance.

Special thanks to the physics postgrads in Kevin street, particularly Vincent Toal's research students, past and present, for their support and friendship during the last few years, and especially to my family and Tim for their encouragement and patience.

I would like to acknowledge Forbairt, formerly Eolas for the provision of a research scholarship.

DECLARATION

This thesis has not been submitted as an exercise for a degree at any other university. Apart from the assistance mentioned in the acknowledgements, the work is entirely my own. I agree that Trinity College Library may lend or copy this thesis upon request.

Signed Martin

A new photopolymer recording material for holographic applications: photochemical and holographic studies towards an optimized system.

by

Suzanne Martin

ABSTRACT

Photopolymer materials are a practical alternative to high resolution silver halide photographic emulsions for the recording of holograms and high spatial frequency holographic gratings.

The new holographic recording material reported in this thesis consists of a green sensitive dye (erythrosin B), an electron donor (triethanolamine), and a monomer mixture (acrylamide and methylene bisacrylamide) in a polyvinyl alcohol binder. On illumination with light of the appropriate wavelength the dye absorbs a photon and the excited triplet state of the dye reacts with the electron donor to produce free radicals. These free radicals may then initiate local polymerization of the monomer. The changes in density and molecular polarizability which accompany polymerization cause a change in local refractive index and the hologram is thereby recorded as a volume phase hologram. After recording no further chemical or physical processing steps are required.

The chemical and physical processes leading to the refractive index modulation are investigated in detail. The relative contributions to the refractive index change, of density change through diffusion and decrease in molecular polarizability are discussed. The conclusions drawn lead to a new understanding of the processes of hologram formation in this type of material.

An original non-holographic technique for the investigation of the initiation processes and comparison of sensitizing dyes is presented. The comparison of quantum yields of bleaching in the absence and presence of monomer is used to estimate the amount of initiation occurring in monomer containing layers.

This, and other more conventional holographic methods are used to optimize the chemical composition of the material for sensitivity, diffraction efficiency, shelf life and layer quality. Thick layers of the optimized material require only 50mJ/cm^2 for an 80% diffraction efficiency or 80 mJ/cm^2 for a 96% diffraction efficiency. The optimized material is found to perform well in transmission mode for slanted or unslanted gratings and has a resolution of up to 3000 lines/mm. However the material, in its present formulation, will only record weak reflection gratings (<2% efficiency).

A demonstration of the suitability of this self developing material for holographic interferometry is carried out with excellent results.

Summary

This thesis is the result of an extensive and detailed investigation into an acrylamide based photopolymer material.

Chapter 1 begins by introducing the basic ideas of holography, its uses and the currently available holographic recording materials. The theoretical background needed to analyze recorded gratings in thick photopolymer layers is outlined here.

Chapters 2, 3 and 4 are closely related and involve the optimization and improvement of the shelf life, optical quality, grating lifetime, diffraction efficiency and sensitivity of the material. A better understanding of the chemical processes occurring under 514nm illumination was required to optimize the system efficiently so a separate investigation was carried out into the photochemistry of the system in chapter 3.

Chapter 5 details the investigation of the recording characteristics of the optimized material and gives a demonstration of holographic interferometry, an application for which this material is particularly suitable.

Chapter 6 is a further study into the recording mechanisms, in particular the physical processes which lead to the refractive index change on exposure to light. Care is taken to determine what type of grating is being recorded and several examples are analyzed using coupled wave theory to determine the magnitude of the refractive index change.

All the chapters are liberally cross referenced. This allows the reader to refer to relevant ideas in other sections as the results observed are often due to a combination of different processes some of which may have been dealt with in another chapter.

The thesis concludes by outlining the progress made and the conclusions reached. The recording material has been greatly improved and thick layers of the optimized material require only 80 mJ/cm^2 for a 94% diffraction efficiency. The optimized material is found to perform well in transmission mode for slanted or unslanted gratings and has a resolution of up to 3000 lines/mm. The chemical and physical processes leading to the refractive index modulation have also been investigated in detail. The relative contributions to the refractive index change, of density change through diffusion and decrease in molecular polarizability have been determined and the conclusions drawn lead to a new understanding of the processes of hologram formation in this type of material.

1. General Introduction to holography.

Holography was invented in 1948 by Dennis Gabor[1] as a method of improving images obtained with an electron microscope. Although unable to demonstrate the validity of his principle with electron waves he was able to do so with visible light. However it was not until the invention of the laser provided a coherent light source of sufficient intensity that holography found any real application, and in the mid 1960's Leith and Upatnieks[2,3] showed that three dimensional images could be generated by illuminating a photographic plate with laser light.

Holography is now a widely used technique whose range of applications has extended considerably from a method of producing three dimensional images to non destructive testing [4,5], optical information processing [6,7] and mass data storage [8]. Holographic optical elements[9], optical interconnects for communications and computing applications[10], as well as optical neural networks for artificial intelligence[11] are all technologies likely to benefit greatly from holography.

1.1 Holographic recording materials.

Since Leith and Upatnieks work there has been an ongoing search for the ideal holographic recording material. For general holography the most widely used and investigated materials have been silver halide photographic emulsions and dichromated gelatin. Specific holographic applications, however, have specific material requirements and there are several other widely used recording media.

Ferroelectric crystals, for example, are almost ideal for optical information storage, as they record real-time, erasable, thick, phase holograms, whereas for an application requiring mass production of holographic components, permanent surface relief holograms recorded in photoresist would be an obvious choice.

In order to record a hologram, the recording material must respond to exposure and/or development by changing its optical transmission properties. The recorded hologram is called an absorption hologram if the absorbance of the material changes as a function of exposure, or a phase hologram if either the thickness or the refractive index changes. As will be described below, recording a hologram usually involves recording the interference pattern produced when light scattered by the object interferes with a reference beam. Since the nature of the interference pattern depends not only on the amplitude of the light scattered by the object but also on the phase, enough information is recorded to reconstruct a three dimensional image of the object. Due to the fact that the interference fringes in a typical hologram are less than a micron in width, the recording material must have a resolution much higher than the few hundred lines/mm typical of photographic recording materials. High sensitivity is also very important as it allows exposure times to be short, thereby reducing the very high levels of environmental stability required for holographic recording.

The following review attempts to provide a brief introduction to each of the main types of holographic recording material. In each case a simple explanation of the recording mechanism is included and their recording characteristics are compared.

1.1.1 Silver Halide Photographic Emulsion

When the helium-neon laser first became accessible for holography in the early 1960s silver halide photographic emulsion was the only readily available material which had the required resolution and sensitivity to this wavelength. The emulsion is suitable for recording amplitude and phase holograms, and can be used in transmission or reflection mode. Its sensitivity is unequaled by other materials; only a few microJoules per square centimeter is required to record a hologram, and the resolution of some of the commercially available films is excellent[12]. Unfortunately wet processing and development is always required making silver halide unsuitable for certain applications, and erasure / re-writing is not possible.

Photographic emulsion consists of a gelatin film in which submicroscopic crystals of silver halide are suspended. Absorption of a photon causes the ionization of the halide (usually Bromine). The free electron may move through the crystal lattice to one of the crystal defects where it is trapped. Here it will attract an interstitial silver ion and form a single silver atom which will attract another free electron so that the cycle repeats itself.

$$Br^- + h\nu \rightarrow Br + e^-$$

$$e^- + Ag^+ \rightarrow Ag$$

Only two silver ions are needed to form a stable subspeck, but a speck of at least three or four atoms is necessary to catalyze development[13]. The number of developable grains is proportional to the exposure that area receives, so the film records a latent image of the spatial variation of intensity across the film. This latent image can be converted into a hologram in the following way. The film is developed to convert each grain which contains a latent image speck to a grain of silver; this is where the huge

amplification involved in silver halide materials is achieved. A grain containing only three or four specks of reduced silver is entirely reduced to metallic silver during development. The amplification effect depends on grain size, but is usually of the order of 10^6. The film can then be either fixed or bleached or both. Fixing will produce an amplitude hologram and bleaching will produce a phase hologram, where the refractive index (or thickness) rather than the absorption properties of the material vary in accordance with the original exposure.

Fixing involves the removal of all undeveloped silver halide. This means that the unexposed areas now consist of almost nothing but pure gelatin. This renders the film insensitive to further exposure but unfortunately not only causes a reduction in refractive index but also a shrinkage of the film by about 15%. In transmission holograms this will distort the image by altering the slant angle of the recorded fringes, but in reflection holography it is particularly problematic. The fringe spacing itself is altered (because the fringes are actually layers in the plane of the film) and a hologram recorded in red light may give a green image. For this reason fixation free processes are often used. Bleaching is achieved by one of two processes depending on whether thickness or refractive index modulation is preferred. In the 'tanning' bleach process the developed silver grains are removed and the gelatin in the vicinity of the removed grains becomes tanned or hardened due to crosslinking of the gelatin molecules. The modulation in emulsion thickness is achieved when the film is dried and the hardened areas don't shrink to the same degree as the less hardened areas. Resolution is limited (<1200 lines/mm) with this process because modulation depth decreases at high spatial frequencies.

For high resolution phase holograms the alternative bleaching process is preferred. In this process the developed silver in the absorption hologram is replaced by a transparent silver salt with a higher refractive index than the gelatin. The diffraction efficiency of the hologram is therefore increased but so is the amount of scatter. Noise levels are therefore higher with this bleaching process.

Silver halide photographic emulsions always suffer some degree of scatter due to the inherent graininess of the material. This is reduced with smaller grain size but there is a corresponding reduction in sensitivity.

In general, at the grain sizes required for holography (typically 0.05-0.1μm) the required exposure is of the order of 10s of microJoules per square centimeter. Film thickness is typically 5-15μm. Because of their high sensitivity silver halide photographic emulsions are the most widely used material for holography, the main disadvantage being the need for wet development and processing.

1.1.2 Dichromated Gelatin:

The main competitor to photographic emulsion is dichromated gelatin (DCG). It surpasses photographic emulsion in both diffraction efficiency and optical quality (it is essentially a grainless material). However as it has a useful life of only a few hours, it must be prepared in the laboratory before use and is not available commercially. Processing and development are complicated and time consuming, and results are often difficult to reproduce.

DCG consists of a gelatin layer impregnated with Ammonium Dichromate. Depending on development techniques, the hologram can be recorded as a thickness variation (surface relief hologram) or refractive index modulation (volume hologram). In both

cases the information is recorded as a pure phase hologram. In holography DCG is usually developed to produce refractive index modulation and form a thick phase grating. After exposure the gelatin layer is sequentially treated with at least two different baths, water and isopropanol. The stresses induced by the swelling with water followed by rapid drying in isopropanol are thought to cause submicroscopic cracks and voids to appear in the regions which are softer due to lack of exposure, but the exact mechanism is still unclear. By some means a phase shift is produced between the exposed and unexposed areas and since the voids are much smaller than the wavelength of light the optical quality is excellent and the noise is low.

Absorption of light of the appropriate wavelength causes the chromium ion to be reduced to a lower ionization state forming Cr_2O_3. The trivalent chromium ion crosslinks the gelatin altering its hardness and solubility[14]. The photochemical processes are quite localized; only a few dichromate ions and the surrounding gelatin molecules are involved so the theoretical limit of the resolution is very high. The modulation transfer function is essentially uniform to a resolution of 5000 lines/mm.

Since the gelatin is water absorbing it will swell in humid environments. The gelatin can however, be hardened by chemical or photochemical treatment to alleviate this problem; some prehardening is required anyway for volume holograms. For long-term storage of recorded holograms the gelatin must always be sealed off from the environment to avoid re-absorption of moisture from the atmosphere.

Although exposure levels are higher than those for photographic emulsion, its low noise, high diffraction efficiency (>95%) and high resolution (>6000 lines/mm) make

DCG a popular choice for many commercial applications[15]. The exposure required is of the order of tens of milliJoules per square centimeter at 488nm and hundreds of milliJoules per square centimeter at 514nm[16] The sensitivity can be extended to the red end of the spectrum using suitable dyes[17].

1.1.3 Photoresists.

Photoresists are an extremely important class of photocrosslinking recording media. The intensity pattern is recorded as a surface relief hologram i.e. the phase change between high and low intensity areas is produced by thickness variation as opposed to refractive index variation, creating a thin phase hologram. Their main application is in master holograms for mass production by hot foil stamping, because of the ease of replication offered by thin phase holograms. Unfortunately sensitivity is low but the lack of granularity of the material means that spatial frequency response is very high (>5000 lines/mm) and scatter is low.

There are two types of photoresist; positive and negative, differing only in mechanism of image formation. In negative photoresist, only the areas of high incident intensity crosslink and become insoluble so that suitable processing washes away the unexposed areas leaving a surface relief modulation which corresponds to the original fringe pattern. With positive photoresist the opposite occurs, i.e. the incident light causes the scission of crosslinks in the photoresist and the exposed area becomes soluble. Positive photoresists are more often used in holography, because the bulk of the material remains insoluble and only the exposed areas are washed away. With negative photoresists there is a certain minimum exposure required to ensure that the material remains adhered to the substrate during processing, and this may often exceed the

optimum exposure for the hologram[18]. Kodak supply several photoresists which require exposures of only a few mJ/cm^2 in the blue end of the spectrum.

1.1.4 Polymer based crosslinking materials:

In crosslinking photopolymer materials, the phase change in the hologram is caused by modification of the local refractive index when crosslinks between polymer strands are broken or formed (due to the fact that the molecular polarizability of these bonds has been altered). The refractive index change is small, so it is usually necessary to work with thick layers. The majority of materials in this group are based on metal ion doped polymers in which thick volume gratings are recorded. The properties vary considerably with formulation. Photoresists could also come under this heading since recording involves the making and breaking of crosslinking bonds, but they have been dealt with separately because the type of hologram formed is quite different.

Dichromated polyvinyl alcohol (DCPVA) has been studied with a view to improving the real time diffraction efficiency by Lessard and co workers[19]; pH variation has been found to play a significant role in the recording process. Diffraction efficiency has been improved to 60% at high pH and the resolution is good[20] (>3500 lines/mm). An alternative to polyvinyl alcohol, dichromated polyvinyl acetate (DCPAA) has also been used by the same authors[21] to record volume holograms; however the diffraction efficiency and sensitivity were very low (exposure of 4000 mJ/cm^2 for a 28% diffraction efficiency). For DCPAA, however, the increase in sensitivity and diffraction efficiency with increased electron donor concentration is even more dramatic than for DCPVA. The high pH material needed an exposure of only 400mJ/cm^2 for a diffraction

efficiency of 70%. Since no post processing is required, this makes it an attractive holographic recording material.

A crosslinking photopolymer material which has a higher resolution than the ion doped polymers is polyvinylcarbazole (PVCz). Diffraction efficiency, sensitivity and durability are good and the refractive index change is large, the only disadvantage being wet development. A sensitizer (Thioflavine T) and an initiator (Camphorquinone) cause the latent image to be recorded on exposure to light. Development processes are similar to those for DCG in that the film is swollen in a good solvent and then shrunk in a poor solvent. An advantage of the material is its resistance to humid conditions and it has actually been used by the Canon research center to manufacture a holographic optical element in a commercialized 8 mm movie camera[22]. Carbon tetrachloride was the sensitizer and 46% diffraction efficiency was achieved with $50mJcm^{-2}$ at a resolution greater than 3500 lines/mm.

1.1.5 Photopolymerizable recording media.

This thesis is concerned with photopolymerization as a recording process. Photopolymerizable systems have the advantage of self development, ease of preparation and low cost and are therefore particularly suited to applications such as holographic interferometry and fabrication of holographic optical elements.

Like crosslinking photopolymer materials, the sensitivity of photopolymerizable materials is lower than silver halide and dichromated gelatin but varies greatly for the different formulations. The layers usually consist of a polymerizable monomer , an initiator and a

sensitizer. If the layer is a solid composition then there will also be a polymeric binder present in the mixture.

During holographic recording the sensitizing dye molecules in a region of high light intensity absorb photons, allowing them to form excited triplet states which react with the initiator or electron donor to form an initiating radical. This radical initiates local polymerization in the high intensity regions changing the refractive index in proportion to the incident intensity.

Liquid layer systems are usually based on a liquid multifunctional acrylate[23,24] or a mixture of liquid acrylate monomer and acrylamide[25,26,27], with xanthene dyes or methylene blue as the sensitizer. The liquid layer is trapped between two glass plates and has the advantage of recording in real time. High diffraction efficiencies are achieved and the recording of reflection holograms is possible[28]. Methacrylate monomers sensitized with xanthene dyes have also been used [29], and even liquid crystals loaded into Rose Bengal sensitized acrylate photopolymer systems[30] have been studied with diffraction efficiencies approaching 100%. In liquid systems resolution is generally of the order of 3000 lines/mm.

Dry photopolymerizable formulations generally have a higher resolution than liquid formulations. In particular Duponts Omnidex series has resolution greater than 6000 lines/mm and an exposure of the order of tens of mJ/cm^2 required for diffraction efficiencies of 99%[31,32,33]. The materials in this series also work well in reflection mode. The Dupont photopolymer, which is commercially available, is based on an acrylate monomer in a cellulose binder. It can be coated onto a glass substrate to a thickness of 1-200μm. Although the material is self developing, the refractive index modulation can be significantly

enhanced by a uniform post exposure with a fluorescent lamp. The recording mechanism involves a polymerization and diffusion mechanism which leads to a high refractive index modulation. This will be discussed further in chapter 6. The Polaroid Corporation also supply a dry photopolymer based material marketed as DMP-128. It consists of lithium acrylate, acrylic acid and methylene bisacrylamide in a poly-vinyl-pyrolidone matrix. Sensitivity is higher than the Dupont material, with exposures of only 5mJ/cm^2 giving diffraction efficiencies of 80-95%. However some wet processing is required[34].

There are several films based on polymerized polymethyl methacrylate films[35,36]. Refractive index modulation is due to the polymerization of residual monomer in the film[37]. Diffraction efficiency and resolution are high but sensitivity is very low at thousands of milliJoules per square centimeter.

The use of several multicomponent systems has been reported[38,39] in which two monomers of different reactivities, or a monomer and a neutral component, are incorporated. Sensitivity is of the order of hundreds of milliJoules per square centimeter. The advantage of having a high and a low reactivity monomer is that the interdiffusion of the two components during recording leads to a greater refractive index modulation[40].

Dry layers based on acrylamide and triethanolamine in a polyvinyl alcohol binder and sensitized with methylene blue have been investigated by Calixto[41]. Diffraction efficiencies reported were of the order of 10% at exposures of around 100mJ/cm^2. A system sensitized with a photochromic sensitizer (indolino-spiropyran) has been reported[42,43], which has the advantage that the material is only sensitive to the laser wavelength when it is illuminated with UV light. Diffraction efficiencies are higher (80%) at approximately the same

exposure. The primary problem with these acrylamide based layers is the short lifetime of the recorded hologram.

A mixture of acrylates and acrylamide contained in a dry a protective polymer matrix such as methyl cellulose or polyvinyl acetate has been studied. These layers have greatly improved environmental stability and resolution is very high ≈ 5000 lines/mm[44].

There are many different types of photopolymer and much work is needed in the area. In this thesis a dry photopolymer based on Calixto's system is studied. The aim is to optimize the sensitivity and diffraction efficiency and broaden the range of wavelengths to which the material is sensitive. Long shelf life and high resolution are also a priority. Much progress has been made with this material, and it will be shown that the improved formulation has many advantages over other recording media.

1.1.6 Dyed Plastics and photochromic materials:

A small yet interesting class of photopolymer materials are those in which photochromes or dyes are suspended in polymer hosts. Dye doped polyvinyl alcohol [45] and dyed plastics[46] are good examples. Diffraction efficiencies are quite low since the hologram is recorded as an amplitude hologram. The materials are simple to prepare, require no post processing and have sensitivities in the order of milliJoules per centimeter squared, so if high diffraction efficiency is not a requirement, they are useful materials. Xanthene dyed polyvinyl alcohol has also been used as a medium for degenerate four wave mixing [47].

A variety of materials exhibit *reversible* colour changes on exposure to light. Examples of these photochromic materials are spyropyrans[48,49] silver halide doped glasses[50] and

methylene blue dye[51]. The disadvantages are low diffraction efficiency and the transience of the hologram.

1.1.7 Thermoplastics

Thermoplastics are particularly useful in holographic interferometry for non-destructive testing applications as the material is quickly processed in situ. However, the equipment needed is expensive and the format is rather small. Holograms can be recorded either by normal interference of light or using an electron beam to record a computer generated hologram. In either case the processing is the same and a thin surface relief hologram results.

A layer of insulating thermoplastic is deposited on a conducting substrate and placed in a vacuum with the substrate grounded. Before illumination the surface of the thermoplastic is charged uniformly to create a uniform internal electric field within the material. When the thermoplastic is exposed to the intensity variation of the interference pattern pairs of charge carriers of opposite sign are generated in the high intensity regions. These are separated by the internal electric field and each migrates to the oppositely charged surface partially neutralizing the surface charge density. Further charging adds charge where neutralisation has ocurred. The latent image is developed by heating the layer above its softening temperature so that the electrostatic pressure can deform it. Thus the surface relief hologram is created. Most thermoplastics are amorphous organic polymers such as styrene and methacrylate copolymers and polyvinyl carbazole[52]. The response of all thermoplastics is limited to a band of spatial frequencies and the spatial frequency

corresponding to peak response is dependent on the thickness of the layer, but is usually around 800 lines/mm. Sensitivity is of the order of milliJoules per square centimeter.

1.1.8 Ferroelectrics (electro optic crystals)

The main advantage of ferroelectric crystals is their very large storage capacity[53]. This is due to their large dynamic range and high angular selectivity (the crystal can be centimeters thick). Ferroelectrics are extremely versatile with regard to the mode of data storage. They can be fixed to store permanent data for read only memories or used in read/write mode. An added advantage is that even fixed data can be deliberately erased by heat and the crystal re-used without any degradation. The disadvantages are the cost and the restrictive size of the crystals. The most commonly used ferroelectrics are LiNbO3, BGO, BSO and BaTiO3.

During recording free electrons are generated in regions of high intensity; these migrate to the areas of low light intensity and become trapped at crystal defects. This sets up a pattern of net space charge. This electric field pattern alters the local refractive index through the electro-optic effect producing a phase hologram. A uniform beam of light will reverse this process by freeing all the electrons and allowing them to redistribute themselves uniformly throughout the lattice. Unfortunately this also means that readout even at lower power will eventually erase the hologram. However, permanent fixing can be achieved by heating the crystal to a temperature where ionic conductivity can neutralize the space charge pattern. This will cause the diffraction efficiency to disappear, but on cooling the ionic pattern is 'frozen in' and illumination with the recording wavelength will free trapped electrons so

that the space charge pattern, and hence the refractive index modulation returns. The hologram can then be read without erasure.

Since the recording process depends on the movement of charge carriers through the crystal lattice to localized sites called electron traps, the density of unoccupied traps is one of the factors which limits the dynamic range of the material. This can be improved by doping with an impurity such as Fe. Impurity doped crystals normally have trap densities in excess of 10^{18} cm^{-3} . Sensitivity of suitably doped crystals is high requiring 0.1mJ/cm^2 for 1% diffraction efficiency. Resolution is extremely high and in theory limited only by the distance between traps (~ 10nm) [54] Inherent noise due to scatter is very low but ferroelectrics suffer a number of problems associated with any material which has no latency period. For example the refractive index change appears as the hologram is being recorded and so begins to modulate the field even during recording. Beam coupling and the build up of optical scatter are common problems at high diffraction efficiency.

1.2 Holographic Recording

Holography is unique because both the phase and the amplitude of the light wave is recorded. Unlike photography, where only the intensity is recorded, enough information is recorded to reconstruct a three dimensional image of the object. The image posseses the depth and parallax properties normally associated with a real object. The method of holography applies to all waves: electron waves, light waves, acoustic waves and microwaves provided they are coherent enough to produce the required interference pattern. It is the availability of intense coherent sources (lasers) in the visible region of the spectrum which has led to the practical success if *optical* holography.[55]

1.2.1 Basic Principles of Holography

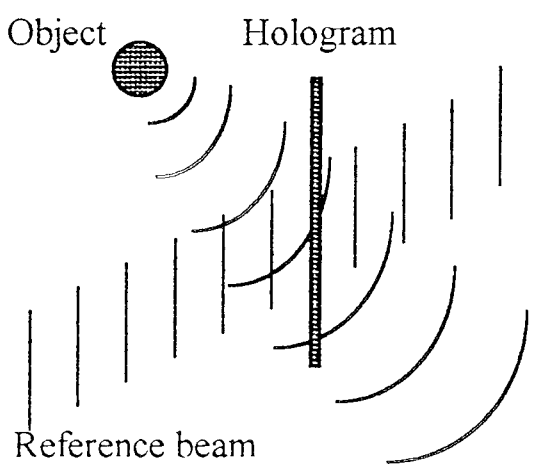

Figure 1.1 Recording a hologram

The recording of a hologram involves illuminating a film, capable of recording a high spatial frequency interference pattern, with two beams of coherent light (Figure 1.1). The reference wave may be a plane wave and the object wave is scattered by the object and carries the relevant information. They interfere in the plane of the recording medium and the resulting interference pattern is recorded by the photosensitive film.

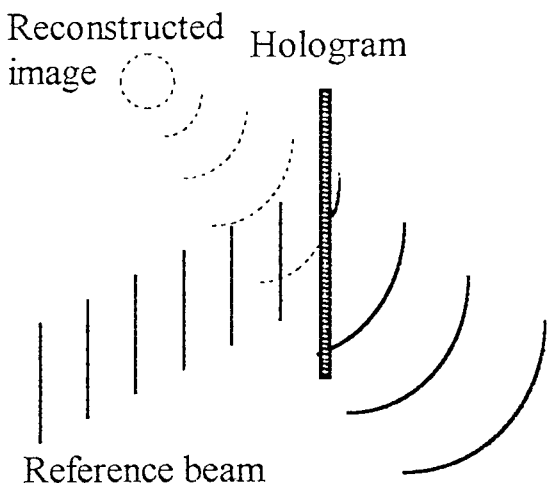

Figure 1.2 Reconstruction of the object wave.

This recorded interference pattern contains all the relevant phase and amplitude information necessary to construct an image of the original object. This is done by illuminating the processed film with the original reference beam (Figure 1.2). The hologram will diffract the reference beam to produce a reconstruction of the original object beam. An observer looking through the hologram will see a three dimensional image of the object. A simple mathematical description of the process now follows.

Let the photographic plate lie in the x,y plane and let the disturbance at the plate due to the wave diffracted by the object be

$$a(x, y)\ \exp[j\ \phi(x, y)]$$

where $a(x,y)$is the amplitude and $\phi(x,y)$ the phase. Let the disturbance at the plate due to the reference beam be

$$b\ \exp[-jk\, y \sin\theta\ ]$$

i.e. the reference wave is plane and travels at an angle θ to the normal to the plate. The intensity distribution at the plate is then

$$a^2 + b^2 + ab\exp[j(\phi(x, y) + ky\sin\theta)] + ab\exp[-j(\phi(x, y) + ky\sin\theta)].$$

If the plate is processed so that the amplitude transmittance is proportional to the original illuminating intensity distribution then at the reconstruction stage (Figure 1.2) when the processed plate is illuminated with the reference beam only, the complex amplitudes of the transmitted waves are

$$b(a^2 + b^2)\exp[-jky\sin\theta].$$

$$+b^2 a(x, y)\exp[j(\phi(x, y)].$$

$$+b^2 a(x, y)\exp[-j(\phi(x, y) + 2ky\sin\theta)].$$

The first of these terms is directly proportional to the reference wave i.e. it is the zero order wave. The second term is directly proportional to the original object wave and includes the phase information. The observer sees a three dimensional image of the original object known as the orthoscopic image. The third term describes a conjugate version of the

original object wave traveling at an angle $\sin^{-1}(2 \sin \theta)$ to the plate normal . Note that if a wave conjugate to the original reference wave is used to illuminate the plate the third term becomes

$$b^2 a(x,y) \exp[-j \phi(x,y)]$$

which is the conjugate version of the original object and produces a real image in front of the plate , known as the pseudoscopic or conjugate image. The conjugate image can be used as the object for a second hologram to produce a final image which is both real and orthoscopic.

In the above treatment we made the assumption that the photographic plate is processed so that the *amplitude transmittance* of the plate is proportional to the original illuminating intensity distribution. This type of hologram is called an amplitude hologram. If the recording material produces a *refractive index* or *thickness* variation proportional to the intensity distribution the hologram is called a phase hologram and the image is reconstructed in the same way. The advantage of phase holograms is that the hologram can be completely transparent and 100% diffraction efficiency is theoretically possible in thick media. Our mathematical description must now be extended to take account of the phase variations in the direction normal to the plane of the hologram in order to take account of layer thickness.

1.2.2 Recording a diffraction grating with two plane waves in a medium of finite thickness.

If both the object beam and the reference beam are plane waves then a simple periodic grating is formed in the recording medium rather than the complex interference pattern that is recorded in a normal hologram. Our mathematical description must now be extended to take account of the phase variations in the direction normal to the plane of the hologram because of the layer thickness.

Let the two incident waves be

$$a \exp[-j\beta p_1]$$

$$b \exp[-j\beta p_2]$$

where $p_1 = x\cos\theta_1 + y\sin\theta_1$ and $p_2 = x\cos\theta_2 + y\sin\theta_2$

where θ_1 and θ_2 are the angles with respect to the normal to the recording medium. β is the propagation constant and is equal to $2\pi/\lambda$.

The intensity distribution at the plate is then

$$a^2 + b^2 + ab \exp[j\beta(p_1 - p_2)] + ab \exp[-j\beta(p_1 - p_2)]$$

and if it is assumed that the permittivity ε_r of the recording material will exhibit a small change proportional to the square of the modulus of the electric field, then

$$\Delta \varepsilon_r = k|E|^2$$

where k is a proportionality constant. The permittivity modulation in the medium will then be

$$\Delta \varepsilon_r = k\left[a^2 + b^2 + ab\exp(j\beta(p_1 - p_2) + ab\exp(-j\beta(p_1 - p_2))\right]$$

which reduces to

$$\Delta \varepsilon_r = k\left[a^2 + b^2 + 2ab\left[\cos\beta(p_1 - p_2)\right]\right]$$

which consists of a constant and a modulation term.

It can be seen from Figure 1.3 that φ_2 is the slant angle and if $\theta_2 = -\theta_1$ then this slant angle is zero,

i.e. an unslanted grating is formed.

$$\varphi_1 = \frac{1}{2}(\theta_1 - \theta_2) \qquad \varphi_2 = \frac{1}{2}(\theta_1 + \theta_2)$$

It should be noted that θ_2 may be larger than 90° in which case wave two is incident from the other side.

The period of the grating may be obtained, using simple geometry, as

$$\Lambda = \frac{\lambda}{2 \sin \varphi_1}$$

where Λ is the fringe spacing.

If the grating is recorded in a thin photosensitive layer reconstruction is very straightforward; if the reconstructing wave is identical to one of the original recording waves, the other recording wave will be reconstructed. However diffracted waves will be produced in some direction whatever the value of λ and φ_1. The recording geometry for a thick medium is identical to that for a thin medium, but because of its finite thickness[56] the intensity modulation recorded in the medium takes the form of parallel layers whose absorption coefficient or permittivity varies sinusoidally along a direction normal to the fringe planes. Spacing is the same as for a thin hologram .

Because of this the condition for producing a diffracted wave from the thick hologram differs from that of the thin grating. Geometric considerations show that rays scattered from successive layers will be in phase only if the following conditions are satisfied

$$\varphi'_1 = \varphi_1$$
$$m\lambda = 2\Lambda \sin \varphi_1$$

Where φ_1 is the angle the recording beam made with the fringe planes, and φ'_1 is the angle the reconstructing beam makes with the fringe planes and m is an integer. These are the well known Bragg conditions. They are more stringent than the condition for the thin hologram.

Three conclusions may be drawn: (1) reconstruction with the same wavelength and angle of incidence will reproduce the object wave. In this way the thick hologram behaves like a thin hologram. (2) If the wavelength is varied but the angle of incidence kept the same no diffracted wave will be produced. (3) If both wavelength and angle of incidence are varied so that the second condition for the thick grating is still satisfied a new diffracted wave will be produced. For these reasons the characteristics of the thick hologram are very different to those of the thin hologram. The thick hologram has spectral or angular filtering characteristics not present in the thin hologram. There is of course no sharp division between thick and thin holograms. As the thickness is reduced there comes a point where the Bragg condition begins to break down and the less restrictive condition for the thin hologram takes over.

This distinction is usually made using the Q parameter defined as

$$Q = \frac{2\pi\lambda d}{n\Lambda^2}$$

Where λ is the wavelength of the light at reconstruction, d is the grating thickness, n is the average refractive index of the material and Λ is the fringe spacing. Holograms are usually considered thick if $Q > 10$ however the thick hologram theory which is discussed below is quite accurate even for Q values of 1.

1.3 The Coupled Wave Theory

When dealing with thick holograms it must be taken into consideration that the diffraction efficiency may be very high and so the illuminating wave may be strongly depleted as it passes through the material. At some point within the material there will be two mutually coherent waves of comparable magnitude traveling together. This is the basis of coupled wave theory which has been applied to the problem of thick holograms by Kogelnik[57]. His analysis gives the angular and wavelength selectivities for all the possible hologram types, transmission or reflection, amplitude or phase, with and without loss and with slanted or unslanted fringe planes. The equations also give the maximum achievable diffraction efficiency for unslanted gratings illuminated at the Bragg angle.

Although the theory is based on the assumption that the hologram is relatively thick and therefore the Bragg effects are very strong, the results are quite accurate even for Q values as low as 1.

There follows an outline of the underlying ideas and principal results of Kogelniks coupled wave theory

A one-dimensional grating is assumed extending from x = 0 to x = d, in which both the relative permittivity (ε_r) and the conductivity (σ) vary in a harmonic manner:

$$\varepsilon_r = \varepsilon_{r0} + \varepsilon_{r1} \cos \hat{K}.\hat{r} \qquad (1.1)$$

$$\sigma = \sigma_0 + \sigma_1 \cos \hat{K}.\hat{r} \qquad (1.2)$$

The grating vector $\hat{K}$ is perpendicular to the planes of constant permittivity and conductivity, the fringe planes, (as in Figure 1.3) and has magnitude $2\pi/\Lambda$. Absorption

losses are assumed to be small and the absorption and refractive index modulations are assumed to be small compared to the average values for the material i.e. $\varepsilon_{r0} >> \varepsilon_{r1}$ and $\sigma_0 >> \sigma_1$.

The electric field vector points in the direction perpendicular to the x,y plane (i.e. perpendicular to the plane of incidence) so the vectorial problem is reduced to a scalar one and a solution to the wave equation, with electric field as a scalar quantity, is sought.

$$\nabla^2 E - \gamma^2 E = 0 \qquad (1.3)$$

where E is the electric field and γ is the spatially varying propagation constant in the grating, γ is expressed in terms of complex permittivity as

$$\gamma = j\omega(\mu\varepsilon)^{\frac{1}{2}}[1 - j\frac{\sigma}{\omega\varepsilon}]^{\frac{1}{2}}$$

The wave equation comes from a treatment of Maxwell's equations in a material of conductivity σ, permeability μ and permittivity ε, for a frequency ω[58]. Since we can assume that conductivity is small,

$$\gamma \approx j\omega(\mu\varepsilon)^{\frac{1}{2}}[1 - j\frac{\sigma}{2\omega\varepsilon}]$$

Substituting in equations 1.1 and 1.2 , this gives

$$\gamma^2 = -\omega^2 \mu \varepsilon_0 \varepsilon_{r0}(1 + \frac{\varepsilon_{r1}}{\varepsilon_{r0}}\cos\hat{K}.\hat{r})[1 - j\frac{\sigma_0}{\omega\varepsilon}(1 + \frac{\sigma_1}{\sigma_0}\cos\hat{K}.\hat{r})]$$

This can be expressed as

$$\gamma^2 = -\beta^2 + 2j\alpha\beta - 4\kappa\beta \cos\hat{K}.\hat{r} \qquad 1.4$$

with

$$\beta = \omega(\mu \varepsilon_0 \varepsilon_{r0})^{\frac{1}{2}},$$

$$\alpha = \frac{\sigma}{2}\left(\frac{\mu}{\varepsilon_0 \varepsilon_{r0}}\right)^{\frac{1}{2}}$$

$$\kappa = \frac{\varepsilon_{r1}\beta}{4\varepsilon_{r0}} + j\frac{\sigma_1}{4}\left(\frac{\mu}{\varepsilon_0 \varepsilon_{r0}}\right)^{\frac{1}{2}}$$

β is the average propagation constant, α is the average absorption constant and κ is the coupling constant. The coupling constant describes the interaction between the reference wave R and the signal wave S. If there is no modulation of permittivity or conductivity (therefore no modulation of refractive index or absorption) then κ=0 and there is no diffraction.

The solution to the wave equation is assumed as the sum of two waves of the form

$$E = R(x)\exp[-j\hat{\rho}.\hat{r}] + S(x)\exp[-j\hat{\sigma}.\hat{r}] \qquad (1.5)$$

Where $\hat{\rho}$ is chosen to represent the wave vector of the input wave R , taken inside the medium, so that we do not need to consider the boundary conditions for the wave vectors. Similarly $\hat{\sigma}$ represents the wave vector of the signal wave S. When the Bragg condition is satisfied the wave vectors are related by the vector triangle

$$\hat{\sigma} = \hat{\rho} - \hat{K} \qquad (1.6)$$

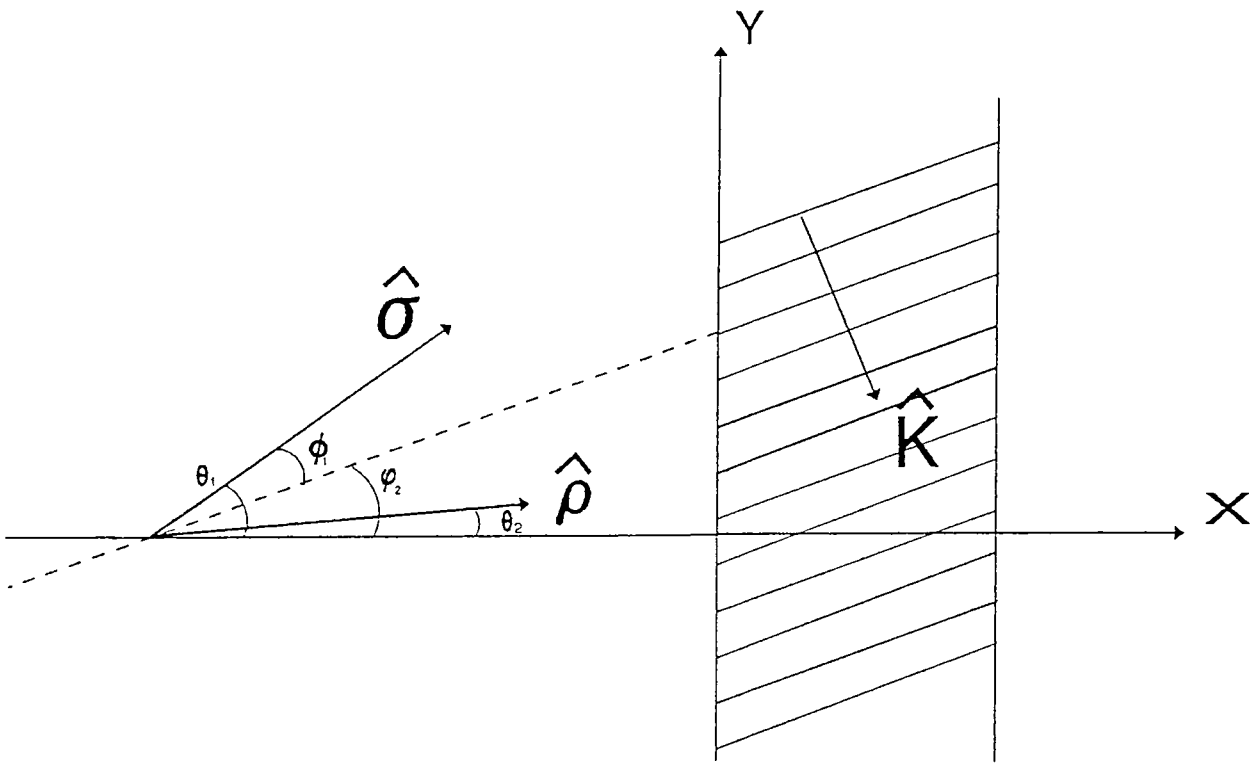

Figure 1.3 Illumination of a slanted volume grating with a reference wave $\hat{\rho}$ *to produce the reconstructed wave* $\hat{\sigma}$ *The slant angle is* φ_2. *The grating vector* $\hat{K}$ *has the absolute value* $2\pi/\Lambda$, *where* Λ *is the fringe spacing..*

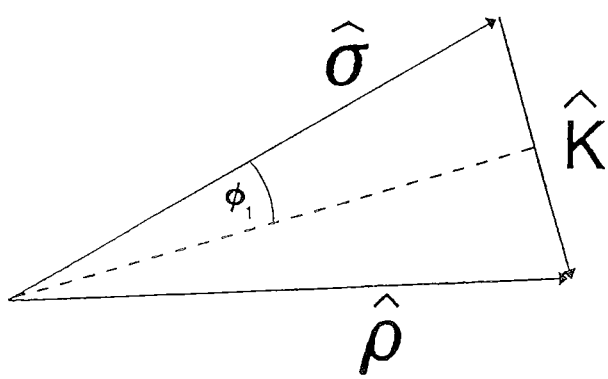

Figure 1.4 The vector diagram illustrating the relationship between the illuminating wave, the grating vector and the reconstructed wave when the Bragg condition is satisfied.

Where $\hat{K}$ is the grating vector. At Bragg incidence the magnitude of the two wave vectors is equal to β, that is to the value appropriate to an unperturbed medium of permittivity ε_{r0} at a frequency ω. If it is specified that no change in the average permittivity of the medium has occurred during the recording and processing of the hologram and that the frequency of the light is the same in recording and reconstruction then the two waves propagating in the recorded hologram are assumed to be the same as the recording waves. The Bragg condition may still be satisfied if these conditions are not met but it is preferable at this stage to proceed with the analysis without reference to the recording conditions. For the moment small deviations from the Bragg angle shall be permitted while the requirement of equation 1.6 is retained. The magnitude of σ will not consequently be equal to β unless the Bragg condition is satisfied.

Substituting equation 1.5 into 1.3 (with equation 1.4 inserted) and performing the operations, we get

$$\exp[-j\hat{\rho}.\hat{r}]\{\frac{d^2R}{dx^2} - 2j\,\rho_x\frac{dR}{dx} - 2j\alpha\beta R + 2\kappa\beta S\}$$

$$+ \exp[-j\hat{\sigma}.\hat{r}]\{\frac{d^2S}{dx^2} - 2j\,\sigma_x\frac{dS}{dx} + (\rho^2 - \sigma^2 - 2j\alpha\beta)S + 2\kappa\beta R\}$$

$$+2\kappa\beta\left\{S\exp[-j(2\hat{\sigma} - \hat{\rho}).\hat{r}] + R\exp[-j(2\hat{\rho} - \hat{\sigma}).\hat{r}]\right\} = 0$$

Where ρ_x and σ_x are the components of the ρ and σ vectors taken in the x direction. Two approximations are now made. The first is to disregard the waves propagating in the $\hat{\sigma} - \hat{K}$ and $\hat{\rho} + \hat{K}$ directions, and so equate the coefficients of $\exp(-j\hat{\rho}.\hat{r})$ and $\exp(-j\hat{\sigma}.\hat{r})$ to zero. These waves are called higher order modes and in most cases involving thick

recording media they can be neglected. This results in two differential equations relating R and S. The second is to neglect the second derivative terms, because R and S are slowly varying functions, that is the interchange of power between the waves is small over a distance comparable to the wavelength of light. This leaves us with the following equations.

$$\left(\frac{\rho_x}{\beta}\right)\frac{dR}{dx} + \alpha R + j\kappa S = 0$$

$$\left(\frac{\sigma_x}{\beta}\right)\frac{dS}{dx} + \left[\alpha + j\left(\frac{\beta^2 - \sigma^2}{2\beta}\right)\right]S + j\kappa R = 0$$

Denoting the coefficients ρ_x/β and $\sigma_x\beta$ as C_R and C_S, it can be seen from Figure 1.3 that

$$C_R = \cos(\phi_1 + \varphi_2) \approx \cos\theta_1$$

$$C_S = \cos(\phi_1 + \varphi_2) + \frac{K}{\beta}\sin\varphi_2 \approx \cos\theta_2$$

where θ_1 and θ_2 are the angles associated with waves S and R when the Bragg condition is satisfied. It is useful to introduce an "off Bragg" or dephasing parameter

$$\vartheta = \frac{\beta^2 - \sigma^2}{2\beta}$$

which, from the vector diagram of Figure 1.4 can be re written as

$$\vartheta = K\sin\phi_1 - \frac{K^2}{2\beta} \qquad (1.7)$$

The magnitude K of the grating vector is retained in the expression because it is a fixed characteristic of the grating and is not affected by the nature of reconstruction.

Equation 1.7 shows that changes of angle of incidence and wavelength from the recording conditions can be mutually compensatory.

The differential equations then take the form

$$C_R \frac{dR}{dt} + \alpha R + i\kappa S = 0 \qquad (1.8)$$

$$C_S \frac{dS}{dt} + (\alpha + i\vartheta)S + i\kappa R = 0 \qquad (1.9)$$

The coupled wave equations show that the amplitude of a wave changes along x because of coupling to the other wave (κR, κS) or absorption (αR, αS).

1.3.1 Power conservation

The balance of power between the two waves can be obtained as follows. Equation 1.8 is multiplied by R^* and the complex conjugate of the whole equation is taken. Similarly equation 1.9 is multiplied by S^* and the complex conjugate taken yielding two further equations. All four equations are added together giving

$$\frac{d}{dx}(C_R RR^* + C_S SS^*) + 2\alpha(RR^* + SS^*) + j(\kappa - \kappa^*)(RS^* + SR^*) = 0$$

This equation may now be interpreted as representing the balance of power between the two waves. The power in the transmitted and diffracted waves moves approximately in the $\hat{\rho}$ and $\hat{\sigma}$ directions so the total power moving in the x direction is

$$P = C_R RR^* + C_S SS^*$$

Thus it can be seen that the total power is independent of x in the absence of losses. i.e. when $\alpha = 0$, $\kappa = \kappa^*$. Diffraction efficiency, the efficiency of the grating in converting incident light into the diffracted wave, can now be defined as,

$$\eta = \frac{|C_S|}{|C_R|} SS^* \qquad (1.10)$$

for a reference wave of unit amplitude. This represents the fraction of the incident power diffracted into the signal wave.

1.3.2 Solution of the coupled wave equations.

Solution of the differential equations is sought in the form

$$R(x) = r_1 \exp \gamma_1 x + r_2 \exp \gamma_2 x$$

$$S(x) = s_1 \exp \gamma_1 x + s_2 \exp \gamma_2 x$$

Substituting these equations into the differential equations 1.8 and 1.9 the following equations are obtained

$$\left(C_R \gamma_i + \alpha\right) r_i = -j\kappa s_i$$

$$\left(C_S \gamma_i + \alpha + j\vartheta\right) s_i = -j\kappa r_i$$

where i = 1,2

This leads to a quadratic equation in γ. The solution yields

$$\gamma_{1,2} = -\frac{1}{2}\left(\frac{\alpha}{C_R} + \frac{\alpha}{C_S} + j\frac{\vartheta}{C_S} + \right) \pm \frac{1}{2}\left[\left(\frac{\alpha}{C_R} - \frac{\alpha}{C_S} - j\frac{\vartheta}{C_S}\right)^2 - 4\frac{\kappa^2}{C_R C_S}\right]^{1/2}$$

The boundary conditions are of course different for reflection and transmission gratings. For a transmission grating the boundary conditions for the amplitude of the waves are $R(0) = 1$, $S(0) = 0$. For a reflection grating $R(0) = 1$, $S(d) = 0$.

Concentrating now on transmission gratings, with the appropriate substitutions the following is obtained,

$$R(x) = \frac{1}{C_R(\gamma_1 - \gamma_2)}\left[-(C_R\gamma_2 + \alpha)\exp\gamma_1 x + (C_R\gamma_1 + \alpha)\exp\gamma_2 x\right]$$

$$S(x) = -\frac{j\kappa}{C_S(\gamma_1 - \gamma_2)}\left[\exp(\gamma_1 x) - \exp(\gamma_2 x)\right]$$

In order to obtain values of R and S at the output of the hologram i.e. at x = d, we introduce the notation

$$\nu = \frac{\kappa d}{(C_R C_S)^{\frac{1}{2}}}$$

$$\xi = j\frac{d}{2}\left(\frac{\alpha}{C_R} - \frac{\alpha}{C_S} - j\frac{\vartheta}{C_S}\right)$$

$$\Phi = (\nu^2 + \xi^2)^{1/2}$$

We obtain, for transmission gratings,

$$R(d) = \exp\left(-j\xi - \frac{\alpha d}{C_R}\right)\left[\cos\Phi + j\left(\frac{\xi}{\Phi}\right)\sin\Phi\right]$$

and

$$S(d) = -j\left(\frac{C_R}{C_S}\right)^{1/2}\exp\left(-j\xi - \frac{\alpha d}{C_R}\right)\frac{\sin\Phi}{\Phi/\nu}$$

These are the general solutions for a transmission grating, slanted or unslanted, with or without loss, for absorption, phase or mixed grating as derived by Kogelnik.

Using the definition of diffraction efficiency given in equation 1.10, and letting $\alpha = 0$, the expression for diffraction efficiency for the special case of a lossless phase transmission grating can be found. The following equation is obtained.

$$\eta = \frac{\sin^2(\nu^2 + \xi^2)^{\frac{1}{2}}}{(1 + \frac{\xi^2}{\nu^2})} \qquad (1.11)$$

Using this equation, the effect of angular and wavelength deviation from the Bragg condition can be readily studied. They influence the diffraction efficiency of the grating through the parameter ξ. The parameter ν is representative of the amplitude of the refractive index modulation and the thickness of the grating and determines the maximum diffraction efficiency. Figure 1.5 shows the effect of deviation from the Bragg condition. The diffraction efficiency η is plotted against the 'off Bragg' parameter ξ letting $\nu = \pi/2$ for a diffraction efficiency of 100% at the Bragg angle.

In the special case of a lossless unslanted transmission grating, illuminated at the Bragg angle, the parameter $\xi = 0$ and $\kappa = \pi n_1/\lambda$. Equation 1.11 becomes

$$\eta = \sin^2(\frac{\pi n_1 d}{\lambda \cos\theta_0}) \qquad (1.12)$$

giving a relationship between diffraction efficiency and the amplitude of the refractive index modulation, for a known grating thickness. θ_0 is the angle of incidence in the medium when the Bragg condition is satisfied.

Figure 1.6 shows how maximum diffraction efficiency varies with the amplitude of the refractive index modulation for a volume phase grating. Figure 1.5 and Figure 1.6 are examples of the type of results that can be predicted using Kogelnik's coupled wave theory. They show the characteristic angular (or wavelength) selectivity and the sinusoidal variation of diffraction efficiency with increasing modulation in transmission gratings. Figure 1.6 shows that the grating can be over modulated if it has sufficient dynamic range. In other words, as the amplitude of the refractive index modulation increases, there comes a point where all the power has been coupled into the diffracted beam (when $\nu=\pi/2$), and if the modulation is increased further the diffraction efficiency begins to fall again, because the power is coupled back into the reference beam. The effect of deviation from the Bragg angle for overmodulated gratings can be seen in Figures 1.7 - 1.10. Equation 1.11 is used to plot diffraction efficiency versus ξ for $\nu=3\pi/4$, $\nu=\pi$, $\nu=5\pi/4$ and $\nu=3\pi/2$. Comparing Figure 1.7 with Figure 1.5, it is observed that coupled wave theory predicts that when the refractive index modulation is increased past the value required to give exactly 100% diffraction efficiency ($\nu=\pi/2$), the diffraction efficiency at the Bragg angle decreases while the sidelobes on either side of the main peak begin to increase. By the time the refractive index modulation has reached twice the value it had in Figure 1.5 the diffraction efficiency at the Bragg angle has been reduced to zero and the side lobes have increased to more than 45%. This is shown in Figure 1.8. Increasing the refractive index modulation still further causes the diffraction efficiency at the Bragg angle to increase again, and the side lobes also increase (Figure 1.9). The diffraction efficiency at the Bragg angle eventually reaches 100% again as shown in Figure 1.10.

Kogelnik's coupled wave theory can also predict behavior for pure absorption gratings, lossy phase gratings and slanted or unslanted reflection gratings with or without loss by simple manipulation of the above formulae. In chapter 6 the special case of an unslanted phase grating without loss will be dealt with further, and compared to experimental results obtained in photopolymer materials.

1.3.3 Application to the analysis of photopolymers

As discussed earlier, the main assumptions of Kogelnik's coupled wave theory are that the modulation is sinusoidal and that only the zero and first order diffracted waves propagate within the grating. For this reason it is only suitable for analysis of thick gratings where, even if higher orders are present the Bragg condition does not allow them to propagate. Coupled wave theory is particularly suited to the analysis of the photopolymer materials for three reasons. (1) The refractive index modulation in the material is very small (<0.1%), in accordance with the initial assumptions of coupled wave theory. (2) This necessitates the use of very thick layers, typical Q values are greater than 100. Coupled wave theory is particularly accurate at Q values greater than 10.

(3) The diffraction efficiency of gratings recorded in these layers is very high so the assumption, made by coupled wave theory that the illuminating wave will be strongly depleted as it passes through the material, is justified.

It is also helpful that after exposure these photopolymer layers are almost completely bleached, so the grating can be assumed to be essentially lossless. This simplifies analysis as equation 1.11 can be used. One disadvantage of coupled wave theory might

be that the grating is considered in isolation and boundary conditions at the front and back surface must be introduced separately. Dispersion equation theory, which is the basis from which modal theory[59] is developed, considers the grating in conjunction with the surrounding medium, but is restricted in its application to the interaction of plane waves. The boundary conditions at the surfaces of the grating can be introduced very simply using Snell's law. The predictions of coupled wave theory will be compared to actual results obtained with photopolymers in chapter 6.

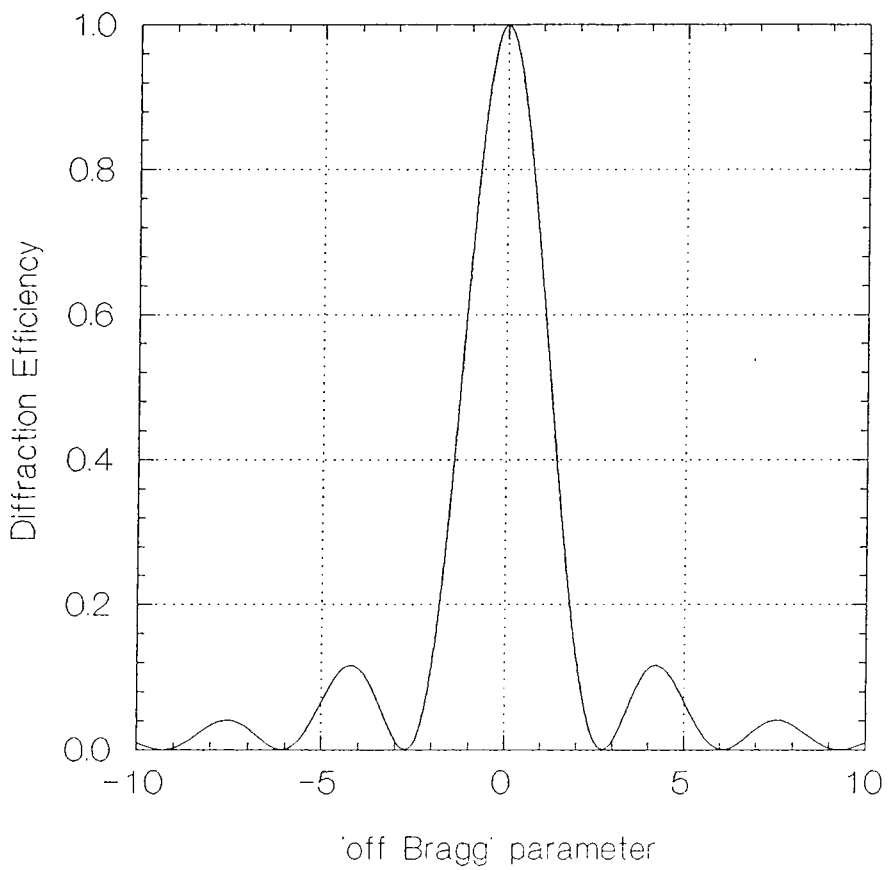

Figure 1.5 The effect of deviation from the Bragg condition on diffraction efficiency, when the diffraction efficiency at the Bragg angle is 100%. (i.e. $\nu = \pi/2$)

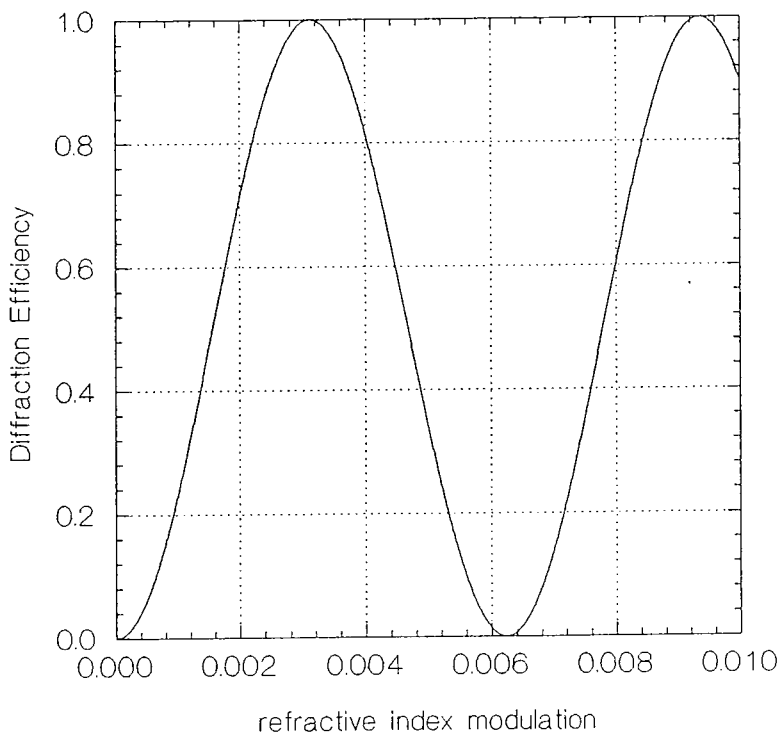

Figure 1.6 Maximum diffraction efficiency versus amplitude of the refractive index modulation (n_1) for a volume phase grating. Diffraction efficiency is calculated for a Bragg angle, θ_0, of 10°, at a wavelength, λ, of 633nm. Grating thickness is 100μm.

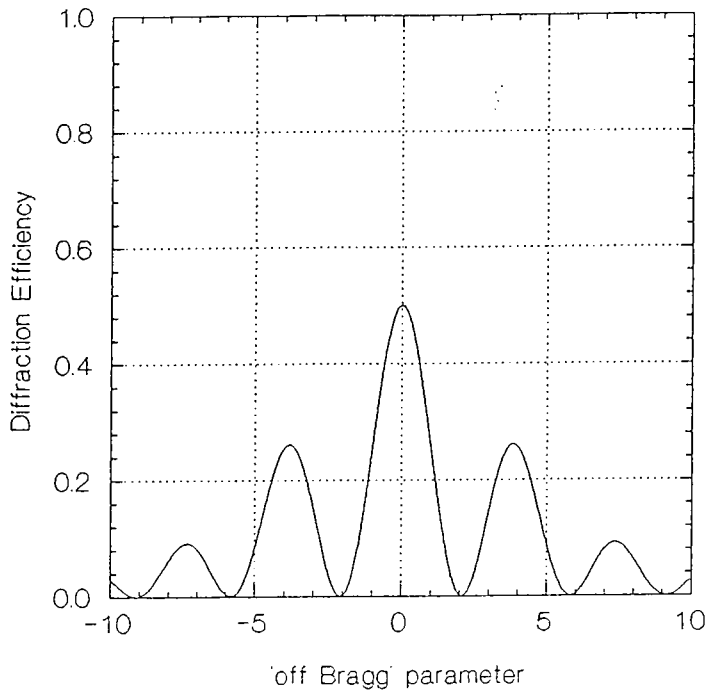

Figure 1.7 The effect of deviation from the Bragg angle for an overmodulated grating. Diffraction efficiency versus ξ for $\nu=3\pi/4$.

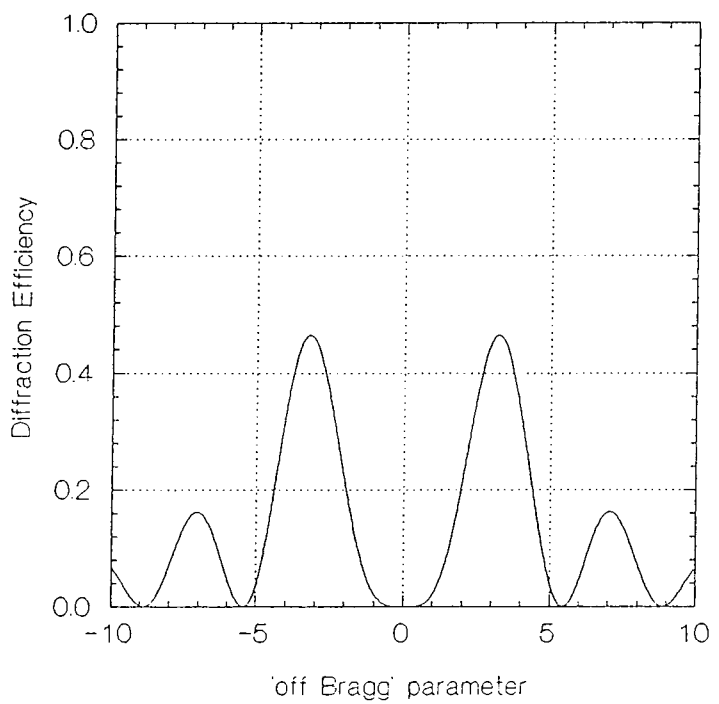

Figure 1.8 The effect of deviation from the Bragg angle for an overmodulated grating. Diffraction efficiency versus ξ for $\nu=\pi$

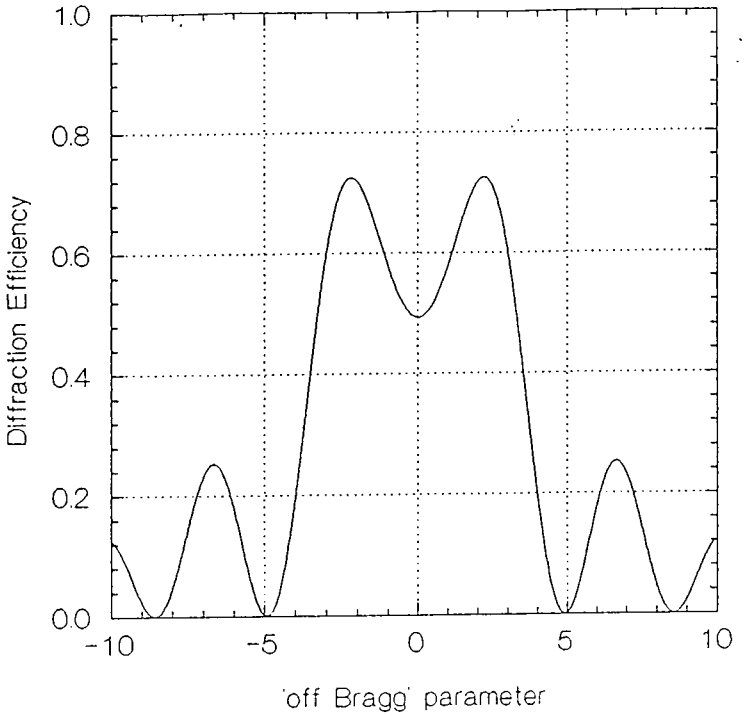

Figure 1.9 The effect of deviation from the Bragg angle for an overmodulated grating. Diffraction efficiency versus ξ for $\nu=5\pi/4$

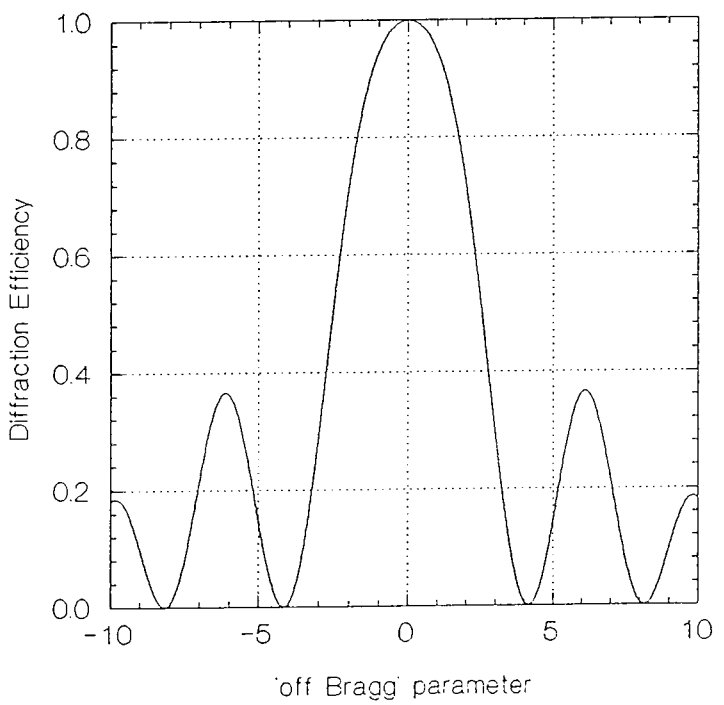

Figure 1.10 The effect of deviation from the Bragg angle for an overmodulated grating. Diffraction efficiency versus ξ for $\nu=3\pi/2$.

[1] D. Gabor, "A new microscopic principle", *Nature*, 161, 777-778, 1948.

[2] E. N. Lieth, J. Upatnieks, "Wavefront reconstruction with diffused illumination and three dinmentional objects" *J. Opt. Soc. Am.*, **54**, 1295-1301, 1964.

[3] E. N. Lieth, J. Upatnieks, "Holographic imagery through diffusing media" *J. Opt. Soc. Am.*, **56**, 523, 1966.

[4] R. K. Erf "Holographic Non-destructive Testing", *Academic Press*, New York, 1974.

[5] R. Jones and C. Wykes "Holographic and speckle interferometry", 2nd edn. *Cambridge University Press*, 1989.

[6] B. D. Guenther, C. R. Christensen, and J. Upatneiks "Coherent optical processing: another approach", IEEE *J. Quant Elect.*, **15**, 1348-1362, 1979..

[7] S. H. Lee, ed. "Optical Information Processing", Springer-Verlag, Berlin, 1981.

[8] A. Kozma "Holographic storage", *Proc. SPIE*, **53**, 77-83, 1974.

[9] J. E. Ludman "Holographic solar concentrator", *App. Opt.*, **21**, 3057-3058, 1982.

[10] J. Parker "ESPRIT II OLIVES - A European Collaborative Programme in Optical Interconnections", *International Topical meeting on Optical computing*, Kobe, 8-12 April, 1990.

[11] A. L. Mikaelian, V. K. Salakhutdinov, "Research on recording holograms in organic media for interconnects", Proc IEE, 379, fourth international conference on holographic systems components and applications, 163-167, 1993.

[12] P. Hariharan, "Optical holography- Principles techniques and applications", chapter 7, *Cambridge monographs on physics*, Cambridge University Press, 1984.

[13] R. R. A. Syms. "Practical Volume Holography", Chapter 5, Oxford engineering series 24, Clarendon Press, Oxford, 1990.

[14] D. Meyerhofer "Dichromated gelatin" in Holographic recording materials, *Topics in Applied Physics*, **20**, ed. H.M.Smith, Springer Verlag, 209-227, Berlin, 1977.

[15] B. J. Chang and C.D leonard "Dichromated gelatin for the fabrication of holographic optical elements", *Appl. Opt.*, **18**, 2407, 1979

H. Owen "Holographic optical components for laser spectroscopy applications", *proc. SPIE*, **1732**, 324-332, 1992

[16] R. R. A. Syms, "Practical Volume Holography", Chapter 5, Oxford engineering series 24, Clarendon Press, Oxford, 1990.

[17] J. Blyth "Methylene blue sensitized dichromated gelatin holograms: a new electron donor for their improved photosensitivity", *App. Opt.*, **30**, No. 13, 1598-1602, 1991.

[18] R.A.Bartolini "Photoresists" in Holographic recording materials, *Topics in Applied Physics*, **20**, ed. H.M.Smith, Springer Verlag, 209-227, Berlin, 1977.

[19] G. Manivannan, R. Changkakoti, R. Lessard, G. Mailhot, M. Bolte, "Primary photoprocesses of Cr(VI) in real time holographic recording material: Dichromated Polyvinyl Alcohol", *Am. Chem. Soc*, **97**, 7228-7233, 1993.

[20] P. Leclère "Etude et caractérisation de films d'alcool polyvinlyique photosensibilisés en vue de leur utilisation en holographie et en cojugation de phase optique" doctoral thesis, University of Liege, Belgium, 1994.

[21] G..Manivannan, R. Changkakoti and R.A. Lessard, "Metal ion doped polymers as media for optical memories", *Polymers for Advanced Technologies*, **4**, 569-576, 1993.

[22] K. Matsumoto, T. Kuwayama, M. Matsumoto, N. Taniguchi, SPIE Proc 600, 9, 1985

[23] C. Carre and D. J. Lougnot "Photopolymerizable material for holographic recording in the 450-550 nm domain", *J. Optics* (Paris), **21**, 3, 147-152, 1990.

[24] S. Sugawara, K. Murase and T. Kitayama "Holographic recording by dye sensitized photopolymerization of acrylamide", *Applied Optics*, **14**, 378 - 382, 1975.

[25] A. Fimia, N.Lopez, F. Mateos , R. Sastre, J. Pineda and F.Amat Guerri "Acrylamide photopolymers for use in realtime holography: improving energetic sensitivity." *proc SPIE* **1732**, *Holographics international*, 105-109, 1992.

[26] C. Carre and D. J. Lougnot, "A photochemical study of the methylene blue / acrylamide system in view of its use for holographic recording under red illumination" *Journal de chimie physique*, **85**, 485-490, 1988.

[27] S. Sugawara, K. Murase and T. Kitayama "Holographic recording by dye sensitized photopolymerization of acrylamide ", *App. Opt.*, **14**, 378 - 382, 1975.

[28] Y. Defosse, C. Carre and D.J.Lougnot "Use of a self developing polymer material for volume reflection hologram recording", *Pure Appl. Opt*,. **2**, 437-440, 1993.

[29] A. Fimia, N. Lopez, F. Mateos, R. Sastre, J. Pineda and F.Amat Guerri "A new photopolymer useful as a holographic recording material" *Appl. Opt*, **32**, 3706-3707, 1993.

[30] R. L. Sutherland, L.V.Natarajan, and V.P. Tondiglia, "Bragg gratings in acrylate polymer consisting of periodic polymer-dispersed liquid-crystal planes", *Chem Mater.*, **5**, 1533-1538, 1993.

[31] B. L. Booth "Photopolymer material for holography", *App. Opt.*, **14**, 593 -601, 1975.

[32] W. K Smothers., T. J. Trout A. M. Weber and D. J. Mickish "Hologram recording in DuPont's new photopolymer materials", IEE Conference Publication no. **311**, *Proceedingsof the Second International Conference on Holographic Systems, Components and Applications*, 1989

[33] A. M Weber, W. K. Smothers, T. J. Trout and D. J. Mickish, "Hologram recording in Dupont's new photopolymer materials" *proc SPIE*, **1212**, 30-39, 1990.

[34] R. T. Ingwall and M. Troll "Mechanism of hologram formation in DMP-128 Photopolymer" *Opt Eng*, **28**, 586-591, 1989.

[35] J. M. Moran, I. P. Kaminow "Properties of holographic gratings photoinduced in polymethyl methacrylate" *Appl. Opt.*, **12**, 1964-1970, 1973.

[36] H. Franke, "Optical refractive index patterns in doped Polymethyl Methacrylate films", *Appl. Opt.*, **23**, 2729-2733, 1984.

[37] M. J. Bowen, E. A. Chandross and I. P.Kaminow "Properties of holographic gratings produced in Polymethyl Methacrylate", *App. Opt*, **13**, 112-117, 1974.

[38] W. J. Tomlinson, E. A. Chandross, H. P. Weber, G. D. Aumiller. "Multicomponent photopolymer systems for volume phase holograms and grating devices", *Appl. Opt.*, **15**, 534-541, 1976.

[39] E. S. Gyulnazarov, V. V. Obukhovskii, T. N. Smirnov, "Theory of holographic recording on a photopolymerized material", *Opt. Spectrosc.(USSR)*, **69**, 109-111, 1991

[40] V. V. Obukhovskii, T. N. Smirnova, "Model of holographic recording on photopolymerizing composites.", Opt. Spectrosc.(USSR), **74**, 462-466, 1993

[41] S. Calixto "Dry polymer for holographic recording", *App. Opt.*, **26**, 3904 -3910, 1987.

[42] M. J. Jeudy, J. J. Robilllard "Spectral photosensitization of a variable index material for recording phase holograms with high efficiency.", *Opt. Commun.*,**13**, 25-28, 1975.

[43] J. J. Robillard, "process and elments for recording phase holograms" French Patent no. **1-471-764**, 1974.

[44] N. Sadlej , B. Smolinska, "Stable photosensitive layers for holography", *Opt Laser Technol.*, **8**, 175-179, 1975.

[45] R. A. Lessard, C. Malouin, R. Changkakoti, G. Manivannnan " Dye-doped polyvinyl alcohol recording materials for holography and nonlinear optics" 1993, *Opt. Eng.*, **32**, 665-670

[46] S. Calixto and R. A. Lessard, "Real time polarizing optical image processing with dyed plastic", *Appl.Opt.*, **24**, 773-778, 1985.

[47] P. Leclère "Etude et caractérisation de films d'alcool polyvinlyique photosensibilisés en vue de leur utilisation en holographie et en cojugation de phase optique" doctoral thesis, University of Liege, Belgium, 1994.

[48] P. H. Vandewyer, J. Hoefnagels and G.Smets, "Photochromic Spiropyrans". *Tetrahedron*, **25**, 3251-3266, 1969.

[49] J. J. Robillard, "process and elments for recording phase holograms" French Patent no. **1-471-764**, 1974.

[50] G. K. Megla "Optical properties and applications of photochromic glass", *Appl. Opt.*, **5**, 945-960, 1966.

[51] R.A.Lessard, R. Changkakoti, D.Roberge and G.Manivannan, "Photopolymers in optical computing: materials and devices", SPIE, **1806**, 2-13, 1993.

[52] P. Hariharan, "Optical holography- Principles techniques and applications", chapter 7, *Cambridge monographs on physics*, Cambridge University Press, 1984

[53] B Ineichen, C. Liegeois, and P. Meyrueis "Thermoplastic film camera for holographic recording of extended objects in industrial applications", *Appl. Opt.*, **21**, 2209-2214, 1982.

[54] H. Sasaki, J. Ma, Y. Fainman, S. h. Lee, "Dynamics of a composite grating in photorefractive crystals for memory application.", *J. Opt. Soc. Am.*, **11**, 2456-2470, 1994.

[55] J.C. Urbach. "Thermoplastic hologram recording" in Holographic recording materials, *Topics in Applied Physics*, **20**, ed. H.M.Smith, Springer Verlag, 209-227, Berlin, 1977.

[56] M. B. Forshaw " Thick holograms: a survey", *Optics and laser technology*, **2**,28-35, 1973.

[57] Kogelnik, H., "Coupled wave thoery for thick hologram gratings", Bell system technical journal, **48**, No 9, 2909-2947, 1969.

[58] Solymar L. and Cooke D. J. "Volume Holography and Volume Gratings", chapter 1, Academic Press, London, 1981

[59] Solymar L. and Cooke D. J. "Volume Holography and Volume Gratings", chapter 3, Academic Press, London, 1981

2. Physical properties of the material; environmental stability, shelf life and optical quality

2.1 Introduction

Regardless of how sensitive a particular material is, or how ideal its holographic recording characteristics are, the practical physical limitations of the material are perhaps the most important factor to be considered. For this reason any new material must be examined not just for its holographic characteristics but also for the practicality of the physical properties of the material for its proposed applications. For example, when choosing an appropriate material for the fabrication of holographic optical elements, a particular material might meet with all the resolution and diffraction efficiency requirements, but if the material is not stable against the environment, it will be of little use for optical component fabrication.

Optical quality is obviously the first priority for any holographic recording material, but other properties such as the shelf life of prepared layers are also important; materials which must be prepared within a few hours of recording (e.g. dichromated gelatin) are more restrictive than those with a long shelf life. The lifetime of the recorded hologram is also of great importance; permanent recording is essential for applications such as holographic optical elements. In this chapter the physical properties of this acrylamide based photopolymer material are investigated with a view to extending the range of practical uses of the material and the lifetime of the recorded hologram.

2.2 Coating methods for high optical quality layers.

The most important requirement of a new holographic recording medium is good optical quality. For this reason a reliable, repeatable method was needed for coating the photosensitive mixture onto glass in layers of uniform thickness and high optical quality. Several well known coating methods were investigated.

2.2.1 Spin Coating

Spin coating involves the rapid evaporation of solvent by high speed spinning to form high quality dry layers ranging from less then one micron in thickness to a maximum of about ten microns with very high viscosity liquids.

With the help of Prof. Werner Blau and Dr. Liam Pender of the Physics Department, TCD, attempts were made to spin coat the photosensitive mixture onto glass substrates. The ideal system for spin coating would have one very high boiling point solvent, one or possibly two solutes, and a concentration of at least 100g/l (in order to produce layers more than one micron thick). The photosensitive mixture was far from ideal for spin coating, having water and ethanol as solvents and four different solutes, and all samples spun (2000rpm and 1000rpm) gave very poor layers with little adhesion to the glass. It was concluded that spin coating was not a suitable method for this system.

2.2.2 Dip Coating

Dip coating involves immersing the substrate (a glass microscope slide in this case) in the coating solution and drawing it out at a constant rate. If there is good adhesion between liquid

and substrate the substrate will be coated with an even layer of the liquid which can then dry by evaporation.

Preliminary investigations produced fairly good quality layers ranging from about one micron to five microns in thickness. This thickness is not sufficient for practical use of this material unless very low diffraction efficiencies can be tolerated. Speeds used were 15 cm/hour achieved using a clock motor and approximately 5 cm/second drawn out by hand. The hand drawn samples gave the best results. The layers were of good optical quality but wedge shaped rather than of uniform thickness. After exposure in the normal way a diffraction efficiency of less than 1% was observed. More viscous solutions of polyvinyl alcohol showed poor adhesion to the substrate and no layer was formed.

2.2.3 Gravity settling

Gravity settling is the simplest method of layer coating and it can produce the thickest layers. A known volume of the photosensitive mixture is placed on a leveled glass substrate and allowed to dry by evaporation.

With care this method can produce very good layers. It was found that the quality of the dry layer was improved by using one solvent (water) rather than two, restricting the airflow by placing an upturned beaker above the drying samples, and by choosing the appropriate concentration of solute. The effect of solute concentration will be discussed in the next section, as it is equally important for layers deposited using bar coaters.

2.2.4 Bar Coaters

A set of six bar coaters was used (from Braive instruments, Liege, Belgium), graded for wet layer thickness of 50, 100, 200, 300, 400, and 500μm. Each bar coater consists of a uniform cylindrical steel bar around which is wound thin steel wire. The diameter of the wire and the spacing between the winds have been chosen to produce the required wet layer thickness. The final dry layer thickness will then depend on the concentration of solutes in the solvent. This method is similar to gravity settling except that the wet layer thickness and uniformity can be controlled; through this the dry layer thickness is controlled. For example if a bar coater spreads a solution of 10% polyvinyl alcohol to a wet layer thickness of 300 microns, the dry layer thickness should be about 30 microns (assuming a density of about 1g/ml).

Solutions of 5%, 10% and 20% polyvinyl alcohol were tested with each of the bars. The binder alone was tested so that the best quality possible for this system could be examined. The average thickness was quite repeatable as can be seen from Figure 2.1, Figure 2.2 and Figure 2.3. However at the lower concentrations, the viscosity was so low that flow became a problem. Thicker wet layers tended to flow off the glass plate, and for thin layers there was flow from the liquid just 'dragged' off the plate back onto it. This explains the lack of repeatability at lower polyvinyl alcohol concentrations.

The optical quality of the dry layers was found to depend more on the concentration of the binder solution than on which bar coaters were used. As an example of the poor optical quality of the layers prepared with the higher viscosity polyvinyl alcohol, Figure 2.4 shows the interference fringes obtained with a Michelson interferometer through a layer prepared with 20% polyvinyl alcohol solution. The layer was placed in one arm of the interferometer and a similar plate of uncoated glass was placed in the other arm. Figure 2.5 shows the

Michelson interference fringes through a layer prepared with 5% polyvinyl alcohol solution for comparison. It is obvious from these photographs that the variations in optical path through the 20% layer are substantial, since the fringe pattern is quite distorted, and it is therefore not of sufficient optical quality for holographic recording. Lower concentrations (which have lower viscosities) gave better optical quality but give less consistent thicknesses with the bar coaters. The 20% polyvinyl alcohol solution gave very consistent results with the bar coater but poor optical quality. The 10% solution performed best in both areas, giving good optical quality and also having sufficient viscosity for use with bar coaters.

In order to use the bar coaters the glass substrate must be placed on a rubber mat designed to prevent slippage. Because of this the substrates could not be leveled properly, and although average thicknesses were repeatable the layer thickness often varied across the substrate due to tilt during drying. The rubber mat was therefore removed and the substrates were placed on a 1.2m × 0.5m leveled granite table with a flatness better than 0.1mm/m.

Although it was difficult to prevent slippage, layers were much improved, with thickness change of less than 2% in a 5cm distance across the substrate. This could be improved by using optically flat substrates (float glass is used here).

In conclusion, although bar coaters proved to be useful , and would perhaps be the method of choice if the preparation process were to be automated, gravity settling produces layers with equally high optical quality. Careful control of the volume deposited and the concentration of the coating solution ensures that final dry thickness can be controlled, and the method is simple. Layers with thicknesses ranging from 1μm to 150μm have been prepared with excellent optical quality, and greater thicknesses can easily be prepared with a small sacrifice in quality.

Solute concentration is actually the factor which most affects the optical quality of the dry layer. For this reason stock solutions of polyvinyl alcohol with concentrations greater than 10% are never used and the coating solution is often diluted further before use.

The gravity settling method has been the method of choice throughout this thesis. It was found that 10 mls of coating solution covered a 5" × 4" glass plate fully and without spillage. This produced a dry layer 140μm thick with good optical quality. Where thinner layers were required, the coating solution was simply diluted appropriately. For example, 56μm layers were prepared by making 4ml of coating solution up to 10 ml with distilled water and pouring this onto the 5" × 4" glass substrate. The resulting layers always had excellent optical quality due to the low viscosity of the coating solution. The layers were dried in an atmosphere where relative humidity was approximately 50% - 60% and usually dried overnight.

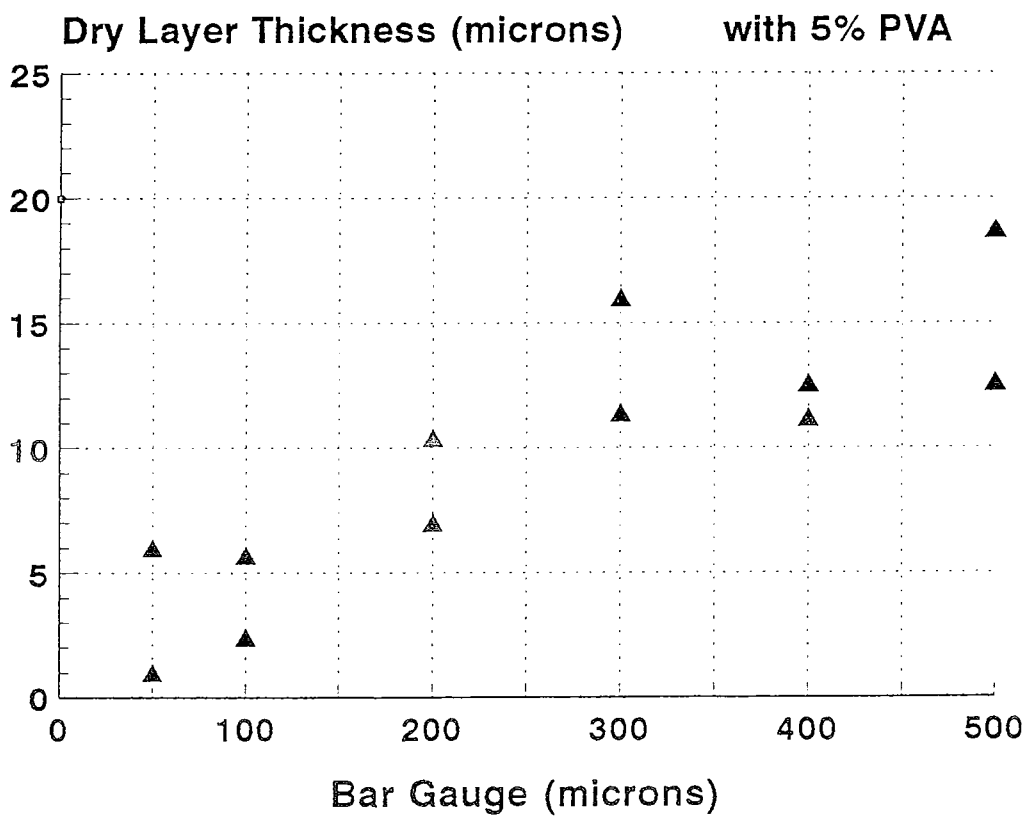

Figure 2.1 Average thickness as a function of bar coater gauge for a 5% polyvinyl alcohol solution.

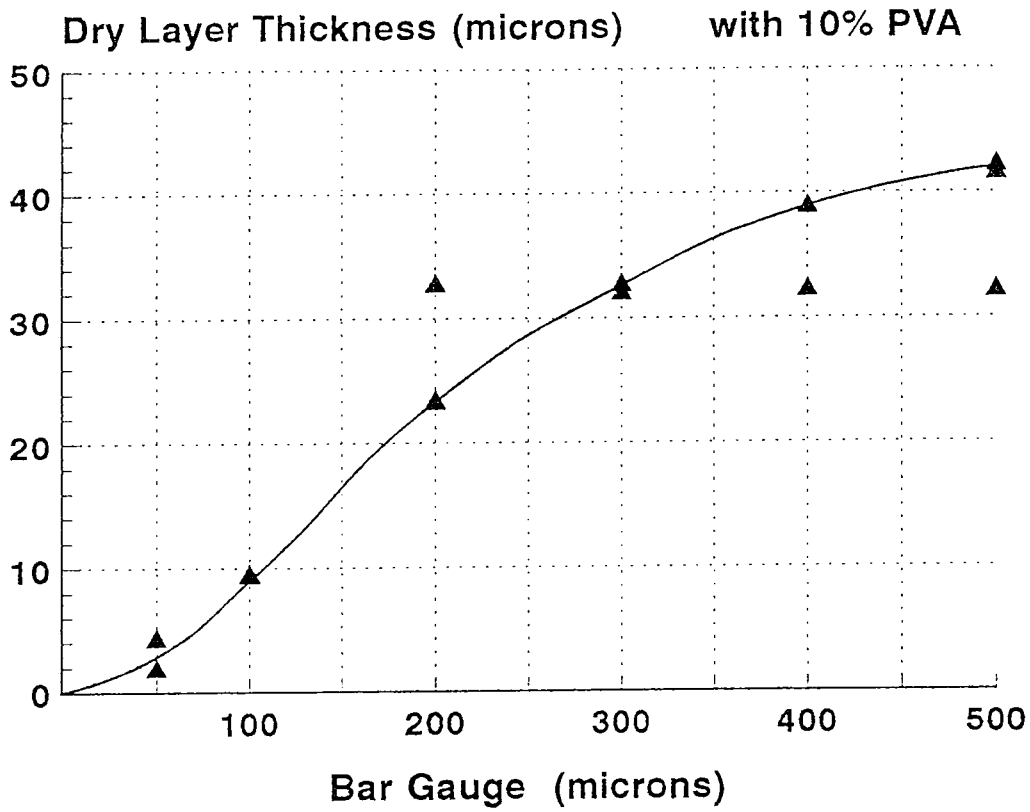

Figure 2.2 Average thickness as a function of bar coater gauge for a 10% polyvinyl alcohol solution.

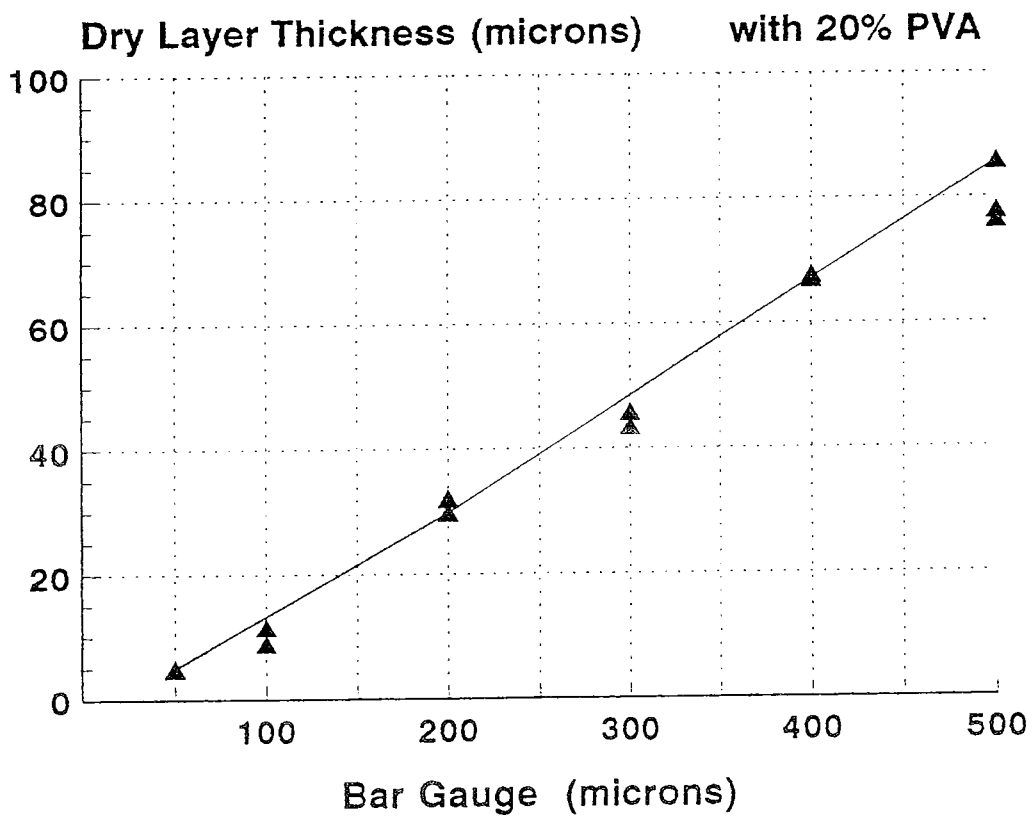

Figure 2.3 Average thickness as a function of bar coater gauge for a 20% polyvinyl alcohol solution.

Figure 2.4 Michelson interference fringes through a polyvinyl alcohol coated glass plate prepared using a 20%w/w polyvinyl alcohol solution.

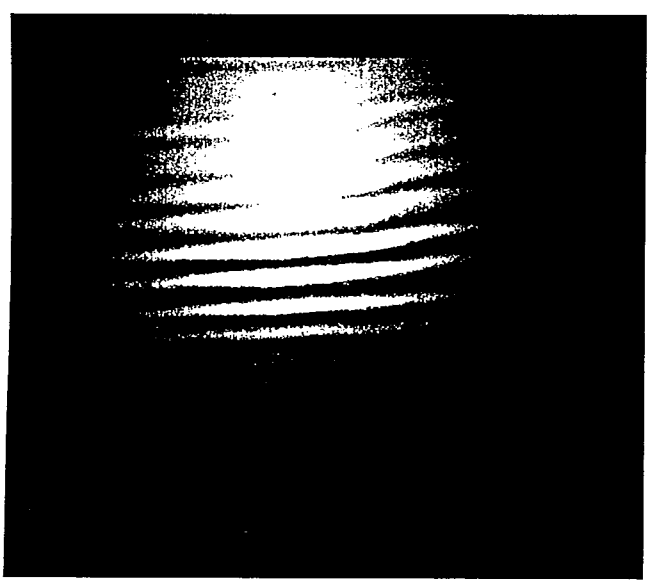

Figure 2.5 Michelson interference fringes through a polyvinyl alcohol coated glass plate prepared using a 5%w/w polyvinyl alcohol solution.

2.3 Environmental stability of recorded gratings

Any system which uses a water soluble binder will be prone to attack from the environment. However, binders which are not water soluble are not suitable for this system as the components themselves are water-soluble and very high compatibility is required to load the monomer into the binder in the required proportions and still achieve optical quality. If droplets of moisture are allowed to condense onto the surface of the polymer layer, its surface optical quality will be permanently damaged, as the water begins to slowly dissolve the binder. The physical problems caused by atmospheric moisture on these layers are only severe when humidities are very high (>70%) and the problem can easily be avoided by storage in a dry atmosphere (a light tight sealed box containing some desiccant is usually used).

As will be seen in the next section, holograms recorded in this material disappear within a few days of recording. Environmental humidity also has an effect on the rate at which the holograms disappear, as will be described below. This problem is more serious than the degradation of the optical quality described above, because the refractive index modulation itself disappears and the hologram cannot be recovered.

2.3.1 Typical decrease in diffraction efficiency after recording.

Figure 2.6 shows the typical fall of in diffraction efficiency observed with layers prepared with the original formulation. these had monoacrylamide alone as the polymerizable

monomer. Diffraction efficiency had decayed to less than half its original value after 2 hours.

It was established, by measuring the halfwidth of the Bragg peak, that the effective thickness of the grating did not change with time. Therefore, it can be assumed that this decrease in diffraction efficiency is due to a decrease in the refractive index modulation. There could be a number of causes for this. In an effort to understand the mechanism by which the refractive index modulation disappears, and try to improve the lifetime of recorded gratings, the diffraction efficiency decay under a number of different conditions was studied.

The first factor investigated was the effect of room light on the recorded grating but it soon became obvious that even complete darkness did not prevent or slow the process to any appreciable extent. It was concluded that the decrease in index modulation could not be due to the polymerization of any unconverted monomer in the dark fringe regions by the room lights. (as will be shown in chapter 6, the diffraction efficiency would not decrease at all if this were the case).

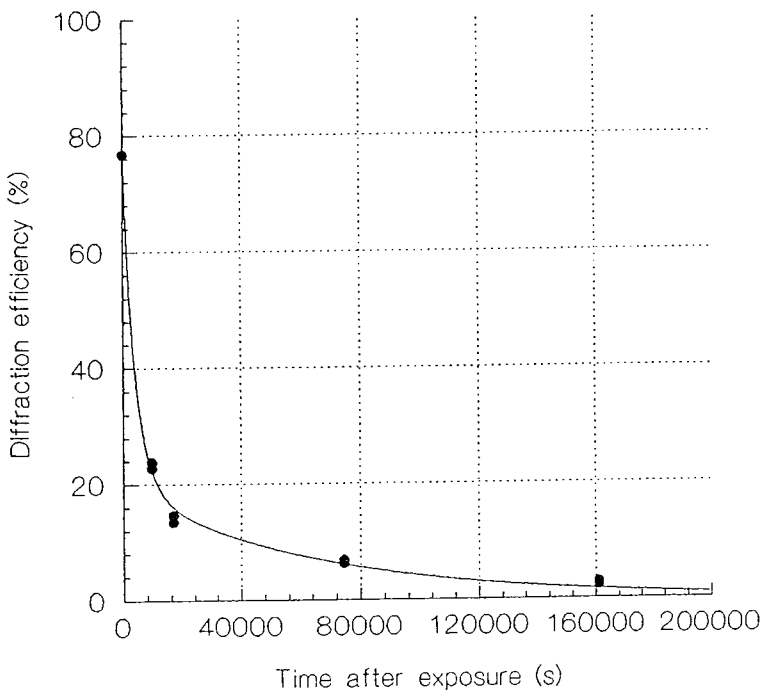

Figure 2.6 Typical decrease in diffraction efficiency with time for a fluorescein sensitized layer with acrylamide only as the monomer. Relative humidity is about 70%..

2.3.2 Effect of sealing the layers between glass plates.

The effect of the environment on the recorded gratings was then investigated. The first step was to observe the effect of sealing layers between glass slides with epoxy resin. Recorded gratings were treated in two ways; one set was sealed immediately after recording and the other was left uncovered both before and after recording.

When unsealed gratings were compared with gratings recorded in the normal way and then sealed, very little difference in the rate of diffraction efficiency decay was observed. However after 9 months the diffraction efficiency of a sealed grating was 7% compared with a fraction of 1% for the unsealed grating. The experiments were complicated by the fact that the difference between the rate of decrease of the efficiency of sealed and unsealed gratings on any particular day, was much less than the difference between the rate of decrease for these and other gratings, recorded on different days. Evidence discussed in the next section shows that the difference in decay rates was due to the different relative humidity values on these days.

2.3.3 The effect of environmental humidity

An experiment was then carried out to determine the effect of humidity on the layers. Layers were prepared and gratings recorded in the normal way at 5 mW cm^{-2} for 150 s (these were fluorescein sensitized layers prepared with the original (unoptimized) formulation and sensitivity was quite low). The diffraction efficiencies were measured and then half the gratings were transferred to a desiccator (20% humidity)and half were left in room conditions (70% humidity). From Figure 2.7 it can clearly be seen that the

gratings kept in a dry environment greatly outlasted the ones kept at 70% relative humidity. After five days the gratings maintained at 20% had more than half their original efficiency while those at 70 % humidity had only 2% diffraction efficiency. The rate of diffraction efficiency decrease of the dry samples was affected by opening the desiccator and exposing the samples to room humidity each time a diffraction efficiency measurement was made, so the number of measurements had to be limited, and each measurement performed quickly.

When removed from the desiccator months later, these gratings still had 18% efficiency. It was concluded that the main factor affecting the permanence of recorded gratings in these layers is the moisture content of the surrounding atmosphere, i.e. the presence of water vapour in some way causes the index modulation to decrease and eventually disappear.

Some high diffraction efficiency gratings were dried in a desiccator and *then* removed and sealed between glass plates. These grating tended to suffer an initial drop in diffraction efficiency and then remain at some lower value permanently. For example, a grating with a diffraction efficiency of 80% was dried in a desiccator for one week and then removed and sealed. Its efficiency dropped quite rapidly after removal from the desiccator to 35% after one week, and 25% after two weeks. After six months the efficiency was 21%. A permanent refractive index modulation of 1.5×10^{-3} remains. Three years after sealing the grating still had a diffraction efficiency of 19.7%.

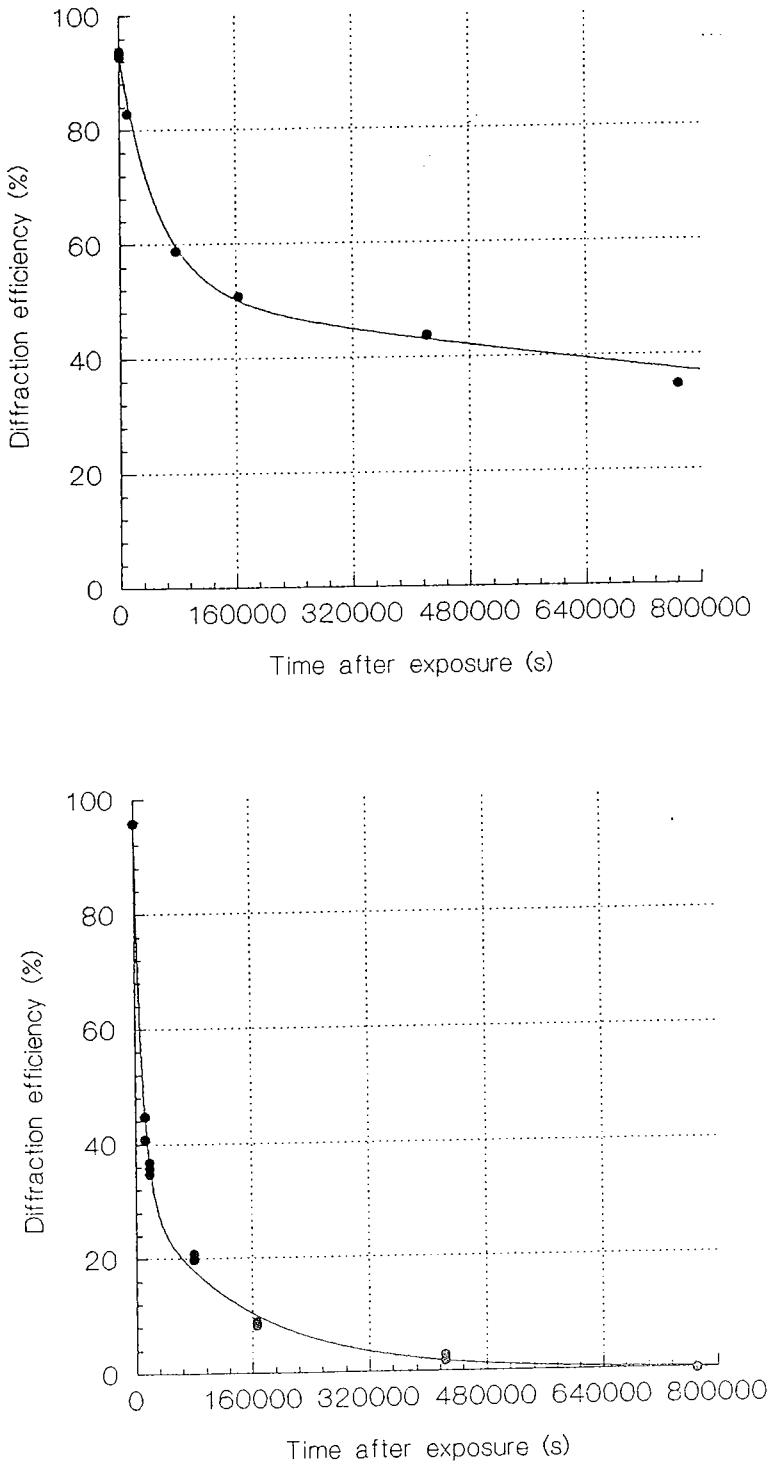

Figure 2.7 The diffraction efficiency decay curve for a grating kept at less than 20% humidity (upper curve) and for a grating kept at approximately 70% humidity (lower curve).

Removing moisture from the layer and sealing to prevent re-absorption is therefore an effective way of making gratings permanent. Refinement of this technique, such as sealing the grating without removing it from the low moisture environment would mean that even higher diffraction efficiencies could be maintained. Many holograms of real objects recorded in this material have been dried and sealed in this way and thus far (after one year) no degradation of the image or reduction in the brightness has been observed.

Even in situations where there is an unavoidable drop in efficiency before the decay process stops, the original grating can be deliberately overmodulated (see chapter 6) to allow for this. The above is a simple effective method for making permanent gratings and holograms.

The question remains as to what the exact cause of diffraction efficiency decrease is. If the decrease in index modulation at high humidities were due to simple absorption of water by the grating it might be expected that the diffraction efficiency could be recovered. However, neither drying in a desiccator nor with low heat in an oven has caused any observed recovery of the gratings.

If the decrease in diffraction efficiency were due to the diffusion of material within the layer, the dependence of the rate of deterioration on relative humidity could be explained by the fact that the permeability of water absorbing polymers such as polyvinyl alcohol and poly acrylamide increases when water content is high[1].

Monitoring the weight of these layers in different humidities has shown that they can contain up to 10% moisture, and the moisture content is known to depend on the humidity of the atmosphere[2].

Since the refractive index modulation is due (in part at least) to a density variation, it seems likely that diffusion of material out of the high density areas may be responsible for the diffraction efficiency decrease, and a more permeable layer would cause a faster deterioration of the diffraction efficiency.

This is due to the fact that in a permeable medium, the density in the bright fringe areas can easily be reduced by migration of acrylamide polymer chains through the polymer binder to the low density dark fringe areas. This migration 'smoothes out' the density modulation and thereby reduces the diffraction efficiency of the grating. This eventually leads to a uniform distribution of polymer and monomer throughout the layer, and the complete removal of the refractive index modulation.

2.3.4 The effect of a crosslinking monomer.

If dry, less permeable, layers decay more slowly then the next obvious step was to investigate other ways of making the layers less permeable in the hope that this might make more permanent holograms. A less permeable binder than polyvinyl alcohol would make a less permeable layer. However, it would be difficult to find such a binder which is water soluble and capable of dissolving the necessary quantities of the system components. Most water soluble binders are, by nature, very permeable. Another problem with a less permeable binder is that the basic processes for the formation of a hologram depend greatly on the fast diffusion of monomer through a permeable host

polymer, so even if a suitable impermeable host polymer was identified it would interfere with the recording characteristics of the material.

After some consideration it was decided that a multifunctional monomer system which tended to crosslink on polymerization would provide a good alternative since highly crosslinked polymer strands would not migrate through the binder as easily as the single strands of polyacrylamide and the recorded hologram may therefore take longer to disappear.

Several triacetates, which tend to have a high degree of crosslinking on polymerization, were investigated but were found to be incompatible with the present system due to their lack of solubility in water. Their solubility in alcohol, however was found to be better so methanol, ethanol and isopropanol were tried as substitute solvents for the photosensitive system. The layers always suffered phase separation as they dried because the triacetates were not compatible with the polyvinyl alcohol binder.

The best alternative turned out to be the addition of methylene bisacrylamide, a crosslinking agent used in the production of acrylamide gels for electrophoresis. Although this is not as water-soluble as acrylamide it will still form stable layers at normal monomer concentrations (higher concentrations produced opaque layers).

Figure 2.8 shows the decay curves for six gratings; the concentrations of the components in the photosensitive mixture are shown in Table 2-1. The overall monomer concentration is reduced to allow for the slightly lower solubility of the bisacrylamide. The total weight of monomer per 30 mls of solution was constant at 1 gram.

Layer Type	Acrylamide (grams)	Bisacrylamide (grams)	TEA (grams)	10% PVOH solution (mls)	Dye (x 10^{-3} g)
(A)	0.00	1.00	1.00	30	6.0
(B)	0.50	0.50	1.00	30	6.0
(C)	1.00	0.00	1.00	30	6.0

Table 2-1 The composition of the coating solutions used to prepare layers with different ratios of acrylamide to bisacrylamide.

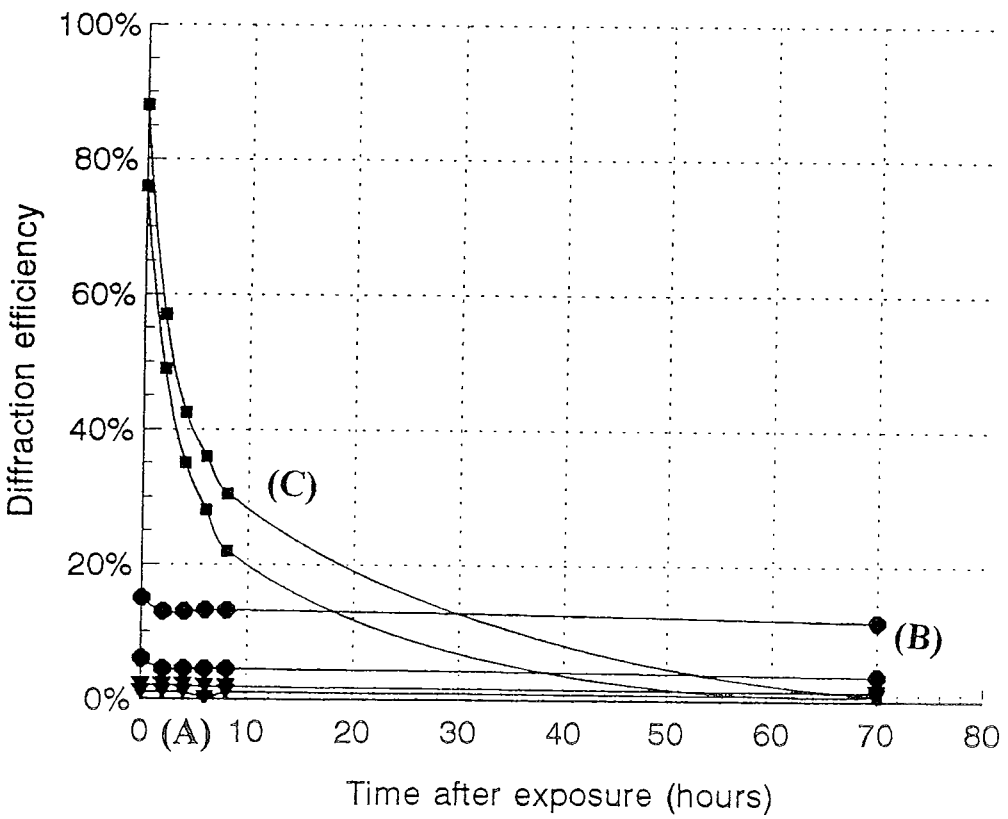

Figure 2.8 Diffraction efficiency decrease with time for different ratios of bisacrylamide to acrylamide. The concentrations of the components in the photosensitive mixture are shown in Table 2-1.

These solutions were used to produce layers by gravity settling and then exposed in the normal way under the same conditions (50-60% humidity). It is clear from Figure 2.8 that gratings recorded in layers with bisacrylamide only have low diffraction efficiency but do not appear to decay very rapidly . The layers which are made from solution B have higher diffraction efficiencies and also a slower rate of diffraction efficiency decay. Lower concentrations of crosslinking monomer therefore seemed interesting, and so the solutions shown in Table 2-2 were investigated and showed very promising results.

Figure 2.9 shows the diffraction efficiencies of layers prepared with these solutions and their rates of decrease after exposure. Layers prepared with solution F gave both a high initial diffraction efficiency and very little decline over the time taken for the acrylamide layer (solution D) to decrease to one percent.

This shows that the composition of the layers can easily be adjusted to facilitate the recording of more permanent gratings and also is further evidence to support the idea that the decay process involves the migration of molecules through the layer from bright to dark fringe areas with the result that the net index modulation is "smoothed out".

	Acrylamide (grams)	Bisacrylamide (grams)	TEA (grams)	10% PVOH soln (mls)	Dye (FLU) (x 10^{-3}g)
(D)	1.00	0.00	1.00	30	6.0
(E)	0.83	0.17	1.00	30	6.0
(F)	0.75	0.25	1.00	30	6.0

Table 2-2 The composition of the coating solutions used to prepare layers with different ratios of acrylamide to bisacrylamide.

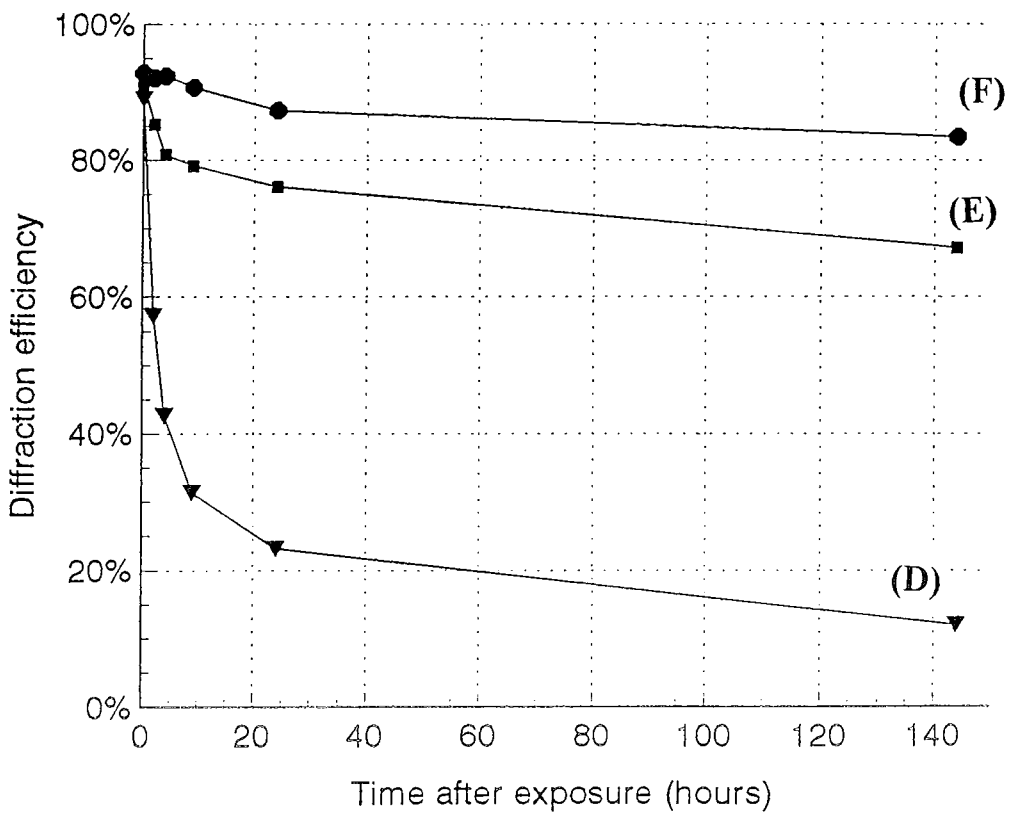

Figure 2.9 Diffraction efficiency decrease with time for different ratios of bisacrylamide to acrylamide. The concentrations of the components in the photosensitive mixture are shown in Table 2-2.

2.4 The effect of bisacrylamide on the photosensitive shelf life of the unexposed layers.

Bisacrylamide also had the added advantage of improving the shelf life of the unexposed layers so that they could be stored for much longer than acrylamide containing layers, while retaining good sensitivity.

Age of layer at time of exposure (hours)	Diffraction efficiency (%) obtained with 360mJ exposure	
	with acrylamide and bisacrylamide	with acrylamide only
0	-	-
8	67.5	74.2
22.5	79.2	64.2
72.5	61.7	22.5
146	46.7	1.8
242.5	39.3	0

Table 2-3

Table 2-3 shows the diffraction efficiencies obtained with the same amount of exposure on layers of increasing age. Unexposed layers were stored in a light tight container. It is obvious from this data that layers containing bisacrylamide have a much longer useful shelf life.

This effect is clearly seen in Figure 2.10. Three weeks after preparation the layers with the higher bisacrylamide content still showed good sensitivity and diffraction efficiency (which reached more than 70% with further exposure) while those with mostly

acrylamide as the monomer were practically insensitive. The reason for the deterioration of layer sensitivity is not understood and so it is difficult to say why the shelf life is improved by the presence of bisacrylamide. Bleaching studies of the type shown in the following chapter have shown that as the unexposed layers age, less polymerization is initiated. However the amount of initiation occurring was approximately the same for all layers of a particular monomer concentration, regardless of the ratio of bisacrylamide to acrlyamide. From this it can be concluded that the increased shelf life is not due to better initiation of polymerization in layers containing bisacrylamide, instead, the increased shelf probably arises from the fact that, being bi-functional, bisacrlyamide can polymerize faster at the same limited rate of chain initiation than pure acrylamide.

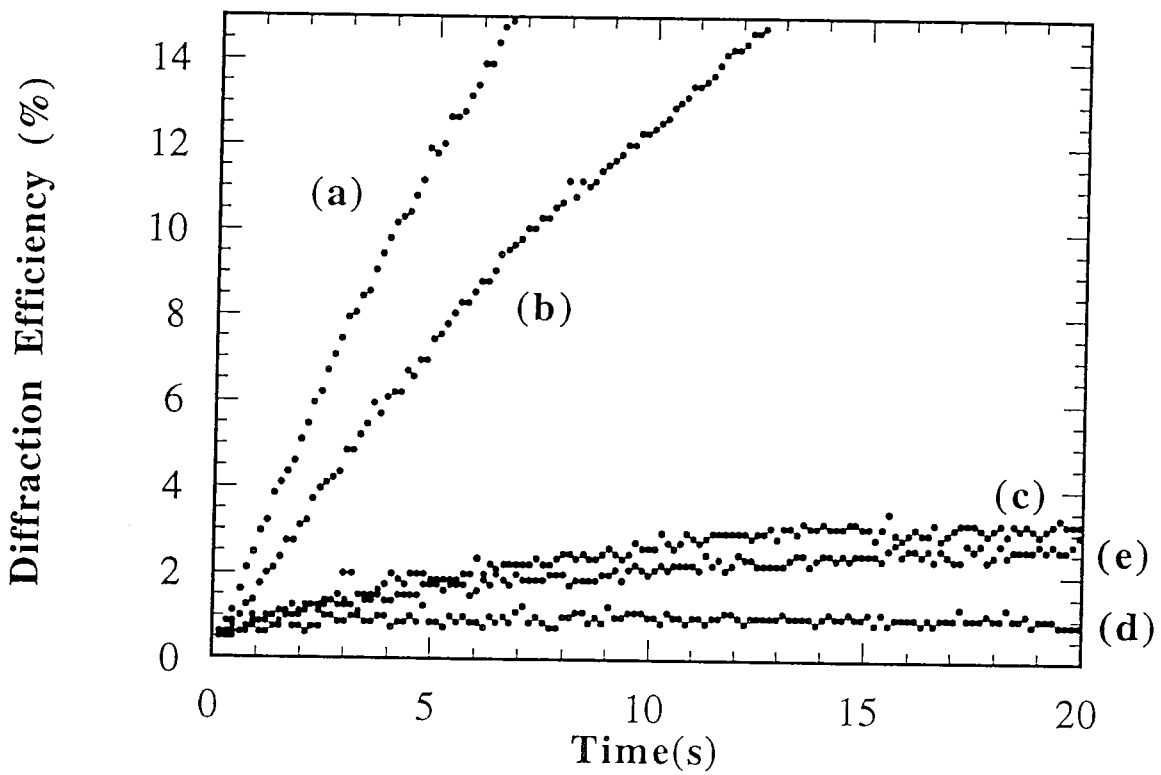

Figure 2.10 Growth of diffraction efficiency with time for three week old layers exposed to 31.5mW/cm^2 total power density. Ratio of bisacrylamide to acrylamide concentration is the parameter. (a) =3:5, (b) =1:3 , (c) = 1:7, (d) =1:15 , (e) = 0:1 The total monomer concentration was constant at 0.8g per 25 ml of coating solution, erythrosin B was the sensitizing dye..

2.5 Conclusion

This chapter addressed the practical physical problems involved with using a water soluble dry photopolymer recording medium. Suitable coating methods for the preparation of thick photopolymer layers were discussed and gravity settling on a leveled surface was identified as the most convenient, reliable method of producing high optical quality layers of sufficient thickness. Because of the practical problems that arise when working with gratings with rapidly decreasing diffraction efficiency, one of the first problems addressed was the causes of the diffraction efficiency deterioration observed in these layers. It was found that the refractive index modulation decreased as a result of diffusion of polymer chains through the permeable binder. The addition of a crosslinker, methylene bisacrylamide, was found to reduce this diffusion by allowing the polymer to form a highly crosslinked network of polymer chains which cannot easily diffuse through the binder and so remain immobile in the bright fringe areas. This preserves the density modulation formed during recording and a more permanent hologram is recorded. Holograms can be made completely permanent by storing in a low humidity environment, or sealing the dried hologram between two glass plates. Holograms of real objects recorded in layers in which the monomer was 25% bisacrylamide, have been protected in this way and stored for more than a year (so far) with no observable degradation of the image. Bisacrylamide also has the advantage of increasing the pre exposure shelf life of these layers.

With improved pre-exposure shelf life, simple, reliable preparation methods and a much improved lifetime of the recorded hologram, the photopolymer material can now be conveniently studied in more detail.

---

[1] J. E. Van Koppenhagen, M. Majda, "Structurally heterogeneous electrode films of polyacrylamide and acrylamide /vinylpyridine copolymeric gels", *J.Electroanal. Chem*, **189**, 379-388,1985

[2] Pritchard "Poly (vinyl alcohol)" Gordon and Breach, 1970.

3. Photochemical processes

3.1 Introduction

The refractive index modulation which is produced when a hologram is recorded in a photopolymerizable material is the result of several different processes occurring simultaneously in the layer. Even when recording the simplest of holograms, the diffraction grating, the rate of growth of diffraction efficiency depends on numerous chemical and physical factors. The main factor is of course the rate of polymerization, but this depends on initiation, propagation and termination rates which in turn depend on the concentration of monomer. The concentration of monomer at any time will depend not only on the percentage conversion which has occurred but also on the rate of diffusion of material from the dark fringe regions, which is an important factor in grating growth (see chapter 6). Furthermore, the refractive index is changing in real-time as the grating grows, diffracting the exposing beams and altering the exposure conditions. Bleaching rates are also important because the optical density of the layer profoundly affects its sensitivity (see chapter 4) so any change in this will affect the growth rate. Understanding the individual contribution of any of these processes is therefore inherently difficult.

The advantage of a detailed photobleaching study is that the physical factors which affect grating growth will not affect the bleaching rate of the layer, since no grating is actually formed, and so the photochemical processes can be studied separately.

In this chapter the photochemical processes that occur in these layers in response to 514nm illumination are investigated.

3.1.1 Polymerization

Polymerization is essentially the process by which many small molecules (monomers) are linked up together to form much larger molecules (polymers). One of the most well known and commonly used processes is free radical vinyl polymerization. In this process the initiating molecule is a free radical, a highly reactive molecule possessing an unpaired electron. The radical attacks the carbon - carbon double bond (the vinyl group) on the monomer and links itself to the monomer molecule. This causes the monomer itself to become a free radical which will attack another monomer molecule and repeat the process. A chain reaction ensues which creates a growing polymer chain which will only terminate when a step occurs which consumes a radical but does not produce one.

A wide variety of unsaturated monomers may be used to yield polymers with different pendant groups attached to the polymer backbone. For example the monomer vinyl chloride is used to form polyvinyl chloride (PVC) and methyl methacrylate yields polymethyl methacrylate (Plexiglas).

Vinyl chloride Polyvinylchloride

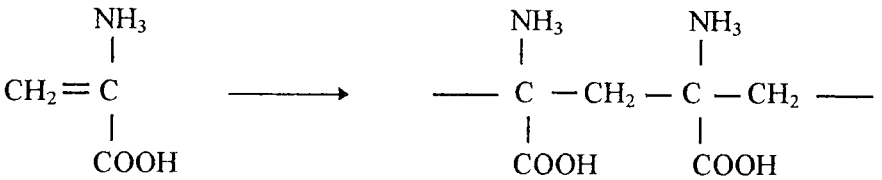

Methyl methacrylate Polymethylmethacrylate

We are mainly concerned with the polymerization of acrylamide, since this is the active chemical component in the holographic recording material.

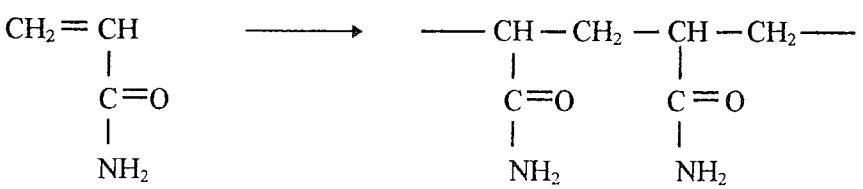

Acrylamide Polyacrylamide

The mechanism of polymerization for each of these examples is free radical vinyl polymerization. Peroxide is a commonly used initiator. It functions by breaking down to form free radicals, but the necessary initiating free radicals may also be formed in other ways; the action of light on a suitable dye, in the presence of an electron donor,

produces free radicals which will initiate polymerization (Initiation processes will be discussed in section 3.1.3.)

3.1.2 Photopolymerization

The first step of the polymerization process involves the initiating radical attaching itself to the monomer molecule by addition across the carbon-carbon double bond.

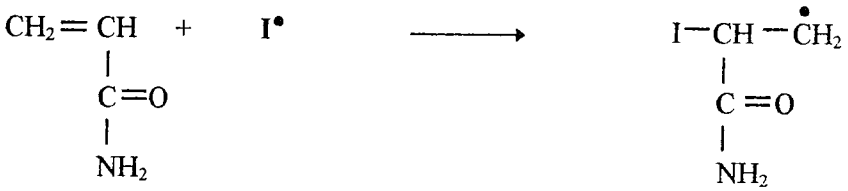

In doing this the free radical uses its odd electron and one of the π electrons from the carbon carbon double bond. The other carbon is left with an odd electron and thus the monomer molecule becomes a free radical.

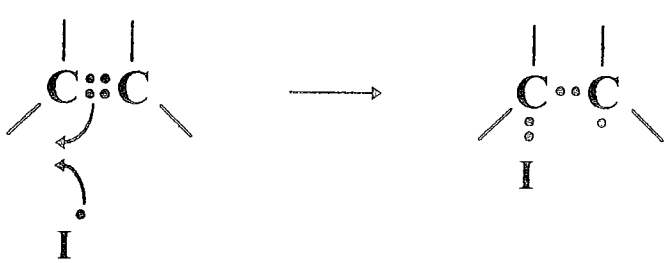

This radical will attack another monomer in the same way, again creating a new free radical.

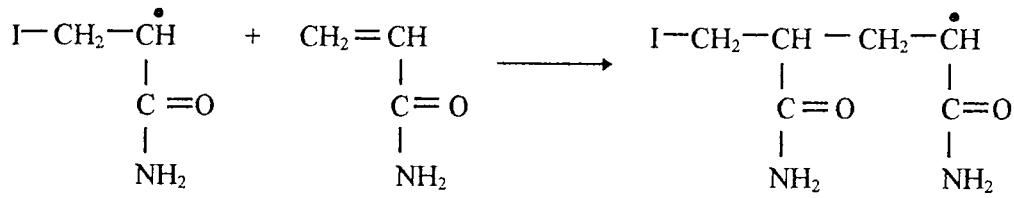

The chain will propagate in this way, growing by one monomer link each time the process is repeated, until finally termination occurs. This can be either by combination or disproportionation. Combination occurs when two radicals meet and the chains join to form one long polymer chain

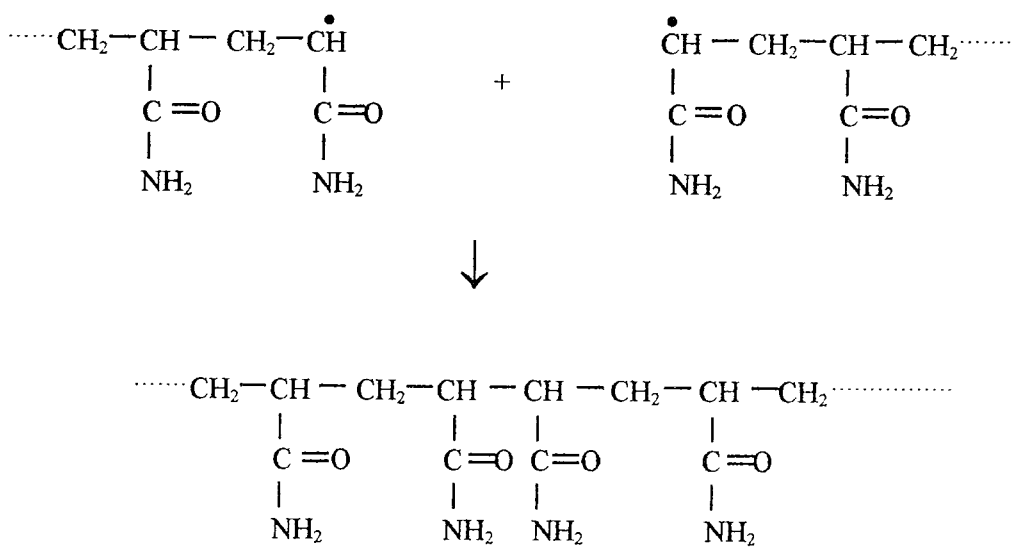

When the chain reaction terminates by disproportionation a hydrogen is abstracted from one growing chain to the other and the double bond reforms. The result is two separate chains.

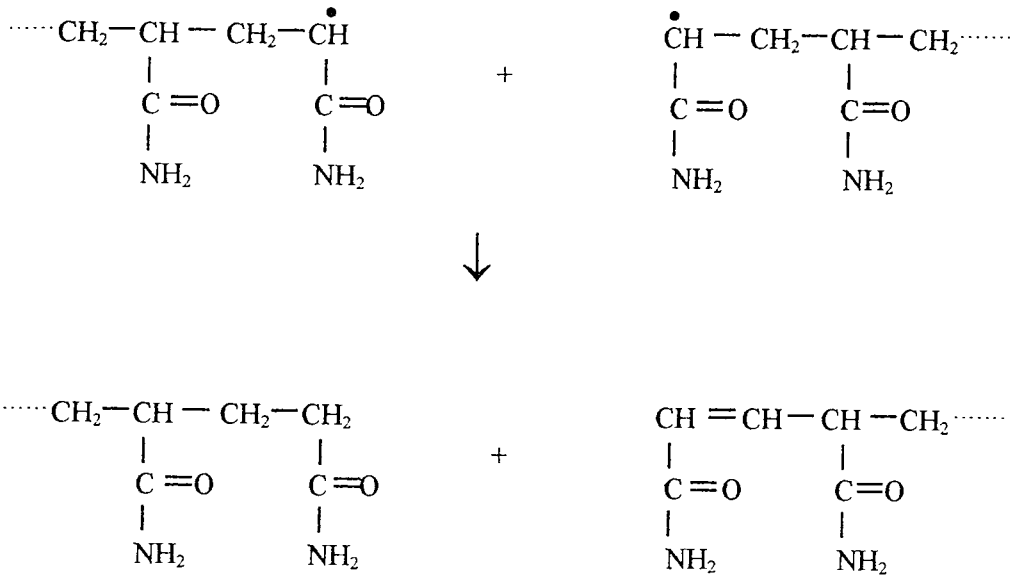

The chemical properties of polymer molecules are not greatly changed from that of the monomer. Functional groups behave in the same way whether they are part of a large or a small molecule. It is their unusual physical properties which characterize polymers. The long chain molecular structure gives them extraordinary tensile strength along the direction of the polymer chain, and also accounts for their elasticity. The optical properties also change. On polymerization, each double bond is replaced by two single bonds, lowering the molar refractivity of the material, but this is usually accompanied by such a large increase in density (10-15%) that the overall refractive index is higher in the polymer than the monomer (chapter 6 has a detailed description of the refractive index change mechanism).

In the photosensitive layers studied here, there is a high content of monoacrylamide, the light induced polymerization of this monomer causes a refractive index change and a phase hologram is recorded.

3.1.3 Initiation and bleaching processes

The generation of free radicals by the incident light is essential to the polymerization process. The light is absorbed by an appropriate dye which reacts with an electron donor to produce the necessary initiating free radicals.

In industry photopolymerization reactions are widely used for printing and photoresist applications. Cationic polymerization is sometimes used (where the reaction is initiated and propagated by a cation rather than a free radical) but the main technology of choice is sensitized free radical polymerization. Acrylic monomer polymerization, for example, is sensitized by xanthene, acridine, cyanine and merocyanine dyes and proceeds by a free radical mechanism[1]. In holographic recording materials the most commonly used sensitizing dye has been methylene blue (an acridine dye). It is used to sensitize dichromated gelatin to the longer wavelengths[2] and to initiate polymerization with both acrylate and acrylamide monomers[3,4]. In this thesis the xanthene dyes are investigated as photoinitiators for vinyl polymerization.

In 1956, discussing the photoreduction of eosin, Oster and Adleman[5] postulated the existence of a long lived excited state of the dye - the lowest triplet state - as being involved in the photobleaching process. After absorption of a photon the xanthene dye is promoted into an excited singlet state.

(1) $XD + h\nu \rightarrow {}^1XD^*$

This may either revert to the ground state by emission of a photon (fluorescence) or by radiationless transfer to another molecule e.g. the electron donor, **ED** (fluorescence quenching).

(2) $^1XD^* \rightarrow XD + h\nu$ (fluorescence)

(3) $^1XD^* + ED \rightarrow XD + ED$ (fluorescence quenching)

or it may cross over to the more stable and long lived lowest triplet state (inter system crossing).

(4) $^1XD^* \rightarrow {}^3XD^*$ (intersystem crossing)

According to Oster and Adelman, the triplet state will react with an electron donor (in their case allyl thiourea) to form the leuco (transparent) form of the dye. It may also revert to the ground state by radiationless transfer (triplet quenching) or by emission of delayed fluorescence or phosphorescence. At high dye concentrations, concentration quenching can occur, whereby an excited dye molecule is deactivated by collision with another dye molecule.

(5) $^3XD^* + XD \rightarrow 2XD$ (concentration quenching of triplet state)

Oxygen quenching is also a significant process[6] leading to the reduction of triplet and singlet state quantum yields. This usually causes an 'inhibition period' at the beginning of the polymerization, during which the oxygen and other inhibitors are used up and no polymerization is initiated.

(6) $^3XD^* + {}^3O_2 \rightarrow XD + {}^1O_2^*$ (oxygen quenching)

(7) $^1XD^* + {}^3O_2 \rightarrow XD + {}^1O_2^*$ (oxygen quenching)

In a more recent paper by Zakrezewski and Neckers[7], rose Bengal (another xanthene dye) was studied under reducing conditions with triethanolamine, $(HOCH_2CH_2)_3N$:, as the electron donor.

The formation of the free radical and subsequent bleaching of the dye is detailed as follows.

Triethanolamine donates an electron to the excited triplet state of the dye molecule leaving the latter with one unpaired electron and an overall negative charge.

(8) $^3XD^* + (HOCH_2CH_2)_3N: \rightarrow XD^{\bullet -} + (HOCH_2CH_2)_3N^{\bullet +}$

The triethanolamine radical cation then loses a proton and becomes an uncharged free radical.

(9) $(HOCH_2CH_2)_3N^{\bullet +} \rightarrow (HOCH_2CH_2)_2NCH^{\bullet}CH_2OH + H^+$

The dye radical abstracts a hydrogen from the triethanolamine radical to form the dihydro dye (transparent) and an unstable triethanolamine intermediate containing a carbon - carbon double bond.

(10) $(HOCH_2CH_2)_2NCH^{\bullet}CH_2OH + H^+ + XD^{\bullet -}$

$\rightarrow (HOCH_2CH_2)_2NCH=CHOH + H_2XD$

The unstable intermediate rearranges to the stable product shown:

(11) $(HOCH_2CH_2)_2NCH=CHOH \rightarrow (HOCH_2CH_2)_2NCH_2CHO$

In short: in order to form the transparent form of the xanthene dye, the excited triplet state of the dye abstracts two hydrogens from the triethanolamine molecule.

(12) $^3XD^* + TEA \Rightarrow H_2XD + TEA_{oxidized}$

If acidic hydrogens are available bleaching can also occur by disproportionation,

(13) $2\,XD^{\bullet -} + 2H^+ \rightarrow H_2XD + XD$

Bleaching of the dye is very important for final hologram transparency, but the primary reason for discussing the above processes has been to show that free radicals are produced by xanthene dyes under 514nm illumination in the presence of triethanolamine. The triethanolamine radical produced in step 8 is the initiating species for the polymerization processes already discussed.

(14) $TEA^{\bullet +} + ACR \rightarrow$ TEA-ACR• (initiation)

In the presence of the acrylamide monomer the triethanolamine radical can follow either of two pathways. It can react with the dye radical to form the leuco form of the dye, or it can react with a monomer molecule to initiate free radical polymerization. Therefore polymerization causes a drop in bleaching rate relative to the bleaching rate in the absence of monomer.

By comparing bleaching rates for layers containing the acrylamide monomer to bleaching rate for identical layers differing only in acrylamide concentration, vital information can be obtained, not only about the rate at which free radicals are produced, but also about the relative proportions of free radicals going into initiation of polymerization and bleaching of the dye. Information vital to the optimization of this photopolymer material can be obtained in this way

3.1.4 Sensitizing dyes

The mechanisms described above show how important the excited triplet state of the dye is to both the polymerization and bleaching processes. It is therefore important to choose a sensitizing dye which will readily form excited triplet states under illumination.

The primary requirement of a good dye sensitizer is of course that it absorbs in the appropriate region of the electromagnetic spectrum. In addition to this the dye should have a high triplet state quantum yield. Physical compatibility with the system is also essential as preparation of stable, optically clear layers must be possible. Xanthene dyes are a group of water soluble organic dyes absorbing in the green region of the spectrum and possessing increasingly high triplet yields as one moves away from the basic fluorescein structure. The structure of each of the five xanthene dyes used here are shown in Figure 3.1. For fluorescein the A, B and C substituents are all hydrogens but for the other xanthene dyes these are replaced with heavy halide atoms according to Table 3-1.

Xanthene dye	A	B	C
Fluorescein	H	H	H
Eosin Y	Br	Br	H
Erythrosin B	I	I	H
Phloxine B	Br	Br	Cl
Rose Bengal	I	I	Cl

Table 3-1 substituents of the five xanthene dyes. H = hydrogen, Br = Bromine, Cl = Chlorine, I = Iodine.

The rigid planar structure and the high level of delocalisation account for the tendency of fluorescein to fluoresce. In aqueous solution its fluorescence yield is 92% so naturally the number of molecules crossing to the triplet state is low (5%)[8]

However the other xanthene dyes posses heavy atom substituents on the aromatic rings which promote the spin forbidden transfer to the triplet state through intersystem crossing. For example the singlet state quantum yield of eosin in aqueous solution is only 19% but its triplet state quantum yield is 71%. In the xanthene dyes absorption of photons can lead to population of the triplet states as a result of singlet triplet intersystem crossing ($S_1 \rightarrow T_1$) following singlet singlet absorption ($S_0 \rightarrow S_1$). These processes are shown in the energy level diagram in Figure 3.2 .

The triplet state quantum yield is defined as the fraction of molecules which are initially excited into singlet states following the absorption of light and subsequently undergo singlet triplet intersystem crossing. It is usually represented by ϕ_T.

Since transfer to the triplet state is necessary for reaction between the excited dye molecule and the electron donor to occur, dyes with high triplet state quantum yields would be expected to be better sensitizers for the initiation of polymerization.

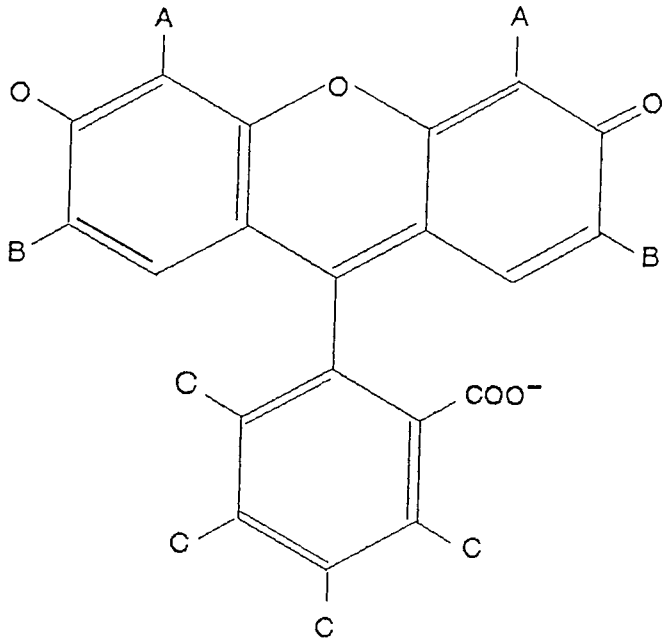

Figure 3.1 Molecular structure of the xanthene dyes.

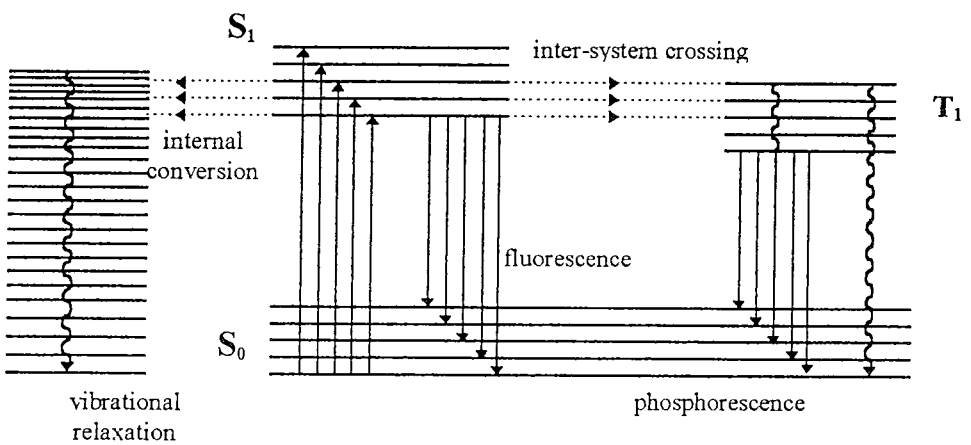

Figure 3.2 Schematic energy level diagram showing the radiative transitions as straight vertical arrows between electronic states and associated vibronic states. Non radiative transitions and vibrational relaxations are shown as wavy arrows.

3.2 Photobleaching Experiments

Several authors have used photobleaching experiments to investigate the photochemistry of dyes either in solution[9] or in polyvinyl alcohol layers[10,11]. It is possible to calculate the quantum yield of bleaching, i.e. that percentage of the incident photons used to convert a dye from its absorbing state to its transparent state, from the bleaching profiles of the layers. The bleaching profile is obtained by monitoring the increase in the transmittance of the layer with time under constant illumination .

3.2.1 Experimental procedure:

Bleaching profiles were obtained by illuminating the samples with an expanded 514nm collimated beam from an argon ion laser (Lexel model 95). As shown in Figure 3.3 the transmitted light was monitored with a photodetector connected to a data aquisition system on a PC.

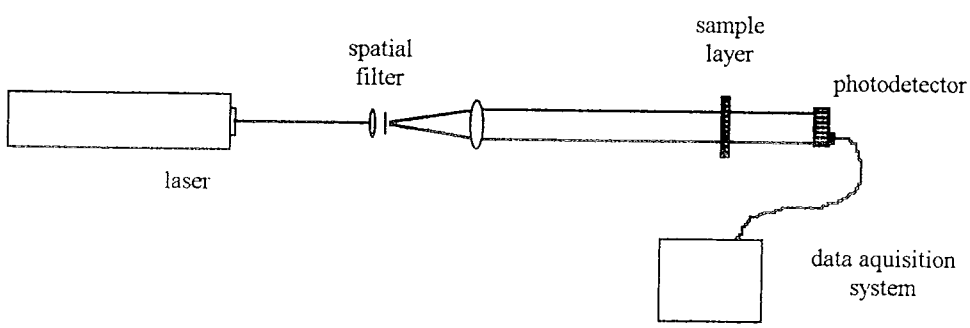

Figure 3.3 The experimental setup used to obtain bleaching profiles.

3.2.2 Photosensitive layer preparation:

The standard concentration layers were prepared as follows, 2.0 ml of triethanolamine was added to 2.7 ml of water and mixed well. The mixture was then added to 17.5 ml of a stock polyvinyl alcohol solution (10% by weight) along with 2.0 ml of dye solution whose concentration was chosen to give each solution approximately the same initial optical density. Finally, for the polymerizable layers, the monomer was added; 0.6g of acrylamide and 0.2 g of bisacrylamide. The total volume was approximately 25 ml. 10 ml of this solution spread on a 5" by 4" leveled glass plate gave a dry layer of 140 micron thickness. All the samples in this chapter were prepared with these concentrations except were otherwise stated. Drying time was usually 36 - 48 hours at 50% relative humidity.

3.3 Theoretical photobleaching model

It has already been shown that the excited triplet state of the triethanolamine molecule will react with the xanthene dye to form the transparent form of the xanthene dye molecule **H_2XD**.

$$\mathbf{ED} \quad + \quad \mathbf{XD} \quad \rightarrow \quad \mathbf{ED_{ox}} \quad + \quad \mathbf{H_2XD}$$

Assuming that the reaction has first order kinetics we can say that the concentration of the non-transparent form of the dye molecule (C) at time (t) and depth (z) can be expressed as

$$\frac{\partial C(x,y,z,t)}{\partial t} = -k_0 C(x,y,z,t) I(x,y,z,t)$$

where k_0 is the bleaching rate constant. Similarly, using the Beer Lambert law , we can express the intensity of light (I) at a given time (t) for a given depth (z) by

$$\frac{\partial I(x,y,z,t)}{\partial z} = -\varepsilon C(x,y,z,t)I(x,y,z,t)$$

where ε is the molar extinction coefficient for the dye. For illumination of a homogeneous layer with a plane wave the equations are simplified to

$$\frac{\partial C(z,t)}{\partial t} = -k_0 C(z,t)I(z,t)$$

and

$$\frac{\partial I(z,t)}{\partial z} = -\varepsilon C(z,t)I(z,t)$$

The initial conditions are $C(z,0) = C_0$, and $I(0,t) = I_0$, since the concentration of dye in the layer is homogeneous and the incident intensity I_0 is constant throughout exposure. Equations expressing the transmission of the dyed films $T(z,t)$ and the evolution of the concentration of dye as a function of time can be obtained as

$$T(z,t) = \frac{1}{1+(e^{\varepsilon C_0 z}-1)e^{-k_0 I_0 t}}$$

$$C(z,t) = \frac{1}{1+(e^{k_0 I_0 t}-1)e^{-\varepsilon C_0 z}}$$

The former can be rewritten as

$$\ln\frac{T}{1-T} = k_0 I_0 t + \ln\frac{T_0}{1-T_0}$$

where $T_0 = T(z,0) = e^{-\varepsilon C_0 z}$

k_0 can be obtained by plotting $\ln(T/1\text{-}T)$ as a function of time.

Since $OD = Log_{10}(I/T)$ the expression for k_0 can be expressed in terms of optical density as follows;

$$\int_{t=0}^{t=t} \frac{dOD(t)}{1-10^{-OD(t)}} = k_0 I_0 t = kt$$

And this integral has been defined as[12,13]

$$B(t) = \int_{t=0}^{t=t} \frac{dOD(t)}{1-10^{-OD(t)}} = -\phi_{bl} \varepsilon l I(0,t) t$$

where l is the thickness of the layer, ϕ_{bl} is the quantum yield of bleaching and I is the incident intensity at a given time.

Therfore

$$k_0 = \phi_{bl} \varepsilon l$$

This allows us to calculate ϕ_{bl} from the bleaching curves if ε, and l are known. In practice the bleaching curve deviates from the theoretical curve for greater than 20% bleaching but the $ln(T/1-T)$ versus t plot gives a good straight line fit in the early part of the curve.

3.4 Photobleaching Results

Figure 3.4 shows the effect of electron donor (TEA) concentration on the bleaching profiles of xanthene dye doped polyvinyl alcohol layers. In the absence of electron donor the transmittance of the layer changes very little (<1%) during the 40 second exposure (a). Addition of a small amount of electron donor causes a marked improvement in the bleaching rate, layer (b) is observed to have a transmittance of about 20% after 40 seconds. Bleaching rate increases with increasing electron donor concentration (d) but the effect saturates at 1.2 ml TEA per 25 ml coating solution and actually decreases slightly for higher concentrations (e) and (f) .

Layer	Electron donor content (ml)	Xanthene dye content (ml)	Polyvinyl alcohol 10% solution (ml)	water content (ml)	total volume(ml)
(a)	0	2.0	17.5	5.5	25
(b)	0.4	2.0	17.5	5.1	25
(c)	0.8	2.0	17.5	4.7	25
(d)	1.2	2.0	17.5	4.3	25
(e)	1.6	2.0	17.5	3.9	25
(f)	2.0	2.0	17.5	3.5	25

Table 3-2 Concentrations of the various components in the coating solution used to prepare the layers studied above. The xanthene dye is erythrosin B(1×10^{-2} mol/l)

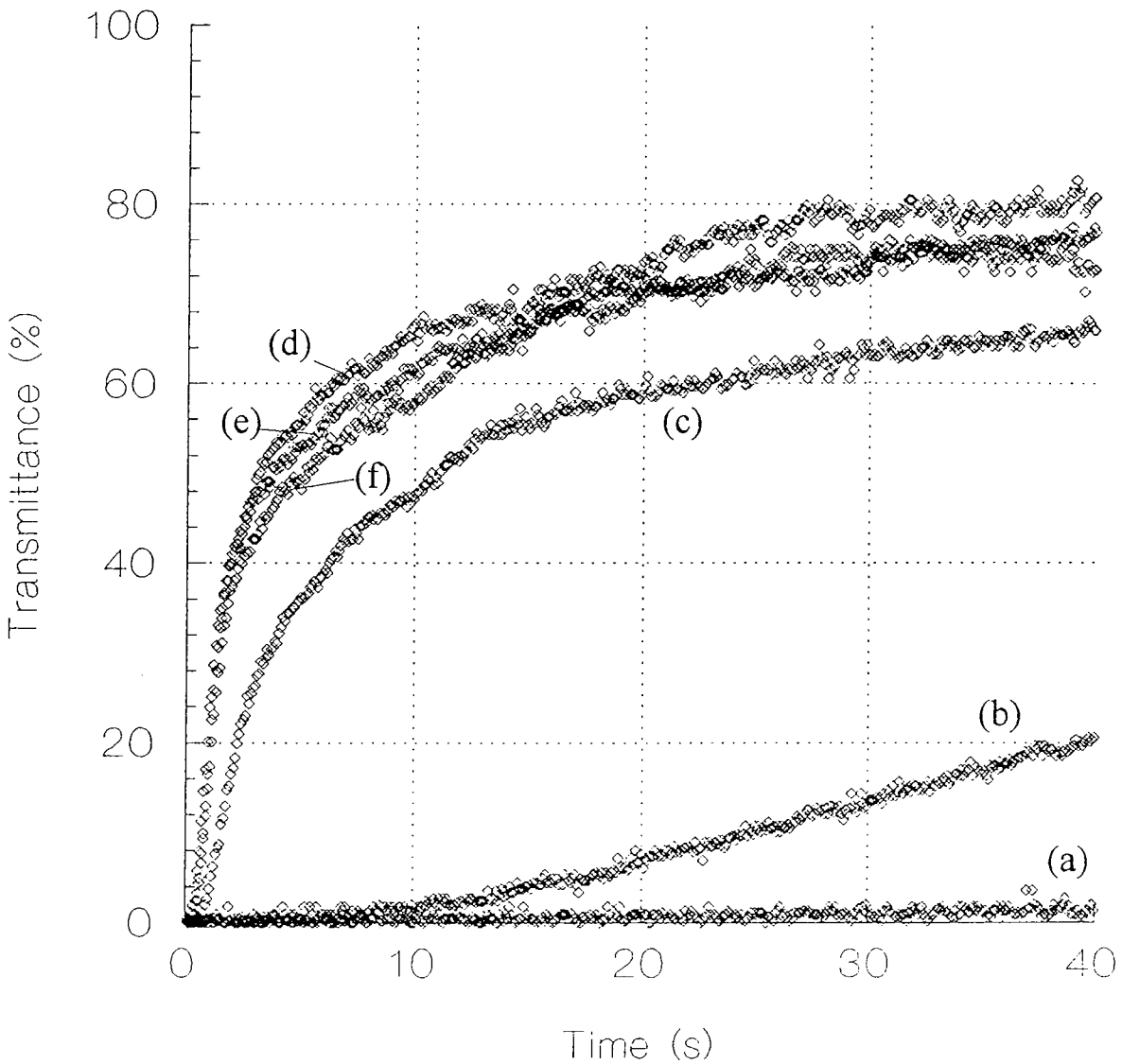

Figure 3.4 the effect of electron donor (TEA) concentration on the bleaching profiles of xanthene dye doped polyvinyl alcohol layers. The concentration of these layers are detailed in Table 3-2. Exposure intensity was 146 mW/cm²

This behavior is in agreement with the photochemical scheme described above. Bleaching occurs when the trethanolamine donates electrons to the excited xanthene dye molecule to form the leuco (transparent) form of the dye. Without triethanolamine this cannot occur and very little bleaching is observed. The slight decrease in bleaching rate observed at higher concentrations is probably due to increased quenching of the excited singlet state of the dye by the triethanolamine molecule (step **(3)** in the photochemical scheme). This would reduce the number of singlet states. The number of molecules transferring to triplet states would therefore be reduced, and with it the bleaching rate.

The optimum concentration of triethanolamine for bleaching, i.e. for the production of free radicals, is therefore about 1.2 ml per 25ml coating solution. However as triethanolamine concentrations must be kept high in order to form a stable optically clear layer it is necessary to work at 2.0 ml per 25ml coating solution even though there will be a slight loss of efficiency.

Although the layers studied in Figure 3.4 do not contain any acrylamide and therefore would be of little use for holography, there are several advantages to studying this system. Without monomer, the quantum yield of bleaching is also the quantum yield of formation of free radicals. Therefore if the quantum yield of bleaching is high for any particular set of conditions, these same conditions would lead to high rate of initiation of polymerization if monomer were present. The fact that the reaction mechanism is much simpler without monomer means that actual quantum yields can be calculated. Also, the fact that monomer is not present means that the effect of electron donor concentration can be studied for a broader range of concentrations because there are no optical quality problems. However, the main advantage of studying photosensitive

layers which don't contain any monomer is that when the bleaching rates are compared to those of similar layers which do contain monomer, valuable information about the polymerization process can be obtained.

The rate at which the layers bleach depends, of course, on the incident intensity. Figure 3.5 shows the effect of varying the incident intensity of the beam used to record the bleaching profiles. (the low triethanolamine content layer was used, concentration (b) from Table 3-2). As expected, the rate of bleaching increases with increasing intensity.

The situation is similar for layers containing acrylamide. The bleaching curves for xanthene dye doped layers containing both triethanolamine and acrylamide are shown in Figure 3.6, for bleaching with various incident intensities. These would be typical layers used to record holograms (2.0 ml triethanolamine and 0.8g acrylamide per 25ml of coating solution, as above; erythrosin B is the sensitizing dye).

If these curves are plotted as a function of exposure energy they overlap exactly. This shows that the photochemical processes which produce the triethanolamine radical responsible for bleaching and initiation are always the same for a particular exposure energy, regardless of incident intensity. An interesting conclusion can be drawn from this. Chapter 4 will show that when these layers are studied holographically they show a serious reciprocity law failure above intensities of 35 mW/cm^2. Since this is not observed when simply bleaching the layers we can conclude that it is not caused by a failure of any of the initiation steps but must be due to some of the physical processes that occur during the formation of a holographic grating. This will be discussed further in chapter 4.

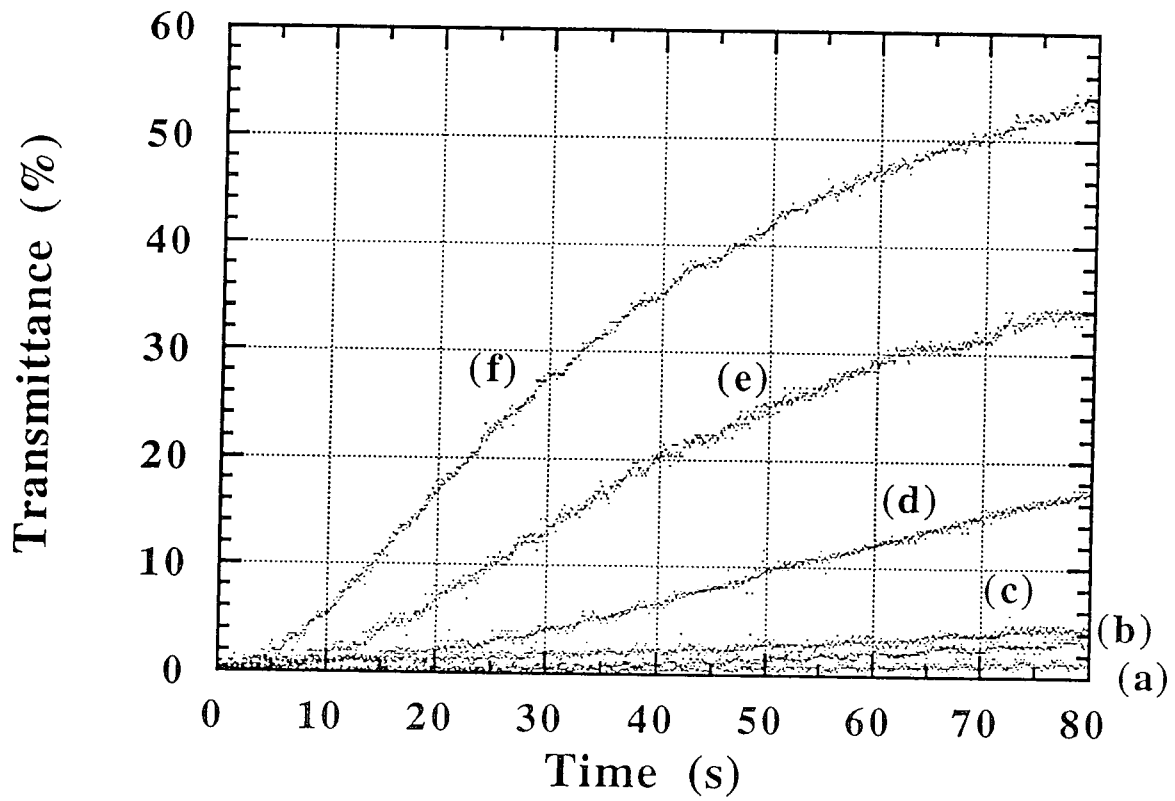

Figure 3.5 The bleaching curves for xanthene dye doped polyvinyl alcohol layers containing only triethanolamine for various incident intensities. The intensities are (a)=42, (b)=67, (c)=120, (d)=146, (e)= 186, (f)=240mW/cm^2.

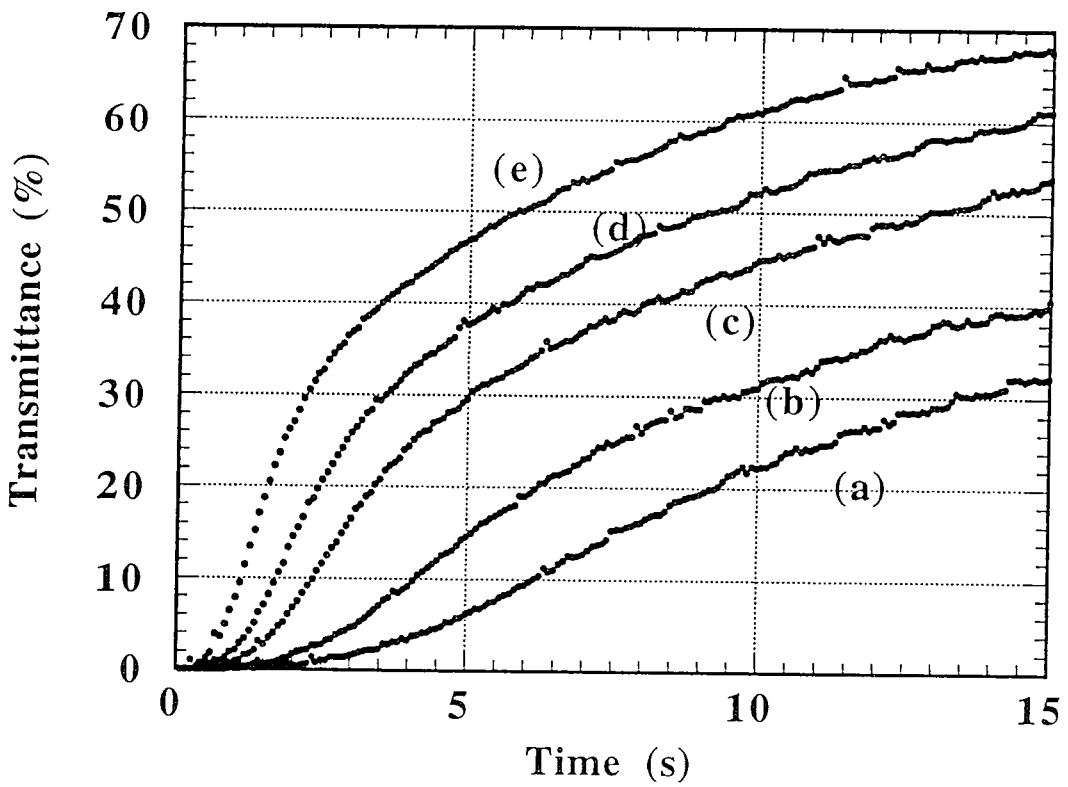

Figure 3.6 The bleaching curves for xanthene dye sensitized polyvinyl alcohol layers containing both triethanolamine and acrylamide. The incident intensities are (a)=40 mW/cm², (b)=60 mW/cm², (c)=100 mW/cm², (d)=140 mW/cm², (e)=200 mW/cm².

3.4.1 The effect of monomer concentration

The reaction between the triethanolamine molecule and the xanthene dye molecule is a one to one reaction during which a triethanolamine radical is formed. This radical reacts with the xanthene dye radical to form the leuco state of the dye. The rate at which bleaching of the dye occurs is therefore an indication of the rate at which triethanolamine radicals are being formed. In the presence of acrylamide monomer these radicals initiate the polymerization process. It is therefore true that conditions which cause a fast bleaching of the dye in a layer containing no acrylamide (high incident intensity, high electron donor concentration) will cause rapid polymerization in a similar layer containing acrylamide monomer. In this way the photosensitive layers can be optimized for free radical production by studying layers containing no acrylamide. However, in a layer containing acrylamide monomer this rapid polymerization will show up as a *drop* in bleaching rate relative to the same layer without acrylamide. This is because although the same number of free radicals are being formed, a large fraction of them are reacting with monomer molecules and initiating polymerization rather than bleaching the xanthene dye. A schematic diagram of the process is shown in Figure 3.7.

There are two pathways for each triethanolamine radical, either initiation of polymerization or bleaching of the dye. A comparison of identical layers which vary only in monomer concentration will reveal what fraction of the triethanolamine radicals is involved in polymerization.

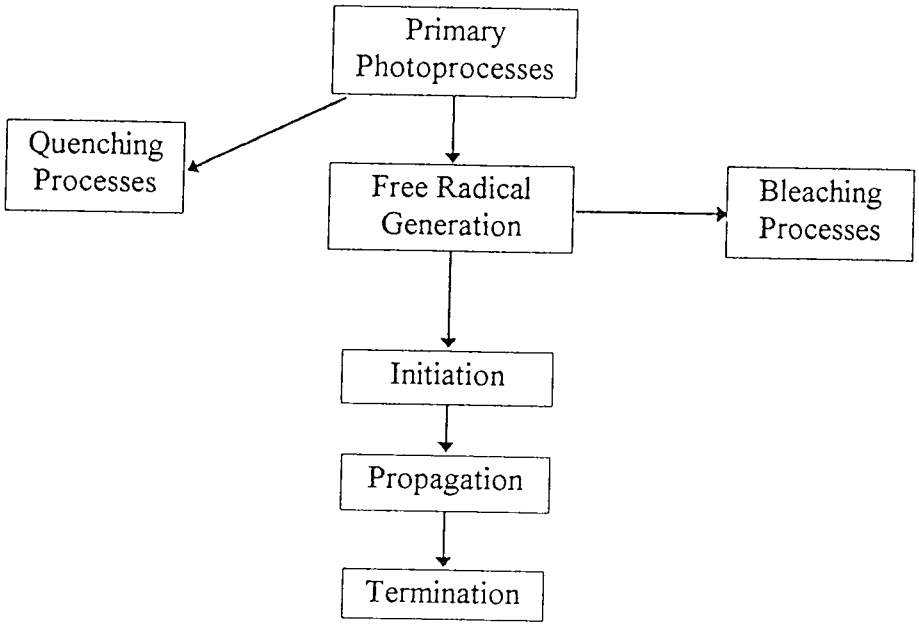

Figure 3.7 Schematic diagram of the photoprocesses occurring in dye sensitized polyvinyl alcohol layers containing electron donor and acrylamide monomer.

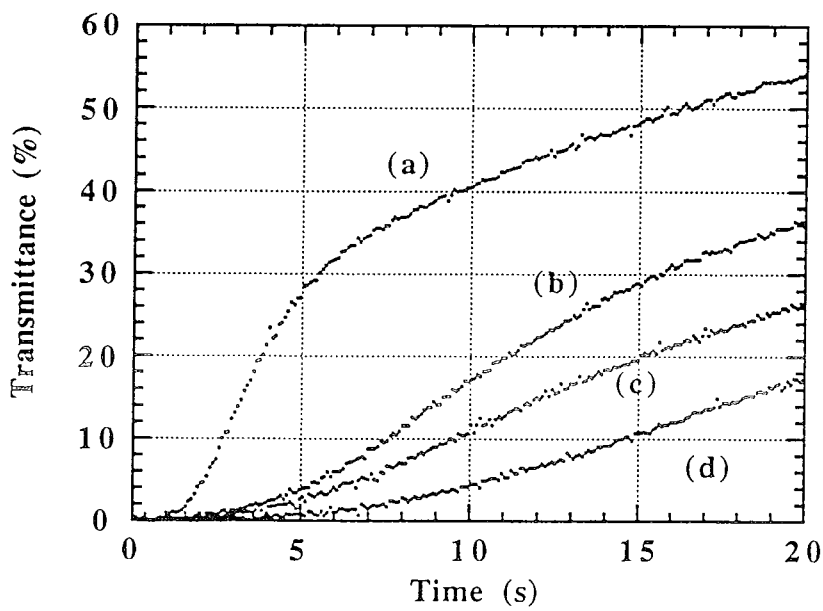

Figure 3.8 The bleaching profiles for layers with different monomer concentrations. (a) =0g, (b) =0.2g, (c)= 0.6g and (d) = 1.0g per 25 ml of coating solution. The incident intensity is 31 mW/cm^2.

Figure 3.8 shows the bleaching profiles for four layers of increasing monomer concentration. The decrease in bleaching rate is clearly seen, indicating that a greater fraction of radicals are reacting with monomer molecules as monomer concentration increases. The concentration of the coating solutions used to prepare each layer are shown in Table 3-3.

Layer	Electron donor content (ml)	Xanthene dye content (ml)	Polyvinyl alcohol 10% solution (ml)	Acrylamide content (g)	Water (ml)	Total volume(ml)
(a)	2.0	2.0	17.5	0	5.5	25
(b)	2.0	2.0	17.5	0.2	5.3	25
(c)	2.0	2.0	17.5	0.6	4.9	25
(d)	2.0	2.0	17.5	1.0	4.5	25

Table 3-3 Concentrations of the coating solution used to prepare the layers used in Figure 3.8

3.4.2 The effect of electron donor concentration.

In Figure 3.9 fluorescein is used to sensitize the layer and triethanolamine concentration is the parameter. The bleaching profiles for three concentrations of triethanolamine in fluorescein sensitized layers containing no monomer are shown, and below them the bleaching profiles of the same three concentrations of dye with 0.8g of monomer added to the photosensitive mixture. The incident intensity is 864 mW/cm^2.

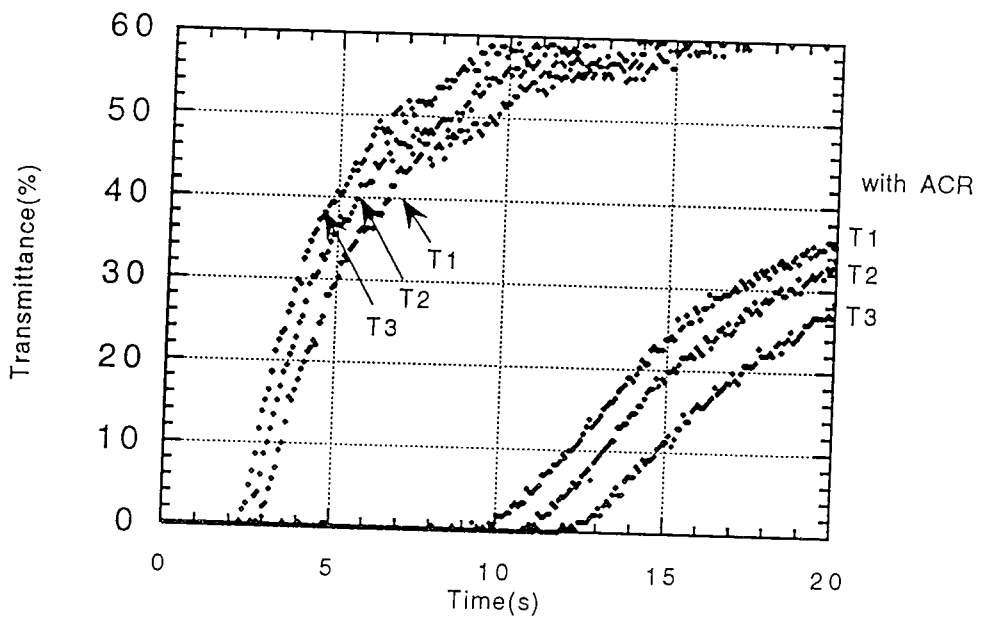

Figure 3.9 The bleaching profiles for three concentrations of triethanolamine in fluorescein / PVA layers containing no monomer are shown , and below them the bleaching profiles of the same three concentrations of dye with 0.8g of monomer added to the photosensitive mixture. The incident intensity is 864 mW/cm^2 . T1 = 0.5ml , T2 = 1.0ml , T3 = 1.5ml , T3 = 2.0ml of TEA per 25ml coating solution.

Increasing concentration of triethanolamine was observed to increase the bleaching rate of layers containing no monomer but decrease the bleaching of layers containing monomer. It is obvious that an increase in the amount of triethanolamine increased the number of available radicals and so in the absence of monomer the bleaching rate increased. However in the presence of monomer this higher number of radicals increased the rate at which polymerization was initiated, resulting in a decrease in the bleaching rate as triethanolamine concentration increased. Rose Bengal and erythrosin B layers were also studied with different electron donor concentrations and the same behavior was observed. This confirms that the electron donor is essential for both bleaching and the initiation of polymerization.

3.4.3 The effect of sensitizing dye concentration on the bleaching curves.

The bleaching curves for Phloxine B at four different concentrations of dye are shown to illustrate the effect of increasing sensitiser concentration. In Figure 3.10 there is a low concentration of dye (0.5 ml of 1.07×10^{-2} M Phloxine B) in the coating solution, so the bleaching is rapid in the absence of acrylamide. As expected in the presence of acrylamide the bleaching is slowed due to radicals being used up in the initiation of polymerization. However, the amount of initiation which can take place is limited by the lack of dye molecules so although the bleaching is slowed, the difference in the two curves is quite small. As the concentration of dye in the coating solution is increased from 0.5 ml of 1.07×10^{-2} M phloxine B (Figure 3.10) to 2.0ml of 1.07×10^{-2} M

Phloxine B per 25ml coating solution (Figure 3.13) the difference between the two curves is observed to increase. indicating that a greater number of radicals is being used up in initiation of polymerization. This indicates that increasing the sensitizing dye concentration in the holographic recording material makes more initiating radicals available and so would lead to faster polymerization and therefore higher sensitivity

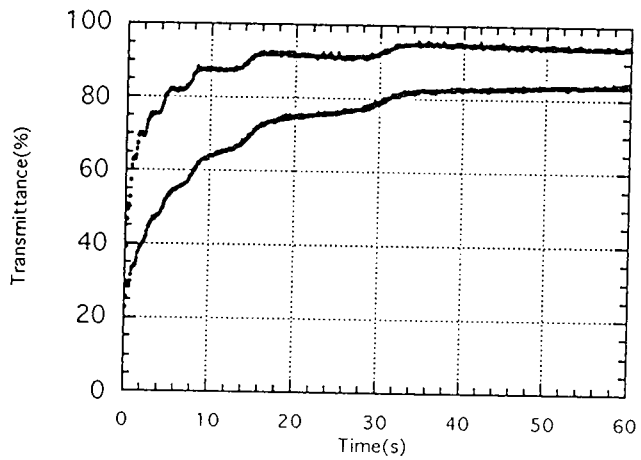

Figure 3.10 Transmittance versus time curves for phloxine B sensitized layers with acrylamide (lower curve) and without acrylamide (upper curve). The layers were prepared with ***0.5 ml*** *of 1.07 mol/l phloxine B per 25ml coating solution.*

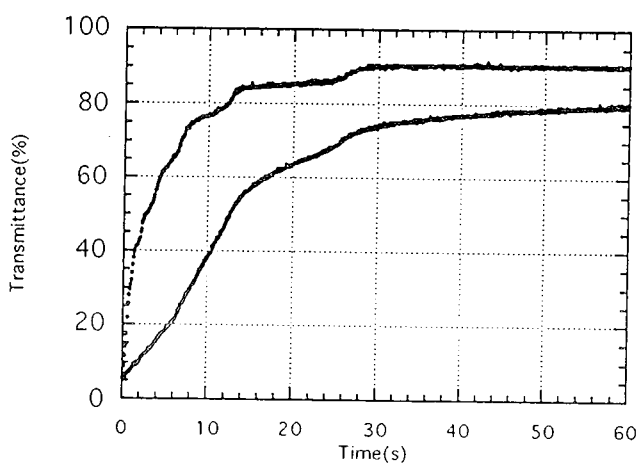

Figure 3.11 Transmittance versus time curves for phloxine B sensitized layers with acrylamide (lower curve) and without acrylamide (upper curve). The layers were prepared with ***1.0 ml*** *of 1.07 mol/l phloxine B per 25ml coating solution*

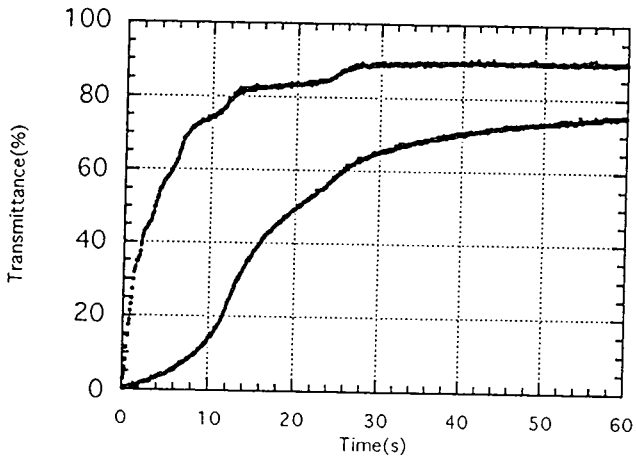

Figure 3.12 Transmittance versus time curves for phloxine B sensitized layers with acrylamide (lower curve) and without acrylamide (upper curve). The layers were prepared with ***1.5 ml*** *of 1.07 mol/l phloxine B per 25ml coating solution*

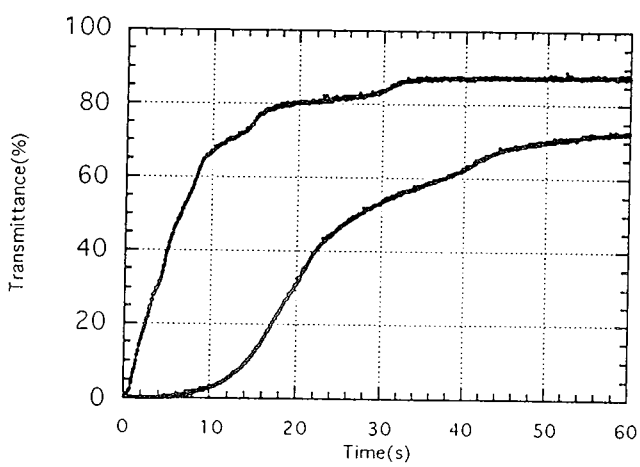

Figure 3.13 Transmittance versus time curves for phloxine B sensitized layers with acrylamide (lower curve) and without acrylamide (upper curve). The layers were prepared with ***2.0 ml*** *of 1.07 mol/l phloxine B per 25ml coating solution*

3.5 Initiation of polymerization with Erythrosin B.

In order to determine the exact relationship between dye concentration and the initiation of polymerization, the calculation of actual bleaching rates and quantum yields is required. Erythrosin B was used for this study, and the extinction coefficient of this dye in the dry layer was first determined, to facilitate accurate calculation of the quantum yield.

3.5.1 Determination of extinction coefficient of erythrosin B in the dry layer

In order to determine the value of the extinction coefficient of erythrosin B at 514nm in the photosensitive layer, 20 layers of various dye concentrations were exposed to an expanded and collimated 4 mW/cm^2, Argon ion beam and their bleaching curves recorded. The initial transmittance of each layer was determined. 10 of the layers contained 0.8g acrylamide per 25ml the other 10 contained no acrylamide. The addition of acrylamide caused no change in the initial transmittance of the layers and therefore has no effect on the extinction coefficient. Figure 3.14 is a plot of the natural log of the reciprocal of transmittance versus the concentration of erythrosin B in the dry layer. The relationship is linear at low concentration but deviates significantly at higher concentrations. According to the Beer Lambert law the slope of the early part of this curve will give $2.303\varepsilon l$ i.e. 2.303 times the extinction coefficient for erythrosin B multiplied by the layer thickness, which in this case is (45 ±2)μm. A value of $3.10\pm.0.15\times10^4$ $dm^3.mol^{-1}.cm^{-1}$ is obtained for ε_{514}. This is slightly higher than the value obtained from reference 15. The difference is probably due to the presence of triethanolamine which may shift the absorption maximum slightly.

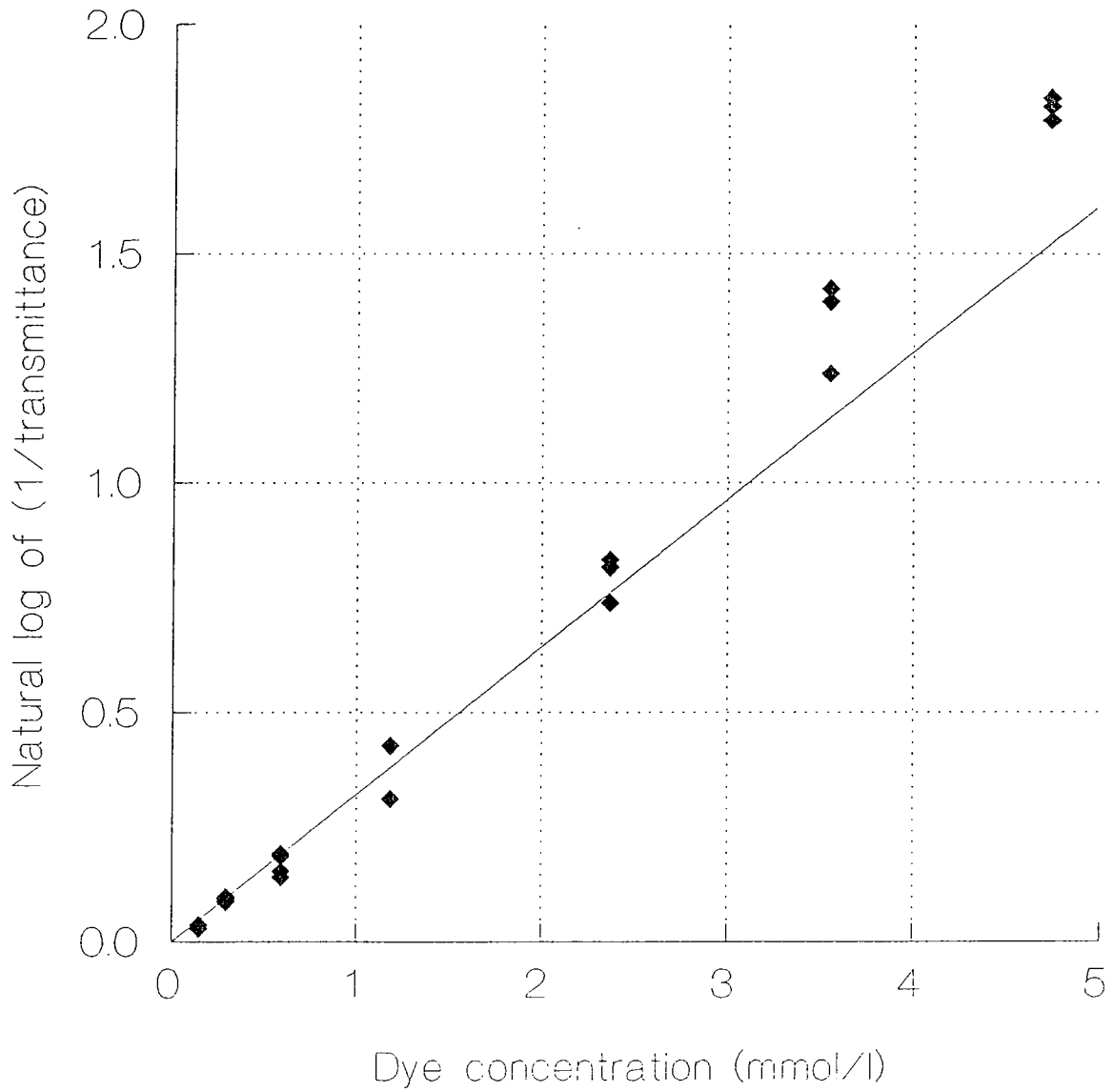

Figure 3.14 The natural log of the reciprocal of transmittance versus the concentration of erythrosin B in the dry layer.

3.5.2 The effect of dye concentration on the initiation of polymerization: calculation of quantum yields.

A detailed study was carried out for the dye sensitizer erythrosin B for 7 different concentrations. The incident intensity was kept low so that the bleaching rates would be slower. This allowed more data to be obtained in the region of interest, that is the early part of the bleaching curve, since the theoretical model is only valid for relatively small changes in the transmittance (< 20%).

Figure 3.15 and Figure 3.16 show typical bleaching profiles for these Erythrosin B sensitized layers containing acrylamide.

The bleaching constant k_0 was calculated as described, by plotting the natural log of $T/1-T$, where T is the transmittance against time. This is done in Figure 3.17 and Figure 3.18. The slope of each of these plots is k_0 from which k, the overall bleaching constant can be obtained since the incident intensity I_0 is known.

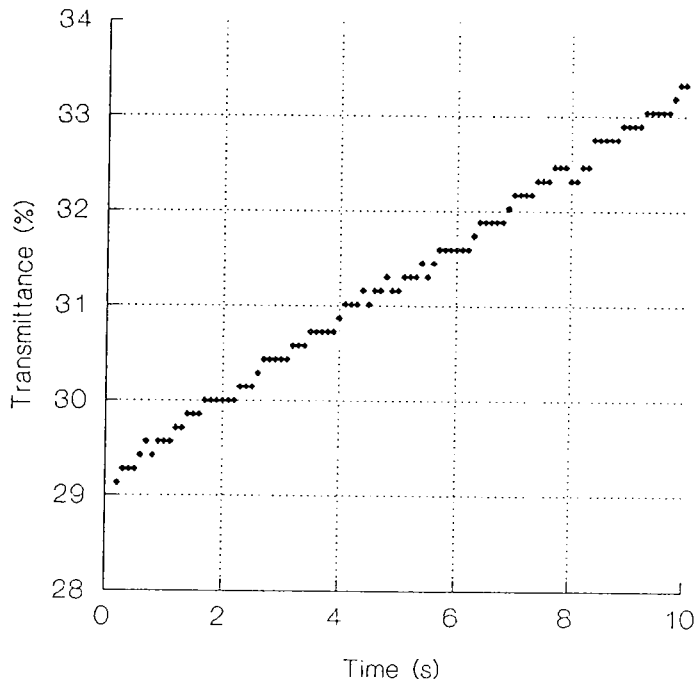

Figure 3.15 Bleaching profile for a layer with ERB concentration 3.36×10^{-3} mol/l.

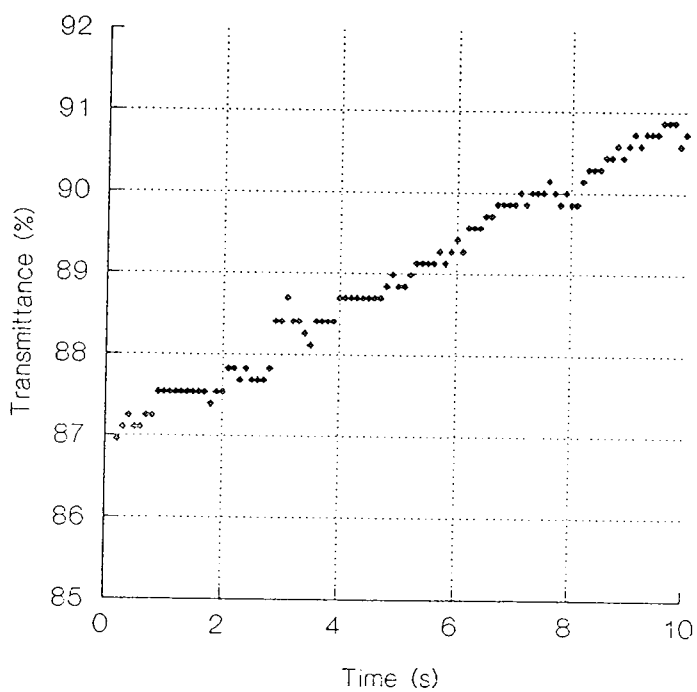

Figure 3.16 Bleaching profile for a layer with ERB concentration 0.56×10^{-3} mol/l.

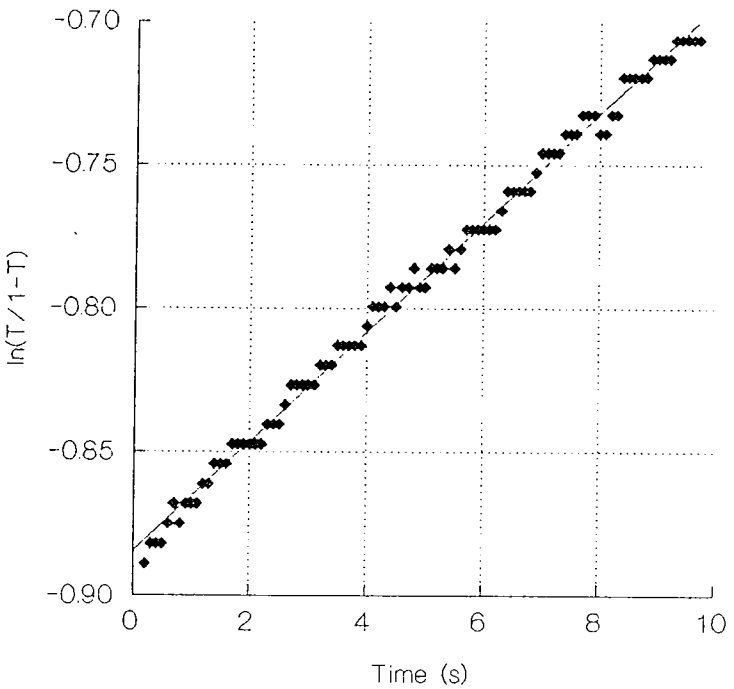

Figure 3.17 Plot of ln(T/1-T) versus time for a layer with ERB concentration 3.36×10^{-3} mol/l.

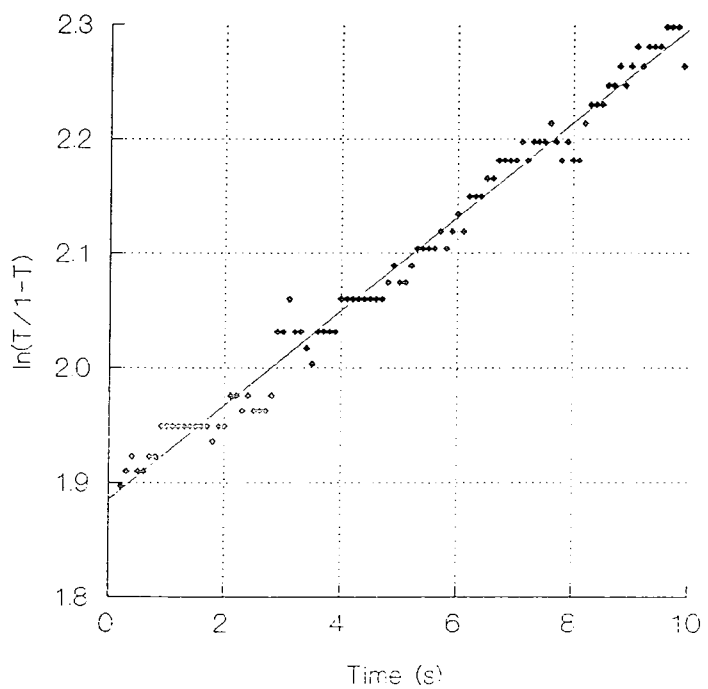

Figure 3.18 Plot of ln(T/1-T) versus time for a layer with ERB concentration 0.56×10^{-3} mol/l.

Knowing the extinction coefficient of the dye and the bleaching constant the quantum yield of bleaching can be calculated as described in section 3.3. Figure 3.19 shows the calculated quantum yield of bleaching for seven different concentrations of erythrosin B, as well as the effective quantum yields of bleaching for layers which are identical except that they also contain the standard 0.8g of acrylamide per 25ml of coating solution.

The percentage of incident photons causing the bleaching of a dye molecule, ϕ_{bl} , is observed to increase and then decrease as the dye concentration increases. If a layer has a quantum yield of bleaching of 6% and this is reduced to 2% in the presence of acrylamide monomer, the difference is the quantum yield of initiation, and we can conclude that 4% of the incident photons produced free radicals which were consumed in the initiation of polymerization of the acrylamide.

This assumes that the increase in triplet quenching due to the presence of acrylamide is negligible. This is a reasonable assumption because the extent of triplet quenching is the same for all acrylamide containing layers since it depends only on the acrylamide concentration. If the quenching was substantial the bleaching rate of layers with and without acryalmide would never be equal even if no polymerization was occurring. Considering Figure 3.19, it is obvious that at a dye concentration of 0.014 mol/l the quantum yields are almost equal and therefore there is negligible triplet quenching occurring.

Figure 3.20 is a plot of the quantum yield of initiation versus dye concentration for 45μm thick, erythrosin B sensitized layers. It shows increasing initiation of polymerization with increased sensitizer concentration. This is similar to the relationship between dye concentration and diffraction efficiency growth rate shown in

chapter 4 except that in that particular example the layers were 140μm thick and at higher dye concentrations the high absorbance became a problem.

Because the layers studied here are only 45μm thick, the initial transmittance is actually quite high, particularly for the lower dye concentrations. For example, see Figure 3.16 where the initial transmittance is 87%. 45μm layers with these low dye concentrations have very low bleaching rates because of the high initial transmittance, so errors are larger in the low concentration region of Figure 3.20.

For further work 140μm layers will be used. This will ensure that all bleaching rates are higher, and therefore the error incurred in estimating the bleaching rate from the *ln(T/1-T)* versus time graph will be reduced.

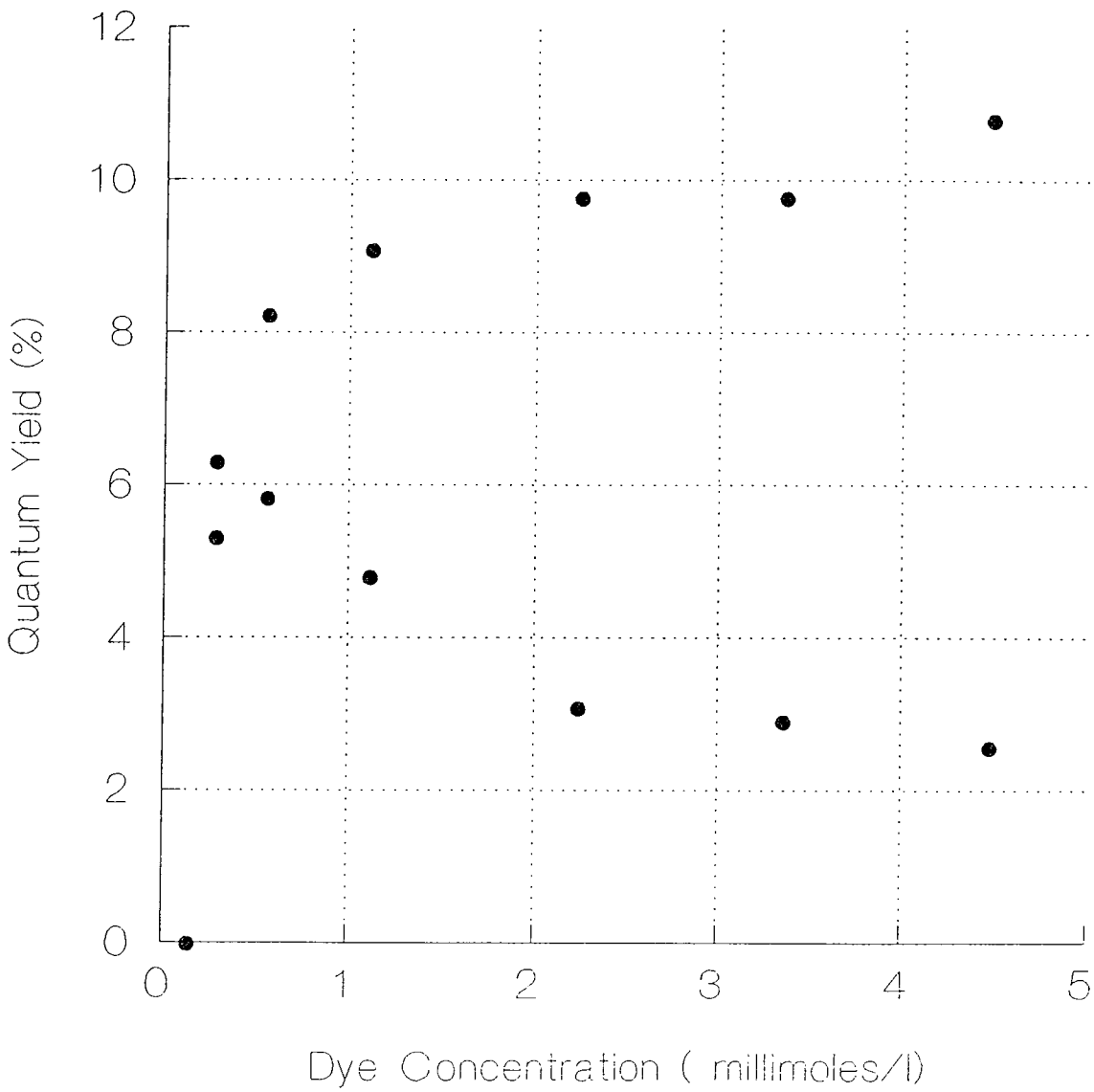

Figure 3.19 Quantum yields of bleaching for layers containing no acrylamide (upper curve) and containing 0.8g acrylamide /25ml coating solution (lower curve) for various concentrations of sensitizing dye (ERB).

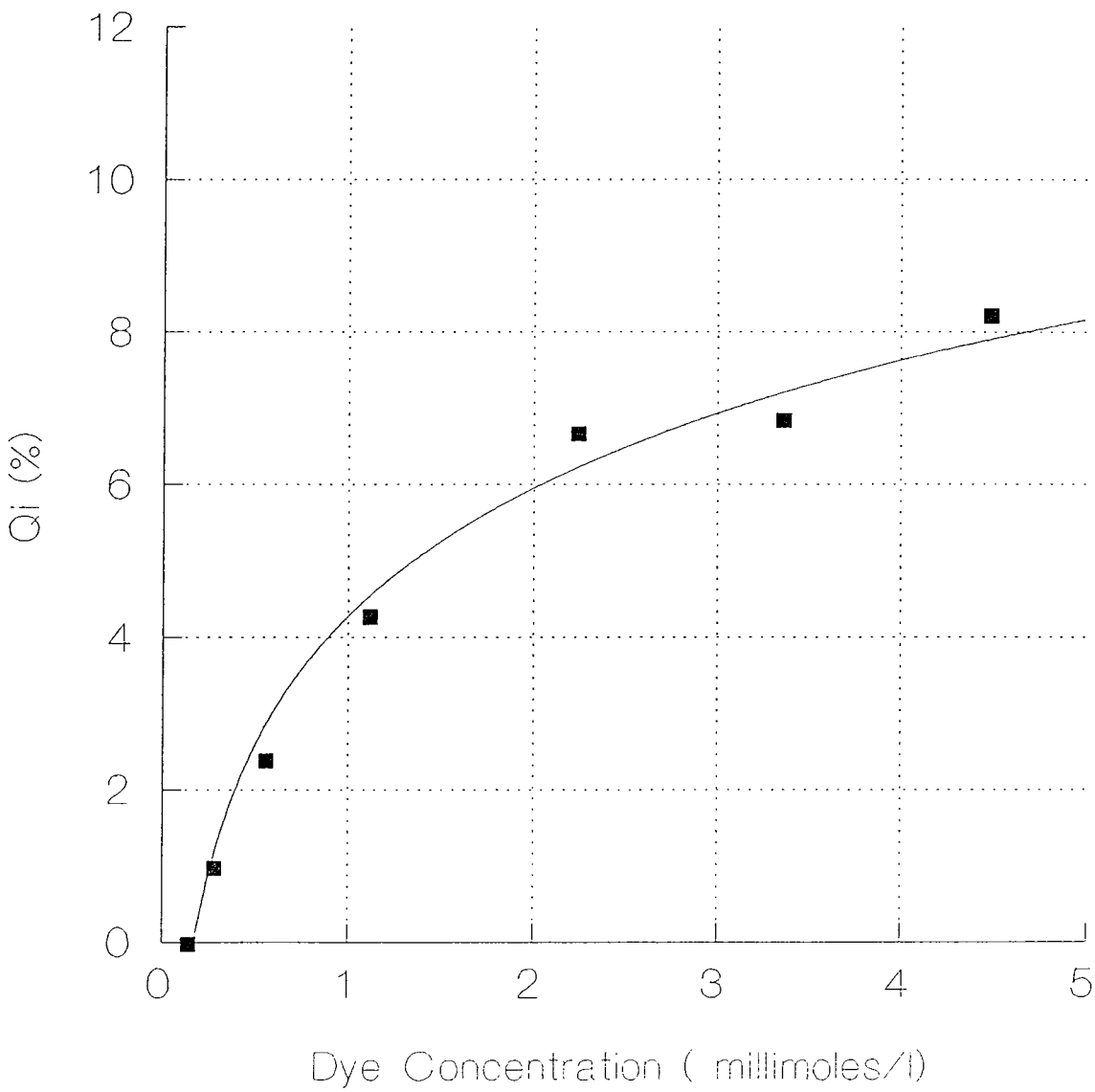

Figure 3.20 The quantum yield of initiation of polymerization for layers containing various concentrations of sensitizing dye (ERB).

3.6 Comparison of xanthene dye sensitizers.

The photochemical scheme summarized in Figure 3.7 suggests that there are three important factors to be considered when comparing dye sensitizers. **(1)** The dye should absorb strongly at the appropriate wavelength i.e. it must have a high extinction coefficient at 514nm so that excited dye molecules are produced. **(2)** The dye should react with the electron donor to produce free radicals. In order to do this efficiently it should have a high quantum yield of excited triplet states. **(3)** A high proportion of the free radicals should initiate polymerization.

The five xanthene dyes we wish to evaluate as possible sensitizers for this system can be compared by calculating their quantum yield of initiation, ϕ_i . As above, this is done by comparing the quantum yield of bleaching in the absence of acrylamide with that in the presence of acrylamide. The relative quantum yields of initiation should indicate how well each dye will perform as a sensitizer for the holographic recording material.

The extinction coefficient of each dye is easily obtained by spectrophotometric measurements of the absorption coefficient at 514nm. The measurements must be taken with the dye in the solid polyvinyl alcohol layer and not in solution as the absorptivity of the dye in a solid matrix is quite different. Other authors have studied various xanthene dyes in polyvinyl alcohol layers[14 15]. The data in Table 3-4 is taken from references 6 and 15 and gives the extinction coefficients for five xanthene dyes in aqueous solution and in a polyvinyl alcohol matrix. Where available, the quantum yield of triplet states (ϕ_T) in aqueous solution is also given.

Xanthene dye	ε_{514} ($dm^3\ mol^{-1}\ cm^{-1}$) in solution (H_2O)	ε_{514} ($dm^3\ mol^{-1}\ cm^{-1}$) in PVOH layer	λ_{max} (nm) in PVOH layer	$\Delta\lambda_{max}$ (nm)	ϕ_T
Fluorescein	38400	30600	502	12	0.05
Eosin Y	101800	39600	528	11	0.71
Phloxine B	30700	26600	553	15	-
Erythrosin B	59200	28600	535	8	1.07
Rose Bengal	33400	18400	564	16	0.76*

Table 3-4 Extinction coefficients for xanthene dyes in solution and in a polyvinyl alcohol matrix. λ_{max} is the wavelength of maximum absorbance of the dyed polyvinyl alcohol layer and $\Delta\lambda_{max}$ is the difference in λ_{max} for the solid layer and λ_{max} for a solution of the dye. Where available, the quantum yield of triplet states for each dye in solution is quoted[6].

All of the above xanthene dyes absorb strongly at 514nm and so fulfill the first requirement for a suitable dye sensitizer. Eosin Y is the most strongly absorbing.

The next requirement is that the dye in the PVOH layer has a high quantum yield of triplet states. As can be seen from Figure 3.7 this is necessary for efficient bleaching and initiation of polymerization. The bleaching rate of a dyed polyvinyl alcohol layer containing no monomer is an indication of the number of free radicals produced and is therefore directly related to the triplet yield of the dye (see section 3.3). The bleaching rates of polyvinyl alcohol layers containing equal concentrations of triethanolamine and prepared to have approximately the same optical density at 514nm were compared by the same authors and the quantum yield of bleaching for each dye was calculated. The data in Table 3-5 is taken from reference 15.

---

* in methanol.

Xanthene Dye	Concentration of Dye solution ($\times 10^{-5}$ mol/l)	Quantum Yield of Bleaching (%)
Fluorescein	6.51	1.0
Eosin Y	2.46	4.1
Phloxine B	8.41	1.4
Erythrosin B	4.22	8.9
Rose Bengal	7.48	2.0

Table 3-5 Quantum yields of bleaching for five xanthene dyes. Layers were prepared by the same method used here with 2.0 ml of triethanolamine and 1.0 ml of xanthene dye solution per 25mls of coating solution. The concentration of each dye solution is given. The layers contain no acrylamide.

All of the above dyes have a significant quantum yield of bleaching and therefore must produce a significant number of triethanolamine radicals. Erythrosin B has the highest quantum yield, fluorescein has the lowest.

The final requirement for efficient initiation of polymerization is that a high proportion of the free radicals that are formed are actually used to initiate polymerization. This can be studied by comparing the quantum yield of bleaching in the presence of acrylamide and comparing it to the quantum yields obtained above.

The present author studied the same five xanthene dyes in polyvinyl alcohol layers containing both triethanolamine and acrylamide to determine how the addition of acrylamide affects the bleaching rate and the observed quantum yield of bleaching.

The quantum yield of bleaching was greatly reduced in layers which contained monomer. Although free radicals are being formed at the same rate in these layers, many of them attack monomer molecules and initiate polymerization. This means that fewer radicals are available for bleaching and the bleaching rate is reduced accordingly. The difference between the two bleaching rates depends on the number of radicals involved in the initiation of polymerization. The quantum yield of initiation could be defined as the percentage of incident photons which lead to the initiation of a polymer chain. It can be determined by subtracting the quantum yield of bleaching in the presence of a fixed amount of monomer (from Table 3-6) from the quantum yield of bleaching in a layer containing no monomer (from Table 3-5).

Table 3-6 shows the quantum yields of bleaching and quantum yields of initiation of polymerization for the five xanthene dyes in layers containing acrylamide. The dye concentrations quoted are the concentrations in moles per liter in the dry layer. They are similar to the concentrations in Table 3-5, for example in preparing the erythrosin B sensitized layers 0.5ml of a 1×10^{-2} mol/l ERB solution was used.

The triethanolamine concentration was constant at 2.0 ml per 25ml of coating solution. The acrylamide concentration was constant at 0.8g per 25ml of coating solution. It can be assumed that the slight differences in dye concentrations between the two studies will not affect the quantum yield values too greatly (at higher dye concentrations the quantum yield changes very little with increasing dye concentration particularly in layers without acrylamide).

Xanthene Dye	Concentration of dye in dry layer ($\times 10^{-3}$ mol/l)	Quantum Yield of Bleaching (%)	Quantum Yield of initiation (%)
Fluorescein	1.13	0.01	1
Eosin Y	0.775	0.52	3.5
Phloxine B	1.16	0.08	1.3
Erythrosin B	1.08	0.66	8.
Rose Bengal	1.66	1.15	1

Table 3-6 Quantum yields of bleaching and quantum yields of initiation of polymerization in layers containing acrylamide. The concentrations of dye in the layers are chosen to give each layer approximately the same initial optical density regardless of which dye is used to sensitize it.

From Table 3-6 xanthene dyes can be listed in descending order of quantum yield of initiation, the order is ERB>EOY>PHB>FLU=ROB. Figure 3.21 shows holographic grating growth curves recorded on similar layers. The results confirm the above study. Erythrosin B is the most efficient sensitizer of the system. Under these recording conditions 40% diffraction efficiency is reached in 6 seconds. Using the above results it would be predicted that eosin Y would reach only 17.5% in 6 seconds since it has a quantum yield of efficiency of only 3.5% compared to 8% for erythrosin B. The grating growth curve for eosin Y fits this prediction very closely. The same method would predict that after 6 seconds phloxine B, fluorescein and rose Bengal would reach approximately 1% diffraction efficiency. They are all in the region of 2-3%. Considering the many sources of error (unavoidable environmental instability during holographic recording, variation in dye concentrations between the two studies, variation of the laser power during illumination of the sample) the holographic results tie in closely with the predictions made by studying the photochemistry of the system.

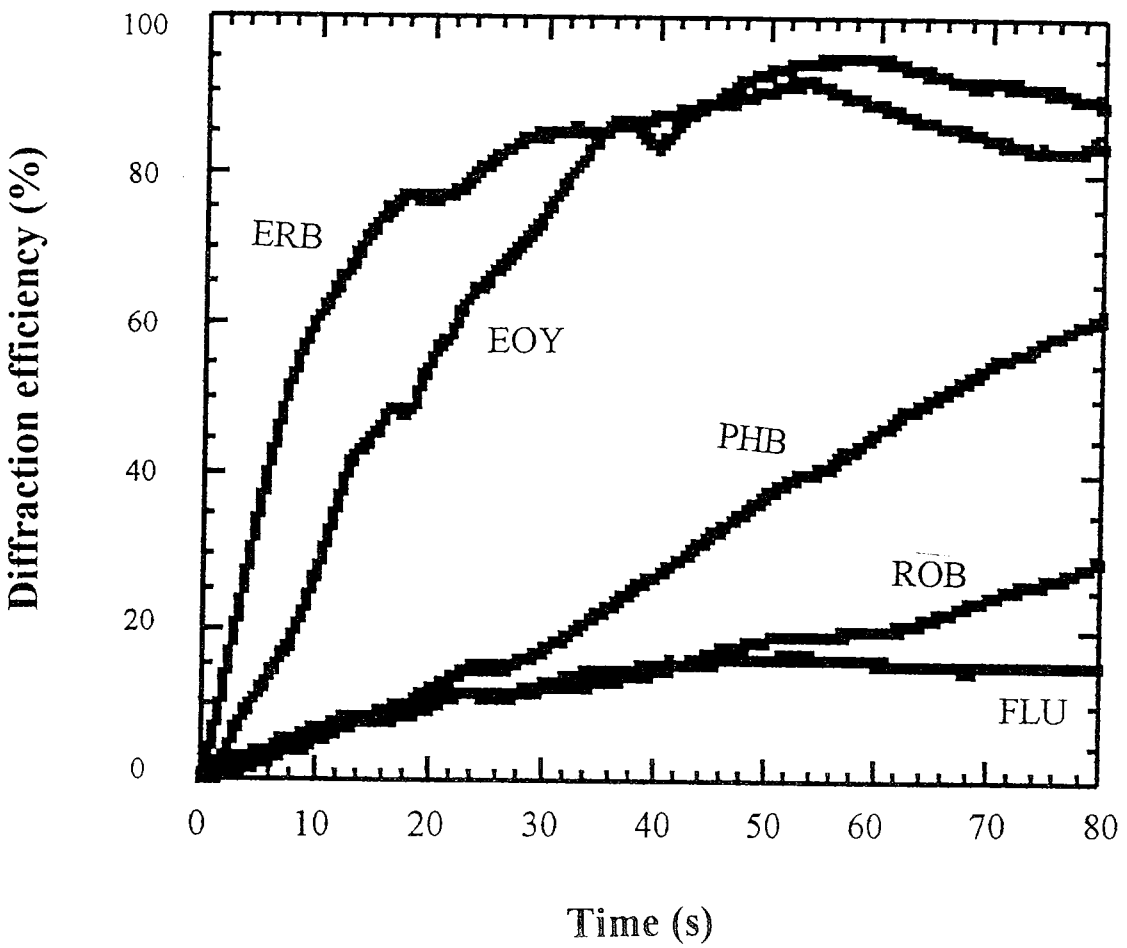

Figure 3.21 Growth of diffraction efficiency with time for identical layers sensitized with different xanthene dyes. The power density was 31 mW/cm^2 and the dye concentrations in the dry layers were chosen to give approximately the same initial optical density at 514nm.

3.7 Conclusion

In this chapter a model for the photochemical interactions which occur during 514nm exposure of the acrylamide based photopolymerizable layers has been proposed; free radicals are generated by the absorption of photons by the sensitizing dye and its subsequent reaction with a triethanolamine molecule. These free radicals can either react with a dye molecule to form the transparent form of the dye or they can attack monomer molecules and initiate polymerization. Both processes occur during the formation of a hologram in this material.

Since the free radicals can follow either of two paths in the photochemical scheme: bleaching of the dye or initiation of polymerization, a comparison of the bleaching rates of layers with and without monomer yields information on the number of radicals involved in initiation of polymerization. The concentrations of electron donor, sensitizing dye and monomer were varied and the effects on the bleaching rate observed.

Actual quantum yields of bleaching were calculated for erythrosin B in layers containing acrylamide. These were compared to the quantum yields for layers containing no monomer. The difference was taken to be the quantum yield of initiation of polymerization. A study of the effect of dye concentration showed the quantum yield of initiation of polymerization increasing with increasing dye concentration.

The quantum yield of initiation of polymerization was then calculated for each of five xanthene dyes, and this was used to predict the efficiency of each dye as a sensitizer for polymerization in this system. As chapter 4 will show, the relative efficiency of the five

xanthene dyes turns out to be almost exactly as predicted by the above work. Erythrosin B was the most efficient sensitizer.

Other authors have studied various dyes in solution and in polyvinyl alcohol layers, but this is the first time that the comparison of quantum yields in the absence and presence of a monomer has been used to determine the quantum yield of initiation of polymerization and thereby predict the efficiency of a particular dye in sensitizing a photopolymerizable holographic recording material.

The advantages of this method are that, in addition to the insight into the photochemical processes that is obtained, the method is simple, and since no hologram is actually recorded, extreme environmental stability is not required. The bleaching curves can be linearized and actual quantum yields calculated or the bleaching curves themselves can be compared qualitatively. Fast bleaching indicates the efficient production of free radicals, and a large difference between the bleaching rate of a layer without monomer and a layer with monomer indicates that most of the radicals produced initiate polymerization.

---

[1] Encyclopedia of polymer science and engineering, **17**, 167-198, John Wiley and son, New York, 1989.

[2] J. Blyth "Methylene blue sensitized dichromated gelatin holograms: a new electron donor for their improved photosensitivity", *App. Opt.*, **30**, 1598-1602, 1991.

[3] S. Calixto "Dry polymer for holographic recording", *App. Opt.*, **26**, 3904 -3910, 1987

[4] C. Carre and D. J. Lougnot "A photochemical study of the methylene blue acrylamide system in view of its use for holographic recording under red illumination", *Jounal de chemie physique*, 1988, **85** , 485-490.

[5] G. Oster and A. H. Adelman "The photoreduction of eosin", *J. Am. Chem. Soc.*, **78** , 913-916, 1956

[6] J. B. Birks, "Organic molecular photophysics", **2**, 153-154, John Wiley and son, New York, 1975.

[7] A. Zakrzewski and D. C. Neckers "Bleaching products of rose Bengal under reducing conditions", *Tetrahedron*, **43**, 4507-4512, 1987

[8] J. B. Birks, "Organic molecular photophysics", **2**, 153-154, John Wiley and son, New York, 1975.

[9] C. Carre and D.J. Lougnot "A photochemical study of the methylene blue acrylamide system in view of its use for holographic recording under red illumination", *Jounal de chemie physique*, 1988, **85** , 485-490.

[10] G. Manivannan, P. Leclere, S. Semal, R. Changkakoti, Y. Renotte, Y. Lion, R. A. Lessard. "Photobleaching of xanthene dyes in a poly(vinyl alcohol) matrix", *Applied Physics B*, **58**, 73 -77, 1994.

[11] P. Leclère "Etude et caractérisation de films d'alcool polyvinlyique photosensibilisés en vue de leur utilisation en holographie et en cojugation de phase optique" doctoral thesis, University of Liege, Belgium. 1994.

[12] P. Fournier de Violet and J. Faure "Etude cinétique de la réaction en chaine entre l'iode et les acides aminopolycarboxliques, initiées par la lumiére. Mise en evidence de leffet cage," *Journal de chimie physique*, 996-1003, 1972.

[13] C. Carre and D.J. Lougnot "A photochemical study of the methylene blue acrylamide system in view of its use for holographic recording under red illumination", *Jounal de chemie physique*, 1988, **85** , 485-490.

[14] G. Manivannan, P. Leclere, S. Semal, R. Changkakoti, Y. Renotte, Y. Lion, R. A. Lessard. "Photobleaching of xanthene dyes in a poly (vinyl alcohol) matrix", *Applied Physics B*, **58**, 73 -77, 1994.

[15] P. Leclère "Etude et caractérisation de films d'alcool polyvinlyique photosensibilisés en vue de leur utilisation en holographie et en cojugation de phase optique" doctoral thesis, University of Liege, Belgium. 1994.

4. Optimization of the material composition.

4.1 Introduction

In Chapter 1 the currently available photopolymer recording materials were discussed. The acrylamide based, dry photopolymer presented by Calixto showed some interesting characteristics. Gratings had reasonable diffraction efficiency (15%) even at the low intensities used (50-750 $\mu W/cm^2$) and the material was also shown to be self developing and to require no post processing.

The aim of the following work was to develop an acrylamide based photopolymerizable recording medium, based on Calixto's formulation but sensitive to 514 nm light. A dry acrylamide based recording material could conceivably have all the advantages of the liquid layer processes (see chapter 1) and yet be in the form of a dry film. Also, finding a suitable sensitizer in the green region of the spectrum would provide greater flexibility in holographic recording since, in general , more power and coherence is available in this area of the spectrum (for example with the argon ion laser). Fluorescein, a readily available laser dye, was used to sensitize the system at first. It is known to undergo some intersystem crossing to the excited triplet state after absorption of a photon. Intersystem crossing is a detrimental pathway for a laser dye, for which fluorescence, the decay from the excited singlet state to ground with emission of a photon, is the primary pathway. Intersystem crossing of the dye molecule into the excited triplet state, however, is a vital step in the initiation process for

photopolymerization that occurs in the material studied here. Fluorescein was a moderately successful sensitizer but the quantum yield of triplet states is low (since it has a high quantum yield of singlet states ~90%)[1]. Improvement would be expected if dyes with higher triplet state quantum yields were used. Xanthene dyes are a group of organic dyes, absorbing in the green, whose basic structure is that of fluorescein with additional heavy halide atoms substituted onto the fluorescein skeleton. The result is a heavier molecule which fluoresces less (i.e. has a lower singlet state quantum yield and a higher triplet state quantum yield) and is therefore a more efficient sensitizer. Chapter 3 has shown that replacing fluorescein with a high triplet state yield xanthene dye will improve material sensitivity.

The following work describes the optimization of the chemical composition of this material and discusses the role of the various constituents in the polymerization process. The chemical composition is optimized for dye, electron donor, and monomer concentration and some alternative systems are considered.

4.2 Experimental procedure

The simplest hologram is a diffraction grating, recorded by interfering two plane waves in the plane of the recording medium. Illumination with one of the original recording beams will then reconstruct the other and vice versa. The efficiency with which the hologram converts one wavefront into the other can be determined by measuring the intensity of the diffracted (1st order) and transmitted (zero order) beams relative to that

of the incident reconstructing beam. Diffraction efficiency is then defined as the ratio of the diffracted 1st order beam intensity (I_1) to the intensity of the incident beam (I_{in}).

$$\eta = \frac{I_1}{I_{in}}$$

However we are often using diffraction efficiency as a figure of merit to compare holograms for which all conditions are similar except the parameter under observation. In this situation the efficiency of a grating in diffracting light into the first order diffracted beam, from the zero order transmitted beam is of interest. The overall characteristics of the material including absorption and reflection losses, are the same for all samples, and the following definition is often more useful. The diffraction efficiency is taken to be the ratio of the intensity of the 1st order beam to the sum of the intensities of the 1st and zero order beams .

$$\eta = \frac{I_1}{I_1 + I_0}$$

4.2.1 Recording and evaluation of gratings.

A schematic diagram of the apparatus used to record gratings in the photosensitive layers is shown in Figure 4.1. The beam from an Argon ion (Lexel ion laser, model 95) was spatially filtered, collimated and split using the halfwave plate/polarizing beam splitter system described in chapter 5. The two 514nm beams were directed to interfere in the plane of the recording material. The angle between these beams could be altered by adjusting the position of the mirror in the path of the collimated 514nm recording beam. This varied the spatial frequency of the recorded grating. An electronic shutter (Uniblitz VS25 from Vincent associates) was used to control the exposure time. During recording a Helium Neon laser beam, incident at the Bragg angle for 633nm light, was

used to monitor the changes in diffraction efficiency. The analog output voltage from an optical power meter (Newport Model 840-C) in the diffracted beam was connected to an Acquisition PC unit which displayed the signal on a PC screen. The diffraction efficiency growth curve was obtained from this data.

4.2.2 Photosensitive layer preparation:

The standard concentration layers were prepared as follows. All the samples in this chapter were prepared with these concentrations except were otherwise stated. 2.0 ml of triethanolamine was added to 2.7 ml of water and mixed well. The mixture was then added to 17.5 ml of a stock polyvinyl alcohol solution (10%) along with 2.0 ml of dye solution (concentration chosen to give each solution approximately the same initial optical density). Finally the monomer was added; 0.6g of acrylamide and 0.2 g of bisacrylamide. The total volume was approximately 25 ml. 10 ml of this solution spread on a 5" by 4" leveled glass plate gave a dry layer of 140 micron thickness. Drying time was usually 36 - 48 hours.

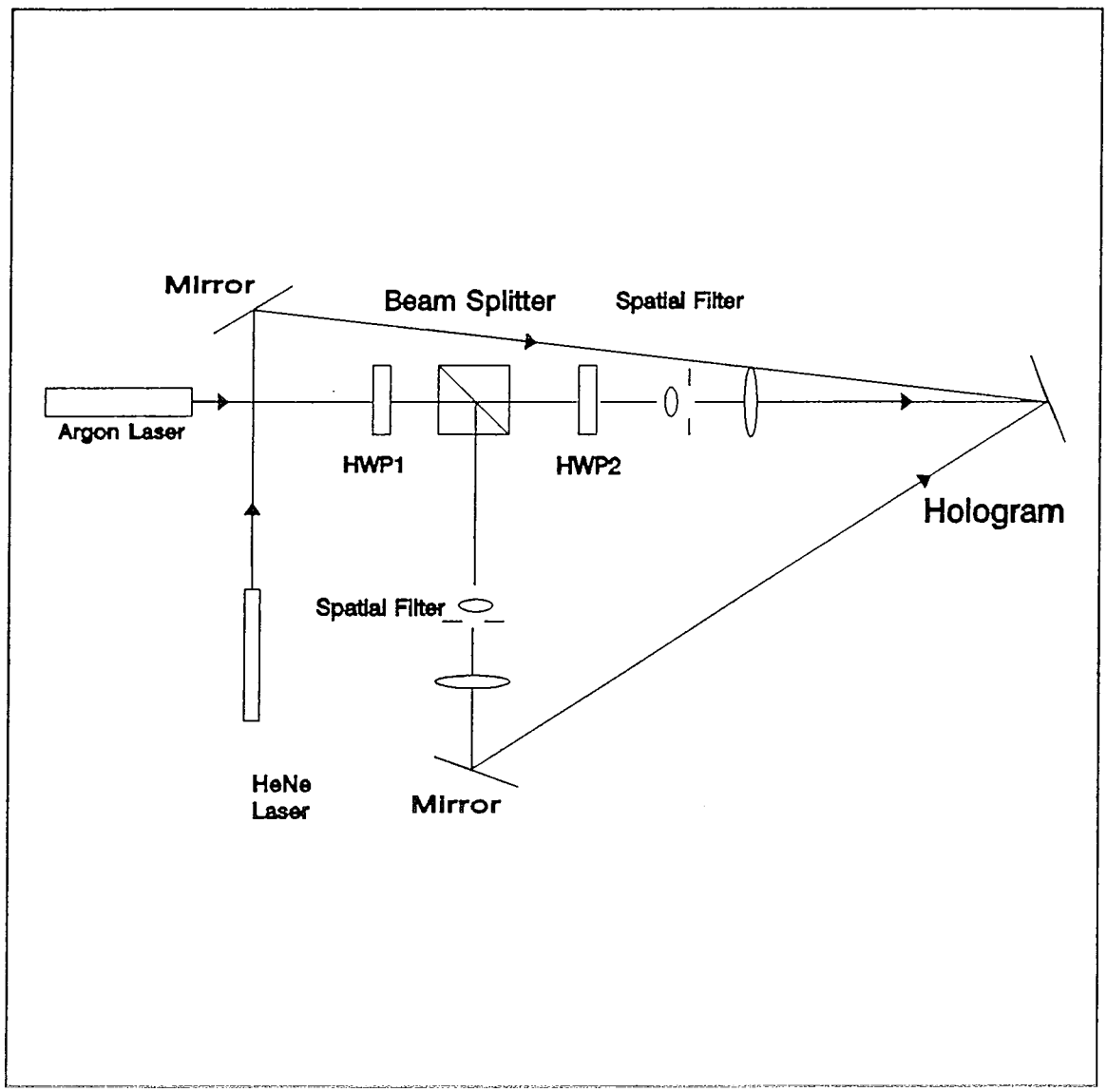

Figure 4.1 Experimental setup for recording and analysis of gratings. HWP1 and HWP2 are half wave plates. Their purpose is explained in chapter 5.

4.3 Optimization of chemical composition

The photosensitive layers consist of an electron donor (triethanolamine), a sensitizer (a xanthene dye), a polymerizable monomer (acrylamide / methylenebisacrylamide) and the inert binder (polyvinyl alcohol). Each of these components was studied individually in order to confirm its role in the photochemical processes and to optimize the composition of the photosensitive layer for holographic recording.

4.3.1 Optimization of monomer concentration:

The sensitivity of the recording medium had a strong dependence on the concentration of acrylamide in the layer. An increased concentration of monomer will of course increase reaction rates making the diffraction efficiency increase more rapidly during exposure. Moreover the total amount of polymer formed must be increased leading to a greater final refractive index modulation as can be seen from Figure 4.2. The layers with higher monomer concentrations became over modulated quite quickly. These are shown in Figure 4.2 (f) and Figure 4.2 (e) whereas the lowest concentration, Figure 4.2 (a), only reached about 6% diffraction efficiency even at long exposures. The highest observed diffraction efficiency is 84%. This is because the diffraction efficiency is not corrected for reflection or absorption. From these curves the grating growth rate for each concentration of acrylamide can be found.

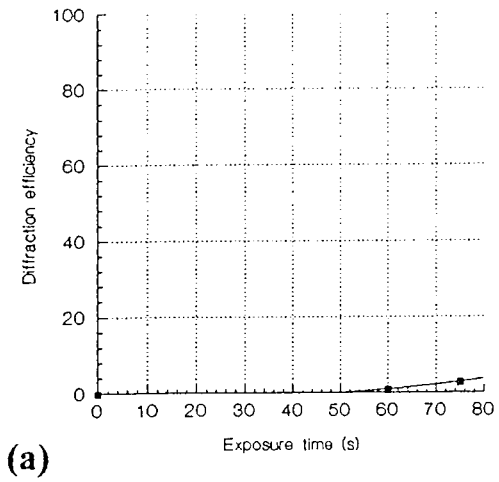

(a)

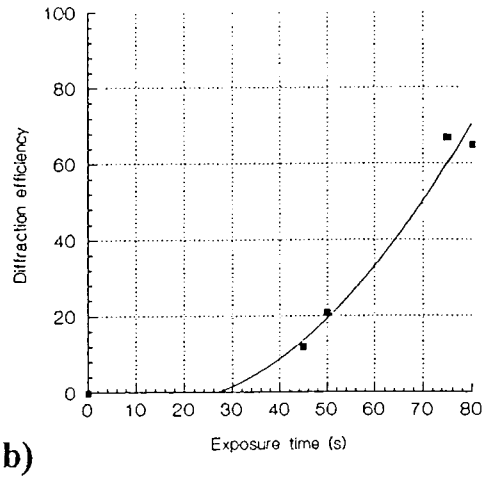

(b)

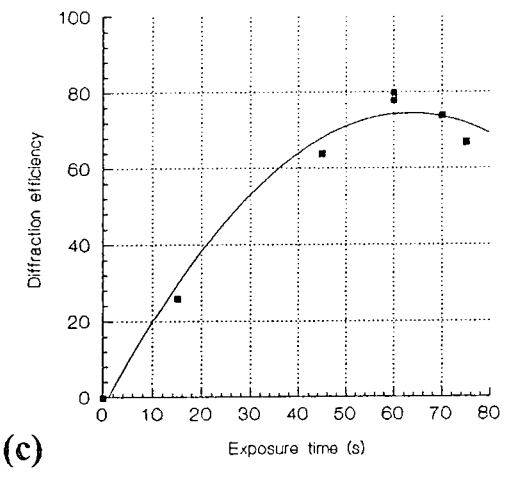

(c)

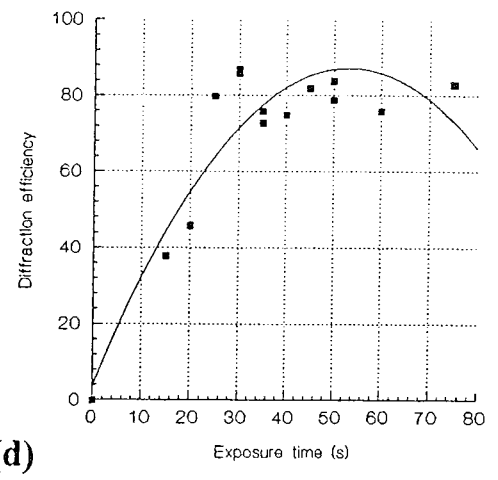

(d)

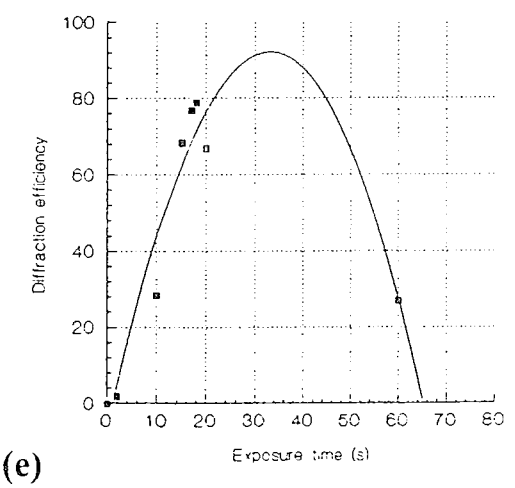

(e)

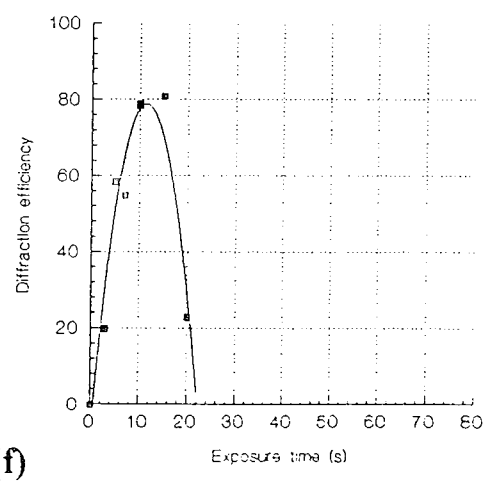

(f)

Figure 4.2 Growth of diffraction efficiency with time for different total monomer concentrations. (a) = 16.0g/l, (b) = 33.3g/l, (c) = 50.0g, (d) = 66.6g/l, (e)= 83.3g/l, (f) = 100.0g/l in the coating solution. The total power density was 5mW/cm^2. The sensitizing dye was fluorescein (1.06×10^{-3} mol/l in the coating solution.).

The relationship between acrylamide concentration and the rate of diffraction efficiency growth is not linear as can be seen from Figure 4.3 which shows the rate of growth of diffraction efficiency for various concentrations of acrylamide (initial slope of each curve in Figure 4.2).

Diffraction efficiency growth rates of 18% per second at 5mW/cm2 incident intensity, (which is very high for this fluorescein initiated formulation) can be achieved. This corresponds to a sensitivity (defined in chapter 5) of about 0.53 cm^2/mJ at high monomer concentration. However, it is difficult to form stable layers at these high monomer concentrations, due to the fact that precipitation of acrylamide (or bisacrylamide) during drying can easily occur.

The relationship between the grating growth rate and monomer concentration (g/l) is an exponential one, and the data can be fitted to the curve

$$R_g = 0.227 \times \exp(43 \times C_{mon} \times 10^{-3})$$

which is shown in Figure 4.3 as an unbroken line. The concentration of monomer is obviously critical to the sensitivity of the layers, with very high sensitivity possible. Unfortunately, as mentioned above, the amount of acrylamide which can be loaded into a given layer without affecting optical quality is limited.

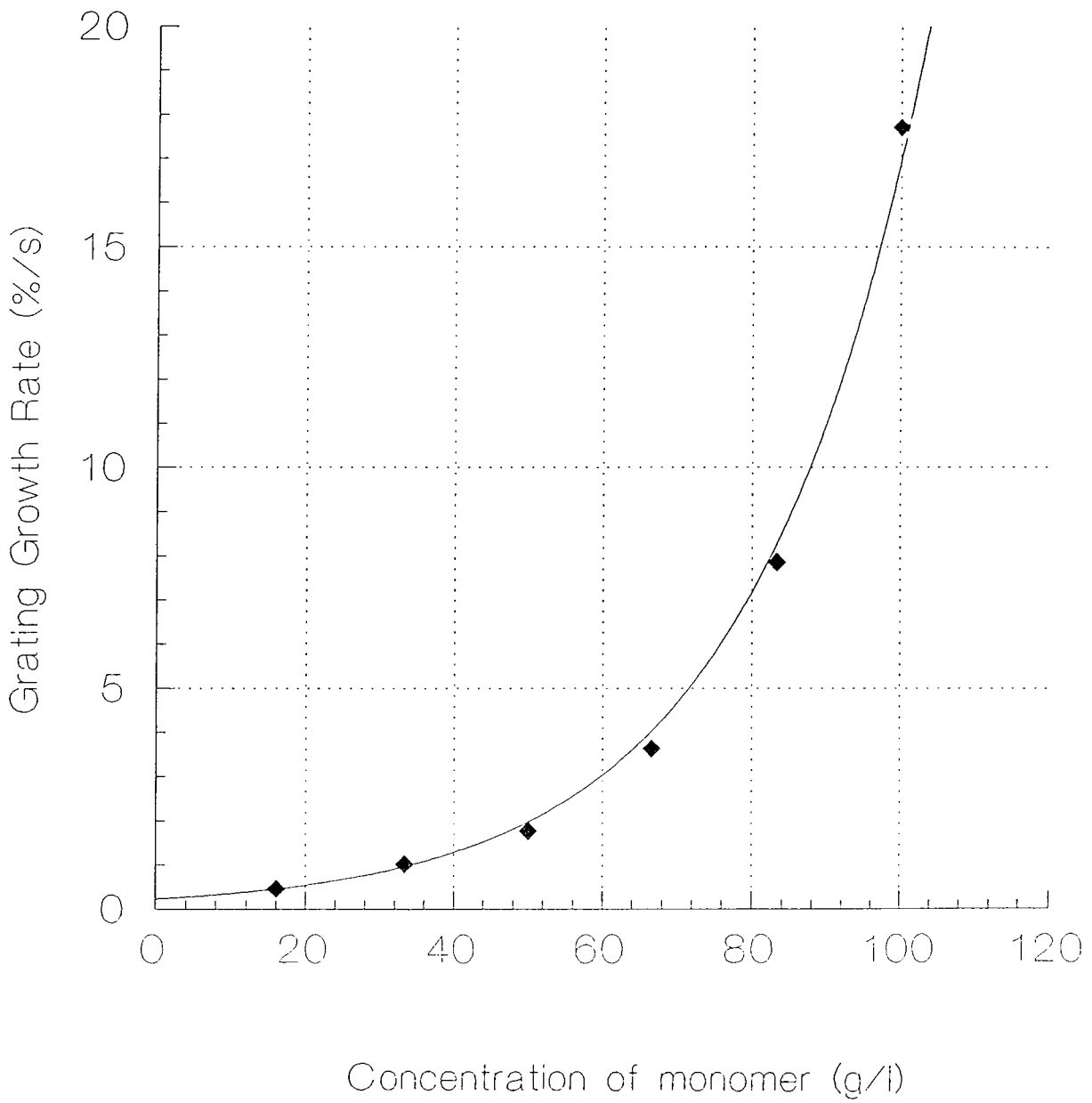

Figure 4.3 Grating growth rate for layers containing various concentrations of acrylamide. Total incident power density 5mW/cm2.

4.3.2 Optimization of dye sensitizer concentration:

The dye / electron donor sensitizing system also required detailed study. The concentration of triethanolamine has to be kept high because this is an important factor in the formation of stable layers. Increased triethanolamine concentration has been found to reduce the occurrence of precipitation on the surface of the layers. This precipitation, which renders the layer unusable, has been identified (by IR scan) as acrylamide. For these reasons the triethanolamine content was fixed at a sufficiently high level (2 ml in 25 ml of coating solution) and the dye concentration was varied.

4.3.2.1 Phloxine B study:

The diffraction efficiency growth curves for layers with various dye concentrations are shown in Figure 4.4 The sensitizing dye chosen for this particular study was phloxine B. It is immediately obvious that within this range of dye concentrations, increasing sensitizer concentration did not increase the performance of the recording material (even though it was shown in chapter 3 that increased dye concentration increases the amount of initiation occurring).

In fact these results show that the dye concentrations we had previously been using with this system were too high. The layers therefore had an excessively high optical density so that much of the light was absorbed by the dye before it had traveled very far into the layer. This results in gratings whose refractive index modulation falls off as the recording beam travels further into the layer. Further study was required, and since phloxine B is one of the least sensitive of the xanthene dyes and the incident intensity used in this study was very high, erythrosin B was used for the next study and gratings

were recorded with a moderate incident intensity. The range of dye concentrations was extended to include much lower values.

4.3.2.2 Erythrosin B study:

At an incident intensity of $4mW/cm^2$, gratings were recorded in 140μm thick layers of standard concentration differing only in the concentration of erythrosin B in the layer. Figure 4.5 shows the rate of diffraction efficiency change at a spatial frequency of 1000 lines/mm. The optimum dye concentration is approximately 1×10^{-3} mol/l. All concentrations shown are the concentration of dye molecules in the dry layer, and not the coating solution.

As the dye concentration increases from zero the sensitivity of the material increases rapidly. The reason is simple; if the concentration of dye molecules is higher, a particular light intensity will produce a greater number of initiating radicals and so increase the initiation rate. This was shown to be true in chapter 3. This increase in initiation rate causes an increase in the polymerization rate and consequently the refractive index modulation and diffraction efficiency of the grating increase at a faster rate. From the data in Figure 4.5 we can see that in layers of low absorbance the relationship between grating growth rate and dye concentration is approximately linear.

Grating growth rate (%/s) = 24.3× dye concentration (mol/l) $\times10^3$.

However, above dye concentrations of 0.3×10^{-3} mol/l in the dry layer the behavior deviates significantly from this due to the increasing absorption of the layers.

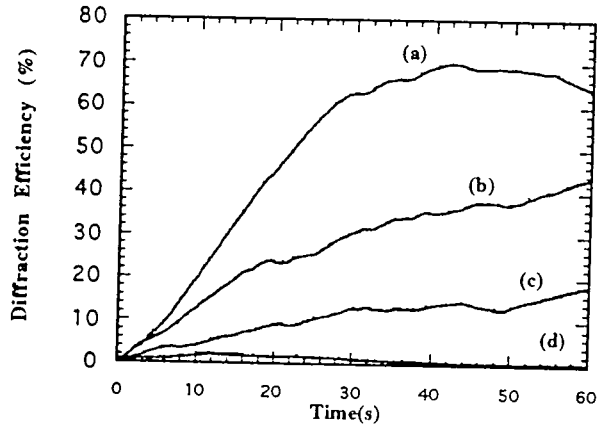

Figure 4.4 Growth of diffraction efficiency with time for layers with different concentrations of phloxine B dye. (a) = 0.5 ml, (b) = 1.0 ml, (c) = 1.5 ml, (d) = 2.0 ml of phloxine B ($1\times10^{-2}M$) in 25 ml of coating solution. The total power density of the exposing beams was $90mW/cm^2$

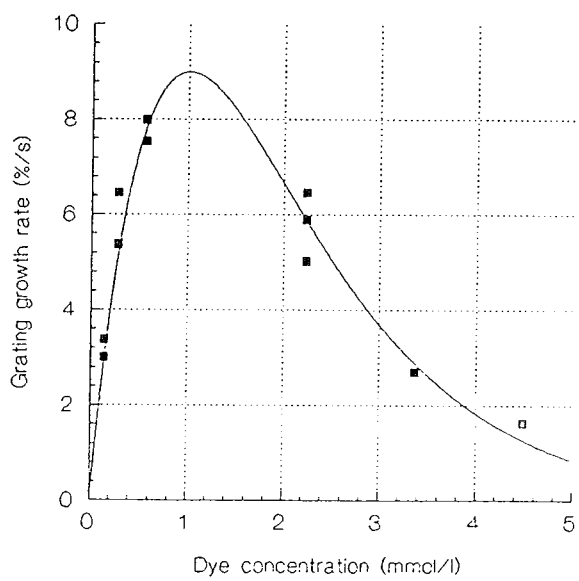

Figure 4.5 The rate of diffraction efficiency growth for 140μm layers as a function of dye concentration (erythrosin B). The incident intensity is 4mW/cm2 and the spatial frequency is 1000 lines/mm. Experimental points(■) and theoretical curve (solid line).

The more highly absorbing the layer, the more of the incident light is absorbed and used to initiate polymerization. However since we are dealing with thick layers we must consider the effect of this high absorption on the bulk of the layer. High absorption means that less of the incident light reaches the back surface of the layer. For example in a typical 100μm layer with a dye concentration of 1.121×10^{-3} mol/l erythrosin B in the dry layer, initially only 67% of the incident intensity reaches the center of the layer, and only 45% is transmitted through the full thickness of the layer (based on the extinction coefficient at 514nm, ε_{514}, of 30.8×10^{3} $dm^3mol^{-1}cm^{-1}$ determined in chapter 3). As the layer begins to bleach (this will occur more rapidly near the surface of the layer) more light will be transmitted through to the deeper regions of the layer. Therefore it should only be the rate at which the grating grows and not its ultimate diffraction efficiency which is affected by high dye concentration. This would appear to be true for (a) (b) and (c) in Figure 4.4 but (d) remains low throughout exposure.

It is possible to predict the effect of this increased absorption using the Beer Lambert law. If we assume that the rate of grating growth in a particular layer varies linearly with intensity at moderate intensities (this is discussed in chapter 5), the actual rate of grating growth can be estimated.

A highly absorbing layer, although exposed to the same initial intensity as a more transparent layer will behave as if it were exposed to a lower intensity. This is because most of the light is absorbed by the surface regions of the layer as described above leaving the bulk of the layer with a much reduced incident intensity. The effect of this absorption can be calculated. According to the Beer Lambert law the transmitted

intensity falls off exponentially as the dye concentration increases. If the ratio of this transmitted intensity to the incident intensity is known, the behavior of the highly absorbing layer can be predicted. We can write,

$$I_T = I_0 e^{-kcl}$$

where I_0 is the incident intensity, I_T is the transmitted intensity and c is the concentration of the dye in mol per liter and l the thickness of the layer in centimeters. k is 2.303 times the extinction coefficient for the dye. For any layer of known thickness and dye concentration apparent sensitivity will depend on the amount of light absorbed by the layer. In fact the photosensitive layer can be treated as if the absorption and sensitizing effects of the dye were separate, and the layer were made up of two separate layers; an absorbing layer which represents the absorbing effects of the dye and a photosensitive layer which represents the sensitizing effects of the dye. Under these particular conditions the grating growth rate of the photosensitive layer depends on the concentration of sensitizer according to the relation determined above,

$$R'_g = 24.3 \times C_{dye} \times 10^3$$

But the fraction of incident light transmitted through the absorbing layer is

$$\frac{I_0 - I_A}{I_0} = e^{-kcl}$$

The actual grating growth rate R_g will therefore be

$$R_g = 24.3 \times C_{dye} \times 10^3 \times e^{-kcl}$$

$$R_g = 24.3 \times C_{dye} \times 10^3 \times \exp(-71000 \times C_{dye} \times 0.014)$$

In Figure 4.5 this curve is plotted on the same axes as the experimental data. The experimental data fits the theoretical curve closely even at very high concentrations of dye. This confirms the model used and is also confirmation of the value of the extinction coefficient for erythrosin B measured in chapter 3. The problem of

absorption is unavoidable in any material, as some fraction of the incident light must be absorbed in order to cause an intensity dependent change in the optical properties of the material. It is particularly troublesome in thick, highly absorbing media. In any particular material of a given thickness there will be an optimum absorbance at which the response of the material is most efficient. With thinner layers we would expect the optimum dye concentration to be somewhat higher, because their grating growth rate would be less affected by the e^{-kcl} factor. Therefore higher concentrations of dye could be tolerated before absorption became a serious problem. This means polymerization would proceed at a much faster rate because of the high concentration of initiating molecules.

It should be pointed out that even with very low dye concentrations, high diffraction efficiency holographic recordings can be made using longer exposure times with the added advantage of extremely low optical density. This would be particularly useful for recording reflection holograms because the interfering beams are incident from the opposite sides of the layer. In this case the beam ratio is only 1:1 at the very center of the layer and the intensities have been greatly reduced by absorption. The ability of these layers to record good holograms at such low dye concentrations means that relatively little attenuation will occur as the beam passes through the layer, greatly improving recording conditions for this kind of hologram. (see chapter 5 for a more detailed discussion of the possibility of reflection holography in this material)

4.3.3 The relationship between electron donor and monomer concentration

Because of the need for high concentrations of triethanolamine to form stable layers, it is of little benefit for the optimization of the system to study the effect of

triethanolamine concentration. It is however important from the point of view of understanding the photochemical processes. Figure 4.6 shows diffraction efficiency growth curves for layers with four different TEA concentrations. The sensitizing dye is fluorescein. The graph shows that as the concentration of electron donor increases, the diffraction efficiency growth rate actually *decreases.*

Increased quenching of the triplet states by the triethanolamine molecule could account for a small decrease in polymerization rate and grating growth at higher triethanolamine concentrations. However, the dramatic decrease in grating growth rate with increasing triethanolamine concentration shown in Figure 4.6 cannot be accounted for by the relatively small effect of increased quenching. It is also true that in chapter 3 increased triethanolamine concentrations were observed to *increase* the rate of initiation of polymerization.

To understand the behavior observed here, it is important to remember that triethanolamine is present in the layer in very large quantities. In fact it constitutes about 45% (by weight) of the dry layer at normal concentrations. A large reduction in triethanolamine concentration will therefore reduce the volume of the dry layer considerably, increasing the concentration of acrylamide per unit volume. This increase in the effective acrylamide concentration is certainly enough to account for the increased rate of diffraction efficiency increase, when we consider the exponential relationship between monomer concentration and grating growth rate discussed in section 4.3.1. In the layer with the lowest triethanolamine content **(a)** the acrylamide concentration is 50% higher than the layer with the highest triethanolamine content **(d).**

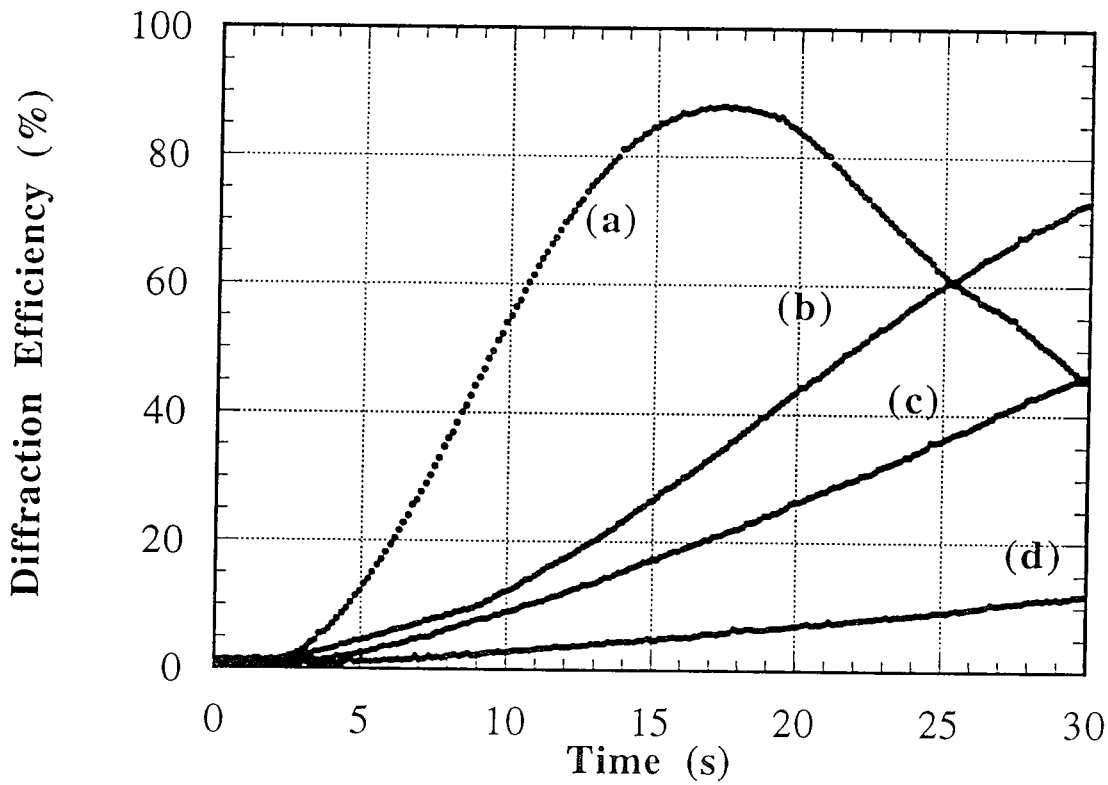

Figure 4.6 Growth of diffraction efficiency with time for four different triethanolamine concentrations. (a) = *0.50ml,* (b) = *1.00 ml,* (c) = *1.50 ml,* (d) = *2.00ml in 25 ml of coating solution. The total power density was 12mW/cm*^{2}

4.4 ALTERNATIVE SYSTEMS:

In order to fully optimize the recording material, each component of the system was replaced by several possible alternatives and the effect on the characteristics of the layer and its sensitivity to exposure was observed. This study was carried out with a view to replacing some or all of the system components with a better alternative.

4.4.1 Study of alternative monomers.

Several alternative monomers have been investigated, primarily with the intention of increasing the long-term stability of the recorded hologram or grating. This is discussed in detail in chapter 2. The choice of alternative monomers for this system is limited due to the fact that in order to be compatible with this system they must be water soluble and capable of being loaded into polyvinyl alcohol to quite a high concentration. Of the monomers investigated, none were able to form stable layers with polyvinyl alcohol. A mixture of methylene bisacrylamide and acrylamide, which forms a crosslinked copolymer on polymerization turned out to be the best choice. Apart from the advantages for hologram stability and shelf life the sensitivity of the material is improved because of the higher reactivity of bisacrylamide. Chapter 2 discusses the effect of bisacrylamide on the properties of the material.

4.4.2 Study of different electron donors.

The following electron donors were studied as possible alternatives to triethanolamine in this system. The dye was erythrosin B for this study and 0.8g of acrylamide per 25ml

of solution was used. Six plates were prepared for each electron donor and allowed to dry for two days. The standard concentrations of monomer, dye and binder were used but the electron donor was varied from 0.5g to 3.0g per 25mls of coating solution. One layer containing no acrylamide and standard electron donor concentration was also prepared in each case.

Four common electron donors were studied along with triethanolamine; these were trimethyldiamine (TMDA), dimethylethylamine (DMEA), dimethylformamide (DMF) and trimethylguanidine (TMG). None of these other electron donors were found to be compatible with this system .

With DMEA: Monomer precipitation onto the layer surface occurred during drying and did not improve at higher electron donor concentrations (as it does with triethanolamine).The optical quality was so poor due to this crystallization that the layers were completely unusable.

With DMF: The layers had a clouding on the surface but no crystals and some bleaching profiles could be obtained. However there were opaque areas and the quality was very poor. The bleaching rate (with and without acrylamide in the layer) was very much slower than with TEA. This indicates that even if the optical quality could be improved to the point where holographic gratings could be recorded, the initiation process would be extremely inefficient (see chapter 3 for explanation).

With TMG: The layers did not dry but remained very tacky and had circular growths of crystal, unlike the usual acrylamide precipitate crystals, which even appeared on the layer which contained no acrylamide. Again the layers were unusable due to poor optical quality.

With TMDA: The layers appeared very similar to DMEA with shrinkage away from the substrate edges and severe acrylamide precipitation.

This failure of these other electron donors, coupled with the fact that triethanolamine concentration cannot be reduced significantly without seriously affecting the optical quality of the photosensitive layer, indicates the importance of triethanolamine. It appears to have a role in helping the binder to hold all the constituents together in a stable and optically clear layer. The layer should perhaps be considered as a triethanolamine/polyvinyl alcohol layer in which acrylamide and dye are suspended (at standard concentrations the dried layer contains slightly *more* triethanolamine than polyvinyl alcohol).

The high triethanolamine content is responsible for the difference in physical properties observed between the pure polyvinyl alcohol and the photosensitive layer. Pure polyvinyl alcohol layers are quite hard and brittle and much more scratch resistant than the photosensitive layer. The photosensitive layer, although completely dry and of excellent optical quality, is easily scratched or indented, and is considerably more flexible than the pure polyvinyl alcohol layer. Thicker layers can be peeled from the glass to give a strong free standing film.

4.4.3 Comparison of xanthene dye sensitizers.

Finally five different xanthene dyes were compared for their efficiency in sensitizing this system for holographic recording. Since fluorescein has the highest quantum yield of excited singlet states, and the other xanthene dyes fluoresce less (i.e. have a higher yield of triplet excited states) they would be expected to be more efficient sensitizers than fluorescein which was originally used. The relative efficiencies of these five sensitizing dyes have been studied in chapter 3. As discussed previously the predicted behavior was in very close agreement with the observed results. Diffraction efficiency growth curves for identical layers sensitized with different xanthene dyes are shown in Figure 4.7.

The dyes studied were fluorescein (**FLU**) , erythrosin B (**ERB**), phloxine B (**PHB**), eosin Y (**EOY**), and rose Bengal (**ROB**). Erythrosin B and eosin Y proved to be the best sensitizers of this system. An improved formulation was then prepared with ERB as the sensitizer , and reduced dye concentration.

Figure 4.8 shows the growth curve for this optimized formulation. The power density in each beam is only 6 mW/cm^2. The layer reached a 96% diffraction efficiency in 6.5 seconds.

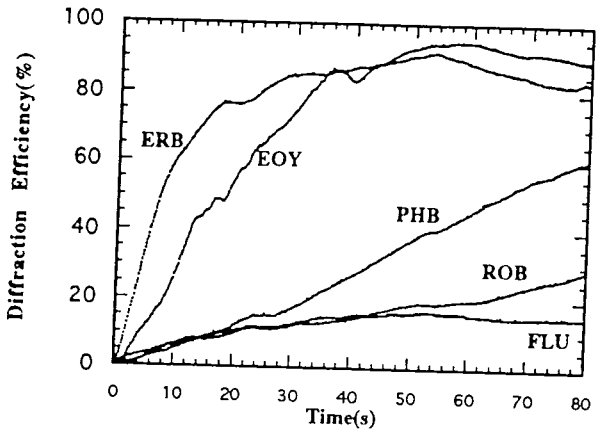

Figure 4.7 Growth of diffraction efficiency with time for identical layers sensitized with different xanthene dyes. The power density was 31 mW/cm^2 and the dye concentrations were chosen to give approximately the same initial optical density at 514nm. [ERB]=4.57×10^{-3}mol/l, [EOY]=3.30×10^{-3}mol/l, [PHB]=4.89×10^{-3} mol/l, [FLU]=4.80×10^{-3}mol/l, [ROB]= 8.36×10^{-3} mol/l *in the dry layer.*

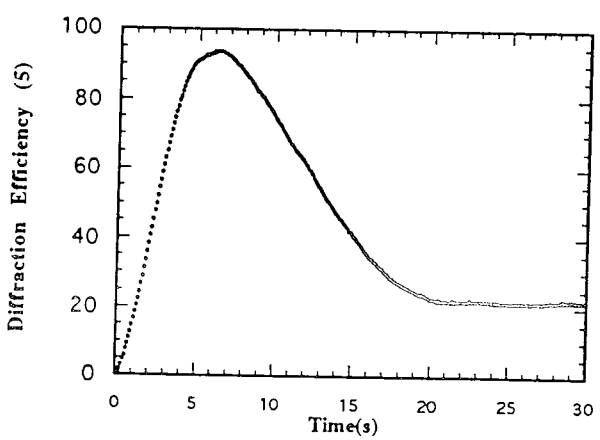

Figure 4.8 Growth curve for grating recorded in a layer prepared using 0.5 mls of ERB (1×10^{-2}M) 2.0 ml TEA and 0.8 g of monomer per 25 ml coating solution. The total power density exposing the layer is only 12 mW/cm^2.

4.4.4 Alternative binders

Several different polyvinyl alcohols were used with this system, but for the main body of the work either 99% hydrolyzed polyvinyl alcohol of 50,000g molecular weight from Aldrich Chemicals or polyvinyl alcohol of unspecified molecular weight from Reidel de Haen Chemicals were used. Both these binders made equally good layers to begin with. However, a film of small droplets of water tended to gather on the surface of a dried layer made with the Aldrich polyvinyl alcohol. This occurred approximately one hour after drying when the relative humidity was greater than 40%. The only way to ensure that this didn't occur was to dry at very low relative humidity i.e. in a desiccator. Alternatively the droplets could be 'dried off' in the desiccator after they have formed but this will not reverse the damage done by the moisture to the surface quality of the layer.

The problem was avoided by working in low humidity environments or by allowing the layers to dry in normal room conditions and then removing them to the desiccator after drying, but before the droplets have had time to form. This is most inconvenient as the layers can take anything from 4 - 48 hours to dry depending on the size of the glass plate, the volume of coating solution deposited, the percentage of water in the coating solution, and the drying conditions (temperature, relative humidity). For example, in a low relative humidity (<20%) at 20-25°C, a 2 by 2.5 inch plate on which 1.5 mls of standard concentration coating solution is deposited, will dry in 3 to 4 hours.

However a 5 by 4 inch plate on which 10 ml of the same solution is deposited in 60% relative humidity and a temperature of 10-15°C could take anything from 24 to 40 hours to dry.

Fortunately the Reidel de Haen product is an equally good binder for the system , and although it takes a little longer to dissolve in water, surface moisture does not become a problem until relative humidity values are greater than 70%.

4.5 Conclusion

The acrylamide based dry photopolymer recording material has been studied and the concentration of each component has been optimized for holographic sensitivity. Possible alternatives for each component were also discussed.

The exposure required for holographic recording has been decreased by a factor of five without increasing the monomer concentration. This was achieved by reducing the dye concentration and replacing Fluorescein with a Xanthene dye with a higher triplet state quantum yield i.e. erythrosin B. The result is an improved formulation which can achieve extremely high diffraction efficiency with relatively low exposure (80 mJ/cm2). The increase in sensitivity obtained by increasing the monomer concentration was observed to be quite substantial and further improvement of the sensitivity of the optimized formulation is certainly possible. However at higher concentrations of monomer layer preparation becomes more difficult. Since repeatability, reliability and ease of preparation are as important in a good recording material as high sensitivity, moderate concentrations of monomer were used in the optimized formulation.

---

[1] J.B.Birks, "Organic Molecular Photophysics", **2**, 153-154, John Wiley and son, New York, 1975.

5. Holographic Characterization.

5.1 Introduction:

In chapter 1 various photosensitive materials were discussed, and their suitability for holographic recording compared. Silver halide is by far the most sensitive and commonly used material. However, as higher power lasers become increasingly available it becomes possible to work with less sensitive materials and still use the short exposure times necessary for good hologram formation. Many of these other materials have advantages over silver halide such as self development, erasability, high angular selectivity or very high resolution which make them more suitable for specific holographic applications.

The self developing photopolymer material studied in this thesis has many advantages over more conventional holographic recording media, particularly for applications such as holographic interferometry. In order to fully understand the advantages and the limitations of this material a study of its holographic recording characteristics in required. In this chapter the acrylamide based photopolymer material is investigated is detail. Its holographic characteristics are studied and compared with the behavior of an ideal material.

Holographic recording materials are usually compared in terms of sensitivity and resolution, but linearity of response, maximum achievable diffraction efficiency and signal to noise ratio are also important.

5.1.1 Characteristics of an ideal holographic recording material.

In order to compare the characteristics of holographic recording materials it is first necessary to describe the behavior of an ideal recording material.

The intensity of the interference pattern produced by the interference of object beam a and reference beam r will be

$$I(x,y) = aa^* + rr^* + ra^* + r^*a$$

The fourth term is the one which carries the relevant information about the object beam. The ideal holographic recording material will record this intensity variation and the reconstructed wave will be a function of the reference wave, the exposure, and the material's response to exposure.

The ideal reconstructed wave complex amplitude w can be defined as

$$w(x,y) = 2Sk_1 t_e rr^* a \qquad (5.1)$$

where t_e is the exposure time, k_1 is a constant introduced because of differing definitions of intensity (see appendix I) and S is a complex constant characterizing the material's response to exposure. The factor of two has been introduced to enable a further reformulation in terms of visibility V.

The visibility, or contrast of an interference pattern produced by interfering two beams a and r, having amplitudes a_0 and r_0, and the same polarization, is given by[1]

$$V = \frac{2r_0 a_0 |\mu_r|}{r_0^2 + a_0^2} \qquad (5.2)$$

where μ_r is the degree of temporal coherence. This can be written in terms of the ratio of the two beam intensities, R, as follows,

$$V = |\mu_r| \frac{2\sqrt{R}}{1+R}$$

The recording arrangement is usually setup so that μ_r the degree of temporal coherence is approximately equal to one.

Returning to equation 5.1 we can determine the ideal reconstructed wave for a hologram recorded with two plane waves.

$$r = r_0 \exp(j2\pi \phi_r x), \qquad a = a_0 \exp(j2\pi \phi_a x)$$

where r_0, a_0, ϕ_r and ϕ_a are real constants. Equation 5.1 then becomes

$$w(x) = Sr_0(2k_1 t_e r_0 a_0) \exp(j2\pi \phi_a x)$$

and since

$$2k_1 t_e r_0 a_0 = k_1(a_0^2 + r_0^2) t_e V = E_0 V$$

$$w(x) = Sr_0 E_0 V \exp(j2\pi\phi_a x)$$

Where E_0 is the exposure. Under the condition of ideal reconstruction

$$S = S_0 \exp(j\sigma) = \text{constant}$$

linear recording is achieved and the reconstructed wave complex amplitude is

$$w = w_0 \exp[j(2\pi\phi_a x + \sigma)]$$

This is also a plane wave with amplitude $w_0 = Sr_0 E_0 V$. The quantity S is the holographic sensitivity. In an ideal material S is independent of average exposure, fringe visibility, and the spatial frequency over the whole hologram area.

Since the diffraction efficiency of the hologram is given by the intensity ratio

$$\eta = {w_0^2}/{r_0^2}$$

the following expression, relating diffraction efficiency to sensitivity, exposure and fringe visibility is obtained.

$$\sqrt{\eta} = SE_oV \qquad (5.3)$$

One holographic recording material is considered more sensitive than another if, for fixed illumination conditions, less exposure is required to produce a hologram of specified diffraction efficiency. If, for a particular recording the visibility is unity then a graph of the square root of diffraction efficiency versus exposure will give a straight line the slope of which is S, the holographic sensitivity. The units of S are m^2/J or cm^2/mJ

Unfortunately, quoting the sensitivity of the holographic recording material gives no indication of the maximum achievable diffraction efficiency; it merely characterizes the speed of response of the material. In the literature quantities of 'energy per unit area' required to obtain a particular diffraction efficiency are often quoted as an indication of sensitivity, instead of simply stating the formal sensitivity S of the material. This is often more informative as a particular material could have a very high sensitivity but only be capable of reaching very low diffraction efficiencies.

A frequent problem with the formal definition of sensitivity is that for a real material the plot of $\sqrt{\eta}$ versus E_o with V constant is rarely a perfect straight line. This is overcome, where possible, by taking the slope of the straight portion of the curve.

The best way to compare materials is actually to compare the shape of the $\sqrt{\eta}$ - V curve, which also gives a straight line for a fixed value of E_0 in an ideal recording material. An example of such a plot for an ideal material is given in Figure 5.1.

For a real material much useful information can be obtained from the $\sqrt{\eta}$ - V curve. The straight line portion of the graph shows the range of visibilities for which recording is linear and the diffraction efficiency obtained for a particular exposure at any value of fringe visibility can be read directly from the graph. Figure 5.2 shows a typical $\sqrt{\eta}$ - V curve for a real material.

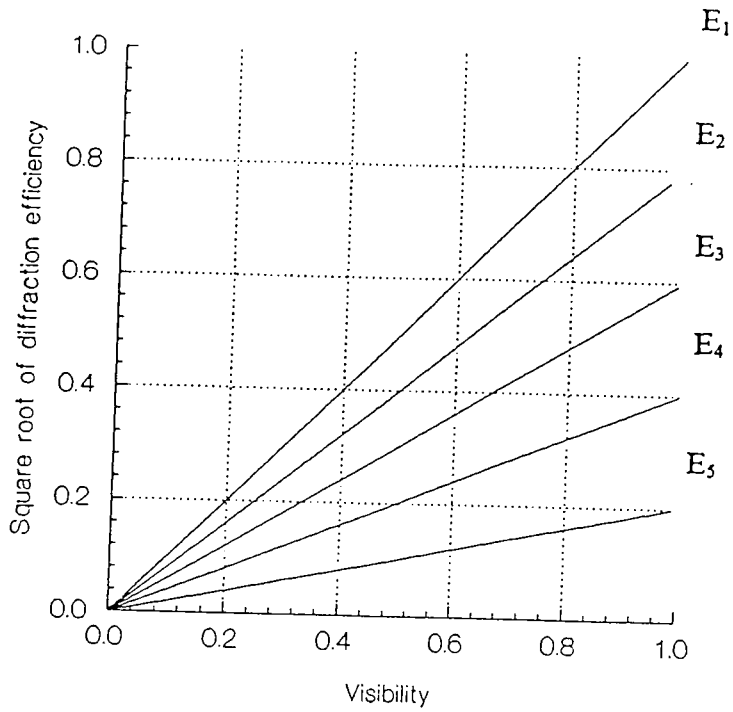

Figure 5.1 $\sqrt{\eta}$ *- V curves for an ideal material at various exposures (E).*

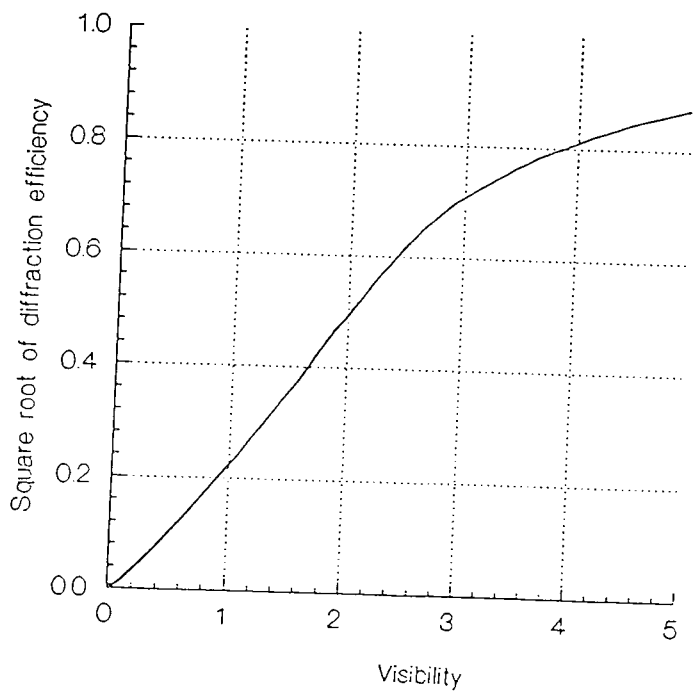

Figure 5.2 An example of a typical $\sqrt{\eta}$ *- V curve for a particular exposure for a real material.*

5.1.2 Modulation transfer function and recording resolution

Successful hologram recording depends first of all on the existence of high contrast ($V\cong1$) interference fringes. High contrast or large modulation depth implies that the amplitude of the spatially varying cosine term is large in comparison with the spatially constant term in the interference pattern. Thus high contrast in the interference pattern implies bright images. Contrast is quantitatively measured by the parameter V defined in equation 5.2. It is affected by the degree of coherence between the interfering beams, the angle between the directions of the polarization of the beams and the ratio of intensities of the two beams measured in the plane of the interference pattern. The contrast of the intensity distribution to which the material is actually exposed, however, is always different. There is always a certain amount of lateral spreading of light within the recording material determined by its scattering properties and coefficient of absorption. Because of this the actual modulation of intensity within the recording material is always less than in the original interference pattern.

For a given spatial frequency f the ratio of $V'(f)$, the contrast of the intensity distribution within the material, to $V(f)$, the input visibility is termed the modulation transfer function. This parameter characterizes the relative response of the material at different spatial frequencies.

$$M(f)=V'(f)/V(f)$$

In an ideal material this would be unity at all spatial frequencies, but in real materials it will always be less than one and is usually only greater than zero for a specific band of spatial frequencies. For most real materials a graph of diffraction efficiency versus

spatial frequency of the recorded grating will show that the modulation transfer function is essentially constant up to a certain cutoff spatial frequency above which the material response decreases rapidly. This cutoff is usually quoted as the maximum resolution of the material.

5.2 Experimental procedure.

It is usually preferable when studying holographic recording materials to record simple diffraction gratings rather than the complex interference patterns which make up most holograms. This makes comparison simple and allows the direct measurement or calculation of several important characteristics such as the refractive index modulation, the diffraction efficiency and the effective thickness of the grating in the layer.

The basic apparatus used to record holographic gratings is shown in Figure 5.3, in which two 514nm beams cross to produce the appropriate interference pattern. The photosensitive material responds and develops a spatial modulation of refractive index which corresponds to the spatial modulation of light intensity in the interference pattern, thus forming a grating.

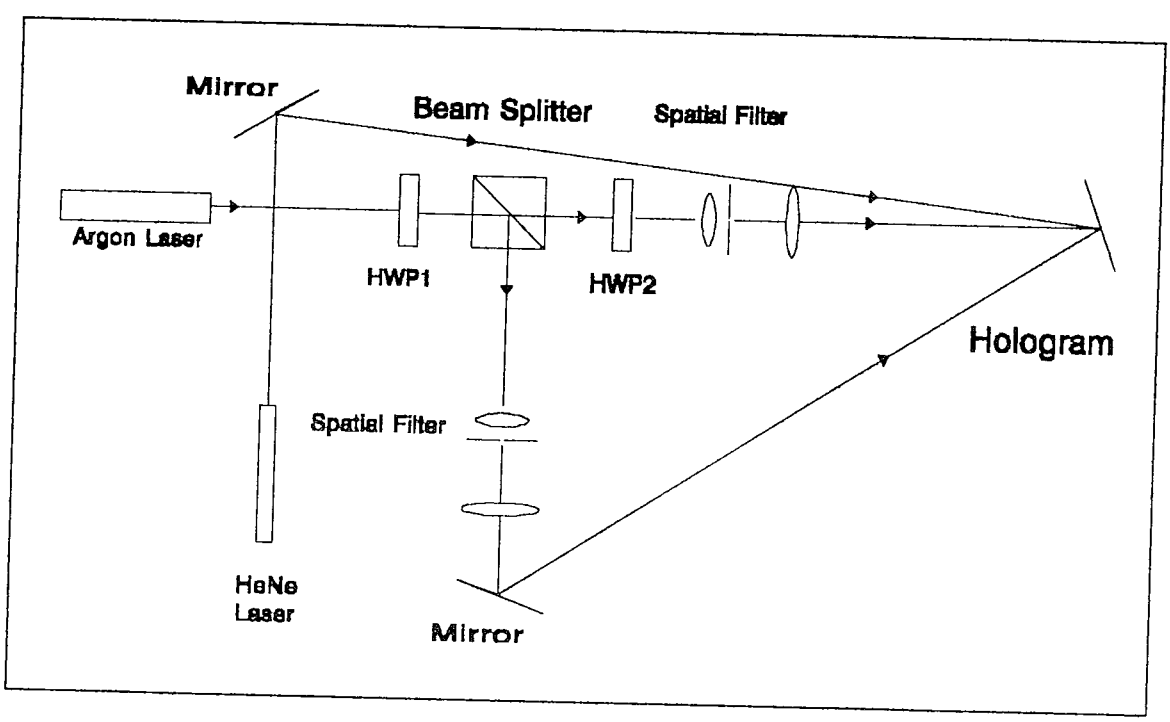

Figure 5.3 Recording apparatus used in the investigation of the relative response of the material at different fringe visibilities.

The Argon ion laser (Lexel Model 95, 514nm) was used in recording and the Helium Neon laser (Unilab, 633nm) was used in reconstruction. This facilitated real-time monitoring of the diffraction efficiency growth *during* recording. The 514nm light from the Argon ion laser was split by the beam splitting system and each beam was spatially filtered, collimated and directed towards the sample as shown. The angle between the incident beams was 30°, so the spatial frequency was approximately 1000 lines/mm. For all experiments the entire setup was arranged on a 3m × 1.3m Newport research table top with pneumatic isolation on all four support legs in order to minimize the transmission of vibrations from the floor to the table. Newport magnetic stands were used to hold the optical components in position. The coated glass plate in which the gratings were to be recorded was clamped in position with the light incident on the coated side, the position of the holder having been previously adjusted so that the two collimated beams overlapped perfectly in the plane of the photosensitive layer and the plate normal bisected the inter beam angle. This ensured that the beam ratio was constant across the illuminated area[2] and that the grating was unslanted.

Care was taken to avoid air currents and temperature gradients during recording and the experiments were always carried out in a darkroom. In order to maintain maximum fringe visibility both beams were vertically polarized. Coherence, however, was not a problem in this case because the laser used had a coherence length of greater than 3 meters. Accurate control of exposure was usually achieved by an electronic shutter system (UniBlitz T132 timer and VS25 shutter) in the path of the unexpanded laser beam as it emerged from the Argon ion laser.

It was necessary to ensure that the Helium Neon laser was incident at the Bragg angle of the recorded grating for reconstruction with 633nm light. It was particularly

important to be precise when recording on thicker layers as angular halfwidths of less than one degree were common and a small deviation from the Bragg angle would cause a large drop in the measured diffraction efficiency.

5.2.1 Experimental control of the beam intensity ratio.

The beam splitter consisted of two 514nm half wave plates and a polarizing beam splitter. The incoming vertically plane polarized light was rotated to an appropriate angle by the first half wave plate (HWP1), and then its vertical and horizontal components were separated by the polarizing beam splitter. The transmitted horizontal component was then rotated to vertical polarization by the second half wave plate (HWP2). The result was two vertically plane polarized beams, whose relative intensities depended on the angle of the fast axis of the first half wave plate relative to the plane of polarization of the incoming beam. For most experiments reported here, the axis of the HWP1 was 22.5° to the vertical so that the plane of polarization was rotated through 45° and the vertical and horizontal components were equal. In those cases where fringe visibilities of less than one were required the beam ratio was easily controlled by rotating HWP1.

5.2.2 Grating analysis

Diffraction efficiency at the Bragg angle could either be monitored in real-time or , if Bragg incidence was not possible during exposure, it could be measured after a specific exposure time by rotating the sample so that the 633nm light from the HeNe laser was incident at the Bragg angle, and measuring the intensity of the diffracted and zero order beams with a Newport optical power meter (model 840). Diffraction efficiency is defined as described in chapter 4 as either the ratio of the diffracted 1st order beam

$$\eta = \frac{I_1}{I_i}$$

intensity (I_1) to the intensity of the incident beam (I_i), or the ratio of the intensity of the 1st order beam (I_1) to the sum of the intensities of the 1st and zero order (I_1+I_0).

$$\eta' = \frac{I_1}{I_0 + I_1}$$

5.2.3 Apparatus for the investigation of the modulation transfer function.

An apparatus was designed which would allow the angle between the recording beams to be easily adjusted in order to facilitate spatial frequency changes. It consisted of a front silvered mirror mounted at right angles to the photosensitive plate, which was held in place against a steel support by two strong ceramic magnets. A single expanded beam was incident half on the mirror and half directly on the photosensitive plate. The beam reflected from the mirror interfered with the directly incident beam to form a grating. The spatial frequency of this grating depended on the angle that the

incident beam made with the mirror surface. Since in practice, the incident beam was Gaussian rather than uniform in intensity, the center of the beam was arranged to fall on the boundary between the mirror and the plate. This ensured that the beam ratio was everywhere equal to one. The apparatus, shown in Figure 5.4 had several advantages over the original setup.

(1) The apparatus was more stable and less susceptible to vibration making measurements more reliable and repeatable. This was because the mirror and photosensitive plate were attached to one another and mounted on the same base; therefore any disturbance affected both in the same way and did not affect the interference pattern.

(2) The spatial frequency of the recorded grating was changed by simply altering the angle at which the incident light approached the mirror. This changed the angle θ between the two beams and therefore the spatial frequency but always recorded an unslanted grating (The geometry of the setup ensures that the plate normal always bisects the angle θ). In the original experimental setup changing the spatial frequency involved resetting one whole arm of the apparatus.

(3) The path lengths of the interfering beams were almost identical, ensuring that coherence is achieved even if a low coherence laser was used to record the grating.

(4) The interference pattern was formed with a wavefront splitting arrangement rather than an amplitude splitting device, effectively doubling the available power of the laser.

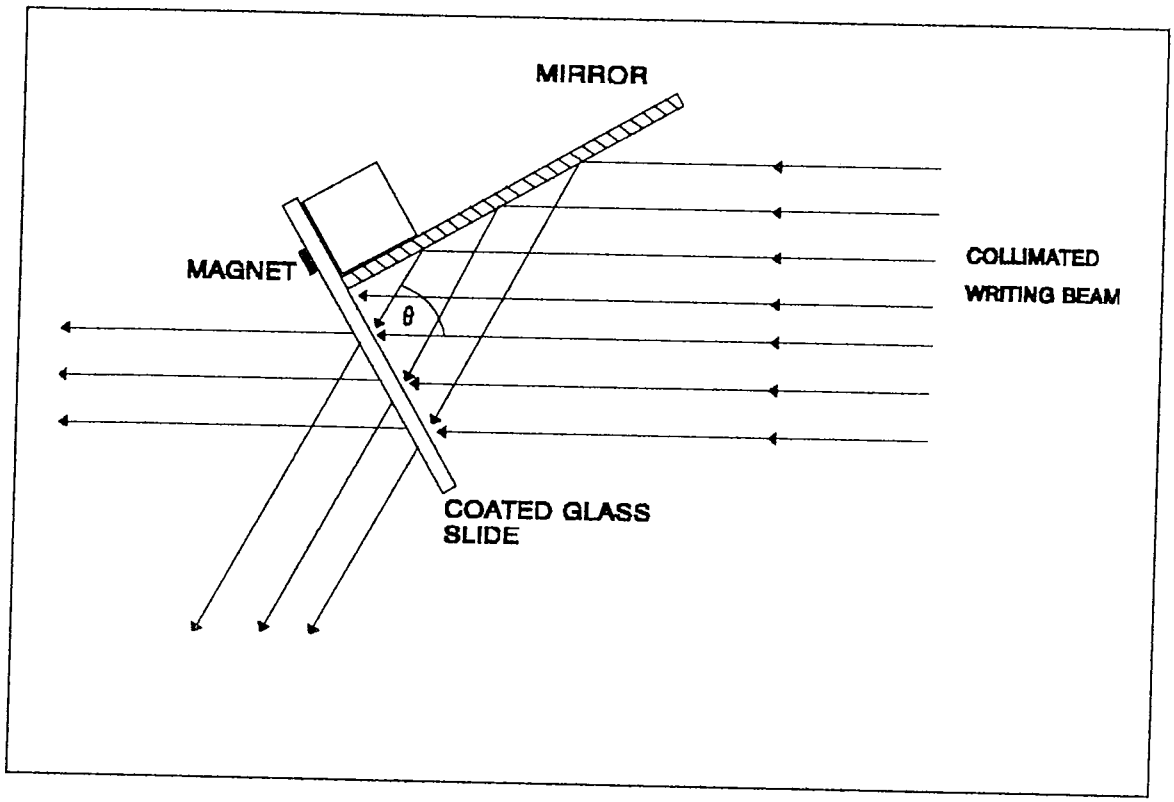

Figure 5.4 Wavefront splitting arrangement used to form an unslanted grating with maximum fringe visibility. The spatial frequency of the interference pattern depends on the angle θ.

(5)The optical power meter monitored the growth of the grating at the Bragg angle during recording and the data obtained was displayed on a Gould storage oscilloscope or, more conveniently, a data acquisition system on a PC .

(6) The table on which the mirror and coated slide were mounted was an ORIEL encoder micrometer motorized driver rotator which was controlled remotely by an ORIEL controller. The center of rotation was fixed at the point in the photosensitive layer where the HeNe beam probed the grating (Figure 5.5). Rotation through the Bragg angle was then simple, allowing the angular selectivity of each grating to be routinely determined.

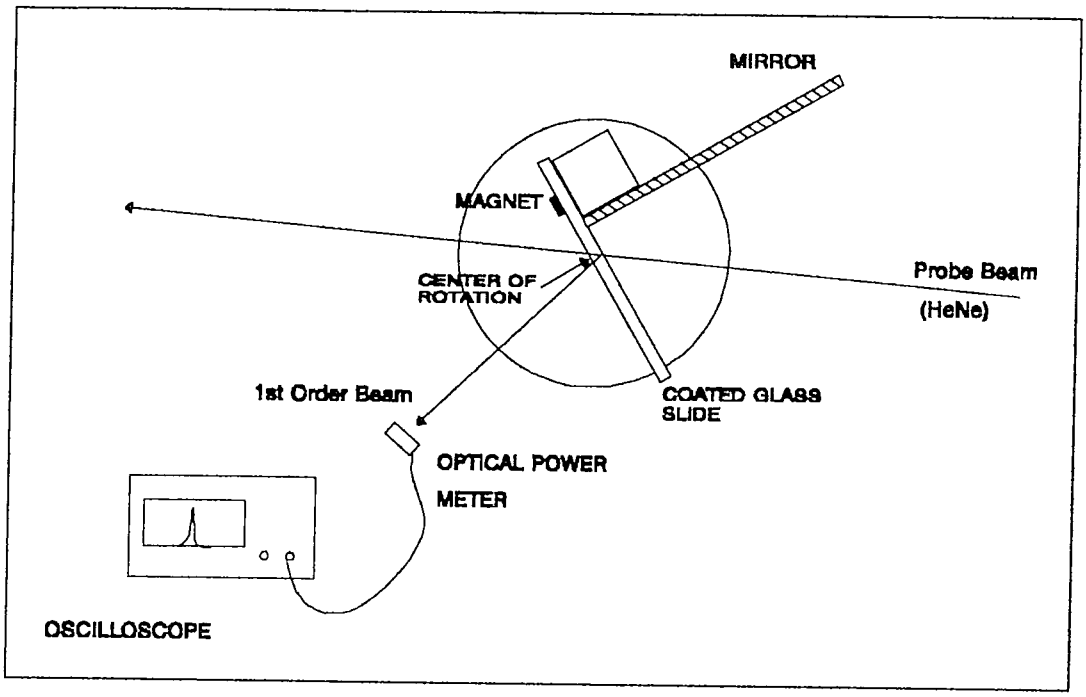

Figure 5.5 Apparatus used in the investigation of the relative response of the material at different spatial frequencies.

5.2.4 Photosensitive layer preparation.

The standard concentration layers were prepared as follows. All the samples in this chapter were prepared with these concentrations except were otherwise stated. 2.0 ml of triethanolamine was added to 2.7 ml of water and mixed well. The mixture was then added to 17.5 ml of a stock polyvinyl alcohol solution (10%) along with 2.0 ml of dye solution (concentration chosen to give each solution approximately the same initial optical density). Finally the monomer was added; 0.6g of acrylamide and 0.2 g of bisacrylamide. The total volume was approximately 25 ml. 10 ml of this solution spread on a 5" by 4" leveled glass plate gave a dry layer of 150 micron thickness. Drying time was usually 36 - 48 hours.

5.3 Holographic characteristics of the recording material.

The characteristics of an ideal holographic recording material were discussed above. In this section the holographic characteristics of the photopolymer material are discussed in terms of sensitivity, diffraction efficiency, linearity of response , material resolution and noise.

5.3.1 Holographic sensitivity of the material.

A typical grating growth curve is shown in Figure 5.6. It shows the increase in diffraction efficiency with exposure time for low diffraction efficiency, and was obtained with the setup shown in section 5.2.1 with a beam ratio of 1:1 and a total incident intensity of 6mW/cm^2. The thickness of the photosensitive layer (standard formulation) was 56 μm and the spatial frequency of the grating was approximately 1000 lines/mm. At low diffraction efficiencies we would expect the square root of diffraction efficiency to be directly proportional to the exposure, and therefore the graph shown in Figure 5.7 would be a straight line. It is observed that the graph is linear at low diffraction efficiencies. The slope of this linear part will give the formal sensitivity of the material, a value of 9×10^{-3} cm^2/mJ. An exposure of 300 mJ/cm^2 was required to achieve an 40% diffraction efficiency.

This photopolymer material usually produces gratings with very high diffraction efficiencies. The linear relationship between the square root of the diffraction efficiency

and exposure clearly only holds at very low diffraction efficiency. Because of this the formal sensitivity is not a very representative parameter for characterizing the photopolymer material's response to exposure. The grating growth curve, where diffraction efficiency is plotted against time for a particular value of total intensity is usually linear to a much higher value of diffraction efficiency. For this reason the initial grating growth rate, that is the initial slope of the grating growth curve, is often used to characterize the response of the material. In Figure 5.6 the grating growth rate has a value of 1.5 %/s.

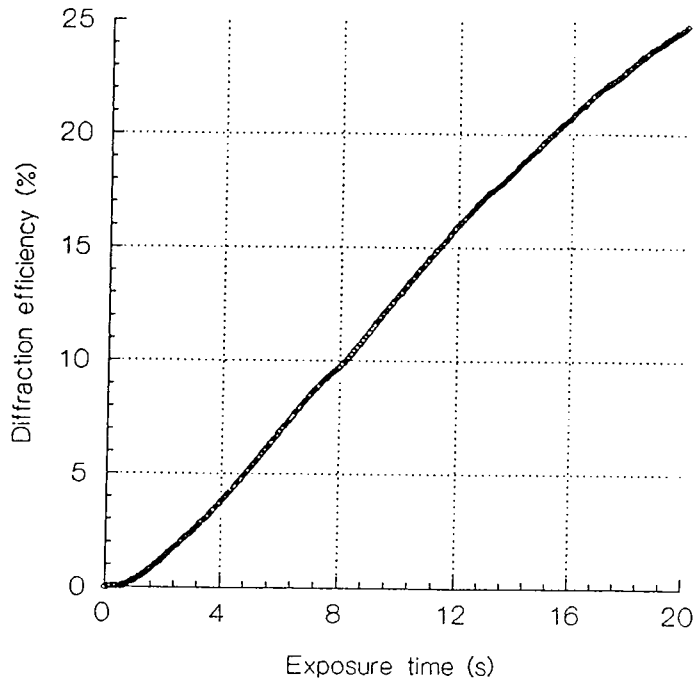

Figure 5.6 Diffraction efficiency growth curve for a 100μm layer of standard formulation.

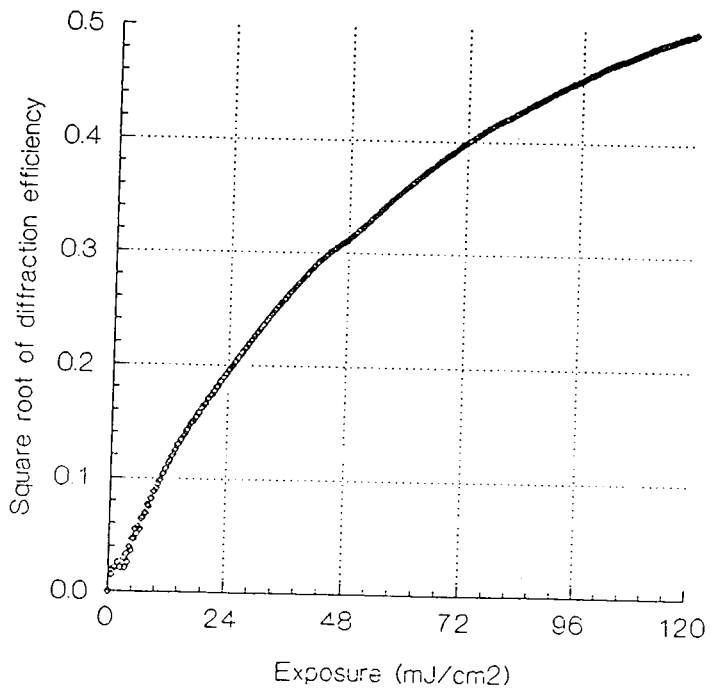

Figure 5.7. Square root of diffraction efficiency as a function of exposure for the layer inFigure 5.6.

5.3.2 The effect of incident intensity on recording

In an ideal material the reciprocity law would be obeyed under all conditions, in other words, the same exposure would always lead to the same diffraction efficiency regardless of the incident intensity. An exposure to 1mW/cm^2 for 200 seconds would produce he same result as exposure to 200mW/cm^2 for 1 second. In real materials there is usually a range of intensities over which this is true, for example silver halide materials have good reciprocity over a broad range of incident intensities but are well known for their lack of reciprocity at very low intensities[3] . The photopolymer material was exposed to a range of incident intensities and in each case the diffraction efficiency increase per second was obtained. This should increase linearly with intensity if there is true reciprocity. It is observed in Figure 5.8 that there is a linear relationship between grating growth rate and incident intensity up to an incident intensity of 30 mW/cm^2. Above this figure little increase is observed , and grating growth becomes erratic and loses repeatability. This is because the polymerization and diffusion rates will not increase indefinitely with an increasing supply of photons, but will reach some maximum rate which cannot be surpassed regardless of how fast initiating radicals are produced. It was pointed out in chapter 3 that there is no reciprocity failure in the bleaching curves obtained in these layers up to incident intensities much higher than 30 mW/cm2. It can therefore be assumed that the actual physical grating growth processes are responsible for this behavior and not the absorption or initiation processes studied in chapter 3. As well as giving an upper limit to the useful intensities that can be used for holographic recording, these experiments also reveal some important information about the physical growth of the refractive index modulation and diffraction efficiency. Regardless of the rate of initiation the polymerization and

diffusion processes cannot proceed much faster than they do at an incident intensity of 30mW/cm^2, so the diffraction efficiency of these gratings (of thickness 140μm) cannot increase at a rate faster than 10-12% per second.

From the point of view of holographic recording characteristics, it can be concluded that the recording will be extremely non linear at intensities greater than 30 mW/ cm^2

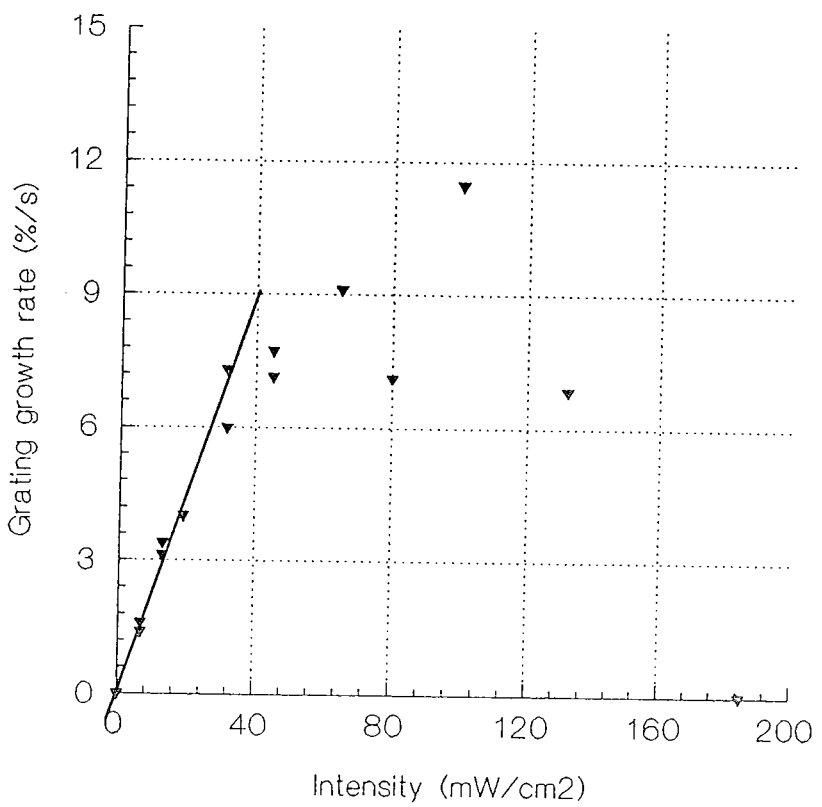

Figure 5.8 Grating growth rate versus incident intensity in mW/cm^2. The standard photosensitive formulation was used to prepare layers with a thickness of 140μm.

5.3.3 Variation of the fringe visibility

Figure 5.9 shows that the diffraction efficiency obtained at a particular exposure decreases as the intensity ratio of the two recording beams is increased.

The same exposure that records a 95% diffraction efficiency at a recording beam ratio of 1:1 will record a grating with a diffraction efficiency of only 35% at a beam ratio of 15:1 even though the combined power of the two beams remains the same. The visibility V associated with each of these beam ratios can be calculated (assuming they are both vertically polarized and the beams are perfectly coherent). The square root of the diffraction efficiency can be plotted against the visibility in order to compare the recording material to an ideal recording material. The ideal response to variations in fringe visibility was discussed in section 5.1.1. Real materials rarely show this linear relationship; more usual is a linear increase from zero followed by a 'leveling out' of the $\sqrt{\eta}$-V curve at visiblilities approaching 1. This is why in practical holography an average beam ratio other than 1:1 is usually used[4]. Figure 5.10 shows a study of the photopolymer material at six different exposures over a range of fringe visibilities. Layer thickness is approximately 100 μm and the standard formulation was used to prepare the layers. Not only does the photopolymer material show a 'leveling out' of the $\sqrt{\eta}$-V at high visibilities, but also shows a fall off in response at very low visibilities. The graph seems to indicate that there is a minimum visibility that is required before the material responds.

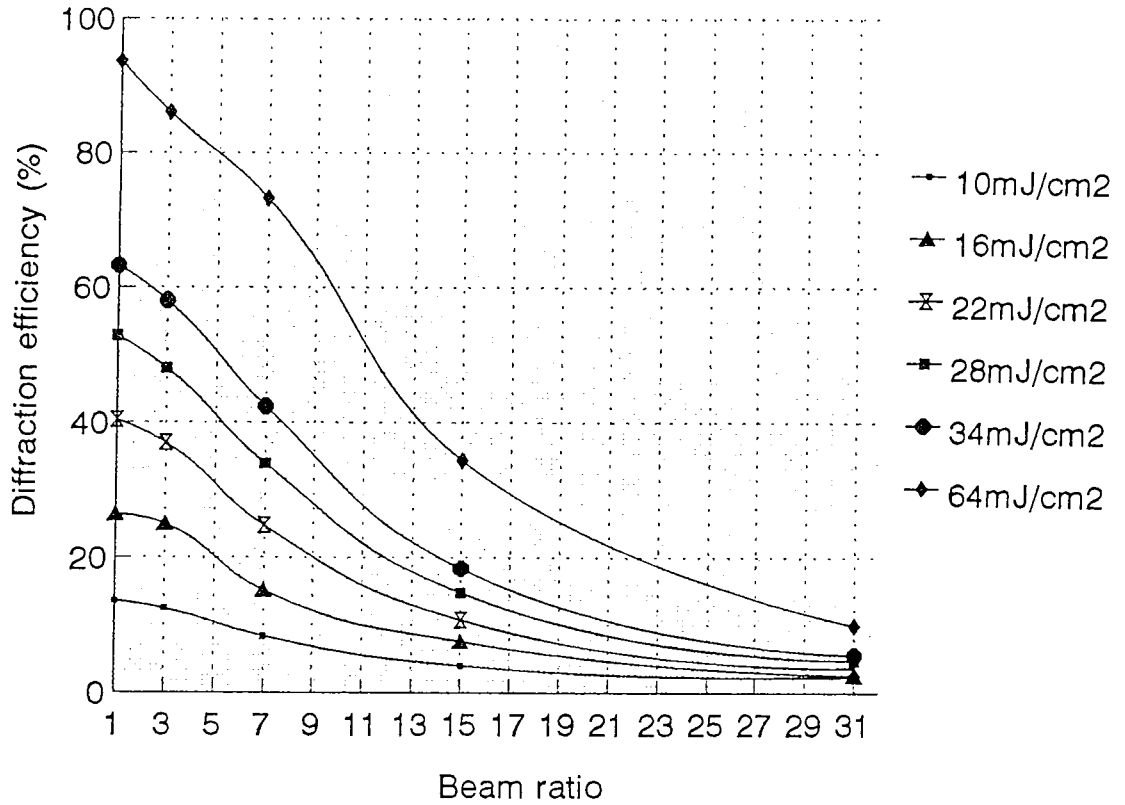

Figure 5.9 Diffraction efficiency as a function of beam ratio for a series of different exposures.

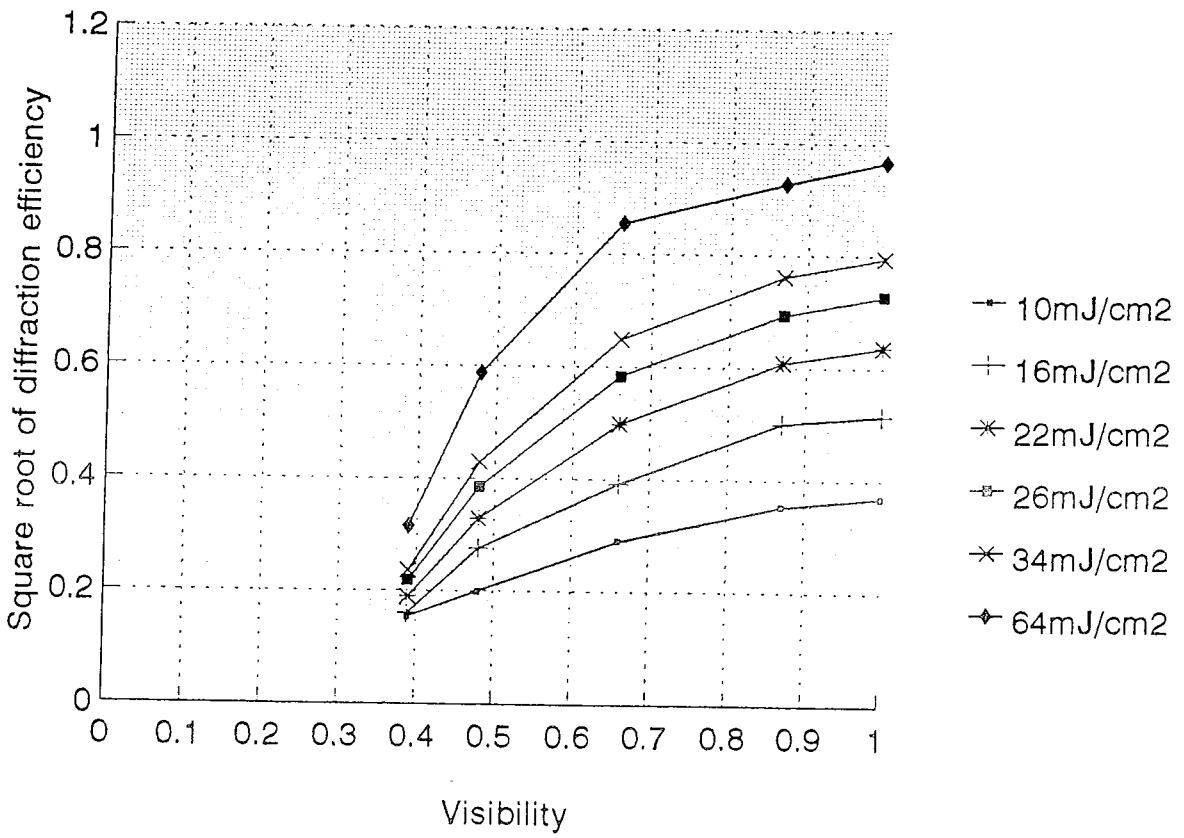

Figure 5.10 Diffraction efficiency versus fringe visibility. Total incident intensity was 6mW/cm^2

Like any self developing material, this self developing photopolymer has inherent lack of linearity. By virtue of the fact that the material records in real-time, the wavefront to which the material is responding is itself affected by the changes it is causing in the material; the result is a nonlinear response to exposure.

In effect, this means that it cannot be assumed that the fringe visibility to which the material is originally exposed is the visibility of the fringes throughout recording. For example take a grating being recorded in a material with a beam intensity ratio of 7:1. When this grating has reached a 60% diffraction efficiency, 60% of each beam has been coupled into the other beam by the time the beams have propagated through the material and reached the back face of the photosensitive layer. This means that the beam ratio at this point is actually $7.6 : 5.2 \approx 3:2$. So as the growing grating reaches 60% diffraction efficiency the beam ratio inside the layer varies from 1:7 at the front surface to 3:2 at the back surface of the photosensitive layer. The corresponding fringe visbilities are 0.66 and 0.98, so obviously there is an overall increase in fringe visibility within the layer and the diffraction efficiency obtained with a particular beam ratio will be greater than the predicted value.

The other major feature of the results obtained here is that unlike other materials there appears to be a cutoff value of visibility below which the material will not respond. This can be explained by the fact that the recording process is dependent on there being a difference between the polymerization rates at the intensity maxima and minima so that diffusion of monomer can occur. If the visibility is greatly reduced the potential for diffusion is reduced and the diffraction efficiency is therefore reduced. From these results it would appear that there is a minimum value of visibility between 0.1 and 0.2 below which essentially uniform polymerization occurs and no grating is recorded. It

can be concluded from theses results that the best linearity for recording is obtained with visibilties below 0.7 but above 0.2. This can be achieved by keeping beam ratios greater than about 7:1 but very low visibility fringes in the hologram will not be recorded and some detail may be lost in the reconstructed image.

5.3.4 Material resolution and modulation transfer function.

In order to investigate the relative response of the recording material at a range of spatial frequencies, gratings were recorded at a range of inter beam angles. As discussed in section 5.1.2, for most materials the graph of diffraction efficiency versus spatial frequency of the recorded grating is essentially flat up to a certain cutoff spatial frequency characteristic of that material. This means that the modulation transfer function does not depend on spatial frequency over that range. For accurate reconstruction the recording material should respond to all spatial frequencies in the interference pattern equally. Unfortunately this photopolymer recording material has a modulation transfer function which is very much dependent on spatial frequency. This can be clearly seen in Figure 5.11. An exposure of 360mJ/cm^2 was used on layers of 60μm thickness and standard formulation, which will usually give a diffraction efficiency close to 100% at 1000 lines/mm and the spatial frequency was varied from 300 lines/mm up to nearly 3000 lines/mm. As can be seen from Figure 5.11 the optimum response is at about 1500 lines /mm with the diffraction efficiency dropping to half the maximum value at 600 lines/mm and 2200 lines/mm This is very interesting from the point of view of understanding the microscopic recording processes within the material but unfortunately means that its holographic response is somewhat unusual. The effect of this peak in the graph on the reconstruction of an image in a

normal off axis transmission hologram would be to form a brighter image of the part of the object from which the scattered rays make an angle between say 30° and 70° with the reference beam (assuming 514nm recording)

The physical explanation for the shape of this curve in terms of the recording processes can be understood as follows.

Chapter 6 will show that in this material the refractive index change is caused, in part, by the diffusion of monomer from the dark fringe regions into the polymerizing bright fringe regions. However the diffusion of monomer occurs very rapidly, and even at a spatial frequency of only 250 lines/mm (fringe spacing 4μm) diffusion is immediate. For this reason the increase in the response of the material at higher spatial frequencies can not be explained by increased monomer diffusion.

The xanthene dye sensitizers, on the other hand are large rigid molecules whose diffusion coefficient is much smaller. This is borne out by the fact that transient amplitude gratings can be recorded in xanthene dye[5] and methylene blue dye doped polyvinyl alcohol layers. However diffusion of dye sensitizer does occur during normal holographic recording in our material. Even in a grating recorded with a high visibility fringe pattern all the dye present gets bleached. This indicates that the unexposed dye in the dark fringe areas must diffuse into the bright fringe areas to replace the dye molecules used in bleaching and initiation, and then be bleached itself.

If the dye being 'used up' in the bright fringe areas can be easily replaced by the dye molecules diffusing in from the dark fringe areas (i.e. if the fringe spacing is small), the growth rate of the grating will be improved. It has already been shown in chapter 4 that the rate of increase of the diffraction efficiency is directly related to the amount of

available dye sensitizer. As can be seen from the graph in Figure 5.11, even at very low spatial frequencies, where diffusion is restricted, the diffraction efficiency reaches 60% in 60 seconds of exposure. As the fringe spacing (and therefore the diffusion distance) decreases, the diffusion time should be reduced (as a function of the square of the diffusion distance) and more dye becomes available for initiation of polymerization in the bright fringe regions. Figure 5.11 shows that the optimum diffusion distance corresponds to a spatial frequency of 1200 lines/mm and is therefore about 0.85μm. At this fringe spacing the diffraction efficiency reached in 60 seconds has almost doubled and is just over 100% (i.e. slightly overmodulated). This is because there was almost twice as much sensitizer available in the bright fringe regions during these 60 seconds than there was when the spatial frequency was low. Diffusion of dye and monomer and the physical processes leading to hologram formation will be discussed further in chapter 6.

The relatively sudden drop in sensitivity at spatial frequencies above 1800 lines/mm can be explained by the limited resolution of the material. In a polymerizable photopolymer recording material, the resolution will be limited by the mobility of the initiating species. If the free radicals are unable to migrate away from the position in which they were formed then polymerization will be very localized to the high intensity fringes and resolution will be extremely high. However, if the free radicals are able to move say 0.2μm during the recording time then the polymerized area will broaden and cause nonlinearity. This is a problem in itself but when the fringe width is reduced it becomes much more serious. If the initiating species can move a distance of 0.2μm during recording then fringe patterns with fringe widths below 0.4 μm cannot be recorded because almost uniform polymerization will occur. This is probably why resolution

capabilities are always lower in liquid photopolymer materials[6] compared to dry photopolymer recording materials; the mobility of initiating species is naturally higher in liquids. The results shown here show a very poor response at spatial frequencies of about 3000 lines/mm. This would correspond to the initiating free radical diffusing a distance of 0.16μm during recording. This may indicate that the characteristics of this material could be greatly improved by decreasing the permeability of the photosensitive layer, although the reduced diffusion would probably mean a reduction in sensitivity. A less permeable type of polyvinyl alcohol binder may be all that is required to achieve this (polyvinyl alcohol can have widely varying solubilities and physical properties depending on its molecular weight and percentage hydrolysis), or perhaps a short uniform pre-exposure to cause a limited degree of polymerization and thereby reduce the permeability of the layer

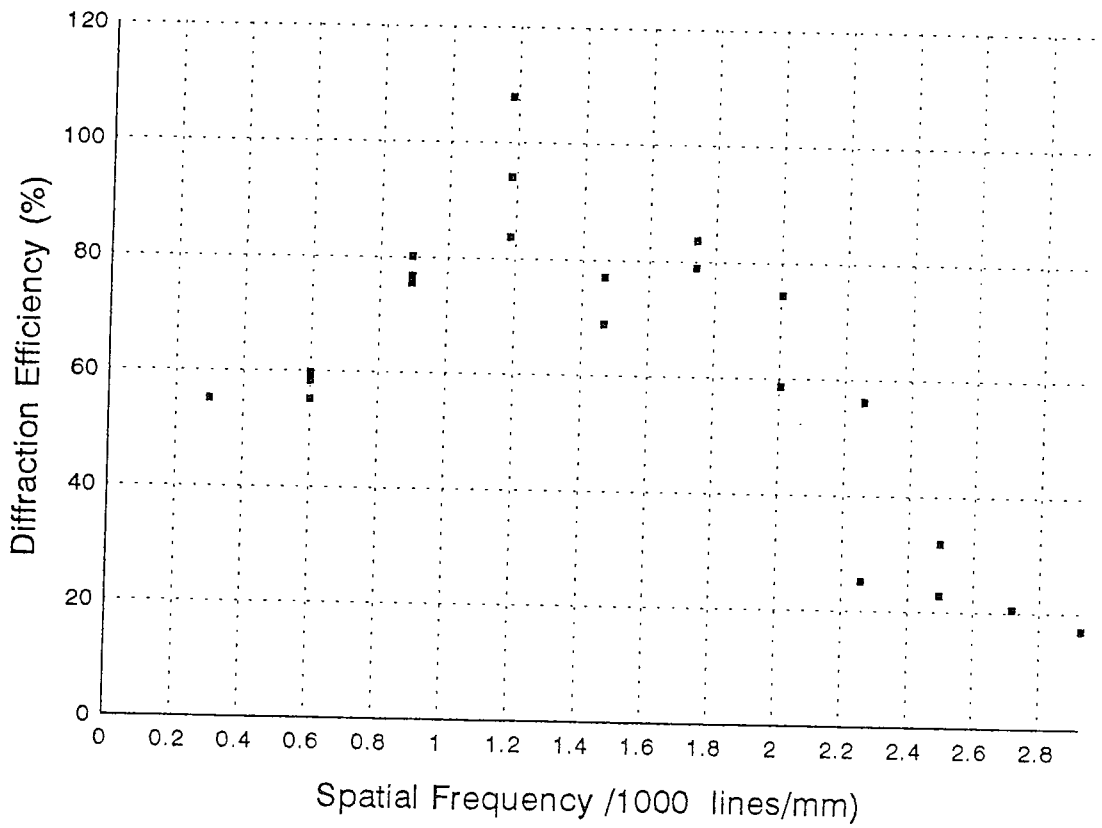

Figure 5.11 Diffraction efficiency as a function of spatial frequency. Layers were prepared with the standard formulation and were 60 μm thick. Exposure was constant at 6mW/cm² for 60 seconds. Overmodulated gratings are shown as diffraction efficiencies over 100%.

5.3.5 Noise and recording nonlinearity.

Noise is unwanted light diffracted or scattered in the same direction as the reconstructed wave. Some of the main sources of noise are: (1) Inhomogeneities and surface deformations of the recording material, (2) random scatter due to the granularity of the recording material, (3) Nonlinear recording of the signal wave.

Poor surface quality is probably the most serious source of noise in this particular photopolymer material. However this can be eliminated by the correct preparation methods and protection from excess humidity (see chapter 2).

The granularity of the recording material can be troublesome in silver halide based materials as the individual grains can scatter light quite strongly. However this only really becomes a problem in situations where the diffraction efficiency is low and the signal to noise ratio is affected. For example, where multiple holograms are to be superimposed in the same plate film grain noise often determines the upper limit of the number of holograms that can be superimposed. In general photopolymers, like dichromated gelatin are essentially grainless materials and therefore produce much less scatter than silver halide.

Perhaps the most important source of noise is non linear recording of the signal wave. In section 5.1.1 it was established that for an ideal recording material the graph of square root of diffraction efficiency $\sqrt{\eta}$ versus exposure E_0 for a particular fringe visibility is a perfectly straight line whereas for practical materials it is only a straight line over a specific range of exposure values. If exposure exceeds this range the recording is not perfectly linear and a non-sinusoidal grating results. A non-sinusoidal grating will produce higher order diffracted waves along with the desired first order

reconstructed wave. Fortunately in these very thick photopolymer layers the angular selectivity is usually so high at typical recording spatial frequencies that the higher orders are not observed under illumination at the Bragg angle even though the recording is non-linear.

A lower spatial frequency grating (450 lines/mm) in a thinner layer (56μm) was recorded in order to observe the growth of the second order diffracted beam. Figure 5.12 shows the growth of the first and second order diffracted beams during recording with 4mW/cm^2 total power density (at 514nm).

An interesting observation is that there is no delay before the appearance of the second order beam. This indicates that even at very low exposures the recording mechanism is intrinsically non linear. This is true of most photopolymers probably because the refractive index change is achieved by a complex process of polymerization and diffusion.

The distribution of light into the different diffracted waves after the layer had been exposed to saturation (<700s) at 4mW/cm^2 is shown in Table 5-1. The grating is illuminated at the appropriate Bragg angle for maximum diffraction efficiency in the first order beam.

Order of diffracted beam	3	2	1	0	-1	-2
Diffraction efficiency	0.10%	5.9%	42.5%	48.3%	3.2%	0.05%

Table 5-1 Diffraction efficiency in each of the observed orders in a non sinusoidal grating recorded in the photopolymer material. Diffraction efficiency is defined as the ratio of the intensity of light in a particular order to the total transmitted intensity.

The existence of second and higher order waves in the reconstructed image of a real object produces "ghost" images to either side of the true image. Figure 5.13 is a photograph of the reconstructed image from a double exposure hologram of a vertical cantilever which has been rather overexposed. The layer is also thinner than usual, being only about 50μm in thickness. The ghost images that arise from nonlinear recording obscure the true image.

Details of the recording of this type of hologram will be given in section 5.4.

Figure 5.13 is a good example of the worst effects of nonlinear recording in this material. However, this is usually not a problem if the standard thick layers are used and care is taken not to over expose the layer.

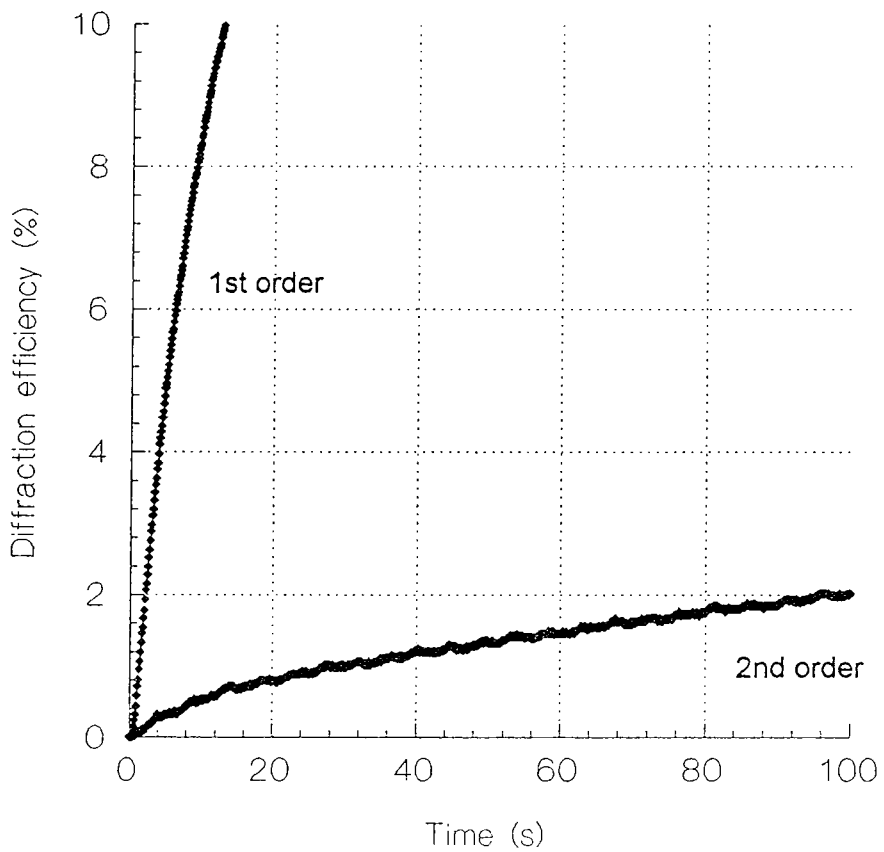

Figure 5.12 the growth of the first and second order diffracted beams during recording with 4mW/cm² total power density (at 514nm).

Figure 5.13 photograph of a double exposure hologram of a cantilever illustrating the detrimental effects of non-linear recording on the reconstructed image.

5.3.6 Variation of the grating slant angle.

According to coupled wave theory the diffraction efficiency of a lossless grating, illuminated at the Bragg angle should not depend on the slant angle φ_2 of the fringe planes (Chapter 1).

Slant angle φ_2 (degrees)	Diffraction efficiency(%) 40mJ/cm^2 exposure.	Diffraction efficiency(%) 60mJ/cm^2 exposure.
0	17.5	31
10	20	32
20	13.5	28
30	16	31
40	16	30
50	10.5	18

Table 5-2 Diffraction efficiencies obtained in gratings recorded at various slant angles. The fringe spacing is 1 μm and the layer thickness is 56 μm.

As can be seen from the above table this photopolymer material can tolerate up to a 40° angle between the grating vector and the plate normal without loss of efficiency. This is without compensating for the increased reflection losses at high angles of incidence. This is an important result as some photopolymers perform poorly at high slant angles.

The Bragg angle of incidence for maximum diffraction efficiency during reconstruction was the same throughout. This indicates that no shrinkage occurred during recording (see below).

5.3.7 Reflection gratings

So far we have dealt solely with transmission holograms. Reflection holograms, in which the fringes are parallel to the layer surface, have unique properties; reflection holograms can be reconstructed with white light. The fringe spacing in a hologram is determined by the wavelength of the illuminating light and upon reconstruction the hologram will reflect only that wavelength. This eliminates the need for a coherent monochromatic source for reconstruction.

There are three main features of reflection holograms which make recording more difficult in some materials.

(1) If the material undergoes shrinkage during recording or development the reflection hologram will be much more severely affected than the transmission hologram. Silver halide sensitized gelatin is an example of a material which shrinks on development. The result is usually negligible in a transmission grating; the shrinkage is in the direction normal to the plane of the substrate, so the film thickness is merely reduced. In a transmission hologram or slanted transmission grating where the fringe planes are basically perpendicular to the plane of the substrate but have some parallel component, some distortion of the image due to variation of the slant angle may be observed. In a reflection grating however, the fringe planes are perpendicular to the direction of the shrinkage and the fringe spacing will actually be reduced, causing the reconstruction wavelength to be shortened. A hologram recorded with red light could therefore be reconstructed as a blue image, or if shrinkage is severe, the reconstruction wavelength

could be shortened beyond the visible spectrum into the near ultra violet, so that no reconstructed image is observed.

In a self developing material, shrinkage would be an even more serious problem, since the shrinkage would be occurring even as the recording is proceeding. Fringe stability would be impossible in a material where the recording medium itself moves in a direction perpendicular to the fringe planes during recording.

During the above study of slanted gratings no change was found in the Bragg angle for reconstruction at 633nm relative to the recording angle at 514nm. Since the variation in the measured Bragg angle was less than 5 arc minutes on these 56μm layers at slant angles of up to 50° it can assumed that if any change in layer thickness occurs at all it must be less than 0.3%.

(2) The recording geometry for reflection holography is such that the two interfering beams are always incident from opposite sides of the photosensitive plate. This means that both the exposing intensity and the beam ratio varies throughout the layer depth, since the beams will always be attenuated as they pass through the material. In highly absorbing media such as this xanthene dye sensitized photopolymer, the variation of beam ratio can be particularly severe. However, since the absorbance of the layer can be easily varied by controlling the xanthene dye concentration, this problem has been overcome by using layers with very low dye concentration.

(3) Perhaps the most important characteristic of reflection gratings is that the fringe spacing is particularly small and the recording medium must have the resolution capabilities to record gratings with typical spatial frequencies of 6000 lines/mm.

This figure can be reduced by lowering the angle between the incoming beams from the standard 180° to, say, 90° but the spatial frequency of the recorded grating will still be as high as 5000 lines/mm. Even if the angle (in air) between the two incoming beams is only 30° and they are incident on the plate from opposite sides, the high degree of refraction at the air/photopolymer layer boundary means that the angle between the beams in the medium ($n \approx 1.5$) is 55^0 and the spatial frequency of the recorded grating will be 4775lines/mm. Since section 5.3.4 has shown that the resolution of this material does not extend much past 3000 lines/mm it seems likely that the material in its present formulation may not have sufficient resolution to record reflection gratings.

Experimental procedure for reflection holograms

Unfortunately, despite exhaustive studies, we have been unable to record reflection holograms with diffraction efficiencies greater than 2% in the photopolymer material studied here.

Two main recording geometries were used. The first is shown in Figure 5.14 and simply consisted of a mirror mounted behind the photosensitive plate and at a small angle to it (e.g. 10°). The mirror was tilted so that the grating would be slightly slanted and the reconstructed beam would not overlap with the part of the reconstructing beam reflected at the air/ photopolymer interface. The grating was expected to form in

the area of the photosensitive plate where the directly incident beam overlapped with the beam reflected from the mirror.

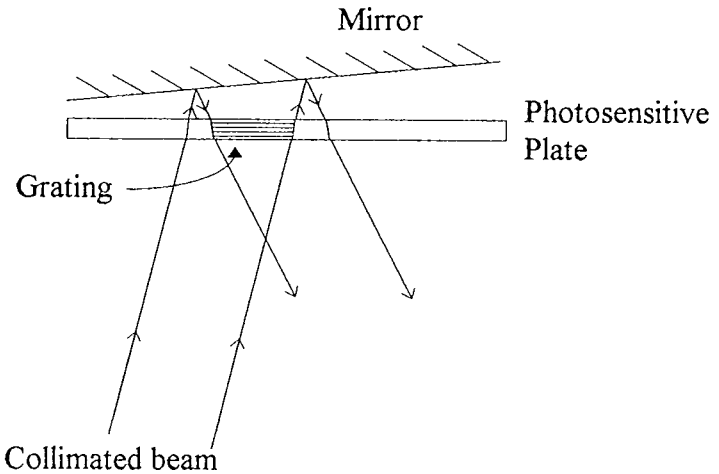

Figure 5.14 Apparatus for recording reflection holograms. Gratings are slightly slanted and have a spatial frequency of frequency of approximately 6000 lines/mm

Reconstruction with an unexpanded helium neon beam produced a weak reflected beam in the appropriate position. Diffraction efficiency was typically 0.4%.

There also appeared to be a weak, low spatial frequency transmission grating, the presence of which was indicated by weak reconstructed beams observed on either side of the undeviated zero order transmitted beam. There were also similar beams equidistant from the part of the reconstructing beam reflected at the air/ photopolymer interface.

This low spatial frequency grating was recorded by the interference between the reflection of the recording beam off the back face of the layer (or glass substrate) and the beam reflected off the mirror. These are shown in Figure 5.15 as beam **(a)** and beam **(b)**. The angle between these two beams depends only on the tilt of the mirror relative to the photosensitive plate and the angle of incidence of the recording beams.

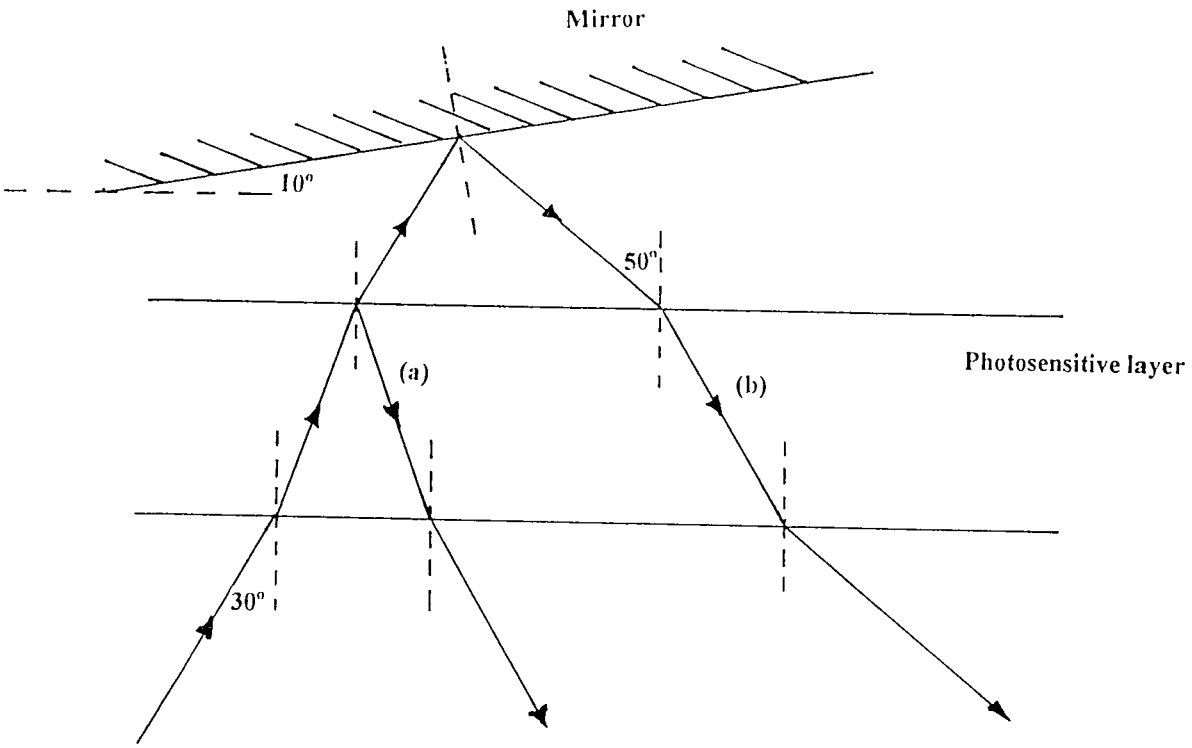

Figure 5.15 Diagram showing some of the reflections and reflections at the boundaries of the photosensitive layer in a typical recording of a reflection grating with the apparatus shown in Figure 5.14. The spurious transmission gratings observed were recorded by the interference of beams (a) and (b).

This type of spurious transmission grating was observed in most cases usually with diffraction efficiencies of a few percent. Thier spatial frequencies were found to be consistent with a transmission grating recorded as described. Even though the beam ratio between beams **(a)** and **(b)** in Figure 5.15 was very high and therefore the visibility of the fringe pattern formed was low, the low spatial frequency meant that the grating was more easily recorded than the high spatial frequency reflection grating.

Figure 5.16 shows the recording geometry used to stop reflections off the layer and substrate surfaces. Orthoxylene was used as an index matching liquid and the light was coupled into and out of the layer with 90°:45°:45° quartz prisms. In gratings recorded with this recording setup, the spurious transmission gratings were eliminated and low diffraction efficiency reflection gratings were observed. The highest observed diffraction efficiency was 2%, and was obtained with 20 seconds exposure to a total power density of 4mW/cm^2. The layer was of standard formulation and 56μm thick.

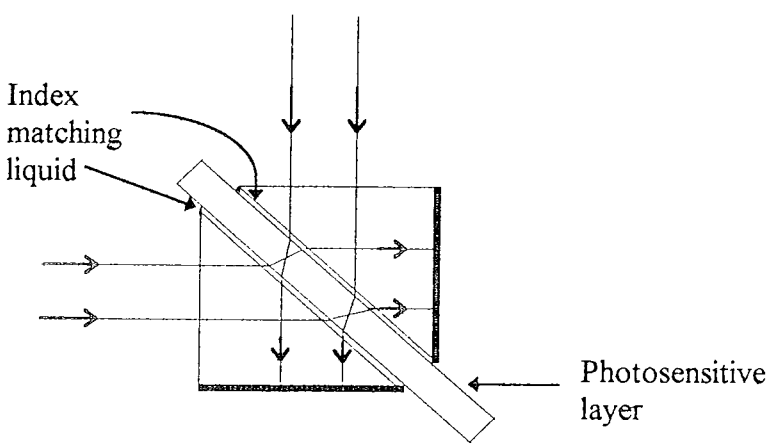

Figure 5.16 Apparatus for the formation of reflection gratings using index matching liquid and prisms to couple the light into the layer. The spatial frequency is approximately 3400lines/mm and the grating is unslanted.

5.4 Holographic applications of the material

Holographic interferometry is perhaps the most important application of holography; it is an extension of interferometric techniques in which at least one of the waves which interfere is reconstructed by a hologram. The unique advantages of holographic interferometry arise from the fact that holography permits storing a wavefront for reconstruction at a later time. Wavefronts which were originally separated in time and space can be interferometrically compared. This makes the technique extremely versatile and changes in the shape of objects with quite rough surfaces can be studied with interferometric precision.

Non destructive testing[7] is the main industrial application for holographic interferometry. Structural weaknesses in the object are detected by interfering the wavefront from the unstressed object with the wavefront produced when the object is stressed either by application of a load or changes in temperature and pressure. Subsurface structural defects are detected as discontinuities or distortions in the fringe pattern. The two most common techniques for forming the interferogram are real-time (live fringe) holographic interferometry and time lapse (double exposure) holographic interferometry. Silver halide photographic emulsions are normally used as the recording material.

5.4.1 Real-time holographic interferometry

In real-time holographic interferometry the object and reference wave interfere to produce the hologram, which is removed and developed and replaced in its original position. Great accuracy is required in replacing the hologram; the exact superposition of object and image wave requires replacement to be accurate to a fraction of a fringe

width. Assuming reconstruction with the original reference wave, the reconstructed wavefront will be identical to the object wavefront if (a) processing of the hologram does not distort the emulsion, (b) replacement has been exact and (c) illumination has been adjusted to equalize the absolute value of the original and reconstructed wave amplitudes. The object may now be placed under stress and allowed to deform (or released from stress and allowed to flow, collapse or expand). As a result the optical path from an observation point to any point on the object's displaced surface is changed with respect to the distance from that observation point to the corresponding point on the reconstructed image surface. The optical path from the illuminating source to that point on the object surface also changes. A phase shift is therefore introduced and an interference pattern which is characteristic of the deformation results. Since the fringes can be observed as the stress is applied this is often referred to as live fringe holographic interferometry.

The exact repositioning of the hologram is one of the most problematic aspects of holographic interferometry. It is usually overcome by processing the hologram 'in situ' using a specially designed container in which the recording plate is immersed. Processing involves filling this container with the series of chemical baths required to develop the hologram This is messy and time consuming but it means that the photographic plate need not be removed from its original position.

Obviously a self developing photopolymer material, easy to prepare and capable of high diffraction efficiency is almost ideally suited to holographic interferometry. There is no processing required so the problems of repositioning, and processing induced distortion are both eliminated. The hologram and fringe pattern can be viewed

immediately. A demonstration of the suitability of this photopolymer material to holographic interferometry was carried out as follows.

A flat disk, with a micrometer driven lever arm which enables it to be rotated through small angles of the order of milliradians was used as an object. It had been spray painted matt white to increase the reflectivity. An expanded beam from the Argon ion laser was split by a beam splitter and one beam illuminated the disk while the other was incident directly on the recording plate. The light scattered from the disk onto the recording plate constituted the object beam. The average power density at the recording plate was 750 $\mu W/cm^2$ The recording plate was a 5"×4" glass plate coated with the standard formulation coating solution to a thickness of 140μm. A recording time of 300 seconds was used. At the end of that time the intensity of the illuminating light was reduced, both to allow readout without risk of further recording, and to increase the visible fringe contrast. The hologram could be viewed by blocking the object from view using a piece of black card, and observing that a bright image of the object could still be seen. At this point there were no fringes visible on the disk surface showing that no movement of the object or distortion of the recording material had occurred during formation of the hologram. A small rotation of the micrometer control produced an in plane rotation of the disk and produced the characteristic parallel fringes associated with in plane rotation. Figure 5.17 shows a photograph of the fringes produced. Further rotation caused an increase in the number of fringes observed as can be seen from Figure 5.18 and Figure 5.19. Very soon the number of fringes increased to the point where the individual fringes could not be resolved. For pure rotation about an axis normal to the surface, fringe frequency is related to the angle of rotation α by the following formula[8]

$$f = \frac{\alpha(\sin\phi_i + \sin\phi_s)}{\lambda}.$$

where ϕ_i is the angle the illuminating beam makes with the surface of the object and ϕ_s is the angle the line of observation makes with the surface of the object. The fringes shown in the photographs of this hologram can be interpreted as follows. Taking ϕ_i to be 45° and ϕ_s to be 90°, we see that the fringes in Figure 5.17 (9 fringes in the 12cm diameter of the disk) correspond to a rotation α of 2.2×10^{-5} radians or 4.6±0.3 arc seconds. Similarly the rotation would have been 8.3±0.3 arc seconds in Figure 5.18 and 16.0±0.3 in Figure 5.19. An error of one half fringe width is assumed. The precision of the measurements is good but for accuracy the values of ϕ_i and ϕ_s would have to be known more accurately.

The above is a simple demonstration of the live fringe holographic interferometry technique and the sort of accurate measurements which can be made by interpretation of the fringes. The technique can be used for much more complex systems such as stress analysis in limb prostheses[9] and machine parts[10].

Figure 5.17 Photograph of the fringes produced by a small in-plane rotation of a flat disk

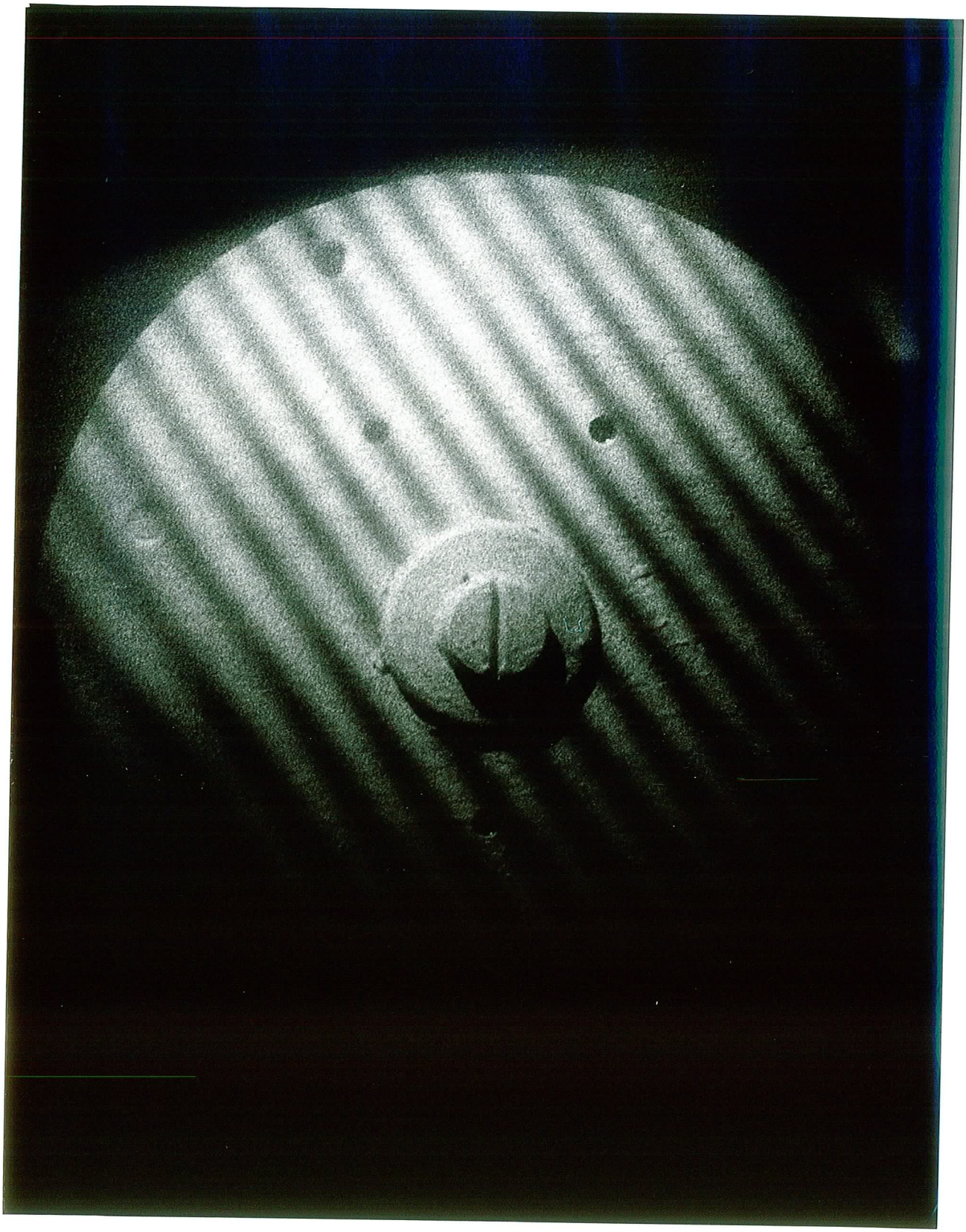

Figure 5.18 Photograph of the fringes produced by further in-plane rotation of the disk

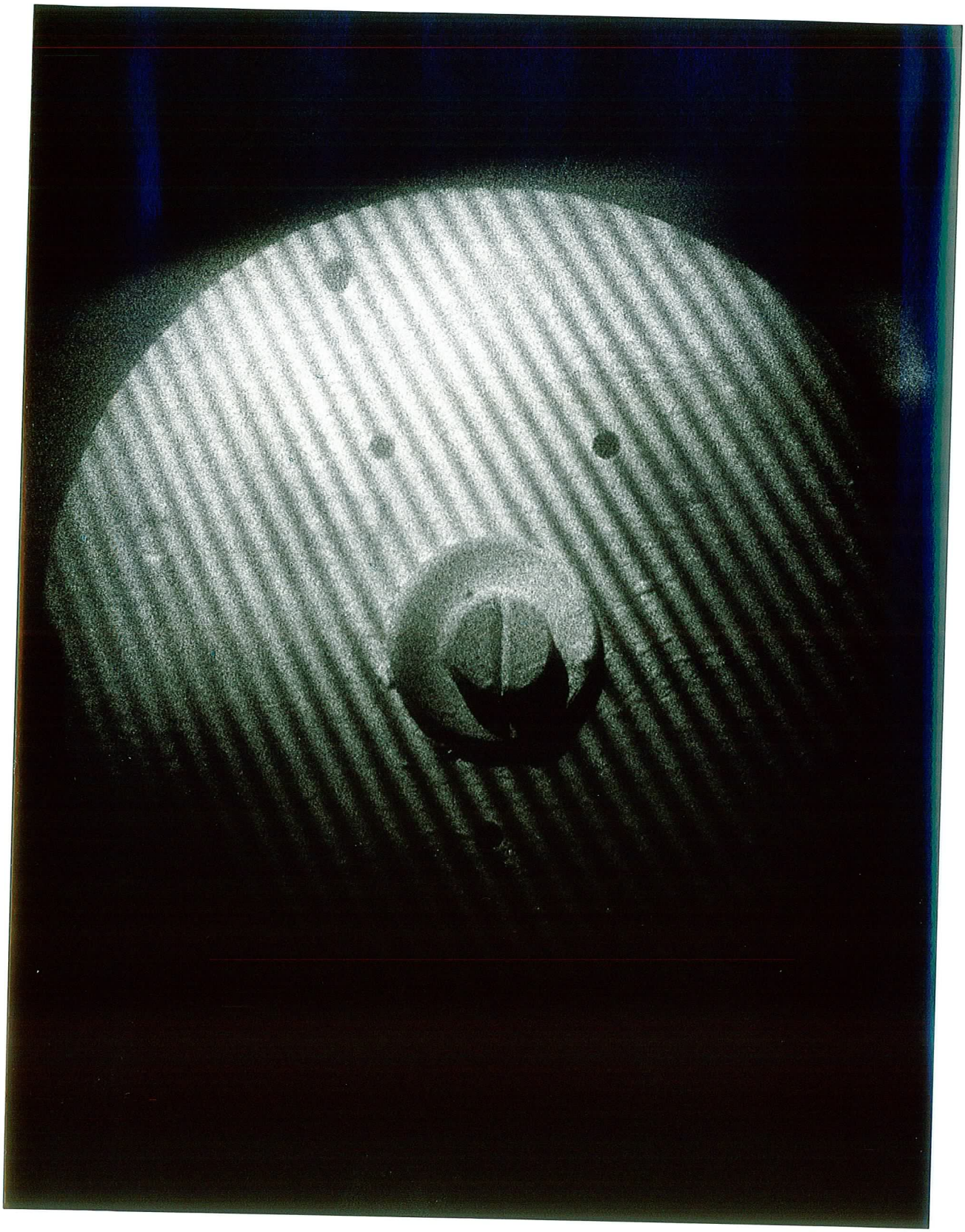

Figure 5.19 Photograph of the fringes produced by further in-plane rotation of the disk

5.4.2 Double exposure holographic interferometry

Double exposure holographic interferometry is similar to live fringe holographic interferometry except that instead of interfering a reconstructed object wavefront with the actual object wavefront, two holograms are recorded one after another on the same plate so that the interference pattern is caused by the interference of two reconstructed wavefronts. The difficulty is usually that the stress or displacement required to give a suitable fringe pattern must be calculated beforehand so that an appropriate change is made during the interval between the two recordings. This is because with most materials the image cannot be viewed until after development. For example if the rotating disk were studied by double exposure holography it would have been easy to rotate it too much and record a double exposure hologram with fringes too narrow to resolve in the reconstruction.

The advantage of the self developing photopolymer material for use with this technique is that the image can be viewed immediately the first exposure is complete, the effect of any changes are immediately visible. Once a suitable fringe pattern is achieved, the second exposure can be carried out to form a permanent double exposure hologram with the consequent improvement in fringe visibility.

Figure 5.20 is a photograph of a double exposure hologram of an aluminium can (painted matt white). The first exposure was done with an elastic band around the center of the can, which was removed for the second exposure. Each exposure was for 240 seconds, and the power density at the recording plate was 500$\mu W/cm^2$. The plate

was prepared with the standard formulation coating solution and had a dry layer thickness of 140μm .

The small deformation of the surface around the region of stress is clearly seen in the interferogram. Fringe contrast is very good. This simple demonstration shows the ease with which bright, high contrast interferograms, can be recorded in this material, without development and at relatively low exposures.

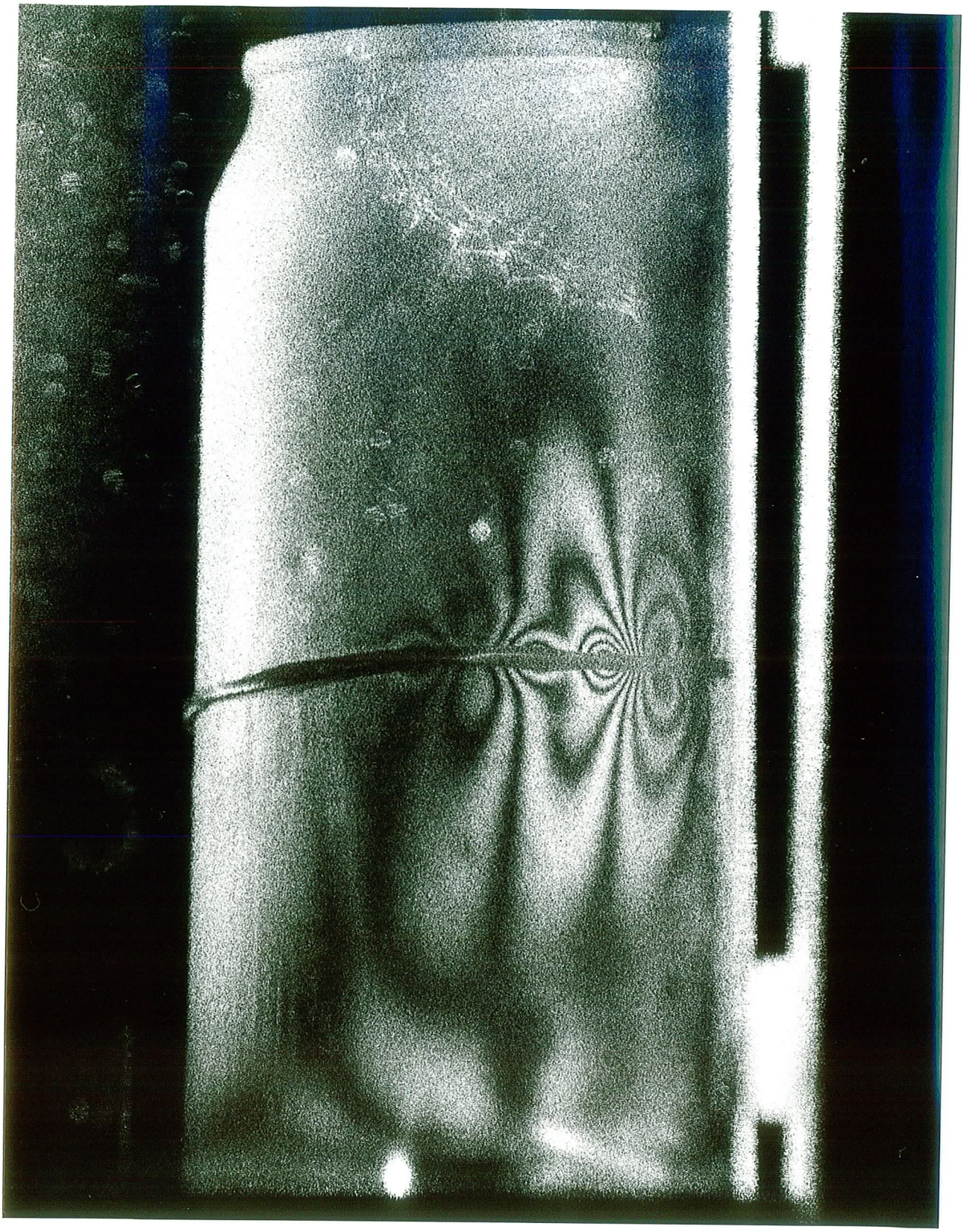

Figure 5.20 Double exposure hologram of an aluminium can, showing the interference fringes produced by the displacement of the surface when stress is applied (by an elastic band).

5.5 Conclusion.

In this chapter the holographic recording characteristics of the material have been examined. This acrylamide based photopolymer material compares very favourably to other photopolymer systems. The thicker layers (100-150μm) compare well in terms of sensitivity and diffraction efficiency with the commercial Dupont photopolymer discussed in chapter 1, and yet the material responds to exposure with greater linearity over a broader range of spatial frequencies. Slanted gratings are also possible without distortion, as no shrinkage occurs during recording. Shrinkage is a frequent problem with many volume holographic materials e.g. silver halide sensitized gelatin, dichromated gelatin and some photopolymers.

One drawback of this photopolymer material is the limited resolution; gratings were not recorded above spatial frequencies of 3000 lines/mm. This means that in its present formulation the material is not a practical recording medium for reflection holograms.

Since this material has the advantage of self development and has very good recording characteristics in transmission mode, it is well suited to applications such as holographic interferometry. Two simple demonstrations of this technique were carried out using the acrylamide based photopolymer, with excellent results.

---

[1] R. J. Collier, C. B. Burckhardt, L. H. Lin, "Optical holography", Chapter 9, Academic Press, NewYork 1971.

[2] P. Leclere, Y. Renotte, Y. Lion "Measurement of the diffraction efficiency of a holographic grating created by two Gaussian beams" Appl. Opt. , 31, 4725-4733, 1992.

[3] R. R. A. Syms, "Practical volume holography", Chapter 5, Oxford engineering series 24, Clarendon Press, Oxford, 1990.

[4] R. J. Collier, C. B. Burckhardt, L. H. Lin, "Optical holography", Chapter 10, Academic Press, NewYork 1971.

[5] P. Leclère "Etude et caractérisation de films d'alcool polyvinlyique photosensibilisés en vue de leur utilisation en holographie et en cojugation de phase optique" doctoral thesis, University of Liege, Belgium, 1994.

[6] G. Manivannan and R. A. lessard " Trends in holographic recording materials", *Trends in polymer science*, **2**, 282-290, 1994.

[7] R. Jones and C. Wykes "Holographic and speckle interferometry", Chapter 7, Cambridge studies in modern optics, Cambridge university press, 1989.

[8] R. J. Collier, C. B. Burckhardt, L. H. Lin, "Optical holography", Chapter 15, Academic Press, NewYork 1971.

[9] S. Blatcher, J. C. Shelton, "Quantitative holographic interferometry for the analysis of surface strains in femurs" Institute of Physics applied optics and optoelectronics conference 1994, abstract no. BO1.3, 63-64

[10] R. Jones and C. Wykes "Holographic and speckle interferometry", Chapter 7, Cambridge studies in modern optics, Cambridge university press, 1989.

6. Physical Aspects Of Grating Formation.

In the previous chapters the chemical processes leading to the initiation of polymerization in these photopolymer layers have been studied. The mechanisms by which the material responds to light of the appropriate wavelength to produce high concentrations of polymer are well understood. However, the question still remains as to the exact mechanism by which the refractive index is changed. The refractive index change was first thought of as being a simple process in which the conversion of immobile monomer molecules to polymer molecules caused a local change in the refractive index. In fact the polymerization of monomer in the bright fringe regions leads to, not only bond conversion, but also to mass transport of material from neighboring unpolymerized regions. It is a complex process in which the two main contributing factors, bond conversion and density change caused by diffusion actually have opposing effects on the overall refractive index. The purpose of this chapter is to examine the physical processes leading to the changes in refractive index.

6.1 Investigation of the variation of refractive index modulation during hologram formation.

The refractive index modulation that occurs during holographic recording cannot be measured directly because the refractive index varies over such small distances. However, coupled wave theory can be used to analyze the recorded gratings and estimate their refractive index modulations. In order to analyze gratings recorded in this material, the type of grating recorded had to first be determined. A spatial variation of the intensity of the incident light may be recorded as a transmittance variation (amplitude grating), refractive index variation (volume phase grating), thickness variation (surface relief grating) or a combination of these. The high diffraction efficiencies routinely achieved in these materials indicate that volume phase gratings must be present, as 3.7% is the theoretical limit on diffraction efficiencies achieved in pure amplitude gratings[1]. Furthermore, as the results in this section will show, the gratings in this material are thick gratings which extend through the bulk of the material. This rules out the possibility of a pure surface relief grating. Since the gratings are analyzed with 633nm light, and the sensitizing dyes do not absorb at this wavelength, we can conclude that there is no modulation of absorption contributing to the diffraction efficiency at this wavelength. It must therefore be concluded that gratings recorded in this material are either pure phase gratings where refractive index modulation alone is present, or mixed gratings with refractive index modulation as the main contributor. However, as section 6.1.1 will show, surface relief gratings are only present at very low spatial frequencies, leading to the conclusion that at spatial

frequencies typical of normal hologram recording the grating recorded in this material can be considered a volume phase grating with negligible loss.

6.1.1 Investigation of surface relief gratings

Several authors[2,3,4] have observed surface gratings in similar (photopolymerizable) materials but usually only at very low spatial frequency. As part of the investigation to determine the type of grating recorded in this material, low spatial frequency surface relief gratings were studied.

A Taylor Hobson talysurf 5M surface profilometer was used to study the surface profile of layers in which low spatial frequency patterns had been recorded. Two large 5"×4" layers of 56μm and 140μm thickness were prepared with the standard formulation coating solution. A uniform collimated beam having a total power density of 6mW/cm^2 (514nm) was used to expose the layers for 60 seconds for each recording. On each layer two low spatial frequency patterns were recorded using suitable masks, and one high spatial frequency grating was recorded using the normal interference method (two beams of 3mW/cm2 each). Mask A had four transparent vertical slits 0.2mm apart on an opaque background. Mask B had 5 pairs of 0.1mm slits; the distance between the slits in each pair varied (0.15mm, 0.175mm, 0.20mm, 0.30mm, 2.10mm). In each case the mask was illuminated with a collimated beam of light and the image of the mask was focused onto the photopolymer layer using a 15cm achromatic lens.

Figure 6.1 shows the surface profile of a 56μm thick photopolymer layer exposed using mask A. The four exposed areas are clearly seen, each peak 4mm from the next

corresponding to the 0.2 mm separation. The peaks on the scan are 5-6mm above the level of the layer surface, this corresponds to 1-1.2μm. The swelling in the exposed regions seems surprising considering that normal polymerization causes volume shrinkage, but these results are in agreement with those obtained by Boiko et al[5], who also found that the surface grating peaks corresponded to the intensity maxima, and suggested that this was due to material being drawn into the polymerized regions by the abrupt change in chemical potential in these areas. In Figure 6.1 there is also some swelling between the peaks. Figure 6.2 shows the same pattern scanned a few millimeters below the previous scan. The four peaks are again clearly visible, and along with the swelling in the exposed areas there seems to be a slight shrinkage in the unexposed regions to either side of the line pattern. Figure 6.3 shows even more swelling, so much that the peaks themselves are poorly resolved. This scan was taken towards the vertical center of the pattern and since the illuminating beam was Gaussian, it would have received more exposure than the previous examples. The peak height is approximately 3μm with respect to the layer surface but only 1μm from peak to trough. The other features that can be seen in this scan are probably due to scratches or pinholes in the mask.

The troughs observed on either side of the exposed area would seem to support Boiko's statement that the swelling is caused by the transport of material from the surrounding areas.

The 140 μm layer behaved in much the same way. Figure 6.4 shows clearly that the exposed area is raised about 2μm above the layer surface, while the surface for about a millimeter either side of the exposed area has clearly shrunk to about 1.2μm below the

level of the layer surface. Figure 6.5 shows the same area scanned with a magnification of 20 on the horizontal axis and Figure 6.6 shows the same pattern scanned in a different area with a horizontal magnification of 50.

Examples of the patterns recorded in layers exposed using mask B are shown in Figure 6.7, Figure 6.8 and Figure 6.9. The first scan shows the profile across two pairs of exposed lines 0.1mm in width. The separation of each pair is, from the left, 0.175mm, and 0.20mm. The other two show the profile across all the five pairs of exposed lines. The separation of each pair is, from the left, 0.15, 0.175mm, 0.20mm, 0.30mm and 2.10mm. The peak heights are approximately 1μm on both the 56μm and 140μm layers.

This simple study demonstrates that the acrylamide based material studied in this thesis behaves in the same way as that reported by Boiko et al[6], in that the material swells in the exposed areas. The authors observed much greater relief depths of up to 15μm on layers 100μm thick 20 hours after exposure. They also observed a linear dependence on film thickness which would indicate that the polymerization occurs throughout the full thickness of the layer and the surface relief is the effect of volume swelling. The photopolymer used in the study by Boiko is essentially a red sensitized version of the one studied here; it is the formulation first used by Calixto[7] upon which the photopolymer studied in this thesis is based. In Boiko's study the surface gratings decreased in depth at spatial frequencies above 15lines/mm and disappeared completely above 45lines /mm. It was also observed with our material that there is no relief grating

whatsoever at high spatial frequencies, and as can be seen from Figure 6.8 and Figure 6.9 the material could not resolve (in surface relief) the slits that were 0.15mm apart. This corresponds to a spatial frequency of 6.66 lines/mm. So, at the spatial frequencies used for holographic recording, of the order of 1000 lines/mm, there is no surface grating. This is possibly because the binder cannot allow alternate swelling and shrinking in regions so close to one another. It must be kept in mind that in the examples shown, although the peaks look sharp there is usually 250 times higher magnification on the vertical axis; for example the sharp peaks shown in Figure 6.9 are actually mounds one micron high and one hundred microns across. It seems reasonable that the binder could not allow sharper features to be recorded in relief. Instead, at high spatial frequencies a dense network of polymer is formed in the bright fringe areas, resulting in a density variation as opposed to a thickness variation.

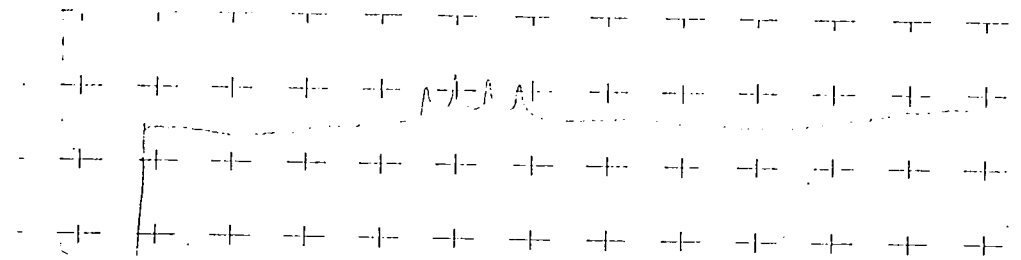

Figure 6.1 Surface profile of a 56μm thick photopolymer layer exposed using mask A. The magnification on the vertical axis is ×5,000 and the horizontal axis is magnified ×20 . The scan was taken approximately one and a half hours after exposure.

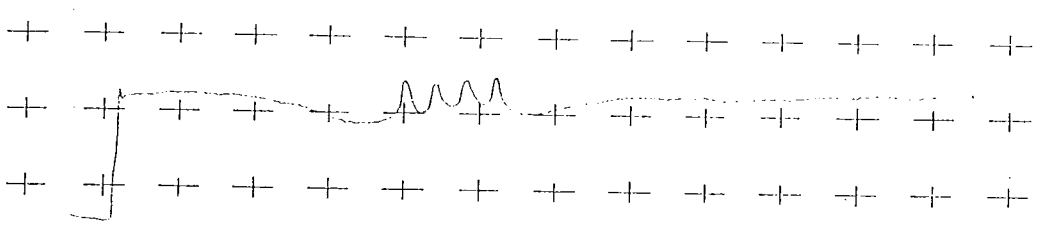

Figure 6.2 Surface profile of the same pattern, scanned in a different position. The magnification on the vertical axis is ×5,000 and the horizontal axis is magnified ×20 . The scan was taken approximately one and a half hours after exposure

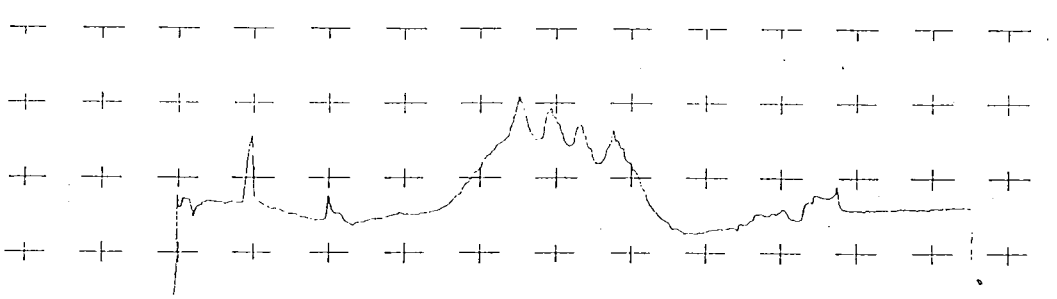

Figure 6.3 Surface profile of the same pattern, scanned in a different position. The magnification on the vertical axis is ×5,000 and the horizontal axis is magnified ×20 . The scan was taken approximately one and a half hours after exposure

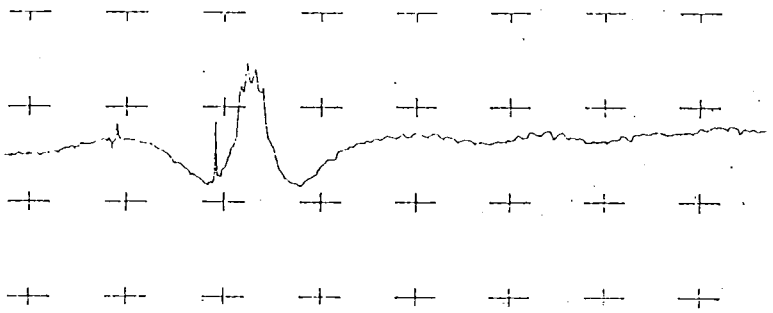

Figure 6.4 Surface profile of a 140μm thick photopolymer layer exposed using mask A. The magnification on the vertical axis is ×5,000 and the horizontal axis is magnified ×5 . The scan was taken approximately two and a half hours after exposure

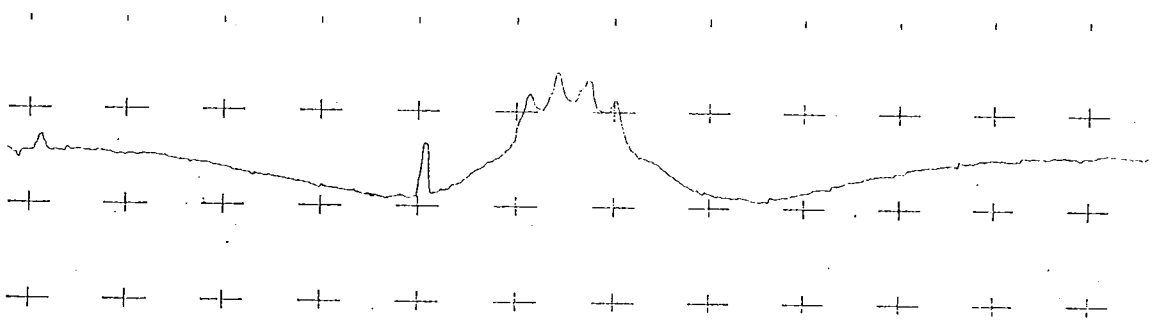

Figure 6.5 Surface profile of a 140μm thick photopolymer layer exposed using mask A. The magnification on the vertical axis is ×5,000 and the horizontal axis is magnified ×20 . The scan was taken approximately two and a half hours after exposure

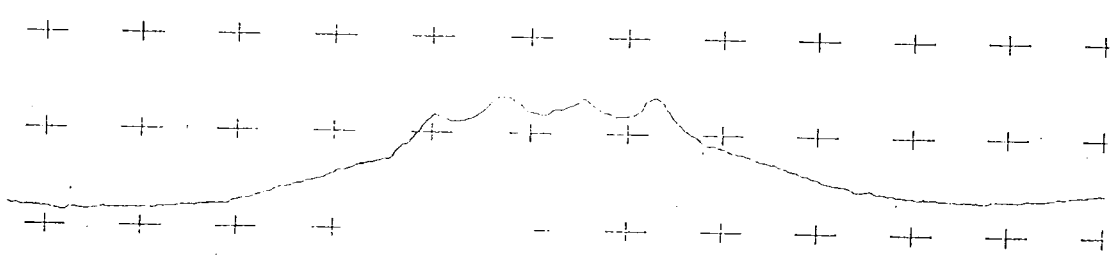

Figure 6.6 Surface profile of a 140μm thick photopolymer layer exposed using mask A. The magnification on the vertical axis is ×5,000 and the horizontal axis is magnified ×50 . The scan was taken approximately two and a half hours after exposure

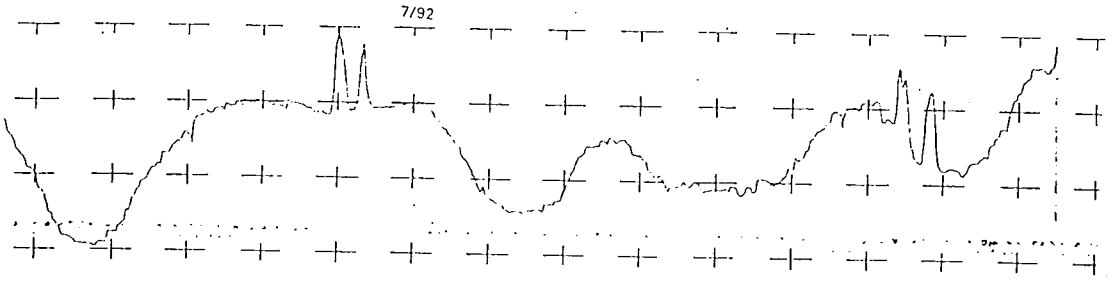

Figure 6.7 Surface profile of a 56μm thick photopolymer layer exposed using mask B. The magnification on the vertical axis is ×10,000 and the horizontal axis is magnified ×20 . The scan was taken approximately three hours after exposure. The scan shows the profile across two pairs of exposed lines 0.1mm in width. The separation of each pair is, from the left, 0.175mm, and 0.20mm.

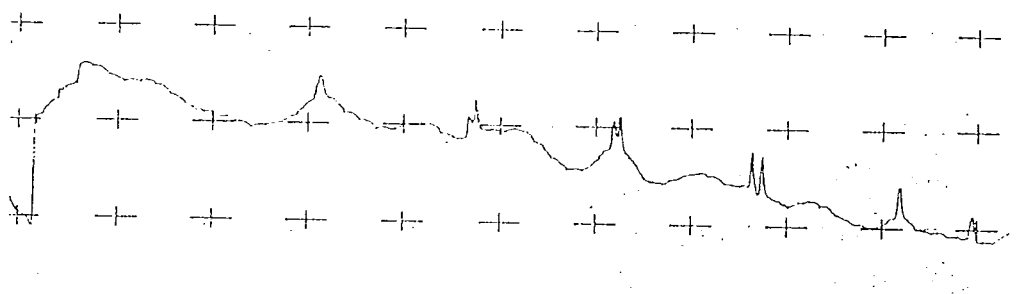

Figure 6.8 Surface profile of a 140μm thick photopolymer layer exposed using mask B. The magnification on the vertical axis is ×5,000 and the horizontal axis is magnified ×5 . The scan was taken approximately three hours after exposure. The scan shows the profile across five pairs of exposed areas 0.1mm in width. The separation of each pair is, from the left, 0.15mm, 0.175mm, 0.20mm, 0.30mm and 2.10mm.

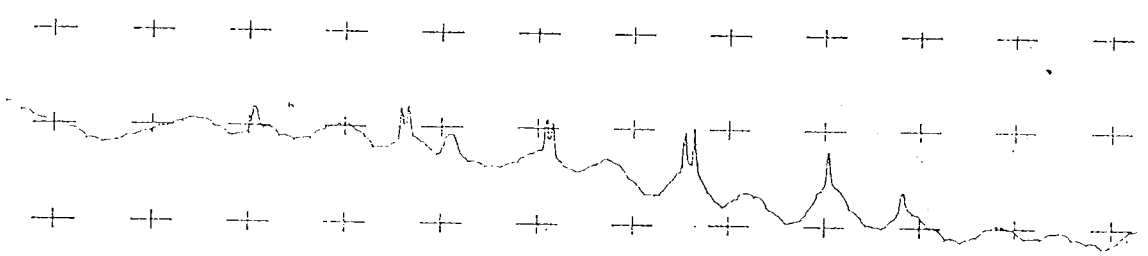

Figure 6.9 Surface profile of a 140μm thick photopolymer layer exposed using mask B. The magnification on the vertical axis is magnified ×5,000 and the horizontal axis is magnified ×5 . The scan was taken approximately two hours after exposure The scan shows the profile across five pairs of exposed areas 0.1mm in width. The separation of each pair is, from the left, 0.15mm, 0.175mm, 0.20mm, 0.30mm and 2.10mm.

6.1.2 Diffraction efficiency growth curve

Having established that at spatial frequencies typical of holographic recording, the grating is recorded as a volume phase grating with no surface relief, coupled wave theory can now be used to analyze the refractive index variation. Figure 6.10 shows a typical diffraction efficiency growth curve for an unslanted grating recorded in a 140μm thick layer. The diffraction efficiency grew from zero and reached a value of 100%* after 30 seconds. After this point the grating became over modulated and light began to be coupled back into the zero order beam. At 60 seconds when exposure ended the diffraction efficiency was still falling, indicating that the refractive index modulation was still increasing.

In order to verify that the recorded grating was indeed overmodulated the grating was rotated with respect to the incident reading beam, so that the dependence of the diffraction efficiency on incident angle could be determined. As detailed in chapter 1, the angle of incidence will affect the diffraction efficiency through the 'off Bragg' parameter ξ, so a curve of the type shown in Figure 1.7 would be expected.

It was shown in Chapter 1 that the diffraction efficiency of a lossless Phase transmission grating is given by

$$\eta = \frac{\sin^2(\nu^2 + \xi^2)^{\frac{1}{2}}}{(1 + \frac{\xi^2}{\nu^2})} \qquad (6.1)$$

* The actual maximum diffraction efficiency reached was 87% without correcting for reflection or other losses. In the graph shown the diffraction efficiencies have been normalized so that the maximum reached is 100%.

Where ν is equal to $\kappa d/(C_s C_r)^{1/2}$ as defined in chapter 1. This becomes $\kappa d/\cos\theta_0$ for an unslanted grating, where θ_0 .is the Bragg angle for the incident beam.

Again from chapter 1, ξ, the 'off Bragg' parameter is

$$\xi = \frac{d\vartheta}{2C_s} \qquad \text{where} \qquad \vartheta = K\sin\phi_1 - \frac{K^2}{2\beta}$$

And since in an unslanted grating $C_s = \cos\theta_0$, this becomes

$$\xi = \frac{d\pi}{\Lambda\cos\theta_0}(\phi_1 - \theta_0) \qquad (6.2)$$

for small deviations from the Bragg angle of incidence θ_0. Letting δ represent the difference between the angle of incidence ϕ_1 and the Bragg angle θ_0 we obtain a simple linear relationship between the off Bragg parameter and the angular deviation from the Bragg angle. For example, for the above grating which is 140μm thick, with a fringe spacing of 1μm and a Bragg angle for the incident wavelength (633nm) of 12.3° inside the medium, the relationship is

$$\xi = 450 \times \delta$$

Where δ is measured in radians inside the material. For convenience the deviation from the Bragg angle, δ, is measured in air and quoted in degrees.

so

$$\xi = 5.2 \times \delta$$

The diffraction efficiency at the Bragg angle (ξ=0) at the end of exposure was measured as 73%. This indicates that $\nu = 2\pi/3$. Substituting these parameters into the equation for diffraction efficiency and plotting diffraction efficiency versus offset from the Bragg angle, the graph shown in Figure 6.11(a) is obtained. The experimental data

obtained when the grating was scanned through a range of angles close to the Bragg angle is shown in Figure 6.11(b) and shows very good agreement with the theoretical prediction. Even the sidelobes correspond well in amplitude and angular position. This close agreement is an indication of how well coupled wave theory is suited to these thick gratings.

6.1.3 Growth of the refractive index modulation during recording.

In chapter 1 it was also shown that the diffraction efficiency at the Bragg angle is given by,

$$\eta = \sin^2\left(\frac{d\pi n_1}{\cos\theta_0 \lambda_a}\right)$$

Where n_1 is the amplitude of the refractive index modulation, d is the grating thickness and λ_a and θ_0 are the wavelength in air of the reading illumination and the Bragg angle in the medium for that wavelength. Using this formula the amplitude of the refractive index modulation can always be calculated as long as the grating thickness is known. Figure 6.12 shows how the refractive index modulation varied with time as the grating shown above was being recorded. The refractive index modulation has been calculated for a series of points on the diffraction efficiency growth curve in Figure 6.10. When exposure ended after 60 seconds the amplitude of the refractive index modulation had reached a value of 0.003. Because the grating was quite thick, even this small refractive index change was enough to cause overmodulation. Refractive index modulations with amplitudes greater than 4×10^{-3} are routinely recorded in these photopolymers and sometimes amplitudes greater than 5×10^{-3} are observed. This means that extremely high diffraction efficiencies can easily be obtained even with thinner layers.

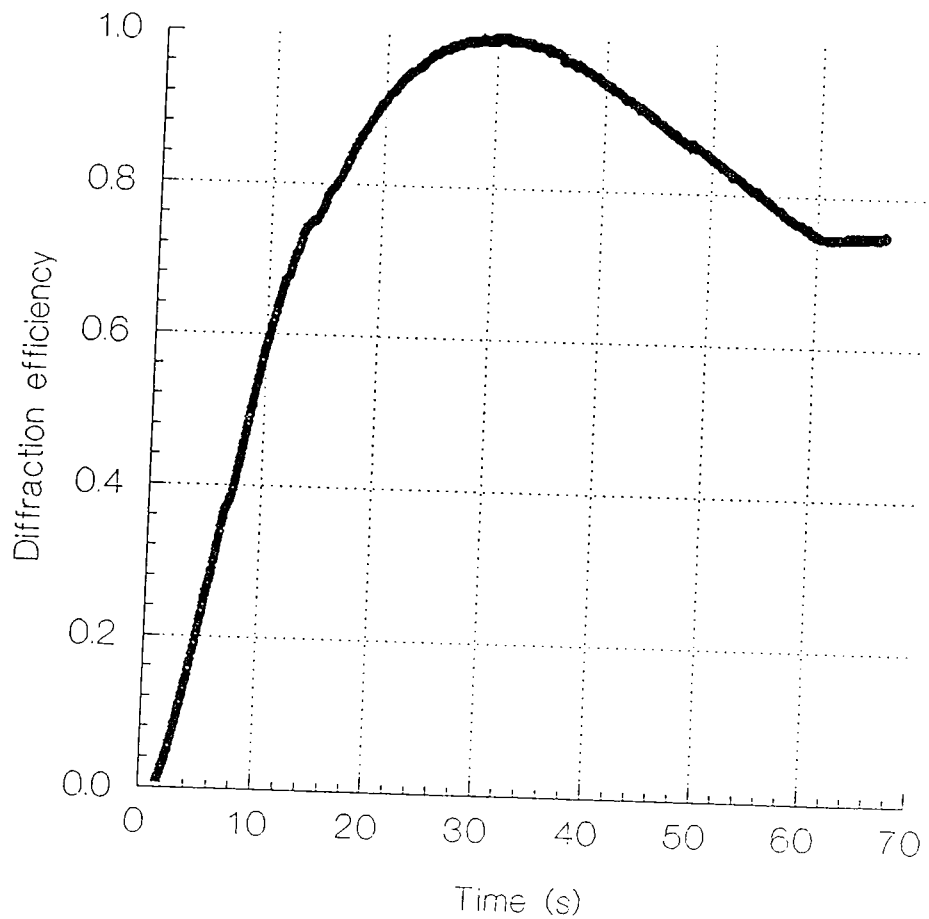

Figure 6.10 The growth of diffraction efficiency with time for a grating recorded in a 140μm layer. The incident intensity was 4mW/cm²

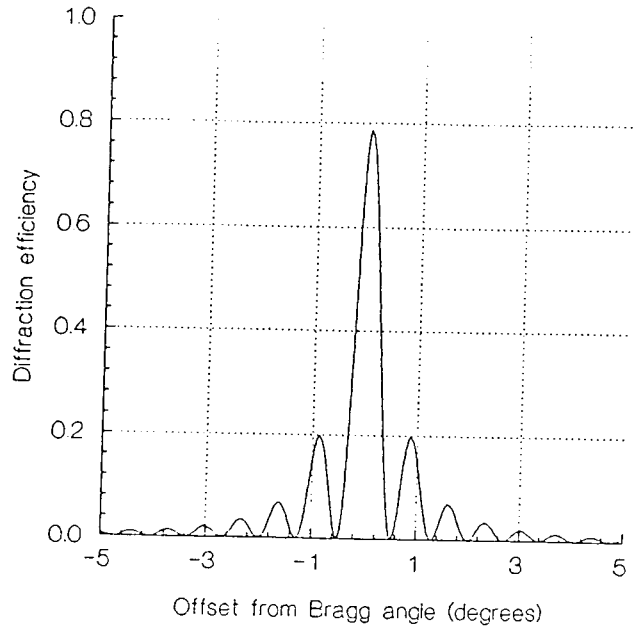

Figure 6.11 (a) Diffraction efficiency as a function of the offset of the incident angle from the Bragg angle, as predicted by coupled wave theory for a 140μm thick grating with a fringe spacing of 1μm, illuminated with 633nm light.

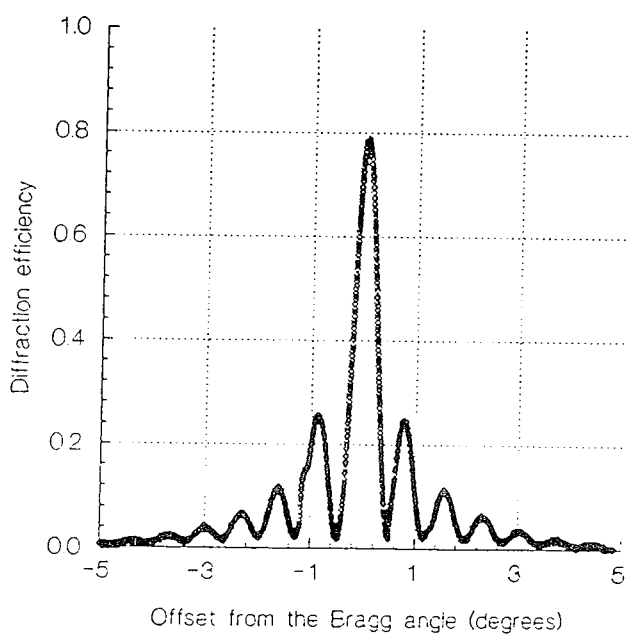

Figure 6.11 (b)Experimental data for diffraction efficiency as a function of the offset of the incident angle from the Bragg angle (δ). The grating, which had a fringe spacing of 1μm, was recorded on a photopolymer layer 140μm thick, and reconstructed with 633nm light

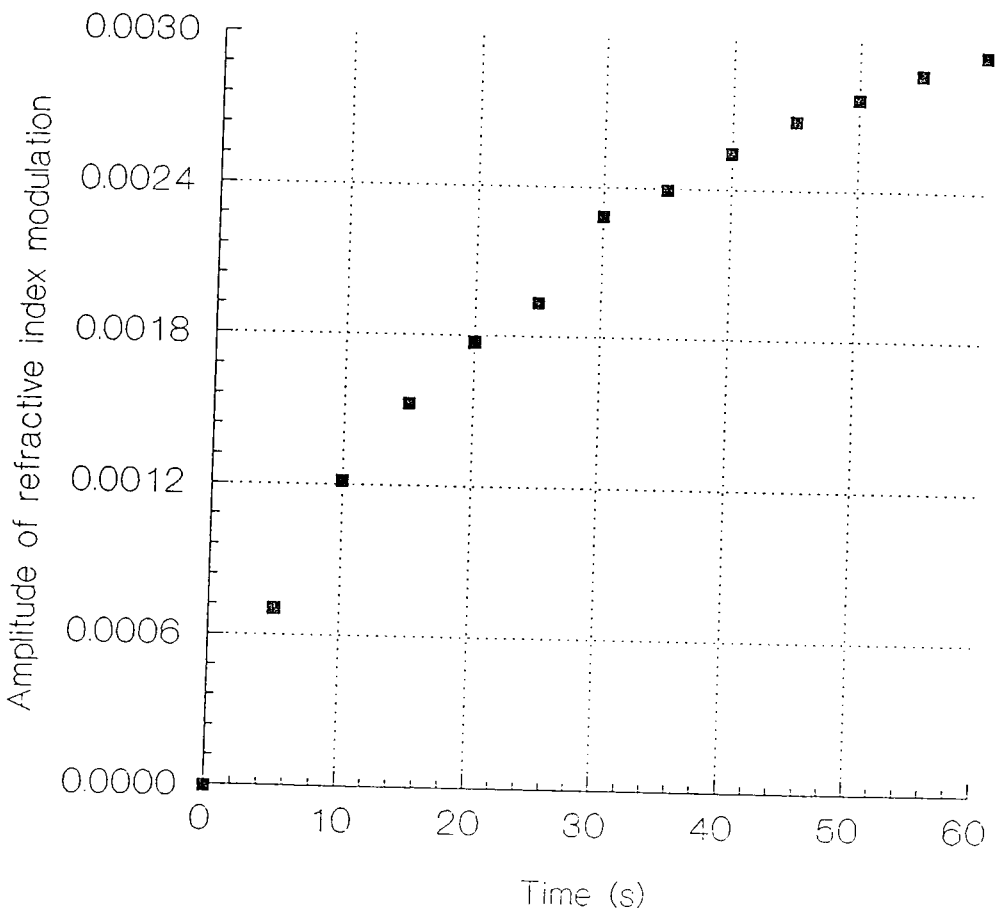

Figure 6.12 The growth of the amplitude of the refractive index variation n_1 with time during the recording of a diffraction grating in a 140μm photopolymer layer.

6.1.4 Angular selectivity data

Plots of diffraction efficiency as a function of the deviation from the Bragg angle such as those shown above demonstrate the angular selectivity of these thick gratings. Of course, as can be seen from equation 6.2, the thicker the grating and the smaller the fringe spacing the greater the angular selectivity. Figure 6.13 shows the angular selectivities of two different spatial frequencies, the broad peak is the response of a 300lines/mm grating and the narrow peak is the response of a 1200 lines/mm grating.

The diffraction efficiency of the higher spatial frequency grating was 95% which gives a value of $3\pi/7$ for ν. Since the layer thickness is 60μm in this example and the Bragg angle (in the medium) is 14.5°, $\xi = 2.7 \times \delta$ is obtained. A theoretical curve calculated with these values is also plotted in Figure 6.13. The fit is so good that the theoretical curve (a solid line) merges with the data points and can only be seen where it deviates slightly from the experimental data points at the maxima of the sidelobes.

The 300 lines /mm grating has an equally good fit with $\nu = 0.3\pi$ and $\xi = 0.66 \times \delta$, calculated for a Bragg angle of 3.6° and a grating thickness of 60μm.

The angular selectivity of a grating is conveniently characterized by the halfwidth of the central peak in these plots. From equation 6.1 it can be seen that for $\nu=\pi/2$ (diffraction efficiency η=100% at the Bragg angle) η goes to zero at ξ=2.7. Using equation 6.2 to relate ξ to δ, the following is obtained

$$\frac{\delta_{\frac{1}{2}}}{} = 1.3 \times \frac{\Lambda \cos\theta_0}{d} \approx \frac{1.3 \times \Lambda}{d}$$

where $\delta_{1/2}$ is the angular halfwidth (in radians), that is the deviation from the Bragg angle required to reduce the diffraction efficiency to half its maximum value. The above relation is only accurate for gratings with diffraction efficiency near 100% but it is a good approximation for any reasonably high diffraction efficiencies (>50%). Taking the gratings in Figure 6.13 as examples, a halfwidth of 0.018 radians or 1° is predicted for the 1200 lines/mm grating and 0.072 radians or 4.1° for the 300 lines/mm grating.

The effect of different layer thickness is similar and halfwidths can also be reliably predicted but it must be remembered that coupled wave theory depends on the assumption that the incident and diffracted waves are the only two waves traveling in the grating. This is not always true of gratings recorded in thinner layers. The Q value discussed in chapter 1 should be greater than 10 if a grating is to be considered 'thick' and analyzed with coupled wave theory. In the example in Figure 6.14 the grating can still be considered 'thick' even though it is recorded in a 5μm layer. The Q factor is 13, so coupled wave theory should be quite accurate. In Figure 6.14 the experimental data is fitted to a theoretical curve plotted with $\xi = 0.18 \times \delta$ and $\nu = 0.19$. Again , the experimental data points merge with the theoretical curve at all angles shown. The waviness is simply noise in the Helium Neon probe beam. It is observed that the angular selectivity is quite low at this thickness. The grating has an angular halfwidth of more than 15°.

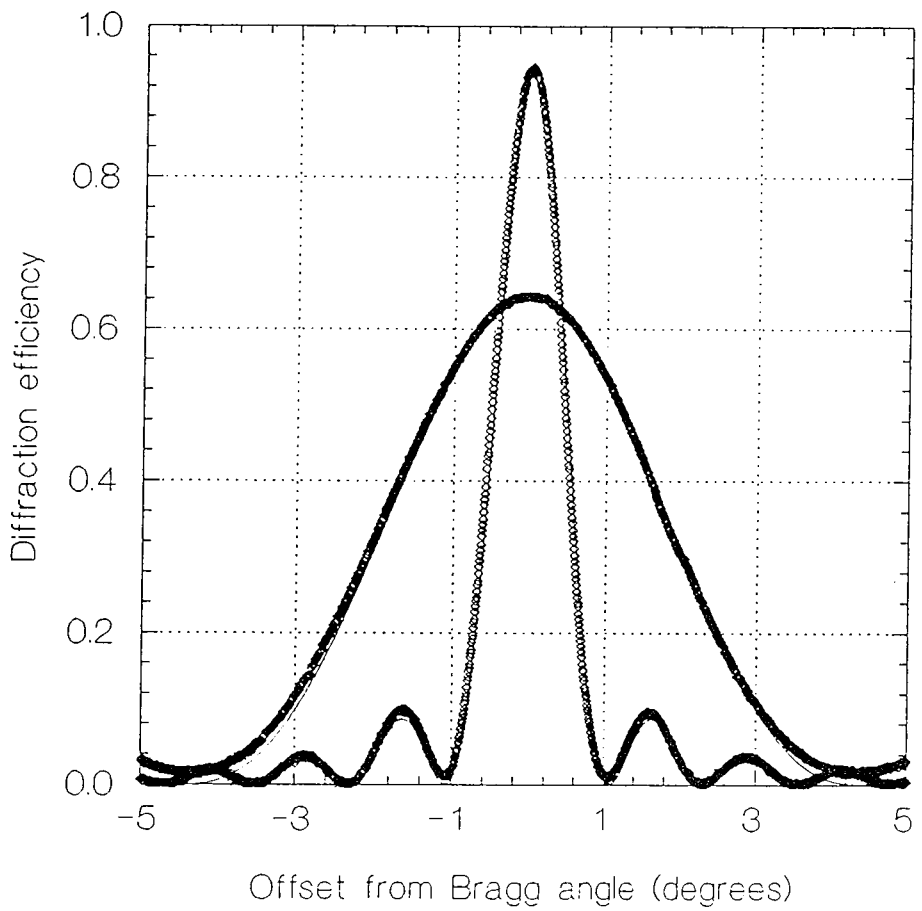

Figure 6.13 Diffraction efficiency as a function of deviation from the Bragg angle for two gratings with different spatial frequencies; 12000 lines/mm (narrow peak) and 300 lines/mm (broad peak). The theoretical curves predicted by coupled wave theory for these spatial frequencies are also shown. Both layers are 60μm thick and were recorded by exposure to 6mW/cm² for 60 seconds.

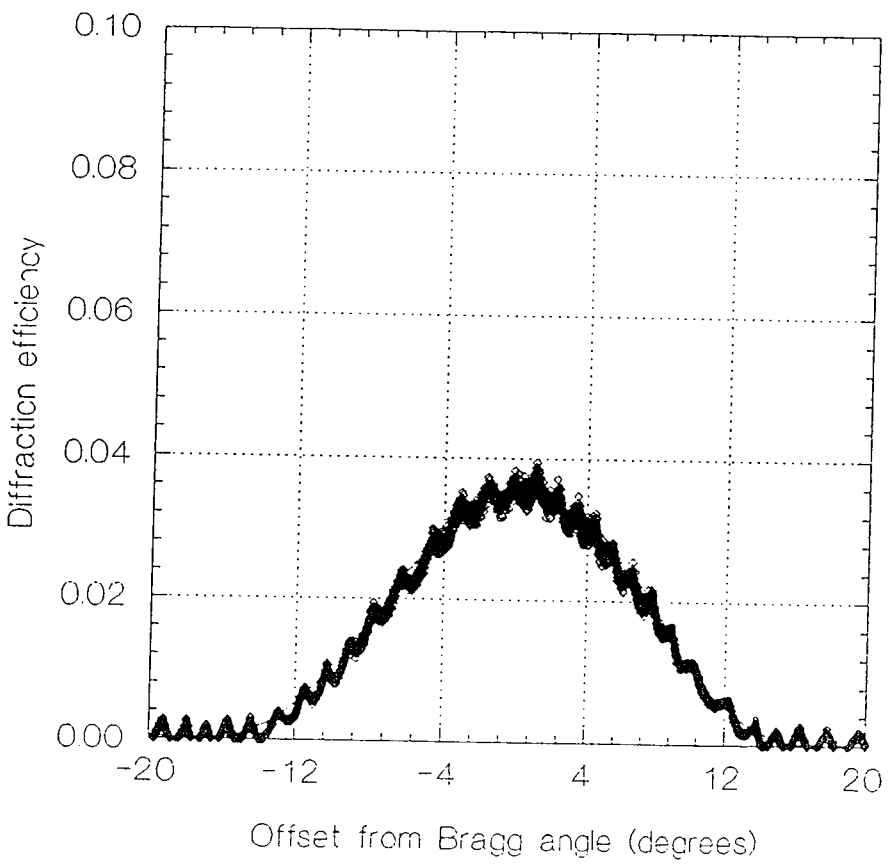

Figure 6.14 Experimental data for the angular selectivity of a grating recorded on a layer approximately 5μm thick at a spatial frequency of 1000 lines/mm. The theoretically predicted curve is shown as a solid line but it merges with the data points.

Throughout these experiments there was a close agreement between coupled wave theory predictions and the experimental data; this confirms that the grating is a phase grating which extends throughout the thickness of the layer. In other words the effective thickness of the grating equals the actual thickness of the layer; proving that the recorded grating extends through the full volume of the photosensitive material in these examples.

Loss (at 633nm) is negligible and the amplitude of the refractive index modulation is usually about 4×10^{-3} at saturation. The actual diffraction efficiency depends on the layer thickness. Very high diffraction efficiencies close to 100% are routinely achieved and thicker gratings (>100μm) can easily be overmodulated.

Figure 6.15 is the angular selectivity curve for an overmodulated grating. The diffraction efficiency at the Bragg angle was 40% and the angular selectivity grating shows the characteristic sidelobes observed for all overmodulated gratings. As chapter 1 showed these sidelobes increase in size as the grating becomes more and more overmodulated and the central peak, the diffraction efficiency at the Bragg angle, decreases. Thicker gratings can easily be overmodulated and gratings of this type have been frequently recorded in these layers.

Angular selectivity can be controlled in overmodulated and undermodulated gratings by setting the thickness and spatial frequency of the grating to the required value. Since good quality layers of 150μm thickness are easily prepared, and spatial frequencies of greater than 2200 lines/mm can be recorded with greater than 50% diffraction efficiency, angular selectivities better than one fifth of a degree are easily obtained.

If the incident angle is held constant and the wavelength of the probe beam is varied the wavelength selectivity of the grating can be observed. A xenon arc lamp with monochrometer was used to determine the spectral selectivity of a typical 140μm thick grating. Figure 6.16 shows the curve obtained. The curve peaks at 514 nm because the probe beam is incident at the Bragg angle for 514 nm light. The spectral halfwidth is about 40nm.

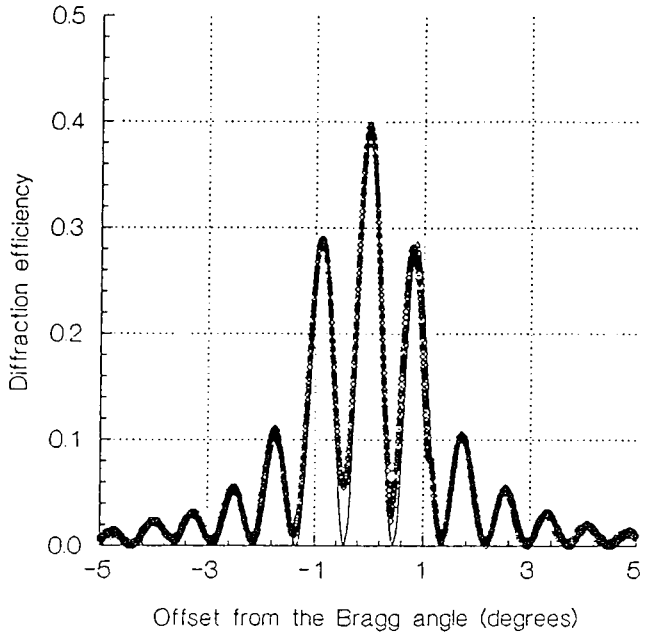

Figure 6.15 The angular selectivity curve of an overmodulated grating 140μm thick.

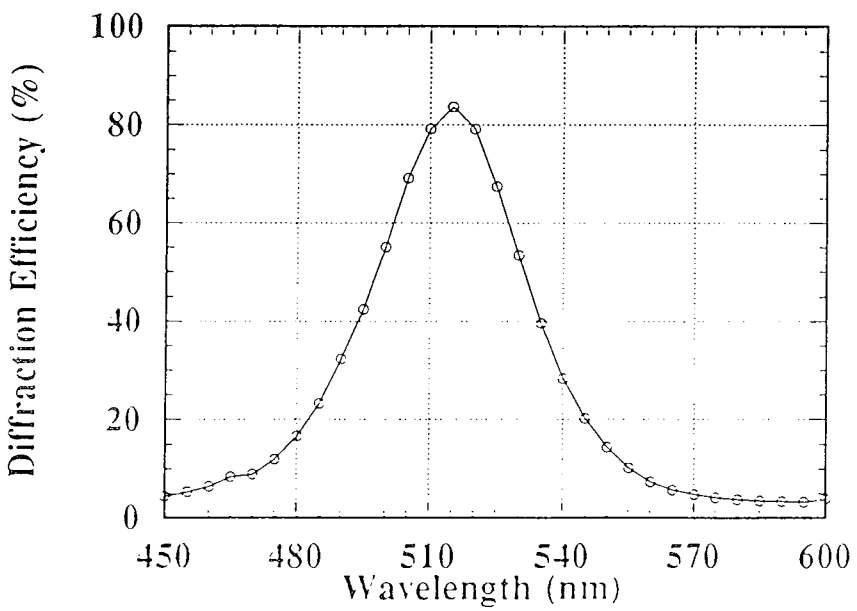

Figure 6.16 The wavelength selectivity curve for a 140μm thick grating.

6.2 Mechanism of refractive index change

The above discussion showed how the refractive index modulation changed during hologram recording. It has already been shown that polymerization is initiated by the absorption of light and this leads to a refractive index change. However, the exact mechanism by which this polymerization causes the refractive index to change is quite complex and inherently difficult to study. This is because the unique conditions under which the polymerization occurs mean that the behavior of the material and its response to illumination, can be quite different to the response under normal polymerization conditions. Observations of bulk photopolymerization of a monomer do not necessarily reveal any information about the polymerization processes occurring on a microscopic scale, in a material where polymerization rates change rapidly over distances of the order of a micron.

6.2.1 Similar systems

In the early 1970's when the first modern photopolymerizable media were appearing Colburn and Haines[8] proposed a diffusion based mechanism for the formation of a refractive index modulation in these materials. They proposed that, during exposure, monomer in areas of higher intensity illumination is polymerized to a greater extent than in lower intensity areas. The binder reduces the shrinkage that would usually occur so initially the effect of exposure is to lower the refractive index because of the reduced polarizability of the polymer (due to the conversion of double bonds to single bonds). The exposure therefore produces concentration gradients and additional monomer diffuses into the regions of higher exposure. An overall uniform exposure fixes the hologram and

polymerizes all the remaining monomer. The resulting polymer concentration is greater in the regions which initially received a higher exposure, thus the refractive index is higher in these regions. Jenny[9] had observed that in his photopolymer material, gratings formed as combinations of surface relief gratings and volume phase gratings. Boiko et al[10] have recently observed surface relief gratings in a red sensitive version of the photopolymer material studied in this thesis, but only at low spatial frequency. In higher spatial frequency gratings volume effects were dominant and surface relief was negligible. In the red sensitive material the surface relief grating disappeared above 45lines/mm.

In 1975 Booth[11] published a review of the Dupont holographic photopolymer which suggested an exposure mechanism close to that described by Colburn and Haines. The Dupont material showed a characteristic initial rise in diffraction efficiency followed by a fall and then a further rise to the final diffraction efficiency. This type of diffraction efficiency growth curve was observed whenever conditions caused the polymerization rate to exceed the diffusion rate, for example at high intensity, low monomer content or low spatial frequency. This was explained by Booth as follows. On exposure to the interference pattern the regions of highest intensity begin to polymerize. If the power density is low ($<2mW/cm^2$) the diffraction efficiency will continue to rise. If it is higher the initial polymerization rate will exceed the diffusion rate and the initial increase in diffraction efficiency will be followed by a decrease which occurs as material begins to diffuse into the exposed regions lowering the refractive index modulation and thus the diffraction efficiency. He has shown that the diffusion time depends linearly on the square of the diffusion distance, confirming the diffusion hypothesis. Figure 6.17 (a) is taken from this reference and shows how the growth curves in the Dupont photopolymer vary at different spatial frequencies. These curves indicate that linearity of recording is not good in this material as the relationship between diffraction efficiency and exposure is complex and very

dependent on spatial frequency. Booth also reported large increases in diffraction efficiency on exposure to a uniform beam of light *after* normal exposure had ended. The increase was rapid, usually faster than the original grating growth during normal exposure, and optimum diffraction efficiency was achieved with a uniform post exposure 2-6 minutes after initial exposure to the interference pattern had ended. This final uniform exposure completes the polymerization process in both the bright and dark fringes but it was not certain why this increased the overall refractive index modulation by such a large factor, Booth suggested that another reaction, perhaps density related, might be occurring which would account for this large diffraction efficiency increase. Examples of the response of the Dupont material to post exposure to a uniform beam are given in Figure 6.17 (b).

In 1976 Tomlinson et al[12] proposed a two way diffusion mechanism to account for the high refractive index modulations they observed in their two monomer systems. The material is similar to other polymerizable materials in that it contains a sensitizer-catalyst system in a polymeric binder, but the active component is a mixture of two or three different monomers, usually a high reactivity monomer and crosslinker and a low reactivity monomer or inert component.

The proposed mechanism involves the preferential polymerization of monomer in the bright fringe areas producing a concentration gradient which causes additional high reactivity monomer to diffuse into the high intensity areas. Thus far the mechanism is the same as for previous systems. However, as the polymerization proceeds, the volume fraction of polymer in the high intensity areas increases and monomer will tend to be excluded from these areas. The resulting refractive index modulation comes from the fact that the higher intensity areas contain a polymer with an excess of the high reactivity monomer and the low intensity areas contain an excess of the low reactivity monomer. Tomlinson et al point out that the two way diffusion system is necessary to explain the magnitude and sign of the

refractive index changes obtained with various similar systems. If the diffusion were one way then the only effect of the low reactivity monomer would be to alter the index of the background material. With a high refractive index material as the low reactivity component, areas of low exposure had a higher refractive index, and vice versa when the low reactivity component had a lower refractive index. These results are consistent with the two way diffusion theory but it should be pointed out that the measurements were made by exposing the material to a mask with 80μm holes and this would correspond to material behavior at very low spatial frequency. Recent studies of similar multicomponent materials have shown similar results[13,14,15] and models based on this diffusion process have been proposed.

The acrylamide based material studied here would be classed as a one component system because methylene bisacrylamide acts as a crosslinker and has similar reactivity to acrylamide, although it is also possible that the very large quantities of triethanolamine present could take the role of a neutral component. However, as the refractive indices of triethanolamine and acrylamide are similar (TEA=1.4835, ACR=1.530) the effect of two way migration would not be very noticeable. Systems of this sort usually use materials with vastly different refractive indices.

This material has been studied for a broad range of material compositions, crosslinking monomer fraction, incident intensity level, fringe visibilities, and spatial frequencies but the characteristic dip in the growth curve observed by Booth in the Dupont material has never been observed. Instead a smooth curve like that observed by Booth when diffusion is fast in comparison with polymerization is observed under all conditions. This is not surprising as the binder used in our system is polyvinyl alcohol which is a very permeable polymer particularly when the water content is high.[16] and diffusion would probably be much faster than in the Dupont material.

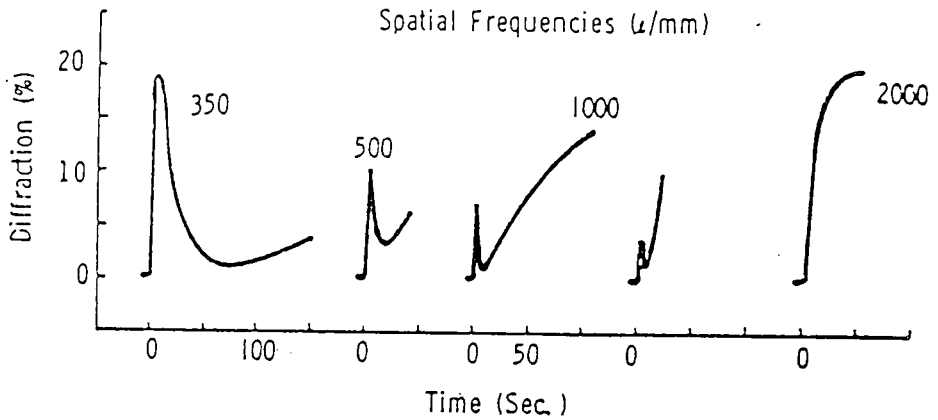

Figure 6.17.(a) The diffraction efficiency monitored during exposure for different spatial frequency gratings recorded in the Dupont photopolymer. Higher spatial frequencies with shorter distances between exposed regions have a faster diffusion rate.(from Booth)[11]

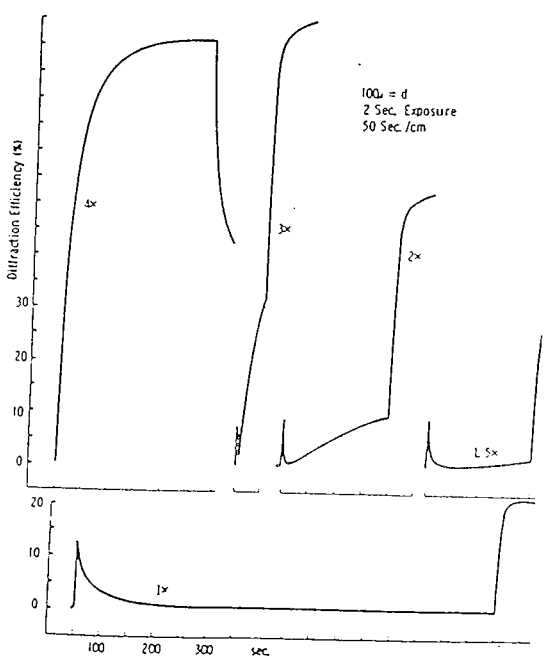

6.17. (b) Grating formation and response to uniform post exposure varies with activator concentration. All exposures are for 2 sec with a sweep rate of 50s/cm. The abrupt change is the post exposure using one of the two interfering beams. (from Booth)[11]

6.2.2 Theoretical analysis of refractive index changes

Tomlinson and Chandross[17] have described the physical and chemical changes leading to refractive index change. The Lorentz Lorenz relation gives us the relationship between refractive index and the optical polarizability per unit volume *P*.

$$\frac{n^2-1}{n^2+2}=\frac{4}{3}\pi P$$

For a pure substance the polarizability per unit volume is equal to the polarizability per molecule, α , times the number density of molecules so the equation can be rewritten in the form

$$\frac{n^2-1}{n^2+2}=\frac{4\pi\rho N\alpha}{3M}=\frac{\rho R}{M}$$

where M is the molecular weight, ρ is the density, N is avogadro's number and the quantity R is usually referred to as the molar refraction. For an ideal mixture (i.e. with no interactions between the components) the following relationship is obtained

$$\frac{n^2-1}{n^2+2}=\sum_i\frac{\rho_i R_i}{M_i} \qquad (6.1)$$

where ρ_i is the density *in the mixture* of the i^{th} component, and R_i and M_i are its molar refraction and molecular weight. From this relationship the three main ways in which the refractive index of a material can be altered are evident. Tomlinson and Chandross describe the three methods as follows.

(1) One can cause a change in the molecular structure of one or more components of the sample so as to change their molar refractions. This does not require the addition or removal of any material.

(2) One can change the overall density of the sample , defined as a fixed volume in space without changing its basic chemical composition This requires that material be either

added or removed. Molecular structure changes, such as polymerization can change molecular packing and thus cause substantial density changes. For example consider the initiation of a typical vinyl polymerization in one region of a liquid monomer. As the higher density polymer is formed from monomer more of the latter is drawn in from the surrounding volume, the result is the addition of material to the sample volume under consideration, allowing it to reach the full (higher) density of the polymer.

(3) One can alter the relative concentrations of the various components of the sample while leaving the overall density unchanged. This requires both the addition and removal of material . Of course, to get a large change in refractive index one must alter the relative concentrations of components that have significantly different refractivities.

Tomlinson and Chandross have presented a model for calculating refractivities, which allows the prediction of the magnitude and sign of the refractive index change associated with simple photochemical changes. At optical frequencies the molecular polarizability is primarily determined by the outer electrons of the atoms making up the molecule. It has been shown that for a considerable variety of molecules it is possible to make reasonably accurate calculations of the polarizability by assigning an empirically determined polarizability to each type of chemical bond and then simply adding up these polarizabilities for all the bonds in the molecule. For example methyl methacrylate has a density of 0.9440g/cm^3 and the molar refraction calculated as described is 26.58 giving a value for refractive index of 1.4228 (the molecular weight is 100.13g). The actual refractive index is 1.4142.

On polymerization the density of the material increases to 1.19g/cm^3 and the chemical structure is altered. In each monomer unit a carbon carbon double bond (bond refraction 4.16cm^3) is replaced by two carbon-carbon single bonds (bond refraction 1.25cm^3). The

calculated molecular refraction becomes 24.2cm^3 which would cause the refractive index of the polymer to be lower than the monomer if the polymerization process did not also cause an increase in density. As is usually the case in vinyl polymerizations the density effect outweighs the drop in molar refraction caused by the chemical changes and the refractive index is increased. In this case the calculated value is 1.5041 and the actual value is 1.488. In most polymerizable systems significant density changes occur and this effect usually outweighs the effect of structural changes in the molecule. Although the above model does not give exact values for refractive index it agrees fairly closely in most cases with experimentally observed values and is very useful for determining the approximate magnitude and the sign of the changes in refractive index caused by specific photochemical changes

6.2.3 Mechanism of refractive index change in the acrylamide based material.

The acrylamide based photopolymerizable material studied here is somewhat different to most polymerization processes in that the material shrinkage is severely restricted by the polyvinyl alcohol binder in which the monomer is dispersed. We have shown that at spatial frequencies typical of holographic recording, there is no surface grating and no shrinkage when polymerization occurs. Any density change that takes place must be due to the addition or removal of material from a particular area by diffusion. This means that the density effects may or may not outweigh the reduction in molecular refraction (depending on how easily diffusion can occur) and no direct comparison can be made between the behavior of the monomer when it polymerizes under normal conditions and its behavior under these circumstances. It is also true that macroscopic measurements of refractive index change obtained with the monomer contained in the binder, but under uniform illumination are equally invalid, as diffusion will be greatly reduced under these conditions

and the material response can be quite different. In fact the refractive index changes in the material must be analyzed while fringe widths are of the order of a micron to get a true picture of the processes that lead to refractive index modulation and hologram formation. This makes analysis more difficult as direct measurements cannot be taken .

The model described above can be useful in determining the relative contributions of each process but the more complex the system the more difficult it becomes to predict the effect of photochemical changes on the refractive index.

In order to determine the exact mechanism of the formation of the refractive index modulation in this material it was necessary to study the response of the material to normal exposure to an interference pattern followed by illumination with a single beam. The shape of the growth curve, response to uniform illumination and effect of varying the delay between the two exposures revealed important information about the growth mechanism.

The following study of the materials response proves that mass transport by diffusion is at least partly responsible for the refractive index modulation because exposing the recorded grating to a uniform beam of light did not erase the refractive index modulation. Post exposure to a uniform beam of light would erase any hologram unless mass transport has occurred. Suppose the refractive index modulation induced during normal recording were due only to the bond conversion that occurs during polymerization and the associated change in molecular refraction, and no mass movement of material was possible in the layers (a substantial reduction of refractive index would result). In that case uniform exposure to a single beam of the recording wavelength would polymerize the monomer in the dark fringe areas and convert it to the same refractive index as the bright fringe areas. No refractive index modulation would remain. Even if the argument were made that

polymerization is known to be favored in areas where there is already a high percentage conversion[18] the decline of the index modulation would only be slowed. Without mass transport, the dark fringe regions would ultimately 'catch up' with the bright fringe regions. Since we can expose a grating recorded in the photopolymer material to a uniform beam of 514nm light without reducing its diffraction efficiency we must conclude that mass transport of material and the subsequent increase in density in bright regions is responsible for the refractive index modulation.

It will be shown that diffusion plays a major role in the formation of a refractive index modulation, and that density variation caused by mass transfer of material from the dark to bright fringe areas is the most important contributor to the refractive index change. This hypothesis is backed up by the observations of grating behavior after recording (see chapter 3). In the original formulation layers (without crosslinking agent) gratings disappear within hours of recording and the rate at which they disappear depends on the layer permeability. This indicates that diffusion is also responsible for he short shelf life of the recorded holograms. In a very permeable layer the density modulation caused by polymerization will smooth out by slow diffusion of the polymer strands into the low density dark fringe regions causing the refractive index modulation to decrease and finally disappear.

Also there is much evidence from our results, to be discussed in this chapter, and those of other authors, discussed above, that in this material[19] and other dry photopolymers[20] diffusion is not only possible but commonly occurring even over relatively large distances (tenths of millimeters). Polyvinyl alcohol in particular is known to be a very permeable polymer host[21,22].

6.3 Diffraction efficiency enhancement by uniform post exposure.

The following section describes post exposure experiments of the type carried out by Booth on the Dupont photopolymer. A detailed study was carried out on the acrylamide based photopolymerizable material. Observation of grating growth curves and the response of gratings to uniform exposure allows us to understand some of the physical processes which occur during the recording of a hologram in this material.

The power density was $4mW/cm^2$ for all exposures in this section and layer thickness was approximately $56\mu m$. The layers were prepared with the standard erythrosin B sensitized coating solution. Diffraction efficiency was monitored throughout by illumination at the Bragg angle with a Helium Neon laser as described in chapter 5.

6.3.1 Shutter system for controlling exposure and uniform post exposure

The post exposure experiments in the next section involve monitoring the effect of uniform exposure on a recently recorded grating. The shutter system had to allow the exposure to be controlled in such a way that there was an initial period of normal exposure, followed by a delay of variable duration, during which the grating was not exposed to light, and then exposure to a uniform beam of light.

The simplest way to achieve this was to allow normal exposure to two beams of light which interfere in the plane of the recording medium, and thus record a grating, then simultaneously block both beams, and after a preset time allow one of the two beams to expose the grating, thus illuminating it with a uniform beam of light.

The Uniblitz electronic shutter was used to control the initial exposure and the delay period, since its timing can be preset and is very accurate. Uniform post exposure was achieved by causing a solenoid controlled shutter to close during the delay period so that when the Uniblitz shutter re-opened there was only one beam illuminating the grating. The experimental setup is shown in Figure 6.19.

Since it was necessary to use the Uniblitz shutter in continuous mode the shutter had to be deliberately disabled after the uniform post exposure had begun in order to prevent it from closing prematurely. A +5V signal in control #3 of the Uniblitz shutter is all that is necessary to force it to remain open, so the circuit was arranged to deliver such a pulse just as the shutter reopened for the uniform exposure.

The Uniblitz shutter has a coaxial output which gives a +5V signal *when the shutter is closed*. As Figure 6.18 shows, this was connected to the clock terminal of a J-K flip flop with J (1J) and K (1K) held high. The output therefore changed state on a negative going transition of the clock pulse (1CLK) as shown below. The output ($1\overline{Q}$) was connected to the clock input (1CLK) of a D type flip flop. Data (1D) and set (1PR) were tied high so that the device triggered on changes from low to high.

The input to the J-K flipflop(7473) from the Uniblitz shutter was

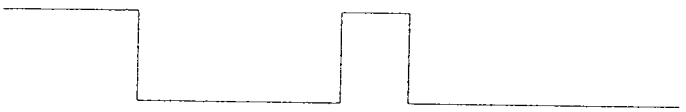

The output $\bar{Q}$ from the J-K flip flop (7473) was

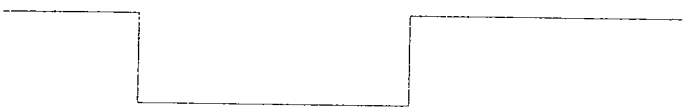

The output Q from the D-type flip flop (7474) was

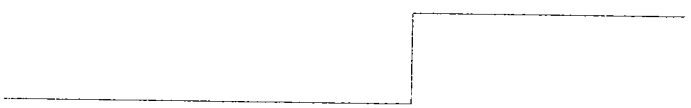

This was connected to control #3 on the Uniblitz shutter so that the shutter was forced to remain open indefinitely as soon as the post exposure period began.

The same input was fed directly into the clock input (2CLK) of the second D type flip flop and its output (2Q) was

The output therefore changed state at the first positive going edge, which triggered the solenoid to close just after the two beam exposure ended and the delay period began.

The +5V pulse from the second D-type flip flop was stepped up to a 12V signal by a transformer and applied to the solenoid. An aluminium blade attached to the solenoid axle blocked the beam when the 12V signal was applied.

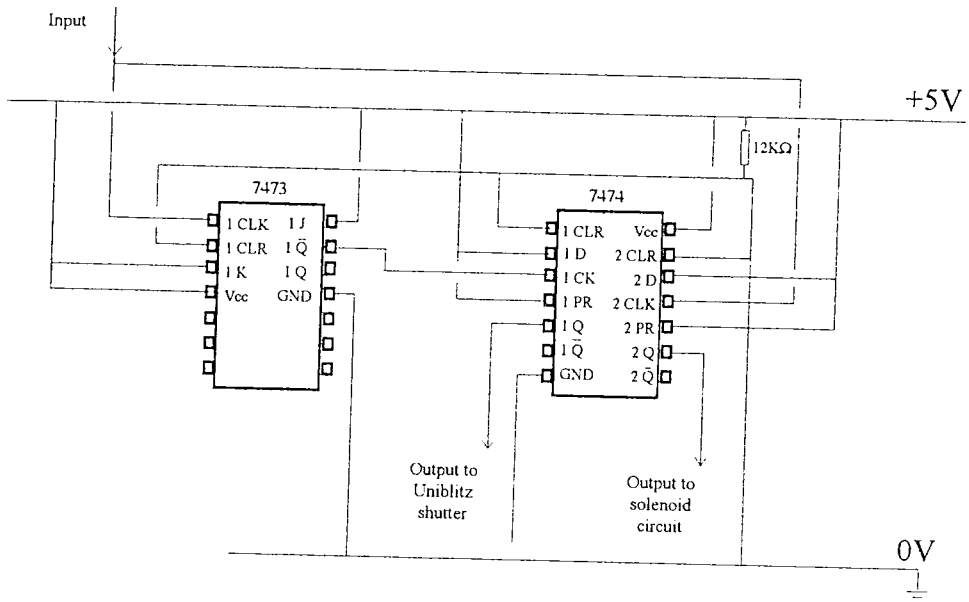

Figure 6.18 Circuit diagram for shutter control system.

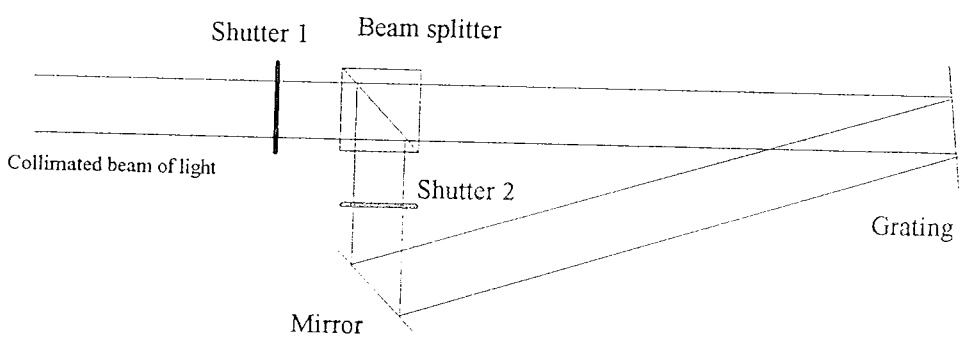

Figure 6.19 Experimental arrangement for the post exposure experiments. Shutter 1 is a Uniblitz electronic shutter and shutter 2 is a solenoid controlled shutter triggered to close by shutter 1.

6.3.2 The effect of uniform post exposure on a recorded grating.

A series of experiments was carried out in order to study grating formation. The photosensitive layers were exposed as follows.

(I) Normal exposure: The layers were exposed to the interference pattern formed by two collimated beams of 514nm light as in normal recording.

(II) Delay: The exposing beams were shut off and the recorded grating was left in the dark for a preset time

(III) Uniform post exposure: One of the exposing beams was used to expose the grating to a uniform beam of light

The diffraction efficiency of each grating was monitored throughout the experiment with an unexpanded 633nm Helium Neon beam incident at the Bragg angle. As discussed above, if mass transport by diffusion has occurred, exposure to the uniform beam in step three would not be expected to erase the refractive index modulation. As the results will show, the recorded grating was not erased, in fact illumination with a uniform beam of 514nm light caused further diffusion to occur and the diffraction efficiency was greatly enhanced, often reaching more than three times its original value. Figure 6.20 shows the typical behavior of a standard concentration layer, exposed as described above. As would be expected, there is an initial increase in diffraction efficiency when the layer is exposed to the interference pattern formed by the two overlapping beams in step one. During step two the diffraction efficiency remains almost constant at the value it had when recording was interrupted. Exposure to a uniform beam during step three causes a further increase in diffraction efficiency, in fact in this example the diffraction efficiency reaches three times its initial value.

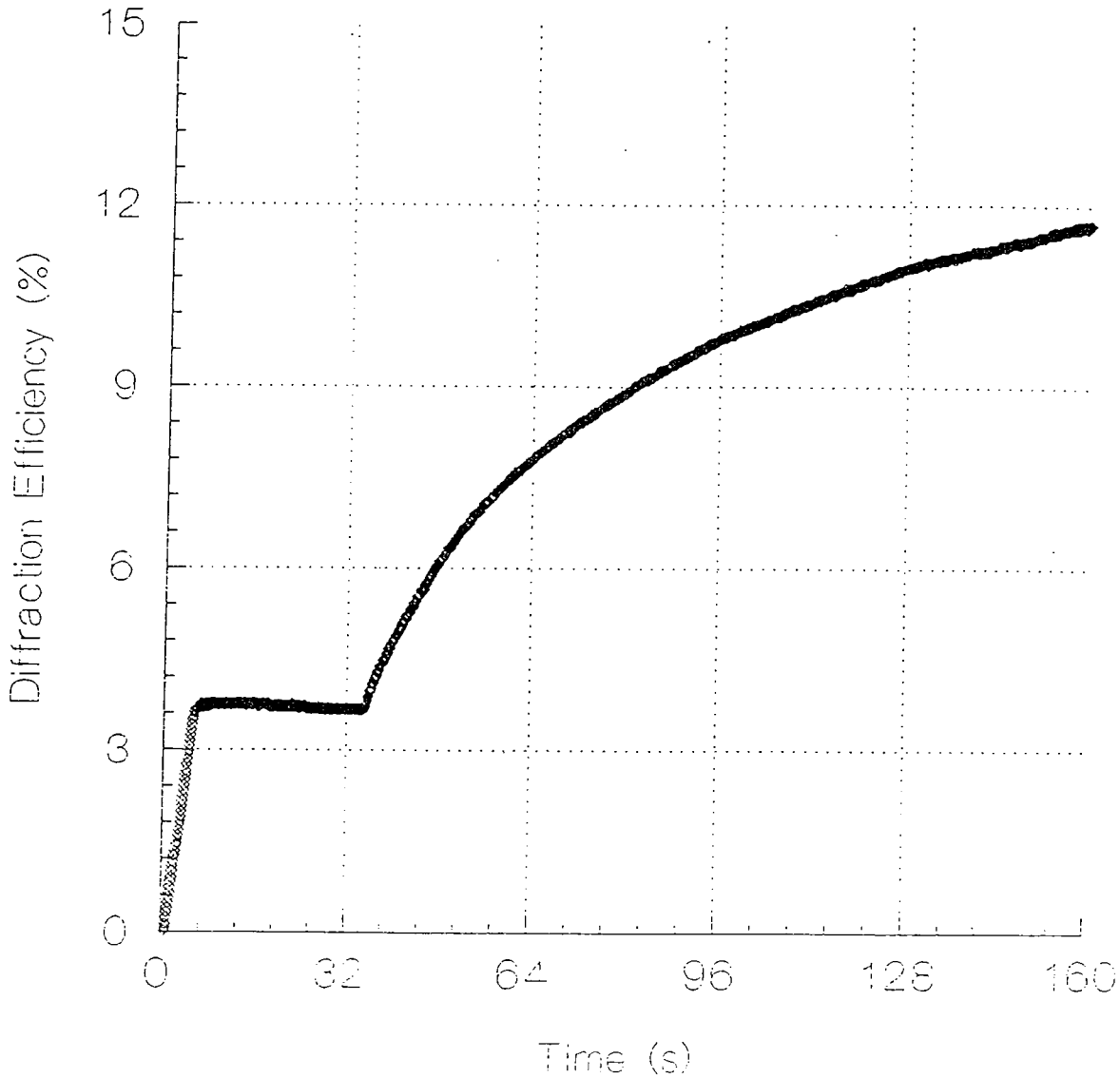

Figure 6.20 The change in diffraction efficiency of a grating recorded by a normal exposure of 5 seconds (step I) followed by a delay of 30 seconds (step II) and then a uniform exposure (Step III). Grating fringe spacing is 2.2μm.

This behavior can be explained as follows. During the normal two beam exposure polymerization occurs at a much higher rate in the bright fringe areas. In fact if the contrast is unity the polymerization rate in the center of the dark fringes should be almost zero (equal to the dark polymerization rate) since the intensity there is zero. As polymerization occurs in the bright fringes a concentration gradient is formed and material is brought in by diffusion from the unpolymerized dark fringe areas. The result is an increasing density in the bright fringe areas and a decreasing density in the dark fringe areas and hence a refractive index modulation.

When the recording is interrupted, polymerization and diffusion stop immediately and the density modulation remains practically unchanged until the grating is further illuminated.

In the next step illumination is uniform and therefore polymerization will occur in both the bright and dark fringe areas[†]. This will reduce the refractive index in both the bright and dark fringes but since there is less monomer in the bright fringe areas, the refractive index will be reduced to a greater extent in the dark fringe areas, increasing the refractive index modulation.

As the results will show (section 6.3.3) diffusion is almost immediate. As normal exposure progresses enough monomer migrates into the bright fringe areas so that the density effect counteracts the drop in refractive index caused by polymerization and causes a small increase in refractive index in the bright fringe areas. At the same time

---

[†] It may be argued that under uniform exposure polymerization will be favored in the bright fringe regions. As mentioned above, it is well known that the polymerization rate is usually higher where some conversion has already occurred and increases further at higher percentage conversion. This is because the chain termination rate is reduced in regions of high viscosity and therefore the overall polymerization rate is increased. However although this may be true in liquid photopolymer formulations where the initial viscosity is low and a very large viscosity increase accompanies polymerization, the effect must be greatly reduced in a material such as this where viscosity is already high because of the polymer binder.

the refractive index in the dark fringe regions has dropped slightly due to the loss of material from this area and the consequent decrease in density. The density modulation has a much greater effect on the overall refractive index than the reduction in molecular refraction that accompanies polymerization, so that a very small amount of diffusion will produce the required effect. The fact that any refractive index modulation remains after uniform post exposure is proof that material migrates from one region to another during normal exposure. However once the grating is exposed to uniform illumination, polymerization of the dark fringe regions will mean that any refractive index modulation which remains must be due to density variations alone.

Furthermore it can be assumed that no more diffusion occurs once normal exposure has ended. It will be shown that negligible diffusion occurs during the delay period (step II) and since polymerization rates in bright and dark fringe areas are approximately equal under uniform illumination, this means that no diffusion occurs during uniform exposure (step III) either. This is important because it means that it can be assumed that the refractive index modulation present after uniform exposure is due only to material diffusion that occurred during normal exposure (step I). This simplifies the analysis somewhat.

Since the effect of post exposure depends on the amount of diffusion which occurred during normal exposure, it will depend on the length of normal exposure time before uniform post exposure. However since diffusion is fast in this material, there is no dependence on delay time.

6.3.3 Effect of varying the delay before post exposure to a uniform beam.

The electronic shutter control described above allowed accurate control of the exposure period and delay times from milliseconds to hundreds of seconds. The effect of varying the delay time was studied over the whole range of delay times at three different spatial frequencies and no significant change was recorded. Figure 6.21, Figure 6.22 and Figure 6.23 are examples. The length of the delay period does not have any significant effect on the diffraction efficiency increase under single beam illumination. The fact that there is no increase in diffraction efficiency during the delay period when the grating is not illuminated indicates that diffusion stops as soon as the illuminating light is removed and is not a slow process which continues on after polymerization has stopped. If it were, some change in diffraction efficiency would be observed, and the effect of uniform post exposure would be different for different delay times, as was observed by Booth in the Dupont photopolymer.

Figure 6.24 is a close up of the point where normal exposure was stopped (after 8 sec) on a standard layer. The diffraction efficiency increase is observed to stop almost immediately the two beam exposure is ended; the diffraction efficiency growth curve is completely level less than half a second after illumination has stopped. The conclusion that can be drawn from these results is that both diffusion and polymerization are fast processes with rates of the same order of magnitude, as neither continues after exposure is interrupted, and that both processes only occur under illumination. If diffusion were the slower process the increase in diffraction efficiency would continue after exposure ended and variation of the delay between writing the grating and uniform post exposure would affect the response to uniform exposure.

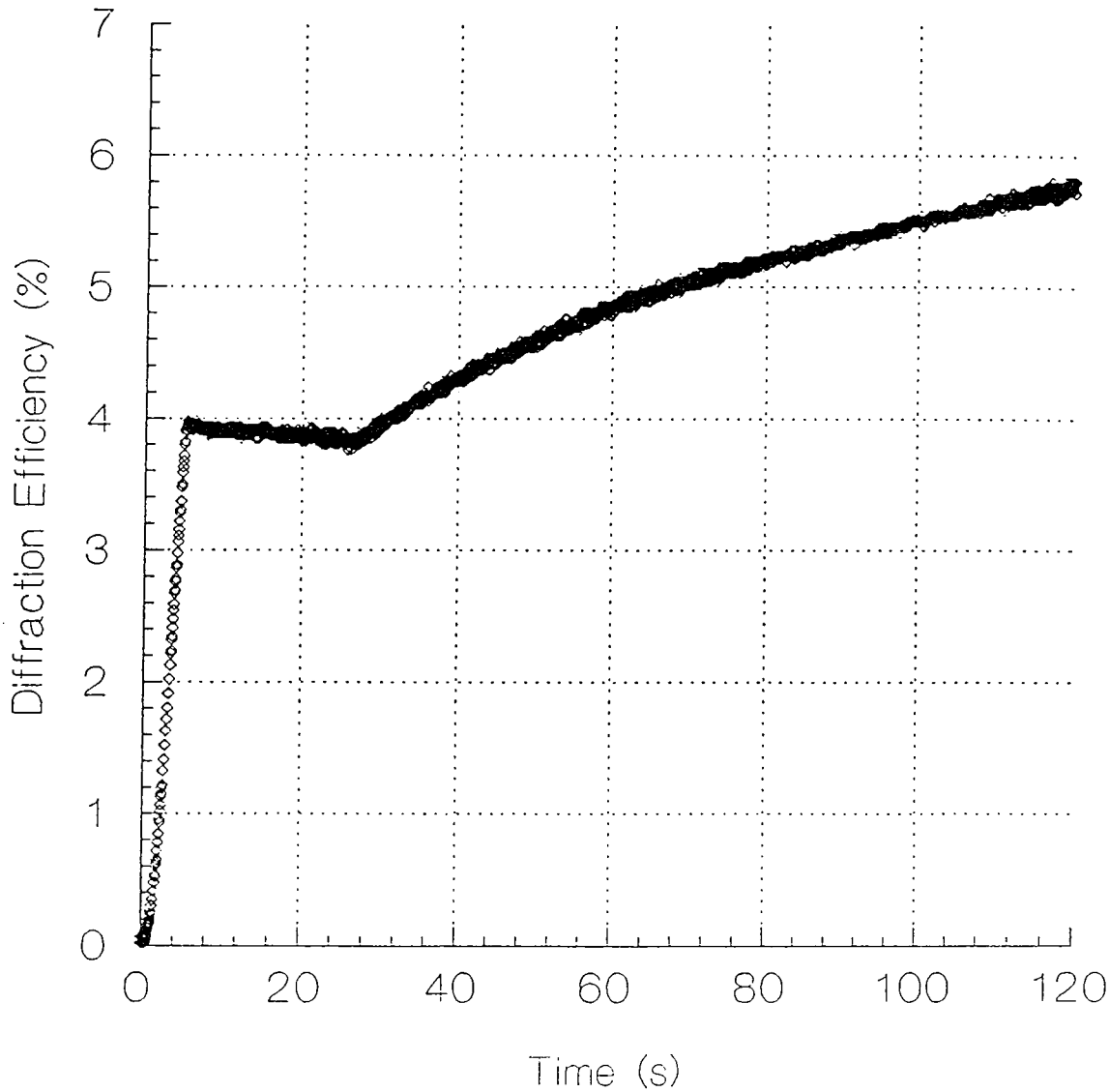

Figure 6.21 The change in diffraction efficiency of a grating recorded by a normal exposure of 5 seconds (step I) followed by a delay of 20 seconds (step II) and then a uniform exposure (step III). Grating fringe spacing is 1 μm.

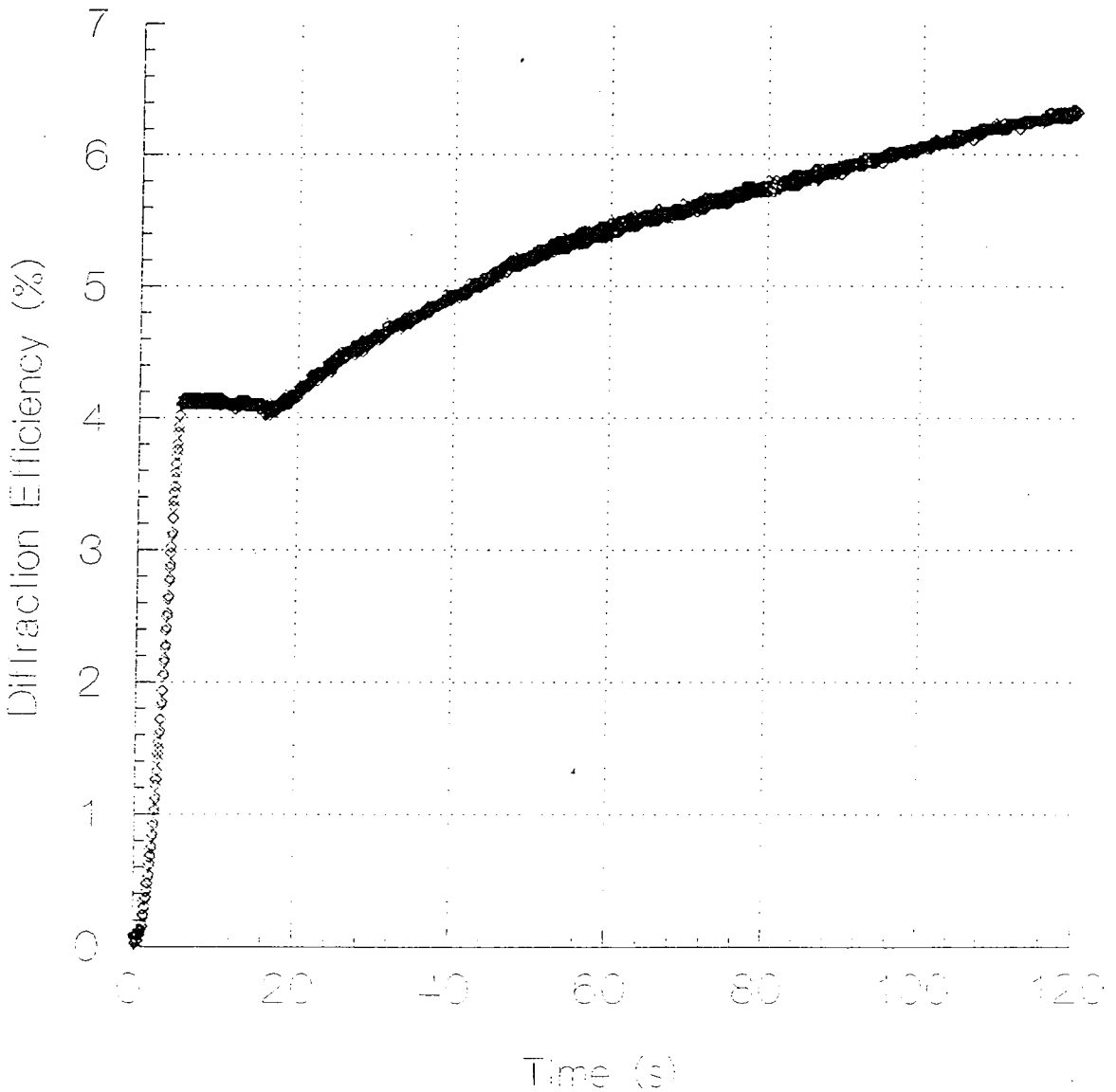

Figure 6.22 The change in diffraction efficiency of a grating recorded by a normal exposure of 5 seconds (step I) followed by a delay of 10 seconds (step II) and then a uniform exposure (step III). Grating fringe spacing is 1 μm.

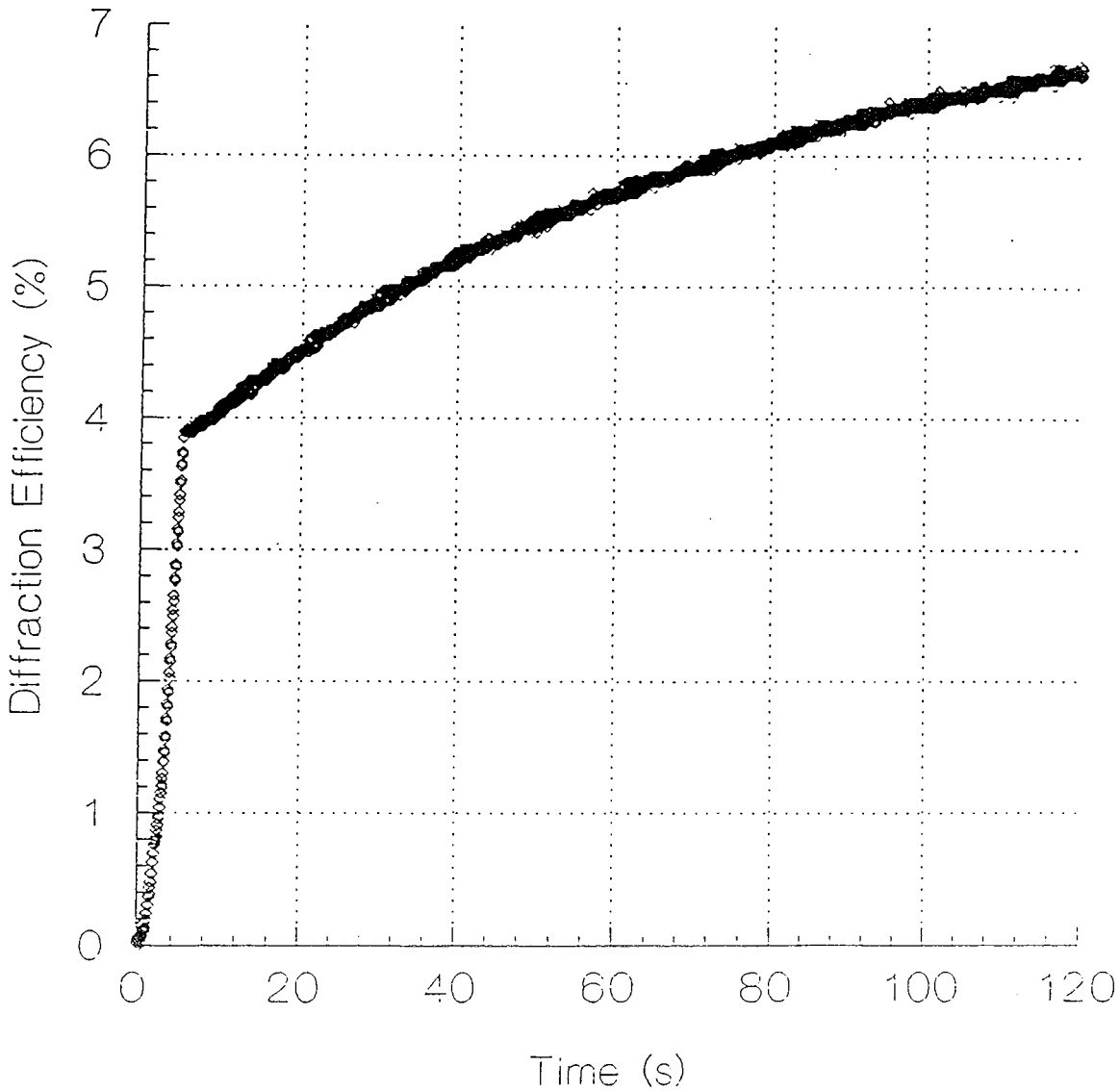

Figure 6.23 The change in diffraction efficiency of a grating recorded by a normal exposure of 5 seconds (step I) followed by a delay of 100 milliseconds (step II) and then a uniform exposure (step III). Grating fringe spacing is 1 μm.

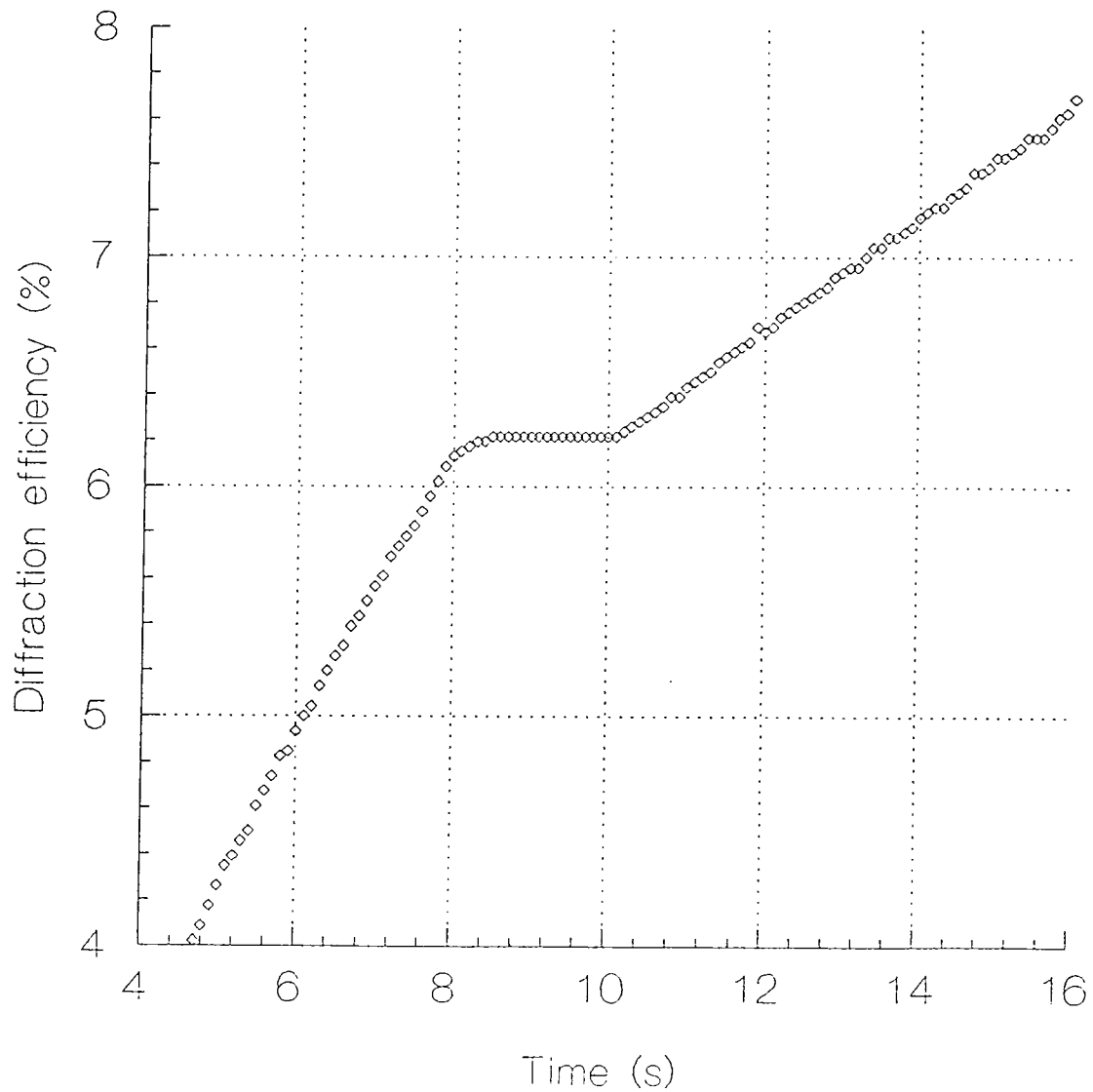

Figure 6.24 The change in diffraction efficiency of a grating recorded by a normal exposure of 8 seconds (step I) followed by a delay of 2 seconds (step II) and then a uniform exposure (step III). Grating fringe spacing is 4μm.

6.3.4 Effect of varying initial exposure to two beams.

A detailed study of the effect of varying the initial exposure to two overlapping beams on the uniform exposure growth rate was carried out. The layers were exposed to the interference pattern for times varying from one tenth of a second to 60 seconds and the effect on the growth rate under uniform exposure was monitored. The delay (step II) was kept constant at 2 seconds. As the initial exposure time was increased the growth rate under uniform exposure also increased, reached a maximum around 15 seconds and decreased again at higher initial exposure time. Figure 6.25, Figure 6.26, Figure 6.27 and Figure 6.28 show four curves for which normal exposure was stopped at one, five, ten and 30 seconds. Although the final diffraction efficiency increases with increasing initial exposure, it is obvious from these examples that in the first 100 s of uniform post exposure the diffraction efficiency increases to approximately 1.5 times its original value. This is true up to about 15 seconds of normal exposure after which, perhaps due to lack of dye sensitizer, the rate of increase under uniform exposure drops. In Figure 6.28 there is no significant increase in the diffraction efficiency under post exposure. The direct relationship between final diffraction efficiency and initial diffraction efficiency would seem to indicate that the amount of diffusion which occurs is linearly dependent on the amount of conversion that has occurred. Since the diffraction efficiency which remains after exposure depends on the amount of diffusion which occurred during exposure it is to be expected that longer exposures to the normal interference pattern will cause a greater percentage conversion of the monomer in the bright fringes and therefore more diffusion and a higher final diffraction efficiency will remain after total polymerization under a uniform beam.

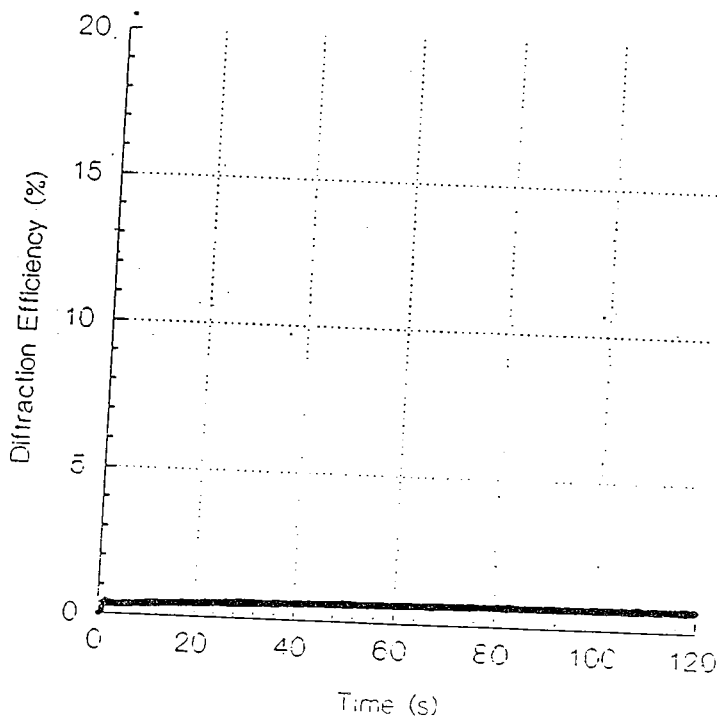

Figure 6.25 The change in diffraction efficiency of a grating recorded by a normal exposure of 1 second (step I) followed by a delay of 2 seconds (step II) and then a uniform exposure (step III). Grating fringe spacing is 1 μm.

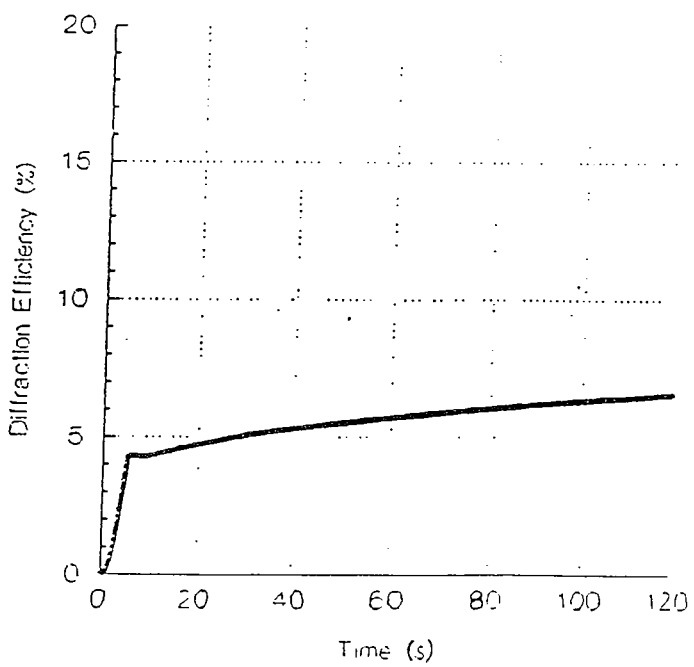

Figure 6.26 The change in diffraction efficiency of a grating recorded by a normal exposure of 5 seconds (step I) followed by a delay of 2 seconds (step II) and then a uniform exposure (step III). Grating fringe spacing is 1μm.

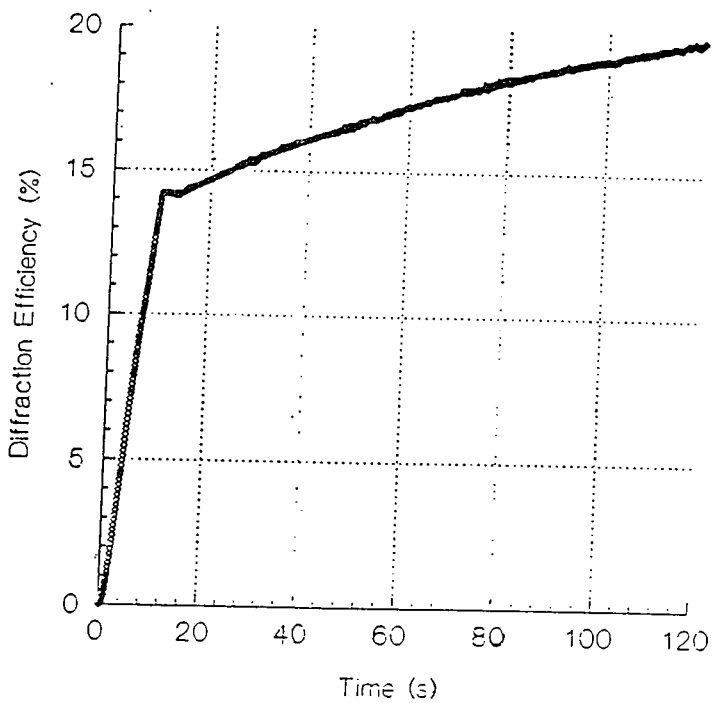

Figure 6.27 The change in diffraction efficiency of a grating recorded by a normal exposure of 10 seconds (step I) followed by a delay of 2 seconds (step II) and then a uniform exposure (step III). Grating fringe spacing is 1 μm.

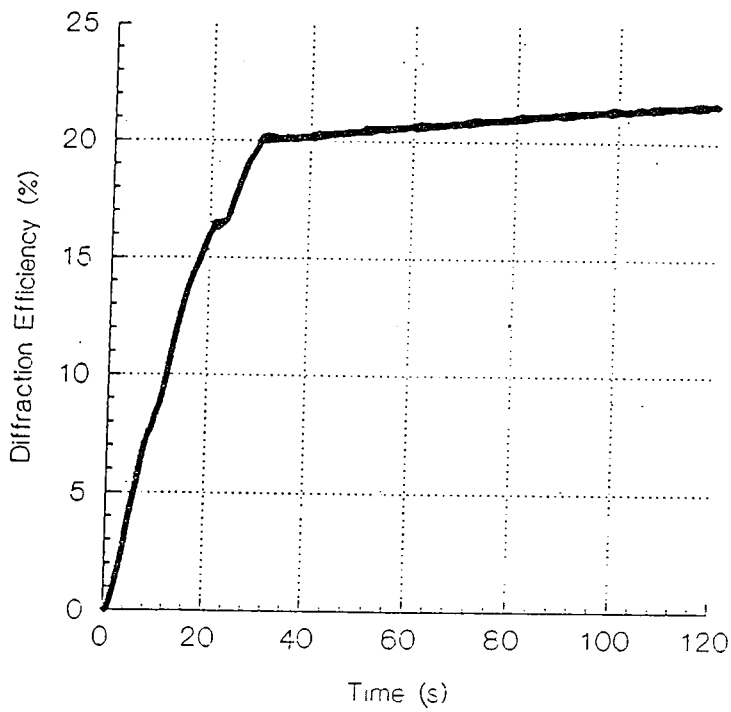

Figure 6.28 The change in diffraction efficiency of a grating recorded by a normal exposure of 30 seconds (step I) followed by a delay of 2 seconds (step II) and then a uniform exposure (step III). Grating fringe spacing is 1 μm.

The effect of uniform post exposure begins to decrease again if normal exposure time is increased further. This is probably because at long exposure times a lot of the sensitizing dye will have been used and further exposure has less of an effect.

Taking a grating recorded at the lowest spatial frequency (250 lines/mm) as an example (the effect of spatial frequency will be discussed in the next section), it can be shown that if fringe visibility can be assumed to be unity[‡,23],.the model described above can be used to calculate the refractive index change, and the contributions made by polymerization and diffusion to that refractive index change.

The final diffraction efficiency which remained after post exposure in this particular example (shown in Figure 6.29)was approximately 30%; this corresponds to a refractive index modulation (n_1) of 1.7×10^{-3}. Since all of the monomer in what were originally the bright and dark regions has now been polymerized, it can be assumed that this index modulation is entirely due to diffusion which occurred during the eight seconds of normal exposure. In other words it is entirely due to the density modulation which exists across the layer.

From equation 6.1 we can obtain an expression which relates refractive index change to density change in this special case of no change in molar refraction.

$$\Delta n = \frac{(n^2+2)(n^2-1)}{6n} \times \frac{\Delta\rho}{\rho}$$

‡ Wopschall and Pampalone have pointed out the importance of recognizing that it is usually a difference in polymerization rates which forms the concentration gradient and the simpler situation where zero polymerization occurs in the dark fringe areas is only approximated at low exposures.

For an average n=1.5 this becomes

$$\Delta n = 0.59 \times \Delta\rho / \rho$$

which allows us to approximate the magnitude of the density change which caused the refractive index to vary with an amplitude of 1.7×10^{-3}. The total difference between the refractive index in the bright fringe areas and the refractive index in the dark fringe areas (Δn) is 3.4×10-3 so $\Delta\rho/\rho$ must be 5.79×10^{-3}. Since the average density of these layers is 1.1g/cm^3 the density difference between bright and dark fringes ($\Delta\rho$) must be 5.24×10^{-3}. This density difference corresponds to 2.86% of the monomer content in the layer (0.183g/cm^3) and would have been caused by 1.43% of the monomer moving from the dark fringe regions (leaving them less dense) and into the bright fringe regions (causing the density to increase). This is a small fraction of the monomer content and yet it creates enough of a density change to cancel the opposing effect of the polymerization and produce enough of an increase in refractive index in the bright fringe areas to give a diffraction efficiency of 6% after the 8 seconds of normal exposure (before uniform exposure). This means that at this point the opposing effects of reduction in molecular refraction and the increase in density combine to give a refractive index modulation of 0.72×10^{-3}. If we now look at the situation which existed in the layer just after normal exposure of 8 seconds had ended, the dark fringe areas would contain no polymer and 98.57% of the original monomer content. Knowing the exact composition of the layer at the position of the intensity minima a predicted refractive index can be calculated using equation 6.1. Table 6-1 shows how the calculated value of 1.47259 was arrived at.

	TEA	Monomer	Polymer unit	Binder	$(n^2-1)/(n^2+2)$	n_{calc}
ρ	0.514	(0.183)×0.9857	0	0.40		
R	38.83	19.02	17.36	10.81		
M	149.19	71.08	71.08	44.0		
$\rho R/M$	0.13378	0.04827	0	0.09827	0.28032	1.47259

Table 6-1 Calculation of the refractive index in a dark fringe.

Since the refractive index of the dark fringe has been calculated and the refractive index modulation is known, a value of refractive index in the bright fringe regions at after 8 second of normal exposure can be calculated as 1.47403. Since the amount of monomer which had migrated into this region at this time has been estimated the only unknown is the percentage conversion of monomer to polymer. Polymerization is the only other contributor to refractive index so this can be calculated using the method described above . It turns out that in order to have a diffraction efficiency of 6% after 8 seconds when 1.43% of the monomer is known to have diffused into the bright fringe areas the percentage conversion of the monomer to polymer must be 16.6%.[§]

These values are only approximate because as was mentioned above refractive indices calculated using this method do differ from the measured values and since the refractive index changes here are small the errors are bound to be quite large. However despite this the method is very useful for determining the sign and approximate

---

[§] The value obtained for percentage conversion agrees closely with the value obtained if it is estimated using the maximum diffraction efficiency achieved when normal exposure was allowed to continue until the diffraction efficiency growth curve was saturated i.e. full conversion was achieved in the bright fringe areas. If 35% diffraction efficiency is obtained (with normal exposure) at 100% monomer conversion in the bright fringe areas then a 6% diffraction efficiency would correspond to a percentage conversion of 17%

magnitude of refractive index changes, and the relative contributions of different processes.

The above explanation can be extended to explain fully the results obtained by Booth. In the light of these calculations it is not surprising that such large diffraction efficiencies were obtained by Booth after post exposure to a single beam. In the case of the Dupont photopolymer the diffusion was occurring just enough to cancel the effect of polymerization (and the consequent lowering of refractive index) and cause a small increase in diffraction efficiency. Both polymerization and diffusion were substantial but as the effects were in opposition the diffraction efficiency growth was quite slow. When the grating was exposed to uniform illumination and the dark fringe areas were polymerized, all monomer was polymerized, but a large density modulation which had occurred during normal exposure remained producing a large diffraction efficiency.

Because diffusion is slower in the Dupont material, time had to be allowed for diffusion to occur, so, in contrast to the material studied here, a dependence on delay time (step II) was observed.

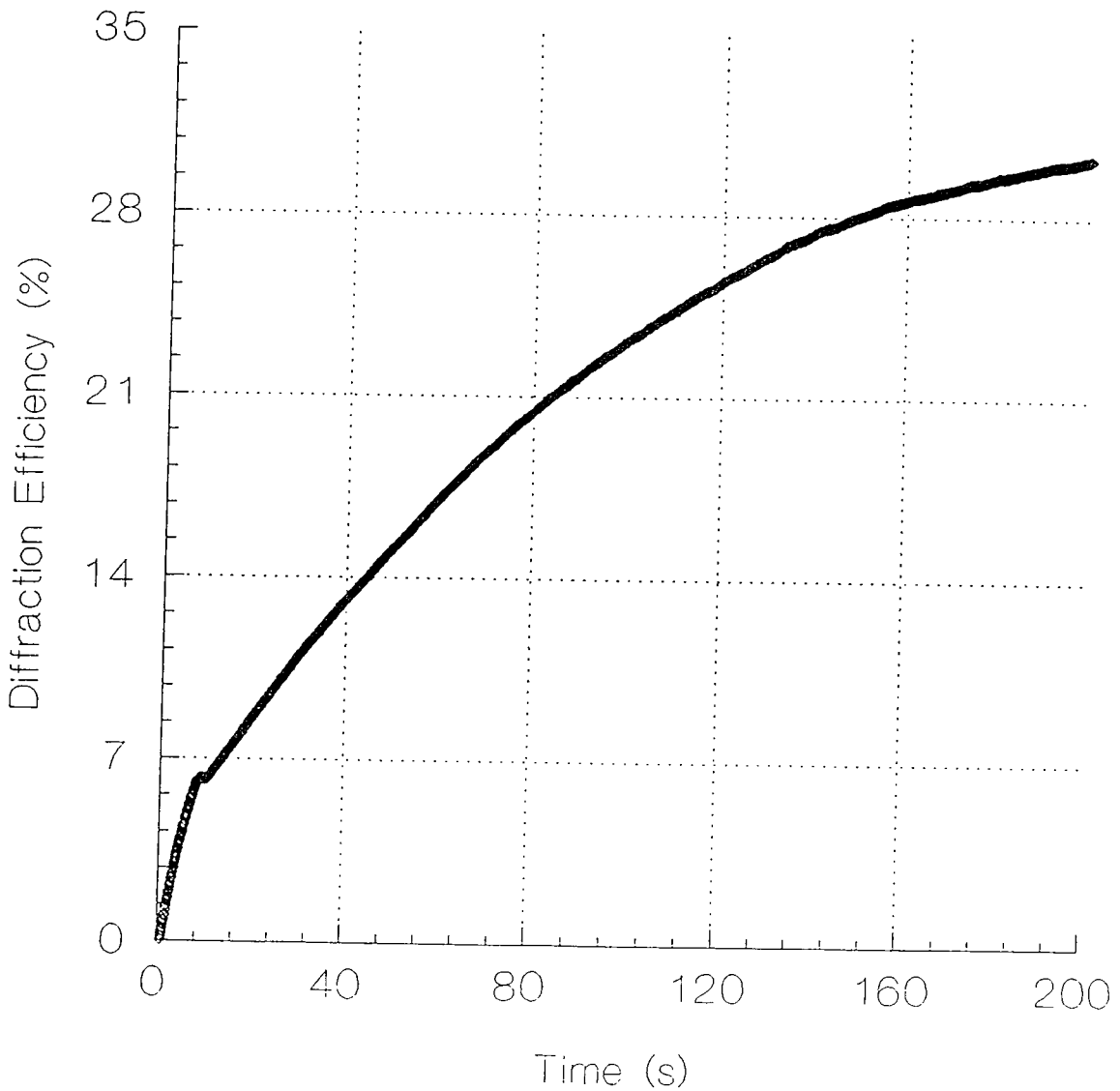

Figure 6.29 The change in diffraction efficiency of a grating recorded by a normal exposure of 8 seconds (step I) followed by a delay of 2 seconds (step II) and then a uniform exposure (step III). Grating fringe spacing is 4μm

6.3.5 Post exposure at different spatial frequencies.

When gratings were recorded for the same exposure time at different spatial frequencies the effect of post exposure to a uniform beam was markedly different. Varying the delay time still had no effect even at a spatial frequency of only 250 lines/mm where the diffusion distance is four times greater than for the 1000 lines/mm gratings. This again confirms that diffusion is a fast process in these layers and does not lag behind polymerization even at large diffusion distances. Since diffusion depends only on the percentage polymerization it would be expected that changing the spatial frequency would have no effect on the response of the grating to uniform post exposure. However, as can be seen from Figure 6.30, Figure 6.31 and Figure 6.32 the final diffraction efficiency which remains after uniform exposure is much greater when the spatial frequency is lower. The same trend was noted throughout these experiments. At the lowest spatial frequency (250 lines/mm) the diffraction efficiencies are increased to, typically, five to ten times the original value by post exposure. Gratings recorded at 450 lines/mm reach three or four times the original value, and the 1000 lines/mm gratings only reach about one and a half to two times the original value.

Recalling the results of chapter 5 this behavior can be explained by the availability of sensitizer in the dark fringe regions. Since recorded gratings are often completely bleached, lossless gratings, it can be assumed that the dye sensitizer also diffuses during normal recording of a grating in this material. If it did not the dye in the dark fringe regions would remain unbleached. In chapter 5 an increase in diffraction efficiency was observed, for a set exposure time, as fringe spacing was reduced. This was explained by the fact that unbleached dye molecules (which are large rigid molecules) could more easily diffuse from the unexposed areas into the bright fringe

areas when the diffusion distance was small. There was therefore more sensitizer available, and more polymerization was initiated under the same exposure than in the gratings with a large fringe spacing. In gratings with a large fringe spacing little diffusion of dye occurred and the concentration of dye in the unexposed areas would have remained at its original value.

This is why gratings recorded with different spatial frequencies respond differently to uniform post exposure. At low spatial frequencies enough dye remains in the unexposed regions to completely polymerize the remaining monomer, lower the refractive index, and cause further increase in the refractive index modulation. However, at high spatial frequencies, where the diffusion distance is low, and less dye remains in the dark fringe areas after normal two beam recording, polymerization will not be completed and the diffraction efficiency will not increase to its full potential. In the calculation in the last section which estimated the contribution of diffusion to the refractive index change, it was necessary to assume that the polymerization process was completed in full during post exposure. This is why the lowest spatial frequency was used.

These results are important, as they show that the post exposure process provides a means of enhancing the low spatial frequency components of a hologram. This means that a well chosen combination of normal exposure and post exposure will ensure a more uniform response to the range of spatial frequencies, and improve the recording characteristics of the material.

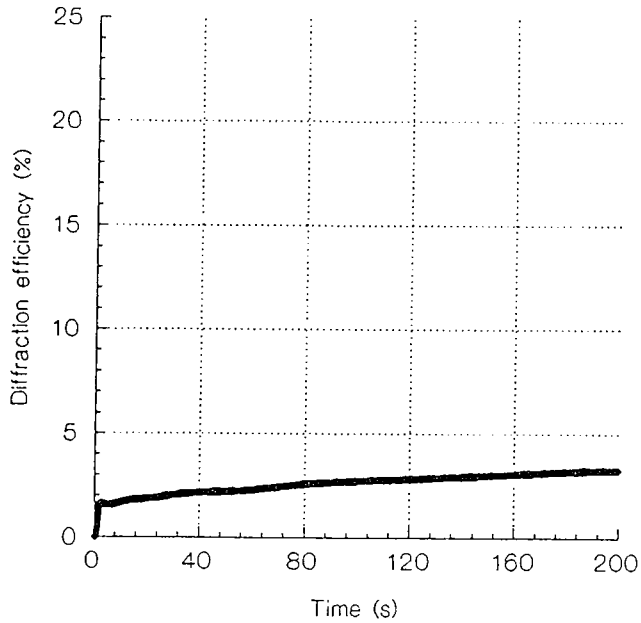

Figure 6.30 The change in diffraction efficiency of a grating recorded by a normal exposure of 2 seconds (step I) followed by a delay of 2 seconds (step II) and then a uniform exposure (step III). Grating fringe spacing is 1 μm.

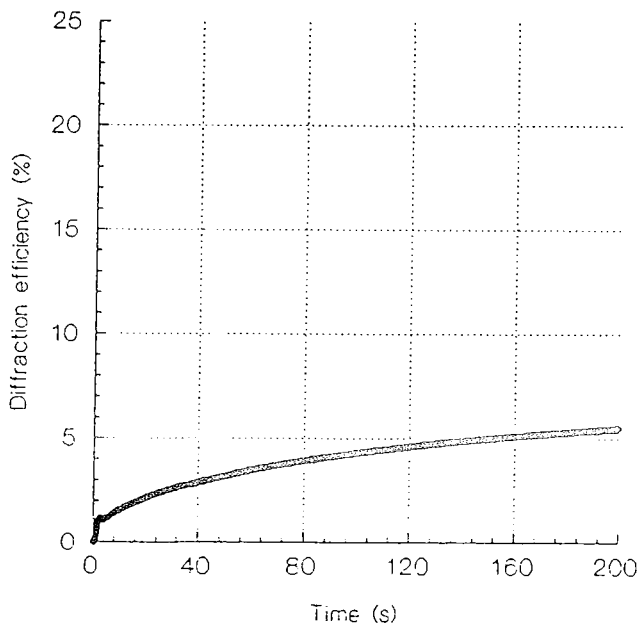

Figure 6.31 The change in diffraction efficiency of a grating recorded by a normal exposure of 2 seconds (step I) followed by a delay of 2 seconds (step II) and then a uniform exposure (step III). Grating fringe spacing is 2.2 μm.

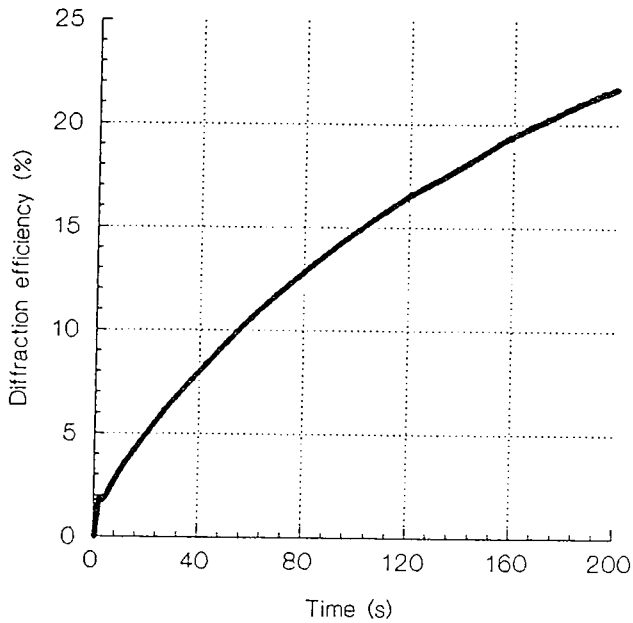

Figure 6.32 The change in diffraction efficiency of a grating recorded by a normal exposure of 2 seconds (step I) followed by a delay of 2 seconds (step II) and then a uniform exposure (step III). Grating fringe spacing is 4μm.

6.3.6 Driving force behind mass transport of material

Although the above results prove that mass transport occurs during recording, and details the contribution which this diffusion makes to the overall refractive index change, the driving force behind the diffusion is still unclear. Many authors simply state that the diffusion is caused by the concentration gradient produced when polymerization occurs at a faster rate in the bright fringe areas. To some extent his is true but it is certainly not a full explanation. If monomer were simply flowing into the bright fringe regions to equalize a difference in monomer concentrations the amount of monomer which moves from the dark fringes would actually be much greater. For example take the situation described in section 6.3.4 . During the eight seconds of normal exposure 17% of the monomer in the bright fringe regions had been polymerized, so a concentration gradient was produced. 8.5% of the monomer in the dark fringe regions would have to diffuse into the bright fringe regions in order to equalize the monomer concentrations. In fact only 1.43% of the monomer moved.

Similarly, full conversion of the monomer in the bright fringes (without even considering conversion of the extra monomer as it diffuses in) would lead to transport of about half of the available monomer in the dark fringes if diffusion were occurring because of the concentration gradient. This would produce an overall density increase of about 10% in the bright fringe areas and a similar decrease in the dark fringe areas. The expected amplitude of the corresponding refractive index change would be of the order of 0.15, thirty times larger than the highest observed values in this material (5×10^{-3}). Clearly the actual levels of mass transport are much lower.

One of the highest diffraction efficiency increases observed after uniform post exposure was an increase from 4.2% to 35% in a 250 lines/mm grating. Even this example corresponds to movement of only 1.57% of the monomer during the initial exposure of 4 seconds. The calculations indicated that approximately 21% conversion was achieved during this time.

This would seem to indicate that in normal exposure 100% conversion would produce movement of about 7.5% of the monomer. In the earlier example 1.43% had moved when conversion was 16.6% so at 100% conversion, 8.6% of the total monomer in the dark fringes would have diffused into the bright fringes.

The real situation is, of course, much more complex. Numerous other factors can affect polymerization and diffusion rates and the interference pattern at recording is not a series of bright and dark lines, but a sinusoidal variation in intensity. Despite these approximations the above results show that diffusion of monomer is undoubtedly very fast and can be said to happen immediately polymerization occurs. The results also show that the amount of monomer that is transported from dark to bright fringe regions is relatively small, and at most between 6% and 8% of the monomer.

Under normal circumstances (in the absence of a binder) polymerization causes volume shrinkage. Polymerization changes the molecular packing by linking the monomer units into long polymer chains, the result is a decrease in the microscopic volume occupied by each polymer molecule. In a straightforward polymerization of a pure monomer, the bulk volume of a typical monomer will shrink by 15% on polymerization. However, in this acrylamide

based photopolymer material the polymerizing material is restricted by the rigid polymer matrix in which it is dispersed. Shrinkage is restricted, and instead material is drawn in from the unpolymerized dark fringe regions on either side of the polymerizing bright fringe. At large fringe spacings (e.g. 10 lines/mm), the binder can withstand some deformation and this increase in material in the polymerized regions causes them to swell slowly over a period of several hours. However at high spatial frequencies no bulk swelling or shrinkage occurs and there must be an increase in the free volume available where polymerization has occurred. Total polymerization in the bright fringe regions could cause a decrease of about 15% in the space occupied by the monomer, but it is likely to be less than this because of restrictions caused by the binder. It is possible that the monomer in the dark fringe regions flows into the bright fringe regions to fill the 'gaps' caused by polymerization. The result is that at high spatial frequencies a density change occurs but the overall volume is not changed.

6.4 Conclusion

This chapter has detailed the physical processes involved in the refractive index changes which lead to the formation of a hologram. It has been concluded that at the spatial frequencies typical of holographic recording, the hologram is recorded purely by modulation of the refractive index and can be considered a lossless phase hologram. The angular selectivity of various gratings has been determined by monitoring the change in diffraction efficiency as the angle of incidence is rotated through the Bragg angle. Coupled wave theory was used to predict angular selectivity curves for these gratings and the experimental data was found to fit very closely to the theoretical curves. From these curves the amplitude of the refractive index modulation in the

grating was determined. 4×10^{-3} is a typical value but modulation amplitudes greater than 5×10^{-3} have been observed. Using coupled wave theory to evaluate the refractive index modulation the evolution of refractive index modulation during a typical recording was shown.

The processes thought to occur in similar materials such as the Dupont photopolymer and other photopolymerizable materials were discussed. Diffusion of material between bright and dark regions was thought to play an important role in the formation of a refractive index change but some behavior, such as the large increases in diffraction efficiency obtained under uniform post exposure by Booth, remained unexplained.

The acrylamide based material studied here was also found to exhibit this phenomenon and a detailed study of the post exposure response was carried out. It was found that diffusion stops as soon as the illuminating light is removed and is not a slow process which continues on after polymerization has stopped. It was also found that a relatively small amount of diffusion was required to produce the magnitude of refractive index modulation normally measured in these materials. Increases in diffraction efficiency under uniform post exposure were substantial and could be explained by the fact that as polymerization occurs the bond conversion and density increase (which occurs as a result of diffusion and not volume change) have opposing effects on the refractive index. The lowering of refractive index which occurs as a result of bond conversion is canceled by the increase of the refractive index caused by the increase in density due to diffusion. Although diffusion is limited its effect on refractive index far outweighs the effect of bond conversion and the net result is an increase in refractive index in the bright fringe areas and a decrease in the dark fringe areas. The effect of post exposure is to polymerize all the remaining monomer (if enough sensitizing dye remains) so that

the decrease in refractive index due to bond conversion is uniform across the layer. This means that the (larger) refractive index modulation due to density variations is the only contributor to the overall refractive index modulation. The resulting diffraction efficiency is therefore much larger. Figure 6.33 is an example of how the refractive index would vary across a typical layer. The broken line represents the refractive index change caused by the bond conversion associated with polymerization and the solid line represents the refractive index variation caused by density variations due to the diffusion which accompanies polymerization. Figure 6.34 shows the sum of these two index variations. This would correspond to the net refractive index modulation that would be measured in the material after a few seconds of normal recording. However looking back at Figure 6.33 it becomes clear the polymerization of the remaining monomer would reduce the refractive index in both the dark and bright fringe regions (more in the dark fringe regions because more monomer remains unpolymerized there). If all the monomer is converted the sinusoidal variation in refractive index due to bond conversion will be reduced to a straight line and will have no effect on the refractive index modulation. It will simply cause a reduction in the average refractive index of the layer. Summing the effects of bond conversion and density variation after post exposure will give a refractive index modulation with the same amplitude as the modulation due to density variation in Figure 6.33 but offset from the original average refractive index by some constant value due to the effects of bond conversion. Since only the amplitude of the modulation affects the refractive index change the resulting diffraction efficiency is much larger.

This also explains the large diffraction efficiency increases observed by Booth.

It was also observed that in order for post exposure to have the full effect on diffraction efficiency sufficient dye sensitizer should remain, or polymerization cannot be completed. This is why a decrease in the response to post exposure was observed at long exposure time (two beam) and high spatial frequency. Unlike Booth's work, no dependence on the delay before post exposure was observed. This is because diffusion is faster in this material than in the Dupont photopolymer.

Since post exposure was observed to have a greater effect on the diffraction efficiency of lower spatial frequency gratings, it was suggested that a suitable combination of exposure and post exposure would improve the spatial frequency response characteristics of this photopolymer.

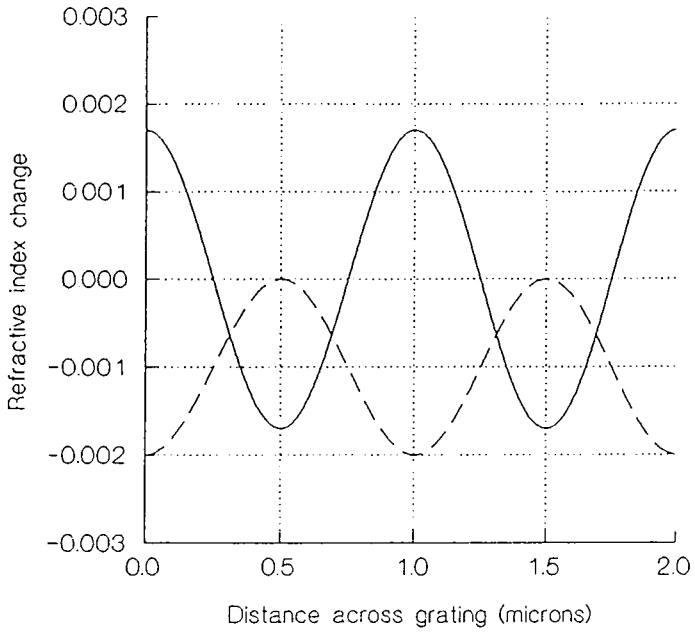

Figure 6.33 An example of how the refractive index would vary across a typical layer. The broken line represents the refractive index change caused by the bond conversion associated with polymerization, and is 180° out of phase with the variation in incident light intensity, and the solid line represents the refractive index variation caused by density variations due to the diffusion which accompanies polymerization.

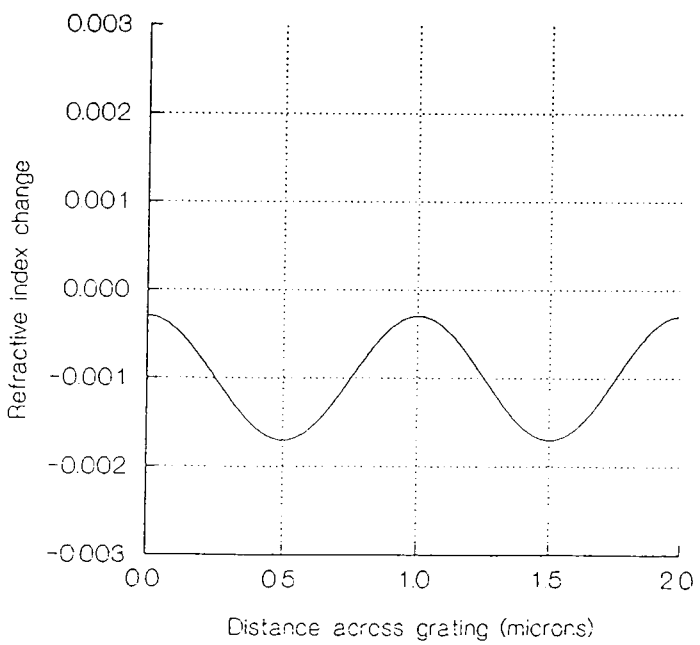

Figure 6.34 The variation of refractive index across a typical layer. The bulk refractive index is the sum of the decrease in overall refractive index due to bond conversion and the change in refractive index due to the density variation caused by diffusion.

[1] R. J. Collier, C. B. Burckhardt, L. H. Lin, "Optical holography", Chapter 9, Academic Press, NewYork 1971.

[2] J. A. Jenney "Holographic recording with photopolymers", *J. Opt. Soc. Am.*, **60**, 1155-1162, 1970

[3] J. A. Jenney "Fixing of photopolymer holograms", *J. Opt. Soc. Am.*, **61**, 1116-1117, 1971.

[4] N. Sadlej and B. Smolinska, "Stable photosensitive polymer layers for holography", *Optics and Laser Technology*, 175-179, Aug, 1975

[5] Y. B. Boiko, V. S. Solovjev, S. Calixto, and D. J. Lougnot, "Dry Photopolymer films for computer gererated infrared radiation focussing elements", *Appl. Opt*, **33**, No. 5, 787-793, 1994.

[6] Y. B. Boiko, V. S. Solovjev, S. Calixto, and D. J. Lougnot, "Dry Photopolymer films for computer gererated infrared radiation focussing elements", *Appl. Opt*, **33**, No. 5, 787-793, 1994.

[7] S. Calixto "Dry polymer for holographic recording", *App. Opt.*, **26**, 18, 3904 -3910, 1987.

[8] W. S. Colburn and K. A. Haines, "Volume hologram formation in photopolymer films", *Appl. Opt.*, **10**, 1636-1641, 1971.

[9] J. A Jenney "Holographic recording with photopolymers", *J. Opt. Soc. Am.*, **60**, 1155-1162, 1970.

[10] Y. B. Boiko, V. S. Solovjev, S. Calixto, and D. J. Lougnot, "Dry photopolymer films for computer gererated infrared rediation focussing elements", *Appl. Opt*, **33**, 787-793, 1994

[11] B. L. Booth, "Photopolymer material for holography", *App. Opt.* , **14**, 593-601, 1975.

[12] W. J. Tomlinson, E. A Chandross, H. P. Weber, and G. D. Aumiller, "Multicomponent photopolymer systems for volume phase holograms and grating devices", *Appl. Opt.*, **15**, No. 2, 534-541, 1976.

[13] E. S. Gyulnazarov, T. N. Smirnova, E. A. Tikhonov, "Mechanisms of phase-hologram recording on photopolymerizing liquid compositions" *Opt. Spectrosc.(USSR)*, **67**, 99-101, 1989

[14] E. S. Gyulnazarov, V. V. Obukhovskii, T. N. Smirnov, "Theory of holographic recording on a photopolymerized material", *Opt. Spectrosc.(USSR)*, **69**, 109-111, 1991

[15] V. V. Obukhovskii, T. N. Smirnova, "Model of holographic recording on photopolymerizing composites.", *Opt. Spectrosc.(USSR)*, **74**, 462-466, 1993

[16] J. E. Van Koppenhagen, M. Majda, "Structurally heterogeneous electrode films of polyacrylamide and acrylamide /vinylpyridine copolymeric gels", *J.Electroanal. Chem*, **189**, 379-388, 1985

[17] W. J. Tomlinson and E. A. Chandross "Organic photochemical refractive index image recording systems" Advanced Photochemistry, **12**, eds. T. N. Pitts Jr, G. S. Hammond, K. Gallnick, D. Grosjier, John Wiley Interscience, 1980.

[18] H. Tobita and A. E. Hamielec, " Crosslinking kenetics in polyacrylamide networks", *Polymer*, **31**, 1546-1552, 1990.

[19] Y. B. Boiko, V. S. Solovjev, S. Calixto, and D. J. Lougnot, "Dry photopolymer films for computer gererated infrared rediation focussing elements", *Appl. Opt*, **33**, No. 5, 787-793, 1994

[20] Booth B. L. "Photopolymer material for holography", *Applied Optics*, **14**, 593 -601, 1975.

[21] J. E. Van Koppenhagen, M. Majda, "Structurally heterogeneous electrode films of polyacrylamide and acrylamide /vinylpyridine copolymeric gels", *J.Electroanal. Chem*, **189**, 379-388, 1985

[22] Pritchard "Poly (vinyl alcohol)" Gordon and Breach, 1970.

[23] R. H. Wopschall and T. R. Pampalone "Dry photopolymer film for recording holograms", *Appl. Opt.*, **11**, 2096-2097, 1972.

7. Conclusion

The purpose of this research has been to develop a new, dry, self processing, holographic recording material based on acrylamide monomers. It was intended that the material could be sensitized for use with a 514nm argon laser and its composition optimized for maximum sensitivity and diffraction efficiency.

The material was sensitized to green using fluorescein, a well known green sensitive laser dye. Detailed consideration was given to the practical problems of layer preparation and pre-exposure shelf life. The lifetime of recorded gratings was improved dramatically from hours to months by the addition of a crosslinking agent: methylene bisacrylamide, and it was discovered that drying and sealing these layers between glass plates made them effectively permanent.

The photochemistry of the system was then studied so that the processes occurring in the holographic recording material under illumination could be better understood. The effect of each chemical component on the bleaching rate of the illuminated layers was studied and, from this, conclusions were drawn about the interaction of the various layer constituents. For example triethanolamine was found to increase the rate of bleaching in layers containing only polyvinyl alcohol, dye and triethanolamine. This indicates that it increases the rate of production of free radicals and will promote polymerization. The role of the electron donor in the proposed chemical scheme was thereby confirmed. This result was important and illustrated the usefulness of bleaching studies, because the response to changes in triethanolamine concentration in the actual recording material is difficult to study holographically.

Studies of the effect of dye concentration, monomer concentration and the effect of different xanthene dye sensitizers were also carried out. Actual quantum yields of bleaching were calculated from the transmittance data, and by comparing the quantum yield of bleaching in the absence and presence of acrylamide the amount of radicals being used for initiation of polymerization was determined. Other authors have used these methods to study various dyes in solution and in polyvinyl alcohol layers. However the comparison of quantum yields in the absence and presence of a monomer has been used to determine the quantum yield of initiation of polymerization, and thereby predict the efficiency of a particular dye in sensitizing a photopolymerizable holographic recording material, and is reported for the first time in this thesis.

The advantages of this method are that, in addition to the insight into the photochemical processes that is obtained, the method is simple, and since no hologram is actually recorded, extreme environmental stability is not required. The method was used to estimate the relative efficiencies of five xanthene dyes as sensitizers for this system by comparing the quantum yield of initiation for the system sensitized by each dye. The predicted results were then confirmed by actually recording holographic gratings in layers sensitized with each of the dyes.

Once the photochemical processes were better understood, the concentration of each of the chemical components was optimized for maximum sensitivity and diffraction efficiency. The sensitivity of the system was increased by a factor of five without increasing the monomer concentration. This was achieved by reducing the dye concentration and replacing fluorescein with erythrosin B which has a higher triplet state quantum yield and is therefore a better sensitizer. Higher monomer concentration

would have produced even more sensitive layers but at higher concentrations of monomer layer preparation becomes more difficult. Therefore, since repeatability, reliability and ease of preparation are as important in a good recording material as high sensitivity, moderate concentrations of monomer were used in the optimized formulation. The result was a much improved formulation which could achieve extremely high diffraction efficiency with relatively low exposure (80 mJ/cm2) without the need for high monomer concentrations. Table 7-1 compares the optimized photopolymer developed here (last line) with other currently available photopolymer materials. The data is taken from a recent review of holographic recording materials by Manivannan and Lessard [1] and from the references cited. The material compares very favourably with other materials, even the commercial DuPont photopolymer.

The holographic recording characteristics of material prepared with the optimized formulation were examined and it was found that slanted gratings were also possible without distortion, as no shrinkage occurs during recording. However one drawback of this photopolymer material is the limited resolution; gratings were not recorded above spatial frequencies of 3000 lines/mm. This means that in its present formulation the material is not a practical recording medium for reflection holograms. One conclusion drawn from this work was the fact that the mobility of the initiating species is responsible for the limited resolution, so it is hoped that it will be possible to improve the resolution of the material by reducing the permeability of the layer through compositional changes. The material was found to have good recording characteristics when used in transmission mode and demonstrations of double exposure and live fringe holographic interferometry were carried out with excellent results.

Material	Preparation method	Thickness (μm)	Recording wavelength (nm)	Sensitivity (mJ/cm^2)	Resolution (lines/mm)	Diffraction efficiency (%)	Processing ?	Ref
Barium and acrylates	Liquid between two glass plates	10-20	694	30	3000	45	optical	2
Multifunctional acrylates	Liquid between two glass plates	50	450-550	100-200	>2500	80	none	3
Methacrylate	Liquid between two glass plates	45	514	40000	~2000	55	none	4
Du Pont's Photopolymer	Coated on glass substrate	1.25-200	350-550	5-50	3000	88-90	heat treatment	5
Du Ponts Omnidex HRF series.	Coated on plastic sheet	6-78	450-650	10-100	6000	99	heat treatment	6
Polaroid's DMP-128	Coated on plastic sheet	1-30	442-647	5-30	5000	80-100	chemical processing	7
Polymethyl-methacrylate	PMMA blocks	2000	325	50000-150000	5000	96	none	8
Acrylamide / bisacrylamide	Coated on glass substrate	140	514	50-80	2800	80-96	none	

Table 7-1 The holographic characteristics of various photopolymer formulations

The angular selectivity of various gratings has been determined by monitoring the change in diffraction efficiency as the angle of incidence is rotated through the Bragg angle. Coupled wave theory was used to predict angular selectivity curves for these gratings and the experimental data was found to fit very closely to the theoretical curves. From these curves the amplitude of the refractive index modulation in the grating was determined. 4×10^{-3} is a typical value but modulation amplitudes greater than 5×10^{-3} have been observed. Using coupled wave theory to evaluate the refractive index modulation the evolution of refractive index modulation during a typical recording was shown.

The physical processes involved in the refractive index changes which lead to the formation of a hologram in photopolymer materials have also been studied in detail. Diffusion of material between bright and dark regions was thought to play an important role in the formation of a refractive index change but some behavior, such as the large increases diffraction efficiency obtained under uniform post exposure by Booth, remained unexplained.

The acrylamide based material studied here was also found to exhibit this phenomenon and a detailed study of the post exposure response was carried out. It was found that a relatively small amount of diffusion was required to produce the magnitude of refractive index modulation normally measured in these materials. The effect of post exposure is to polymerize all the remaining monomer (if enough sensitizing dye remains) so that there is no difference in the molecular refractivity of the material in the bright and dark fringe. This means that the (larger) refractive index modulation due to density variations is the only contributor to the overall refractive index modulation. The resulting diffraction efficiency is therefore much larger. This also explains the large

diffraction efficiency increases observed by Booth. The fact that post exposure was observed to have a greater effect on the diffraction efficiency of lower spatial frequency gratings, could be used to improve the spatial frequency response characteristics of this photopolymer, i.e. a suitable combination of exposure and post exposure could ensure that approximately the same diffraction efficiency is reached at a broader range of spatial frequencies.

The quantitative analysis of the diffraction efficiency growth during uniform post exposure of an underexposed grating provided considerable in sight into the processes involved in grating formation.

The material has been improved dramatically in terms of optical quality, diffraction efficiency, sensitivity and pre- and post exposure shelf life. The relatively low monomer concentration needed to produce these high diffraction efficiencies in this optimized formulation means that high quality layers can be produced reliably and easily without the previously prevalent problem of monomer precipitation. This study has improved our understanding of the photochemical and physical processes that contribute to the refractive index change as a hologram is being recorded. The knowledge of the system that has been obtained facilitates further refinement of this formulation and contributes to the understanding of the behavior of other similar photopolymerizable recording materials. Further work in this area is being carried out in our laboratories on the new photopolymer developed here. Holographic characterization of the optimized material showed that it has good holographic recording characteristics and will be particularly successful as a recording medium for holographic interferometry.

[1] G. Manivannan, R. A. Lessard "Trends in holographic recording materials" *Trends in polymer science* , **2**, No. 8, 282-290, 1994

[2] D. H. Close, A. D. Jacobson, J. D. Margerum, R. J. Brault and F. J. McClung "Hologram recording on photopolymer materials", *Appl. Phys. Lett*, **14**, 159-160, 1969.

[3] D. J. Lougnot, C. Turck "Photopolymers for holographic recording II Self developing materials for realtime interferometry" *Pure Appl. Opt.*, **1**, 251-268,1992.

D. J. Lougnot, C. Turck "Photopolymers for holographic recording III Time modulated illumination and thermal post effect" *Pure Appl. Opt*, **1**, 269-279, 1992.

[4] A. Fimia, N. Lopez, F. Mateos, R. Sastre, J. Pineda, and F. Amat-Guerri "New photopolymer used as a holographic recording material", *Appl. Opt.*, **32**, No. 20, 3706-3707, 1993.

[5] W. S. Colburn, K. A. Haines, "Volume hologram formation in photopolymer materials", *Appl. Opt.*, **10**, 1636-1641, 1971.

[6] W. K. Smothers, T. J. Trout, A. M. Weber, D. J. Mickish, "Hologram recording in Du Pont's new photopolymer materials" *IEE Conference Publication, no. **311**, Proceedings of the Second International Conference on Holographic Systems, Components and Applications*, 184-188, 1989

[7] R. T. Ingwall, M. Troll, "Mechanism of hologram formation in DMP-128 photopolymer", *Opt. Eng.*, **28**, 586-591, 1989.

[8] M. J. Bowden, E. A. Chandross and I. P.Kaminow "Properties of holographic gratings produced in polymethyl methacrylate", *Appl. Opt*, **13**, 112-117, 1974

Appendix I

Classical and holographic definitions of intensity:

In the interaction of light with photosensitive media the optical properties of the material change as a function of the energy absorbed, averaged over a time which is long compared to the light vibration period. From the energy law of Maxwell's theory we know that u the energy per unit volume or energy density in the electric field of a light wave is given in SI units as

$$u = \frac{1}{2}\varepsilon\,\vec{\nu}\cdot\vec{\nu}$$

where ε is the dielectric constant of the material in which the wave is traveling and $\vec{\nu}$ is the electric field vector. The time average of u is

$$\langle u\rangle = \frac{1}{2T}\int_{-T}^{T} u\,dt$$

$$= \frac{1}{2}\varepsilon\cdot\frac{1}{2T}\int_{-T}^{T}\vec{\nu}\cdot\vec{\nu}dt$$

$$= \frac{1}{2}\varepsilon\,\langle\vec{\nu}\cdot\vec{\nu}\rangle$$

where 2T is the time over which the average is taken.

At any point in the light wave the Poynting vector may be interpreted as giving the magnitude and direction of the energy flow per unit time per unit area normal to the

flow. In classical optics the time average of the magnitude of this flow of power per unit cross section is called the *intensity*, I_p of the light at that point.

$$I_p = s\langle u \rangle = \frac{1}{2} s\varepsilon \langle \vec{v} \cdot \vec{v} \rangle$$

where s is the speed of the light in the medium. On the other hand, in holography it is the custom to define intensity in an abbreviated form such that

$$I = 2\langle \vec{v} \cdot \vec{v} \rangle$$

because this intensity I reduces to the square of the amplitude of a light wave. However, the proportionality between I and I_p allows relative intensities to be expressed equivalently in terms of I or I_p and the two definitions of intensity can be related to one another by a simple proportionality constant.

PUBLICATIONS

Martin S., Leclere P., Renotte Y., Toal V. and Lion Y.,"*Characterisation of an acrylamide-based dry photopolymer holographic recording material*" Optical Engineering, Vol. 33, no. 12 , December 1994, pp 3942-3946.

Martin S., Leclere P., Renotte Y., Toal V. and Lion Y.,"*Characterisation of an acrylamide-based dry photopolymer holographic recording material*" Proceedings of Applied Optics and Optoelectronics Conference, Institute of Physics,York, September 1994. pp 323 -325

Martin S., Toal V., "*Dry Photopolymer Layers for Holographic Applications*", IEE conference publication no. 379, Proceedings of Fourth International Conference on Holographic Systems, Components and Applications, Neuchatel, 1993.

Martin S. and Toal V. "*Dry photopolymer layers for holographic recording*", Proceedings of Applied Optics and Optoelectronics Conference, Institute of Physics, Leeds, September 1992. pp 102 - 103.

Martin S. and Toal V. "*Dry photopolymer layers for holographic recording*", Proceedings of Irish Optoelectronics Group annual meeting,University College Dublin , April 1992.